



National Library  
of Canada

Bibliothèque nationale  
du Canada

Canadian Theses Service

Services des thèses canadiennes

Ottawa, Canada  
K1A 0N4

## CANADIAN THESES

## THÈSES CANADIENNES

### NOTICE

The quality of this microfiche is heavily dependent upon the quality of the original thesis submitted for microfilming. Every effort has been made to ensure the highest quality of reproduction possible.

If pages are missing, contact the university which granted the degree.

Some pages may have indistinct print especially if the original pages were typed with a poor typewriter ribbon or if the university sent us an inferior photocopy.

Previously copyrighted materials (journal articles, published tests, etc.) are not filmed.

Reproduction in full or in part of this film is governed by the Canadian Copyright Act, R.S.C. 1970, c. C-30.

THIS DISSERTATION  
HAS BEEN MICROFILMED  
EXACTLY AS RECEIVED

### AVIS

La qualité de cette microfiche dépend grandement de la qualité de la thèse soumise au microfilmage. Nous avons tout fait pour assurer une qualité supérieure de reproduction.

S'il manque des pages, veuillez communiquer avec l'université qui a conféré le grade.

La qualité d'impression de certaines pages peut laisser à désirer, surtout si les pages originales ont été dactylographiées à l'aide d'un ruban usé ou si l'université nous a fait parvenir une photocopie de qualité inférieure.

Les documents qui font déjà l'objet d'un droit d'auteur (articles de revue, examens publiés, etc.) ne sont pas microfilmés.

La reproduction, même partielle, de ce microfilm est soumise à la Loi canadienne sur le droit d'auteur, SRC 1970, c. C-30.

LA THÈSE A ÉTÉ  
MICROFILMÉE TELLE QUE  
NOUS L'AVONS REÇUE

CHEMISORPTION AND THERMAL DECOMPOSITION OF ALCOHOLS  
ON MAGNESIUM OXIDE AND TUNGSTEN OXIDE --- A STUDY  
BY SOLID-STATE NUCLEAR MAGNETIC RESONANCE SPECTROSCOPY

by

Septimus Hsien-Chai Liang

B.Sc. (Hon.) University of Toronto, 1976

M.Sc. Simon Fraser University, 1979

A THESIS SUBMITTED IN PARTIAL FULFILLMENT OF  
THE REQUIREMENTS FOR THE DEGREE OF  
DOCTOR OF PHILOSOPHY

in the department

of

Chemistry

© Septimus H.C. Liang 1985

SIMON FRASER UNIVERSITY

May 1985

All rights reserved. This thesis may not be  
reproduced in whole or in part, by photocopy  
or other means, without permission of the author.

Permission has been granted to the National Library of Canada to microfilm this thesis and to lend or sell copies of the film.

The author (copyright owner) has reserved other publication rights, and neither the thesis nor extensive extracts from it may be printed or otherwise reproduced without his/her written permission.

L'autorisation a été accordée à la Bibliothèque nationale du Canada de microfilmer cette thèse et de prêter ou de vendre des exemplaires du film.

L'auteur (titulaire du droit d'auteur) se réserve les autres droits de publication; ni la thèse ni de longs extraits de celle-ci ne doivent être imprimés ou autrement reproduits sans son autorisation écrite.

ISBN 0-315-30856-7

APPROVAL

Name: Septimus H.C. Liang  
Degree: Doctor of Philosophy  
Title of Thesis: Chemisorption and Thermal Decomposition of Alcohols on Magnesium Oxide and Tungsten Oxide -- A Study by Solid-State Nuclear Magnetic Resonance Spectroscopy

## Examining Committee:

Chairperson: Dr. F.W.B. Einstein

Dr. Ian D. Gay, Professor  
Senior Supervisor

Dr. A.C. Oehlschlager, Professor  
Supervisory Committee

Dr. E.J. Wells, Professor  
Supervisory Committee

Dr. A.G. Sherwood, Associate Professor  
Internal Examiner

Dr. B.A. Morrow, Professor  
External Professor  
Chemistry Department  
University of Ottawa

Date approved:

May 27, 1985

PARTIAL COPYRIGHT LICENSE

I hereby grant to Simon Fraser University the right to lend my thesis, project or extended essay (the title of which is shown below) to users of the Simon Fraser University Library, and to make partial or single copies only for such users or in response to a request from the library of any other university, or other educational institution, on its own behalf or for one of its users. I further agree that permission for multiple copying of this work for scholarly purposes may be granted by me or the Dean of Graduate Studies. It is understood that copying or publication of this work for financial gain shall not be allowed without my written permission.

Title of Thesis/Project/Extended Essay

"Chemisorption and Thermal Decomposition of Alcohols on Magnesium

Oxide and Tungsten Oxide - A Study by Solid-State Nuclear Magnetic

Resonance Spectroscopy"

Author:

(signature)

Septimus Liang

(name)

27th May 1985

(date)

Abstract

The technique of Proton-Enhanced Nuclear Induction Spectroscopy has been applied to the study of chemisorbed alcohol molecules on magnesium oxide (MgO) and tungsten oxide (WO<sub>3</sub>) surfaces. Preliminary studies involved the carbon-13 nuclear magnetic resonance (NMR) and adsorption studies of methanol on four different preparations of MgO. High-resolution C-13 NMR spectra have been obtained together with proton relaxation data at different coverages of methanol. These data indicate the only significant chemisorbed species to be methoxide at room temperature. Coverage-dependent motions of molecules are demonstrated in the adsorbed layer. The adsorbed layer is stable up to 300°C. At higher temperatures, decomposition sets in, yielding a complex mixture of gas-phase products. The only chemisorbed species found from high temperature decomposition is believed to be a bicarbonate species.

This study has been extended to ethanol and isopropanol adsorption on MgO. Both alcohols adsorb in the form of alkoxides, which are stable up to 250-300°C. The decomposition of the adsorbed layer at higher temperature yields a range of dehydration and dehydrogenation products, of both gaseous and chemisorbed varieties. The identification of the decomposition products by employing the Magic-Angle Spinning technique and C-13 enriched ethanol is fraught with some difficulties. The

elucidation of a complete decomposition mechanism is not possible with the present data. The preliminary investigation of adsorbed alkane-diols on MgO has met with some success.

The present technique has been applied to the study of other catalytic systems and, in this dissertation, the methanol-WO<sub>3</sub> system. The result is similar to that of methanol-MgO system, with the observation of surface-methoxide species at room temperature. The study of the decomposition of the methanol-WO<sub>3</sub> system at elevated temperature is hampered by paramagnetic interaction arising from the reduced form of WO<sub>3</sub> (WO<sub>3-x</sub>, where x varies from 0 to 1).

獻給我的父母

果里奇

一九八五年五月



Acknowledgement

I would like to thank Professor Ian Gay for his patient and helpful supervision, and his enlightening encouragement throughout this research project.

I would also like to extend my thanks to Professor R.K. Pomeroy, Professor B.M. Pinto, Mr. W.H. Romines III and Mr. B.D. Johnston, for their helpful discussion. I am also grateful for the help from the Machine Shop and the Glass-Blowing Shop.

Last of all, my thanks go to my good friends Mr. Paul R.C. Saunders and Mr. and Mrs. Danny Ho for their guided tours, fishing trips and good times we shared together, thus making my stay in Vancouver exciting.

# TABLE OF CONTENTS

		vii.
		Page
Title Page		i
Approval		ii
Abstract		iii
Dedication		v
Acknowledgement		vi
Table of Contents		vii
List of Tables		xi
List of Figures		xii
CHAPTER 1	Introduction	1
1.A.	NMR Techniques in Surface Chemistry	1
1.B.	Alcohol Decomposition	5
1.C.	Scope of This Study	5
CHAPTER 2	Survey of Work Done	8
2.A.	MgO	8
2.B.	WO <sub>3</sub>	11
CHAPTER 3	Solid-State NMR Theory	15
3.A.	Theoretical Background	15
3.B.I.	Double Resonance Experiments	19
3.B.II.	Cross-Polarization of Dilute Spins	32
3.B.III.	Cross-Polarization Dynamics	38
3.C.I.	Magic-Angle Spinning (MAS) Technique	42
3.C.II.	Basic Theory of MAS Technique	43
3.D.I.	MAS Combined with Proton-Enhanced NMR (CP/MAS) Technique	52
3.D.II.	Theory of CP/MAS	53

CHAPTER 4	Experimental	59
4.A.	Apparatus - General Description	59
4.A.I.	Probe	59
4.A.II.	R.F. Power	61
4.A.III.	Decoupler Phase Control	64
4.A.IV.	Control Logic	66
4.B.	Magic-Angle Spinner (MAS)	67
4.C.	Preparation of Catalyst	67
4.C.I.	MgO	67
4.C.II.	WO <sub>3</sub>	68
4.D.I.	Experiments	69
4.D.II.	NMR Measurements	71
4.E.	Estimation of Errors and Experimental Difficulties	74
4.F.	Reagents	77
CHAPTER 5	Results and Discussion	79
5.A.I.	Methanol and CO <sub>2</sub> Adsorption Isotherms	79
5.A.II.	Measurements of Relaxation Times and Cross-Relaxation Times	83
5.A.III.	Summary	93
5.B.I.	<sup>13</sup> C Spectra of Adsorbed Methanol	94
5.B.II.	<sup>13</sup> C NMR Measurements of Adsorbed Methanol Treated at Elevated Temperatures	100
5.B.III.	Summary	107

5.C.I.	$^{13}\text{C}$ Spectra of Adsorbed Ethanol on MgO	108
5.C.II.	$^{13}\text{C}$ NMR Measurements of Adsorbed Ethanol Treated at Elevated Temperatures	114
5.C.III.	$^{13}\text{C}$ CP/MAS Studies of Adsorbed Ethanol on MgO	119
	(i) Room Temperature to 200°C	124
	(ii) 250°C, 3 hours	125
	(iii) 275°C, 16 hours	127
	(iv) 300°C, 16 hours	135
	(v) 400°C, 3 hours	135
	(vi) 450°C, 3 hours	137
	(vii) 500°C, 3 hours	138
5.C.IV.	Summary	139
5.D.I.	$^{13}\text{C}$ Spectra of Adsorbed Isopropanol on MgO	142
5.D.II.	$^{13}\text{C}$ NMR Measurements of Adsorbed Isopropanol Treated at Elevated Temperatures	147
5.D.III.	$^{13}\text{C}$ CP/MAS Study of Adsorbed Isopropanol on MgO	160
5.D.IV.	Summary	163
5.E.	$^{13}\text{C}$ CP NMR of Adsorbed Alkanediols on MgO	164
5.E.I.	Adsorbed 1,2-ethanediol	170
5.E.II.	Adsorbed 1,3-propanediol	171
5.E.III.	Adsorbed 1,4-butanediol	176

	Page
5.E.IV. $^{13}\text{C}$ CP/MAS Study of Adsorbed 1,4-butanediol on MgO Treated at Elevated Temperatures	179
5.E.V. Adsorbed 1,3-butanediol	181
5.E.VI. Summary	183
CHAPTER 6 Results and Discussions of Methanol Adsorbed on $\text{WO}_3$	185
6.A. $\text{WO}_3$	185
6.A.I. Methanol Adsorption Isotherm	186
6.A.II. NMR Relaxation Parameters	188
6.A.III. $^{13}\text{C}$ CP Spectra of Adsorbed Methanol	192
6.A.IV. $^{13}\text{C}$ Static CP Spectra of Methanol- $\text{WO}_3$ at Elevated Temperatures	196
6.A.V. $^{13}\text{C}$ CP/MAS of Adsorbed Methanol on $\text{WO}_3$	201
6.A.VI. Summary	208
CHAPTER 7 Conclusions and Future Outlook	211
References	219

## LIST OF TABLES

	Page
Table 5.1 Proton $T_1$ of all methanol-MgO systems and selected samples treated at higher temperatures	85, 86
Table 5.2 Proton $T_1$ and $T_{1\rho}$ and $T_{CH}$ for some selected methanol-MgO systems	87
Table 5.3 Proton $T_1$ of all ethanol-MgO systems	89
Table 5.4 Calculated $^{13}\text{C}$ chemical shifts of some alcohols pertinent to this work	130, 131
Table 6.1 Proton spin-lattice relaxation time ( $T_{1H}$ ) for methanol-WO <sub>3</sub> samples	189

## LIST OF FIGURES

	Page
Figure 3.1 Schematic representation of the coupling between the I and S spins reservoir	20b
Figure 3.2 Schematic representation of different means for reducing spin-temperature	23b
Figure 3.3 Pictorial representation of level matching in the rotating frame	25b
Figure 3.4 Time evolution of the I and S inverse spin temperatures	28b
Figure 3.5 Pulse timing of a typical double resonance experiment in the rotating frame	31b
Figure 3.6 Double-rotating frame transformation	33b
Figure 4.1 Block diagram of the modified spectrometer	62b
Figure 4.2 Block diagram of the phase shifter logic	65b
Figure 4.3 Phase shifter schematic	65c
Figure 4.4 Some pulse sequence use in this dissertation	72b
Figure 5.1 Adsorption isotherms of methanol on all preparations of MgO at room temperature. Samples degassed at 500°C.	80b
Figure 5.2 Adsorption isotherms of CO <sub>2</sub> on all preparations of MgO at room temperature. Samples degassed at 500°C.	80c

- Figure 5.3 Adsorption isotherms of  $\text{CO}_2$  on all preparations of  $\text{MgO}$  at room temperature.  
Samples degassed at  $300^\circ\text{C}$ . 80d
- (Note: All  $^{13}\text{C}$  spectra are not normalized for different number of scans unless specified)
- Figure 5.4  $^{13}\text{C}$  CP spectra of 90%  $^{13}\text{C}$  enriched  $\text{CO}_2$  on all preparations of  $\text{MgO}$  82b
- Figure 5.5  $^{13}\text{C}$  CP spectra of  $2.79 \mu\text{mole}/\text{m}^2$  of 60%  $^{13}\text{C}$  enriched methanol on  $\text{MgO}$ -(2) at different contact times 91b
- Figure 5.6 Plot of  $^{13}\text{C}$  FID signal vs contact times for  $2.09 \mu\text{mole}/\text{m}^2$  of 60%  $^{13}\text{C}$  enriched methanol on  $\text{MgO}$ -(1) 92b
- Figure 5.7 Plot of  $^{13}\text{C}$  FID signal vs contact times for  $2.21 \mu\text{mole}/\text{m}^2$  of 60%  $^{13}\text{C}$  enriched methanol on  $\text{MgO}$ -(2) 92c
- Figure 5.8 Plot of  $^{13}\text{C}$  FID signal vs contact times using data from Figure 5.5 92d
- Figure 5.9 Plot of  $^{13}\text{C}$  FID signal vs contact times for  $2.99 \mu\text{mole}/\text{m}^2$  of 60%  $^{13}\text{C}$  enriched methanol on  $\text{MgO}$ -(4) 92e
- Figure 5.10  $^{13}\text{C}$  CP spectra of methanol adsorbed on  $\text{MgO}$ -(1) at various coverages 95b
- Figure 5.11  $^{13}\text{C}$  CP spectra of methanol adsorbed on  $\text{MgO}$ -(2) at various coverages 96b



- Figure 5.12  $^{13}\text{C}$  CP spectra of methanol adsorbed on MgO-(3) at various coverages 97b
- Figure 5.13  $^{13}\text{C}$  CP spectra of methanol adsorbed on MgO-(4) at various coverages. 98b
- Figure 5.14  $^{13}\text{C}$  CP spectra of  $4.31 \mu\text{mole/m}^2$  of methanol (60%  $^{13}\text{C}$  enriched) on MgO-(1) treated at different temperatures 101b
- Figure 5.15  $^{13}\text{C}$  CP spectra of  $4.97 \mu\text{mole/m}^2$  of methanol (60%  $^{13}\text{C}$  enriched) on MgO-(2) treated at different temperatures 102b
- Figure 5.16  $^{13}\text{C}$  CP spectra of  $3.55 \mu\text{mole/m}^2$  of methanol (60%  $^{13}\text{C}$  enriched) on MgO-(3) treated at different temperatures 103b
- Figure 5.17  $^{13}\text{C}$  CP spectra of  $4.11 \mu\text{mole/m}^2$  of methanol (60%  $^{13}\text{C}$  enriched) on MgO-(4) treated at different temperatures 104b
- Figure 5.18  $^{13}\text{C}$  CP/MAS spectrum of a sample of 90%  $^{13}\text{C}$  enriched  $\text{CO}_2$  adsorbed on MgO-(3), and  $^{13}\text{C}$  CP/MAS spectra of a sample of 60%  $^{13}\text{C}$  enriched methanol on MgO-(3) treated at different temperatures 105b
- Figure 5.19  $^{13}\text{C}$  CP spectra of ethanol adsorbed on MgO-(1) at various coverages 110b
- Figure 5.20  $^{13}\text{C}$  CP spectra of ethanol adsorbed on MgO-(2) at various coverages 111b

Figure 5.21	$^{13}\text{C}$ CP spectra of ethanol adsorbed on MgO-(3) at various coverages	112b
Figure 5.22	$^{13}\text{C}$ CP spectra of ethanol adsorbed on MgO-(4) at various coverages	113b
Figure 5.23	$^{13}\text{C}$ CP spectra of the sample of $8.01 \mu\text{mole}/\text{m}^2$ of ethanol on MgO-(1) treated at elevated temperatures	115b
Figure 5.24	$^{13}\text{C}$ CP spectra of the sample of $7.22 \mu\text{mole}/\text{m}^2$ of ethanol on MgO-(2) treated at elevated temperatures	116b
Figure 5.25	$^{13}\text{C}$ CP spectra of $7.19 \mu\text{mole}/\text{m}^2$ of ethanol on MgO-(3) treated at elevated temperatures	117b
Figure 5.26	$^{13}\text{C}$ CP spectra of the sample of $8.00 \mu\text{mole}/\text{m}^2$ of ethanol on MgO-(4) treated at higher temperatures	118b
Figure 5.27	$^{13}\text{C}$ CP/MAS spectra of 90% $^{13}\text{C}$ -enriched ethanol-1- $^{13}\text{C}$ on MgO-(3), at room temperature and treated at higher temperatures	120b
Figure 5.28	$^{13}\text{C}$ CP/MAS spectra of 90% $^{13}\text{C}$ -enriched ethanol-2- $^{13}\text{C}$ on MgO-(3), at room temperature and treated at higher temperatures	121b

- Figure 5.29  $^{13}\text{C}$  MAS spectra of the same sample as in Figure 5.27, treated at higher temperatures 122b
- Figure 5.30  $^{13}\text{C}$  MAS spectra of the same sample as in Figure 5.28, treated at higher temperatures 123b
- Figure 5.31  $^{13}\text{C}$  CP/MAS spectrum of  $13.92 \mu\text{mole/m}^2$  of acetaldehyde on MgO-(3) 133b
- Figure 5.32  $^{13}\text{C}$  CP static spectra of isopropanol adsorbed on MgO-(1) at various coverages 143b
- Figure 5.33  $^{13}\text{C}$  CP static spectra of isopropanol adsorbed on MgO-(2) at various coverages 144b
- Figure 5.34  $^{13}\text{C}$  CP static spectra of isopropanol adsorbed on MgO-(3) at various coverages 145b
- Figure 5.35  $^{13}\text{C}$  CP static spectra of isopropanol adsorbed on MgO-(4) at various coverages 146b
- Figure 5.36  $^{13}\text{C}$  CP static spectra of ammonium tartronate 148b
- Figure 5.37  $^{13}\text{C}$  CP spectra of  $6.92 \mu\text{mole/m}^2$  of isopropanol on MgO-(1) treated at elevated temperatures 150b

- Figure 5.38  $^{13}\text{C}$  CP spectra of  $5.85 \mu\text{mole}/\text{m}^2$  of isopropanol on MgO-(2) treated at elevated temperatures 151b
- Figure 5.39  $^{13}\text{C}$  CP spectra of  $6.05 \mu\text{mole}/\text{m}^2$  of isopropanol on MgO-(3) treated at elevated temperatures 152b
- Figure 5.40  $^{13}\text{C}$  CP spectra of  $7.02 \mu\text{mole}/\text{m}^2$  of isopropanol on MgO-(4) treated at elevated temperatures 153b
- Figure 5.41  $^{13}\text{C}$  single-pulse NMR spectra of  $6.92 \mu\text{mole}/\text{m}^2$  of isopropanol treated at 300 and 400°C 154b
- Figure 5.42  $^{13}\text{C}$  spectra of adsorbed acetone on MgO-(3) 155b
- Figure 5.43  $^{13}\text{C}$  CP/MAS spectra of  $5.70 \mu\text{mole}/\text{m}^2$  of isopropanol on MgO-(3) at room temperature and after heating to elevated temperatures 161b
- Figure 5.44  $^{13}\text{C}$  CP spectra of 1,2-ethanediol adsorbed on MgO-(3) at various coverages 166b
- Figure 5.45  $^{13}\text{C}$  CP spectra of 1,3-propanediol adsorbed on MgO-(3) at various coverages 167b

Figure 5.46	$^{13}\text{C}$ CP spectra of 1,4-butanediol adsorbed on $\text{MgO}$ -(3) at various coverages	168b
Figure 5.47	$^{13}\text{C}$ single-pulse NMR spectra of 1,4-butanediol adsorbed on $\text{MgO}$ -(3) at various coverages	169b
Figure 5.48	$^{13}\text{C}$ CP/MAS spectra of 1,2-ethanediol on $\text{MgO}$ -(3) at two coverages	172b
Figure 5.49	$^{13}\text{C}$ CP/MAS spectra 1,3-propanediol on $\text{MgO}$ -(3) at various coverages	174b
Figure 5.50	$^{13}\text{C}$ CP/MAS spectra of 1,4-butanediol on $\text{MgO}$ -(3) at various coverages	178b
Figure 5.51	$^{13}\text{C}$ CP/MAS spectra of $7.83 \mu\text{mole}/\text{m}^2$ of adsorbed 1,4-butanediol on $\text{MgO}$ -(3) treated at elevated temperatures	180b
Figure 5.52	$^{13}\text{C}$ CP/MAS spectra of 1,3-butanediol on $\text{MgO}$ -(3) at various coverages	182b
Figure 6.1	Adsorption isotherms of methanol on $\text{WO}_3$ -(1) at room temperature	187b
Figure 6.2	Adsorption isotherms of methanol on $\text{WO}_3$ -(2) at room temperature	187c
Figure 6.3	Plot of $^{13}\text{C}$ FID signal vs contact time for $5.78 \mu\text{mole}/\text{m}^2$ of methanol on $\text{WO}_3$ -(1)	191b

- Figure 6.4  $^{13}\text{C}$  CP spectra of adsorbed methanol on  $\text{WO}_3$ -(1) at various coverages 193b
- Figure 6.5  $^{13}\text{C}$  CP spectra of adsorbed methanol on  $\text{WO}_3$ -(2) at various coverages 194b
- Figure 6.6  $^{13}\text{C}$  CP spectra of  $6.41 \mu\text{mole}/\text{m}^2$  of methanol (14%  $^{13}\text{C}$ -enriched) on  $\text{WO}_3$ -(1), treated at elevated temperatures 197b
- Figure 6.7  $^{13}\text{C}$  CP spectra of  $5.73 \mu\text{mole}/\text{m}^2$  of methanol (14%  $^{13}\text{C}$ -enriched) on  $\text{WO}_3$ -(2), treated at elevated temperatures 198b
- Figure 6.8  $^{13}\text{C}$  CP/MAS spectra of  $0.96 \mu\text{mole}/\text{m}^2$  of 90%  $^{13}\text{C}$ -enriched methanol on  $\text{WO}_3$ -(1), treated at elevated temperatures 202b
- Figure 6.9  $^{13}\text{C}$  CP/MAS spectra of  $0.99 \mu\text{mole}/\text{m}^2$  of 90%  $^{13}\text{C}$ -enriched methanol on  $\text{WO}_3$ -(2), treated at elevated temperatures 203b

## CHAPTER 1

1.A. NMR Technique in Surface Chemistry

The subjects of chemisorption and catalysis are so much related that they are indistinguishable. For a better understanding, chemisorption is defined as the mode of adsorption, while heterogeneous, or contact catalysis is its interesting consequence. The massive development in recent years of appropriate spectroscopic technique (such as infrared, Raman, ultraviolet and magnetic resonance) suitable for low vacuum has brought the field of chemisorption to maturity as a distinct field of surface chemistry. Research interest in chemisorption is very wide indeed, with no particular emphasis toward catalysis (although often related to it). However, the industrial importance of catalytic systems tends to bias the research toward those systems of special catalytic relevance.

The molecular emphasis of modern chemisorption has benefited the field of catalysis by giving depth and scope to the understanding of the surface chemistry of catalytic processes. The complete characterization of an adsorbate-adsorbent system requires the application of diverse analytic procedures. Adsorbents are usually characterized by steady-state measurements (such as XRD, adsorption isotherm etc.), by which the macroscopic properties are determined. For the adsorbates, conventional high-resolution spectroscopies e.g. infrared, Raman, and ultraviolet are used to measure vibrations and

electronic transitions which occur in the frequency range of  $10^{12}$  to  $10^{14}$  hertz.

High resolution NMR studies carried out 20 years ago (1) on molecules adsorbed on diamagnetic solid surfaces indicated that proton resonance frequencies of the adsorbed molecules differ from the free molecule values. This shift, due to a perturbation of the electron distribution, varies with the nature of the functional group, especially when there is a preferred orientation of the adsorbed molecule with respect to the surface. On the other hand, since adsorption decreases molecular motion, apart from changes in chemical shift, we should observe a broadening of the spectral components which will be greater or smaller depending on the component and whether it is associated with a group fixed on the surface or sufficiently remote for it to preserve a certain number of degrees of freedom.

Smaller linewidths and larger chemical shifts of  $^{13}\text{C}$  nuclei yield more favorable conditions for the application of high-resolution NMR spectroscopy of adsorbed molecules. By means of Fourier transform technique, the  $^{13}\text{C}$  NMR spectra and the longitudinal  $^{13}\text{C}$  relaxation times of simple hydrocarbons adsorbed on NaY zeolites have been studied (2). In contrast to the  $^1\text{H}$  resonance spectra of the same systems involving 1-butene and cis-butene, the  $^{13}\text{C}$  spectra show separated sharp lines (2).



In the last ten years, the application of conventional  $^{13}\text{C}$  NMR spectroscopy to surface chemistry and catalysis has become nearly routine. Investigation of surface acidity and acid sites (3,4) and monitoring of surface reactions (5) have been achieved with moderate success. However, these results are based on the premise that the adsorbed molecules undergo isotropic rotation at a rate of at least  $10^5$  Hz. This is because the C-H dipolar coupling is of the order of  $10^4$  Hz and correspondingly rapid motion is required to average this to a small value, permitting high resolution spectroscopy.

It is obvious that this conventional  $^{13}\text{C}$  NMR technique will not be applicable in the case of strongly chemisorbed species which exhibit a more rigid structure and limited freedom of motion. However, what is lacking from a complete picture of the adsorbate-adsorbent system is the analysis of these low frequency dynamic properties of the system; that is, a description of any orientational influence the adsorbent may have on the adsorbate.

Recent developments in high resolution solid-state NMR (6) have shown that C-H dipolar coupling can be suppressed by high power irradiation of the protons and high-resolution  $^{13}\text{C}$  spectra obtained. Combining this with cross-polarization (6-8), the sensitivity (signal to noise ratio) can also be increased. The application of this high power decoupling plus

cross-polarization (CP) technique in surface chemistry and polymers is still relatively new (9-12). The main difficulty in these experiments is that the  $^{13}\text{C}$  chemical shift anisotropies can be large, thus overlapping powder patterns result for species containing more than one carbon. This may also aggravate the sensitivity problem, although the use of selectively enriched  $^{13}\text{C}$  compounds (11c) could solve this problem. To optimize the sensitivity further, pressed pellets of the adsorbent would increase the sample density, thus allowing more adsorbate to be introduced.

To solve the problem of overlapping  $^{13}\text{C}$  chemical shift anisotropies, magic-angle spinning is the solution. However, all the conventional spinners are not really designed for the study of adsorbed systems. The reason is that most interesting systems (catalytically) are sensitive to the presence of air and water and must be prepared on a vacuum line. Some researchers (13-15) have attempted the transfer of adsorbed systems into conventional spinners inside a dry-box. This technique only works for those systems in which the sensitivity to air and water are low or none at all. In some cases, a drastic change in the  $^{13}\text{C}$  NMR spectra were observed (13b, 15) due to the intrusion of air. Previous MAS attempts using sealed samples (16, 17) met with "experimental difficulties".

We have recently developed a magic angle spinner (18) in this laboratory, which permits reliable spinning at 3kHz of

samples sealed in glass tubes. Stable species on surface reactions could thus be monitored with a drastic improvement in resolution (18).

### 1.B. Alcohol Decomposition

The conversion of alcohols to hydrocarbons is a remarkable reaction. The industrial potential of the reaction is tremendous, especially after the discovery by workers at Mobil Oil of the selective catalytic conversions of methanol to high octane gasoline over zeolite catalysts (19-21). This revives a new interest in the surface chemistry of zeolites and the general conversions of alcohols to hydrocarbons over other catalysts (22).

There is clearly a diversity of opinion concerning the mechanism of initial C-C bond formation, and a wide gap separating theory from experiment. Because of the high exothermicity and fast kinetics of the methanol transformation, classical methods of mechanism elucidation e.g. trapping of intermediates, tracer, and kinetic studies, have failed to provide unequivocal answers. Direct observation of the transition state seems beyond reach at present.

### 1.C. Scope of this Study

This dissertation focusses on two aspects of heterogeneous catalysis: difference in catalytic activity due to the different methods of preparation, and the extent of

catalytic conversion of reactant at different temperatures. The systems under investigation are the methanol, ethanol and isopropanol adsorbed on MgO and WO<sub>3</sub>.

The analytical tool used is solid state <sup>13</sup>C NMR (6) employing cross-polarization (CP) and high power C-H decoupling. We have successfully modified our high-resolution 14kG spectrometer for this purpose (see Chapter 4).

A preliminary study of methanol adsorbed on MgO performed in this laboratory (23) has shown great promise. We are able to observe an axially symmetric powder pattern for the adsorbed species, at low coverage of methanol, which resembles that of magnesium methoxide. As coverage is increased beyond 6 μmole/m<sup>2</sup>, another mobile species is observed. It appears as an isotropic peak superimposed upon the underlying powder pattern. From its chemical shift, we conclude that this could be a mobile methanol species on the surface.

To study the differences in the methanol-MgO systems from different preparations, we measure the proton relaxation parameters at various coverages of methanol and the corresponding <sup>13</sup>C CP spectra. We have also extended this to the chemisorption of ethanol and isopropanol on MgO.

It is well known that basic oxides have high activity in catalytic dehydrogenation of alcohols. To investigate this, we

treat the alcohol-MgO systems at successively higher temperatures, and monitor the stable surface species by  $^{13}\text{C}$  spectra. Overlapping powder patterns resulted in the  $^{13}\text{C}$  CP spectra due to the presence of more than one surface species as the alcohols decompose on the surface. Identification of the conversion products in the ethanol decomposition is done by MAS/CP technique using selectively  $^{13}\text{C}$ -enriched ethanol.

For comparison of our present results and to test the applicability of the CP technique to other catalytic systems, we attempt the characterization of the alcohol- $\text{WO}_3$  systems.  $\text{WO}_3$  is a well known acidic oxide which catalyzes the dehydration of alcohols. In this preliminary study, we intend to study the interaction of methanol with the  $\text{WO}_3$  surface, and to investigate the decomposition products from this system at elevated temperatures.

## CHAPTER 2

This chapter surveys the work done so far on MgO and WO<sub>3</sub> surfaces. The list is by no means exhaustive and complete. It selects studies pertinent to the chemisorption of alcohols, to the catalytic activities and selectivities due to different preparation methods, and to the acid/base characteristics of these oxide surfaces.

2.A. MgO

There are several methods of preparation for high surface area MgO. The conventional ones are from the thermal decomposition of the hydroxide, carbonate or oxalate. Comparison of different preparations of MgO relative to catalytic activities have been detailed (24-28). It is agreed that MgO prepared by different routes has different surface morphologies, and thus the catalytic activity and selectivity vary. Other factors, such as the temperature and length of calcination time, and the atmosphere in which the precursor (for MgO) is heated also have great effects on the activity of the resulting product (29, 30). Pretreatment of MgO with H<sub>2</sub> or O<sub>2</sub> also affects the catalytic selectivity as detailed by Davis (31).

As a member of the alkaline earth metal oxides, MgO shows surface basicity (32-36). Some acidity is also observed in the case of MgO calcined at high temperature ca. 1000°C (32, 37). The presence of several types of basic centres at the surface of partially dehydrated magnesium hydroxide has been discussed by Krylov et al. on the basis of studies of adsorption and isotope exchange of carbon dioxide on MgO and on partially dehydrated magnesium hydroxide surface (38). The basic centers are believed to derive from the  $O^{2-}$  ions adjacent to the surface -OH groups (39).

Adsorption studies related to the catalytic activity on MgO have been scarce. These few studies included alkene hydrogenation (27, 40), alkene and alkane oxidation (41, 42), acetone adsorption (43), acetonitrile adsorption (44), and the decomposition of methyl formate (45).

On the other hand, the interaction of alcohols with MgO has been widely explored (31, 46-54). The general consensus is that MgO is a very selective dehydrogenation catalyst. However, dehydration activity is observed when the catalyst is contaminated with carbon dioxide, which may result from an incomplete decomposition of a carbonate precursor (55), or during the various steps of preparation.

Studies of the catalytic conversion products of methanol on

MgO include IR spectroscopy (47, 48), mass spectrometry and flow system (49). Infrared spectroscopy has revealed several adsorbed species formed from methanol on MgO. These include physisorbed methanol plus several chemisorbed methoxide species (48, 49) at room temperature. These methoxide species persist on the surface upon heating until  $300^{\circ}\text{C}$ , at which temperature, formate is observed on the surface. Mass spectrometer analysis of desorbed species indicates  $\text{H}_2$ ,  $\text{CH}_4$ ,  $\text{H}_2\text{O}$ ,  $\text{CO}$ ,  $\text{H}_2\text{CO}$  and  $\text{CO}_2$  (49), similar to the result from Noller and Ritter (54). At even higher temperatures, surface carbonate is observed. This possibly results from the reaction of carbon dioxide (from decomposing surface formate species) with the surface.

For ethanol adsorption, the general consensus indicates that the ethanol is chemisorbed on the MgO surface as an ethoxide species which is stable up to  $150^{\circ}\text{C}$ . At  $250^{\circ}\text{C}$ , the ethoxide species dehydrogenates to acetaldehyde and hydrogen, along with some dehydration to ethylene (51, 53). At much higher temperatures, 1,3-butadiene is observed, along with some hydrogen. This result conforms to the intrinsic dehydrogenation activity of MgO, and 1,3-butadiene arises probably from the dehydration of the reaction products of another ethanol molecule with the aldol condensation product of acetaldehyde (56). Desorption at  $290^{\circ}\text{C}$  reveals acetaldehyde and  $\text{CO}_2$  only (51). This contrasts with the observation of ethanol, water and ethylene in the desorption study by Parrott et al. (50). This seems to indicate different catalytic activity on MgO surface



due to different preparations.

Propene and acetone are the major products from adsorbed isopropanol on MgO at elevated temperatures. This result was obtained via temperature programmed desorption studies in the range of  $30^{\circ}$ - $750^{\circ}$  C (50, 54). However, TPD study employs flow-system analysis, and pays no attention to adsorbed species which inform us of dehydrogenation or dehydration activities. The authors in (54) also prepared a series of silica-magnesium oxides. At  $>80$  mole % MgO, the desorption products are the same as for pure MgO at the same temperature. This may indicate the dehydrogenation or dehydration of alcohols taking place in the basic centres of MgO. Studies of adsorption of other high molecular weight alcohols on MgO (see, for example ref. (31)) usually focus on kinetic data and percentage conversion, rather than the characteristic of adsorbed species leading to decomposition of the original alcohols.

To summarize, past studies indicate that MgO can act both as a dehydrogenation and dehydration catalyst for the alcohol decomposition. Infrared spectroscopy has provided information on the structure of surface species, although there are questions concerning the assignment of the observed bands (57), among other problems (such as the assumption of an invariance of extinction coefficient of molecules upon adsorption etc.). It is the intent of this thesis to shed light on the structure and type of slow-moving species (usually chemisorbed species) on the

MgO surface, upon the adsorption of alcohols.

## 2. B. WO<sub>3</sub>

According to Krylov (58), tungsten oxide at its highest oxidation state i.e. WO<sub>3</sub>, is a dehydration catalyst for alcohols, although some dehydrogenation activities were observed. WO<sub>3</sub> has been scarcely studied. The existence of several forms of tungsten oxide, WO<sub>3-x</sub> (x varies from 0 to 1), and the generally low surface area of the prepared WO<sub>3</sub> make the study of WO<sub>3</sub> slightly difficult (because of the amount of adsorbate per gram of WO<sub>3</sub> may be too small to be detected). Most of the studies on WO<sub>3</sub> were carried out with WO<sub>3</sub> supported on SiO<sub>2</sub>, Al<sub>2</sub>O<sub>3</sub>, MgO and TiO<sub>2</sub> (59). These supported WO<sub>3</sub> catalysts are found to be extremely active in the metathesis and isomerization of alkenes. The active sites on these metathesis catalyst have not been elucidated. One school of thought is the precursor for the active site in metathesis is a surface compound, and not the "free" oxide as such (60). However, no detail of this surface compound was given.

In view of all these catalytic activities, WO<sub>3</sub> is thus, one component of industrially important catalysts. Tungsten oxide itself is known to catalyze the oxidation of 1-butene to carbon dioxide (61). Tungsten oxide reduced with hydrogen was reported recently to catalyze the isomerization and hydrocracking of heptane, the dealkylation of isopropylbenzene, and the dehydration of isopropanol, where the variation of catalytic

action with the change in oxidation state and acidic property of tungsten oxide was studied (62, 63).

$WO_3$  can be reduced to lower oxides e.g.  $WO_{2.96}$ ,  $WO_{2.90}$ ,  $WO_{2.72}$  and  $WO_2$  by hydrogen at elevated temperatures. All of these oxides are stoichiometric but have different structures (64). It was proven recently that the blue oxide of tungsten,  $WO_{2.87}$ , is a selective dehydration catalyst for a series of alcohols (65). Pretreatment in hydrogen or oxygen did not alter the dehydration selectivity but did alter the alkene distribution.

This blue oxide of tungsten, which is stable to heating at 440°C for a long period of time (62) will contain a combination of tungsten at the +5 and +4 states (in addition to the +6 state). This creates another problem for our NMR study of the surface. No doubt, tungsten at the +4 or +5 states may be paramagnetic, and the  $^{13}C$  NMR spectra obtained will be broadened due to electron dipole interactions, and there may be shifts in the chemical shifts of the carbon nuclei under investigation (66).

Since the electronic magnetic moment is about 1000 times greater than nuclear moments, all spectral information may be obscured by this electron-dipole broadening. This effect may hamper the investigation of the tungsten oxide surface by NMR spectroscopies.

To summarize,  $WO_3$  has not been extensively studied despite its catalytic importance. Hopefully, NMR spectroscopy with the cross-polarization and strong decoupling technique may give some insight into the catalytic activities in relation to the adsorbed species present, on the tungsten oxide surface.

## CHAPTER 3

3.A. Theoretical Background

It is not the intention of this dissertation to build up the subject of NMR systematically from first principles. Rather, it discusses concepts at levels appropriate to the interfacing of solid-state NMR to surface studies.

High-resolution NMR in liquids has been proven to be a useful tool for structural and dynamical analysis of chemical systems. However, it is less successful in the study of solids (the reasons will be discussed later). So, why is there a need to try high-resolution NMR in solids?

There are several reasons for performing high-resolution NMR in solids. A pragmatic one is that the system of interest need not be dissolved in any solvent to obtain a high-resolution NMR spectrum. Consequently, the signal to noise ratio (S/N) could be much better in a solid sample if its solubility is very small in the appropriate solvent. A more fundamental variation of this theme is that the physical and even chemical properties of a molecule will, in general, not be the same for a solid and a dissolved sample. Thus extrapolation may be required to draw conclusion about molecules in a solid from a high resolution NMR spectrum in solution. So, why isn't solid-state NMR done conventionally? The reason is well known: the direct nuclear magnetic dipole-dipole interaction is averaged to zero in

liquids due to rapid translational and rotational diffusion, no such motions are available to solids, and their absence leads to spectral broadening. This dipolar broadening is normally in the order of several kilohertz, compared to the few hertz required for the resolution in the spectral structure due to chemical shifts and spin-spin couplings. We can see that it is a real feat to bring solids into the realm of conventional high-resolution NMR.

This nuclear dipolar interaction contains a wide range of information pertaining to lineshapes (67), spin-diffusion (68), spin temperature (69) etc. In addition, it can be used in both structural and dynamical studies, as in wide-line dipolar structures (70) and by second-moment and spin-lattice relaxation studies of motion (71). However, the above information could only be obtained via complicated mathematical analysis.

If it were possible to suppress this dipolar broadening (by techniques to be discussed later), a considerable increase in information could be obtained, such as the interaction due to chemical shift anisotropies and indirect nuclear spin-spin couplings. This type of interaction is generally obscured in liquid systems due to averaging to zero, but because of the restriction of molecular reorientation in solids, such anisotropies (e.g. chemical shift anisotropy) are preserved.

A simple example is the benzene molecule, which is a planar hexagon. At the corner of the hexagon, where there is a carbon atom, the effects of the chemical bond should have a directional character governed by the shape of the molecule. The covalent bonds which hold the molecule together are made up of electrons, and the nuclei on the molecule feel the effects of bonding (and other) electrons in the form of additional small magnetic fields induced by the experimental field, which give rise to the well known chemical shifts. Since the site at the corner of the hexagon is not tetrahedral or of higher symmetry, the chemical shift must depend on the orientation of the molecule with respect to the external magnetic field. Such chemical shift tensor properties could only be observed when this benzene molecule is "frozen", or in the solid form. In liquid benzene, when the benzene molecule reorients itself rapidly, the directional character at each carbon nuclei changes rapidly also, and all these chemical shift anisotropies are "averaged" to a scalar value (the isotropic chemical shift usually observed in high-resolution NMR).

There exist to date, several approaches to bring solids into the realm of high-resolution NMR. These can be discussed in terms of the Hamiltonian for the "truncated" dipolar interactions (72) in a substance containing two nuclear species, I and S of different gyromagnetic ratios  $\gamma_I$  and  $\gamma_S$  :

$$[1] \quad \mathcal{H}_d^0 = \mathcal{H}_{II}^0 + \mathcal{H}_{SS}^0 + \mathcal{H}_{IS}^0 \quad \text{where}$$

$$\mathcal{H}_{II}^0 = \chi_I^2 \hbar^2 \sum_{i < j}^{N_I} r_{ij}^{-3} P_2(\cos \theta_{ij}) (\vec{I}_i \cdot \vec{I}_j - 3I_{iz} I_{jz})$$

$$\mathcal{H}_{SS}^0 = \chi_S^2 \hbar^2 \sum_{m < n}^{N_S} r_{mn}^{-3} P_2(\cos \theta_{mn}) (\vec{S}_m \cdot \vec{S}_n - 3S_{mz} S_{nz})$$

$$\mathcal{H}_{IS}^0 = 2\chi_I \chi_S \hbar^2 \sum_{i=1}^{N_I} \sum_{m=1}^{N_S} r_{im}^{-3} P_2(\cos \theta_{im}) I_{iz} S_{mz}$$

The techniques and their effects differ according to the nature of the sample and to which part of equation [1] they choose to affect.

In the magic-angle spinning (MAS) experiments (73-75), the  $\theta$ 's are modulated rapidly giving  $\langle P_2(\cos \theta(t)) \rangle = 0$ , for all  $i, j, m, n$ ; so that all dipolar interactions are erased. At the same time, all other anisotropic interactions which are transformed as second rank tensors, such as the anisotropic part of the chemical shift, is also removed. However, it was pointed out by Maricq and Waugh (76) that this is not possible when the homonuclear dipolar interactions are coupled with other interactions (such as those arising from quadrupolar nuclei). In multiple-pulse NMR (77-80), in an appropriate reference frame, it is the I spins which are modulated, leaving  $\langle 3I_{iz}(t) I_{jz}(t) - \vec{I}_i \cdot \vec{I}_j \rangle = 0$ . Thus the dipolar interactions are fully removed only in single-species sample ( $N_S = 0$ ). Dipolar interactions from unlike spins ( $\mathcal{H}_{IS}$ ) can be removed by strong irradiation of these spins at their resonance frequencies (81).



The anisotropic chemical shift is, however, not lost. Both methods (MAS and Multiple-Pulse) have met with considerable success, despite some experimental difficulties.

In this dissertation, we are mainly interested in the double-resonance experiments and the proton-enhanced NMR of dilute spins in solid (6, 82), and a combined technique of the proton-enhanced NMR with magic-angle spinning (MAS).

### 3.B.I. Double Resonance Experiments (82)

To start with, we consider a system of abundant I and rare S spins (i.e.  $N_I \gg N_S$ , N the number of spins). Each spin system is coupled to the lattice and approaches the lattice temperature with the spin-lattice relaxation time  $T_{Iz}$  and  $T_{Sz}$  respectively, as shown in Figure 3.1,  $T_I$  and  $T_S$  are the spin temperatures of spins I and S respectively.

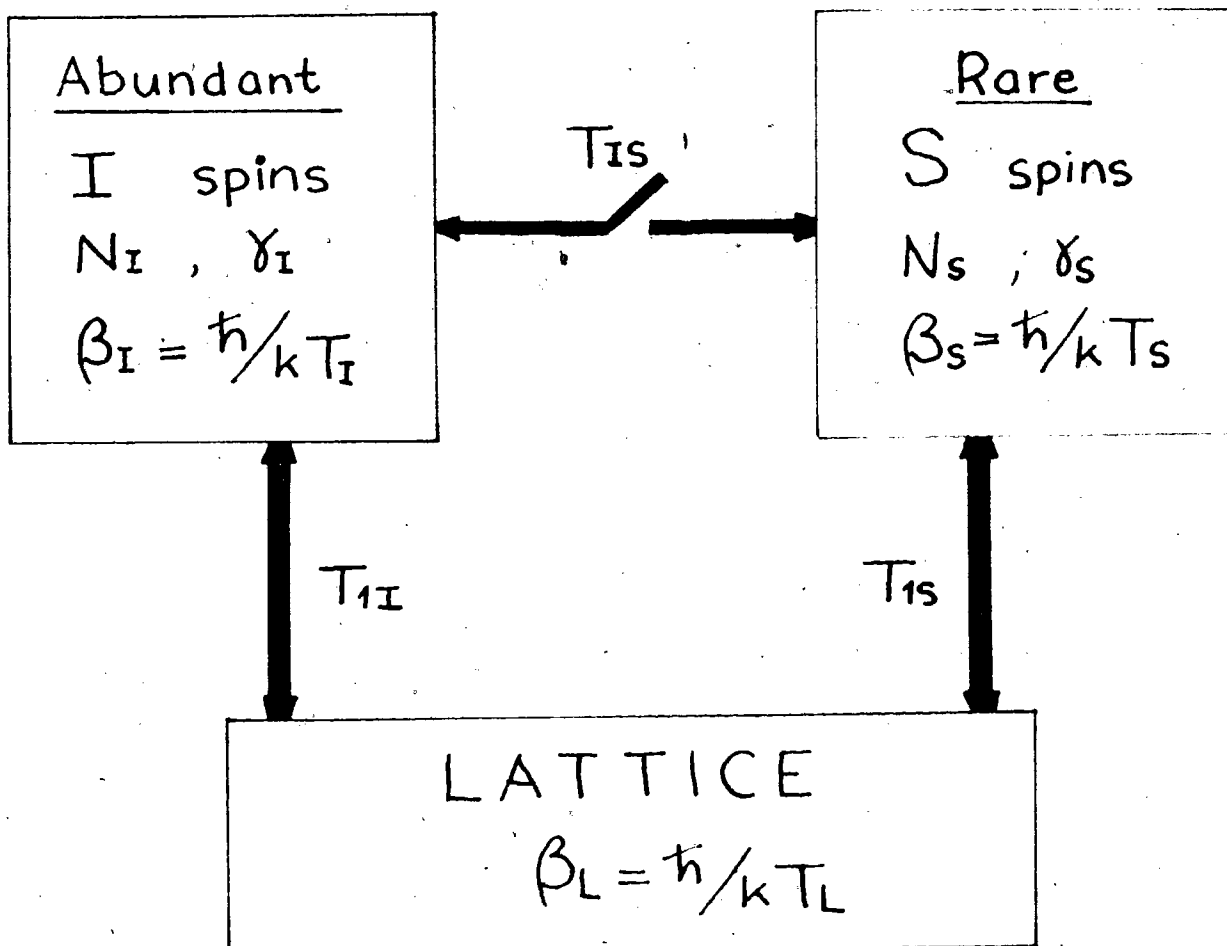
The I and S spins may be coupled by some interaction represented by the cross-relaxation time  $T_{IS}$ . Applying the concept of spin temperature (69c, 70, 83, 84), and using the high temperature approximation, the spin density matrix can be written as:

$$[2] \quad \rho = Z^{-1} (1 - \beta \mathcal{H}) \quad \text{where}$$

$$Z = \text{Tr} \{ \hat{1} \} = (2I+1)^{N_I} (2S+1)^{N_S}$$

The quantities of interest are the energy, magnetization and entropy, which are given by:

Figure 3.1 Schematic representation of an abundant I spin reservoir and a rare S spin reservoir, which are coupled to the lattice by their spin-lattice relaxation times  $T_{1I}$ , and  $T_{1S}$ . The coupling between the 2 reservoirs as represented by the cross-relaxation time  $T_{IS}$  can be varied at the experimenters discretion by a suitable application of rf fields.



$$[3a] \text{ Energy} \quad E = k \text{Tr} \{ \rho \mathcal{H} \} = -\beta k \text{Tr} \mathcal{H}^2$$

$$[3b] \text{ Magnetization} \quad M_i = \hbar \gamma \text{Tr} \{ \rho I_i \} \quad i=x, y, z$$

$$[3c] \text{ Entropy} \quad S = -k \text{Tr} \{ \rho \log \rho \}$$

In the case of Zeeman interaction with a magnetic field  $H_0$ , these quantities reduce to:

$$[4a] \quad E = -\beta \cdot C \cdot H_0^2$$

$$[4b] \quad M_z = \beta \cdot C \cdot H_0 \quad C = \frac{1}{3} N I(I+1) \gamma^2 \hbar$$

$$[4c] \quad S = \text{constant} - k \cdot \beta^2 \cdot C \cdot H_0^2$$

After waiting several times  $T_{1I}$ ,  $T_{1S}$  the I and S spins reach the magnetization, in a static magnetic field:

$$[5a] \quad M_{0z} = \beta_L \cdot C_I \cdot H_0 \quad \text{and}$$

$$[5b] \quad M_{0s} = \beta_L \cdot C_S \cdot H_0$$

where  $\beta_L$  is the inverse lattice temperature.

Double resonance can now be achieved by the following steps:

(i) Cooling the abundant I spins system.

This can be achieved e.g. by locking the spins in a field  $H_I \ll H_0$ . In which case:

$$[6] \quad M_{0I} = \beta_L \cdot C_I \cdot H_0 = \beta_I \cdot C_I \cdot H_I \quad \text{with}$$

$$\beta_I / \beta_L = H_0 / H_I \gg 1$$

There are two basic approaches by which a spin system is cooled, they are schematically represented in Figure 3.2. There are:

(a) Spin-locking (6-8, 83-88) in the rotating frame with a field  $H_{Ix} = 2H_{Iz} \cos(\omega_I t)$ .

$$[7] \quad \beta_I = H_0 \beta_L / H_{Ix}$$

$$M_I = \beta_I \cdot C_I \cdot H_{Ix} \quad ; \quad E = -\beta_I \cdot C_I \cdot H_{Ix}^2$$

The inverse spin temperature  $\beta_I$  will approach the inverse lattice temperature  $\beta_L$  with the time constant  $T_{1\rho}$ , the spin-lattice relaxation time in the rotating frame.

(b) Adiabatic demagnetization in the rotating frame (ADRF) (89) by turning off the  $H_{Ix}$  field adiabatically, leaving the spins in the "dipolar field"  $H'_{LI}$ , where

$$[8] \quad \text{Tr} \{ H_D'^2 \} = \delta^2 H_{LI}'^2 \text{Tr} \{ I_3 \}^2$$

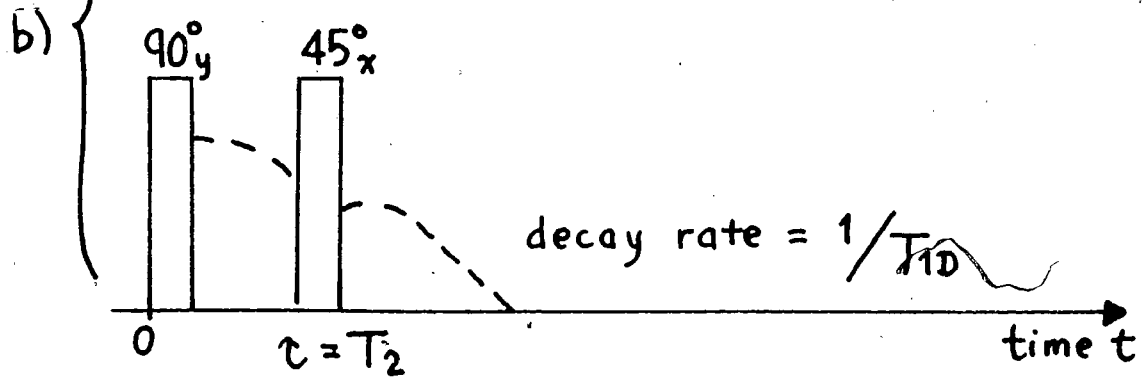
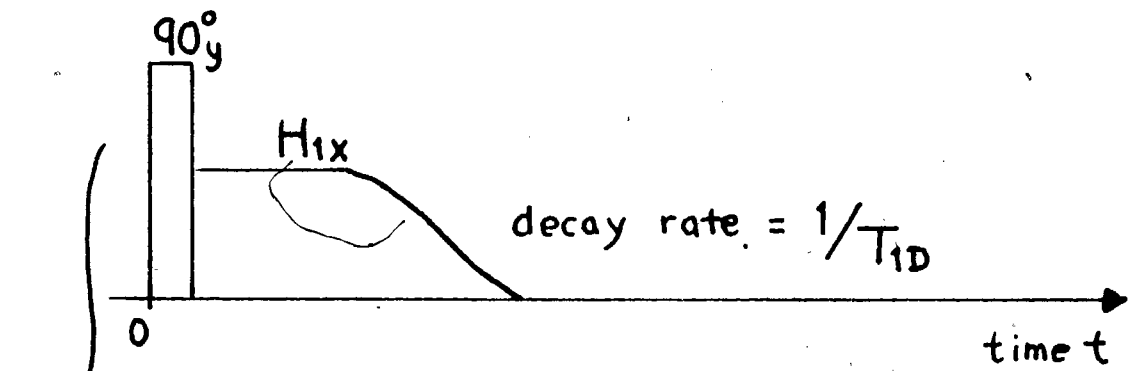
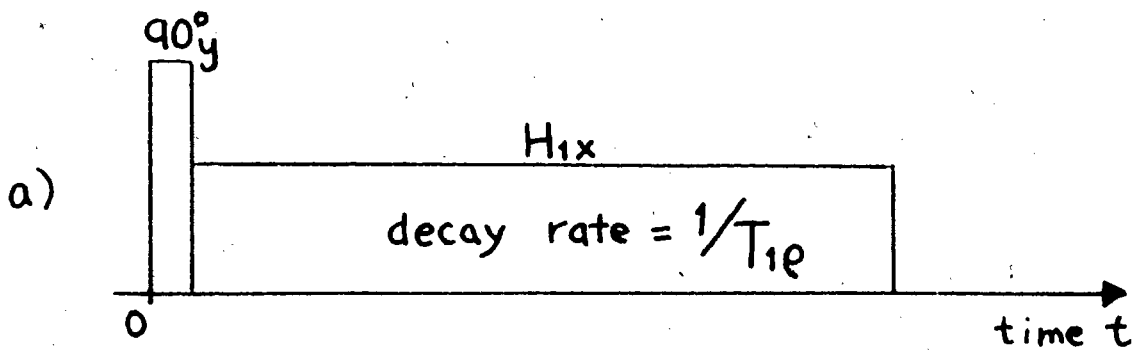
$$\beta_I = \frac{H_0}{H_{LI}'} \beta_L \quad ; \quad E_I = -\beta_I \cdot C_I \cdot H_{LI}'^2$$

Figure 3.2 a)-b)

Schematic representation of different means for reducing the spin temperature in the rotating frame.

- (a) Spin locking;
- (b) Adiabatic demagnetization in the rotating frame (ADRF) and Jeener-Broekaert two pulse experiment;

4



The inverse spin temperature  $\beta_I$  will approach the inverse lattice temperature  $\beta_L$  with the time constant  $T_{ID}$ , the spin-lattice relaxation time in the dipolar state.

A different way of achieving a dipolar state was proposed by Jeener and Broekaert (90), applying a  $90^\circ - \tau - 45^\circ$  pulse sequence. Since this process is not adiabatic, a somewhat smaller inverse temperature  $\beta_I$  is achieved, and from ref. (69c).

$$[9] \quad \beta_I \approx 0.525 \frac{H_0}{H'_{LI}} \beta_L$$

nevertheless, this is a very convenient method for cooling the abundant spin system.

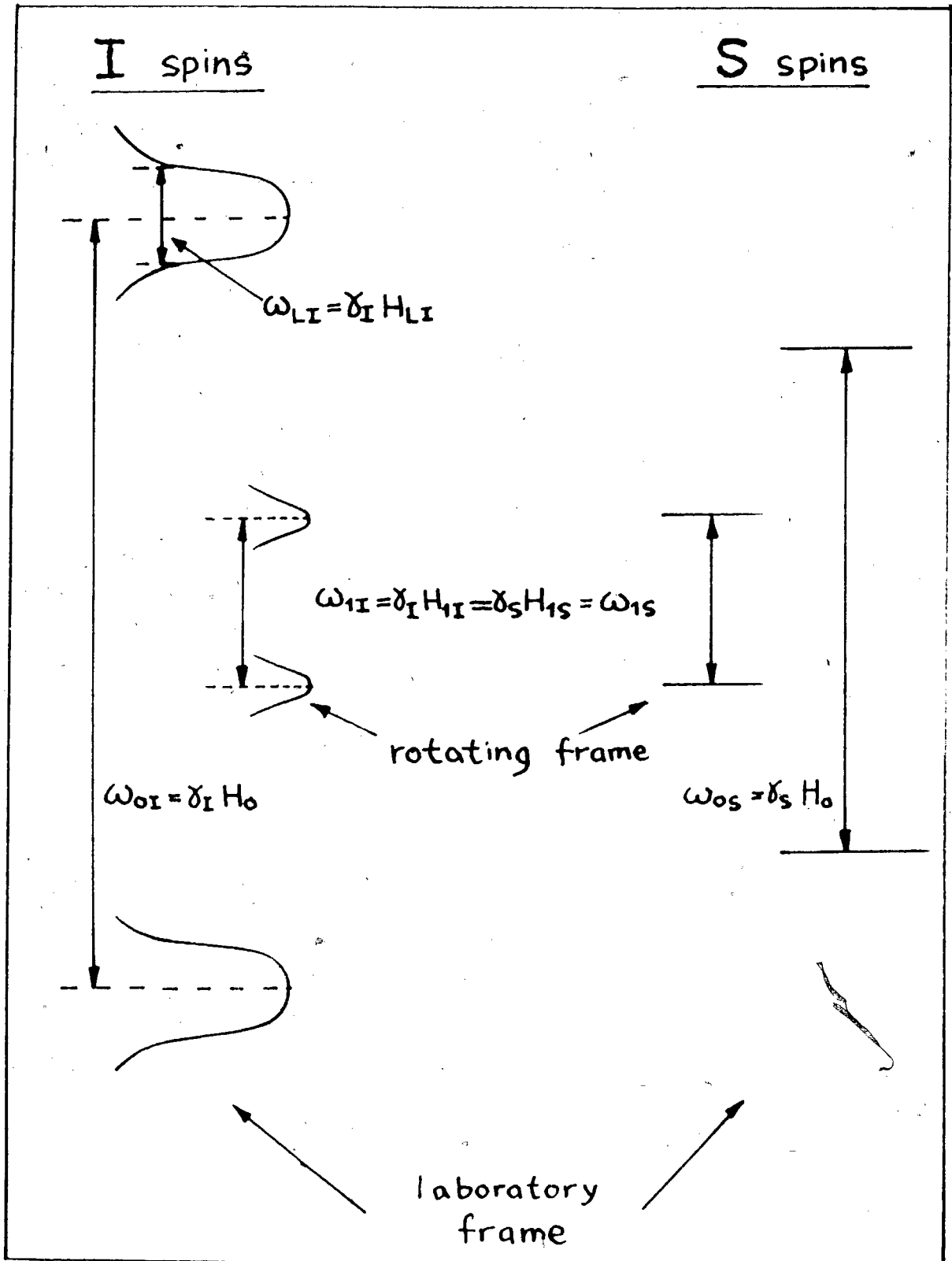
The next step in double-resonance is:

(ii) Bringing the I and S spins into contact.

Since the I spins are cold and the S spins are hot, there will be a calorimetric effect (86), and energy exchange may proceed with the time constant  $T_{IS}$ . Only if  $T_{IS} \ll T_{ID I}$ ,  $T_{ID S}$ , is this energy exchange considerable and can be utilized for a double resonance effect. Rapid energy transfer is possible only under total energy conservation. No such transfer is possible in the laboratory frame. However, in the rotating frame a matching of the energy levels is possible as shown schematically in Figure 3.3, allowing rapid transfer under



Figure 3.3 Pictorial representation of level matching in the rotating frame (Hartmann-Hahn condition) for spin = 1/2 systems.



energy conservation (in the rotating frame) if the Hartmann-Hahn condition (7, 85)

$$[10] \quad \gamma_S \cdot H_{IS} = \gamma_I \cdot H_{II} \quad \text{for } I = S = 1/2 \text{ or}$$

$$\omega_{IS} = \omega_{II}$$

is satisfied, where  $H_{II}$  and  $H_{IS}$  are the rf fields in the rotating frame of the I and S spins respectively. Of course, these fields may be effective fields, and then the  $\omega_{II}$ ,  $\omega_{IS}$  becomes the "effective frequencies"  $\omega_{eI}$  and  $\omega_{eS}$ , respectively.

As will be shown later (Section 3.B.III), the transfer rate can be expressed as (91, 92).

$$[11] \quad \text{ADRF case: } \left(\frac{1}{T_{IS}}\right)_{\text{ADRF}} = \sin^2 \theta_S M_2^{IS} J_{\text{ADRF}}(\omega_{eS})$$

and

$$[12] \quad \text{Spin-locking case: } \left(\frac{1}{T_{IS}}\right)_{\text{SL}} = \frac{1}{2} \sin^2 \theta_S \sin^2 \theta_I M_2^{IS} J_{\text{SL}}(\Delta \omega)$$

$$\omega_{eS}, \omega_{eI} \gg \omega_{LI}$$

$$\text{where } \tan \theta_I = \frac{\omega_{II}}{\omega_{0I} - \omega_I} \quad \tan \theta_S = \frac{\omega_{IS}}{\omega_{0S} - \omega_S}$$

$$\Delta \omega_e = \omega_{eS} - \omega_{eI}$$

and where  $M_2^{IS}$  is the second moment of the I-S coupling Hamiltonian. The spectral distribution function for the cross-relaxation process  $J(\omega)$  decreases monotonically to zero for increasing  $\omega$ , i.e. with increasing mis-match of the Hartmann-Hahn condition. This results in a drastic decrease of the transfer-rate  $1/T_{IS}$ . McArthur et al. (91) have used an intuitive approach, based on the experimental data to express the functional form of  $J_{ADRf}(\omega_{es})$  as

$$[13] \quad J_{ADRf}(\omega_{es}) = \frac{1}{2} \tau_c \exp(-\omega_{es} \tau_c)$$

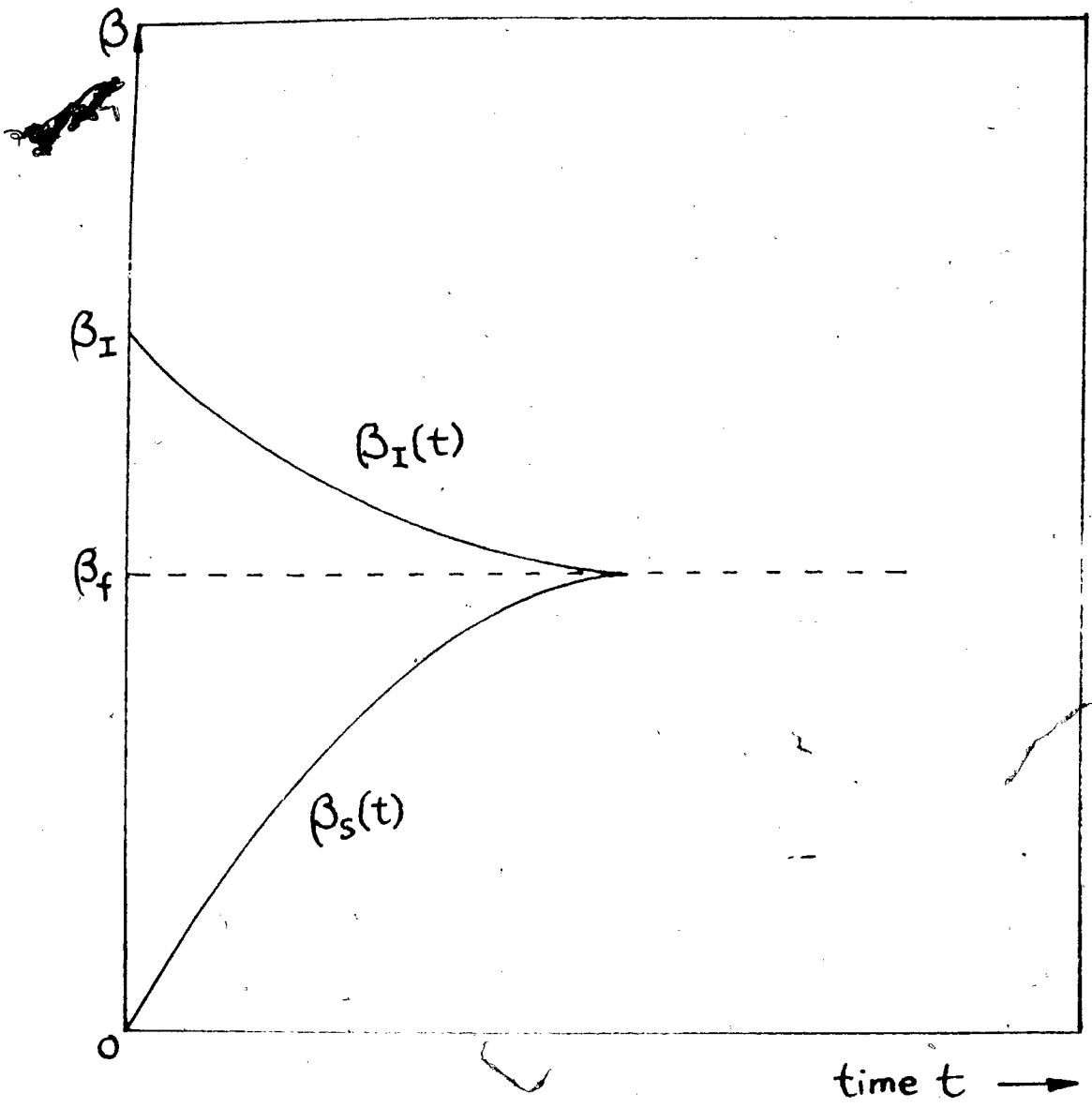
where  $\tau_c$  is the correlation time. A more general approach using the memory function technique was applied by Demco et al. (92).

The spin temperature occurring in a single I-S contact is shown schematically in Figure 3.4. Assuming a high inverse spin temperature  $\beta_I$  and a zero inverse temperature  $\beta_S$  at the beginning of the contact ( $t = 0$ ), neglecting spin-lattice relaxation, both spin temperatures will finally reach the same value  $\beta_f$  assuming exponential relaxation as:

$$[14] \quad \beta_I(t) = (\beta_I - \beta_f) \exp(-t/T_{IS}) + \beta_f$$

$$[15] \quad \beta_S(t) = \beta_f [1 - \exp(-t/T_{IS})]$$

Figure 3.4 Time evolution of I and S inverse spin temperatures  $\beta_I$  and  $\beta_S$ , when the spin systems are brought into contact at  $t = 0$ . Initial condition:  $\beta_I \neq 0$ ;  $\beta_S = 0$ . A final inverse spin temperature  $\beta_f$  is reached after several  $T_{IS}$ .



Assuming energy conservation

$$[16] \quad \beta_I \cdot C_I \cdot H_I^2 + \beta_S \cdot C_S \cdot H_S^2 = \beta_f [C_I \cdot H_I^2 + C_S \cdot H_S^2]$$

and with  $\beta_S = 0$ , eqn. [16] leads to

$$[17] \quad \beta_f / \beta_I = 1 / (1 + \epsilon') \quad \text{where}$$

$$[18] \quad \epsilon' = C_S H_S^2 / C_I H_I^2$$

is the ratio of the heat capacities of the S and I spins.

If the Hartmann-Hahn condition  $\gamma_S H_S = \gamma_I H_I$  is satisfied, one obtains

$$[19] \quad \epsilon = \frac{N_S S(S+1)}{N_I I(I+1)} \ll 1$$

with  $M_I^{(f)} = \beta_f \cdot C_I \cdot H_I$  and  $M_S^{(f)} = \beta_f \cdot C_S \cdot H_S$ , the final I and S spin magnetization reaches

$$[20] \quad M_I^{(f)} = \frac{1}{1 + \epsilon} M_I^{(i)} \quad \text{and}$$

$$[21] \quad M_S^{(f)} = \frac{\gamma_I}{\gamma_S} \frac{1}{1 + \epsilon} M_{0S}$$

where  $M_I^{(i)}$  is the initial magnetization of the I spins and

$M_{0S}$  is the Zeeman magnetization of the S spins. Since  $\epsilon$  is

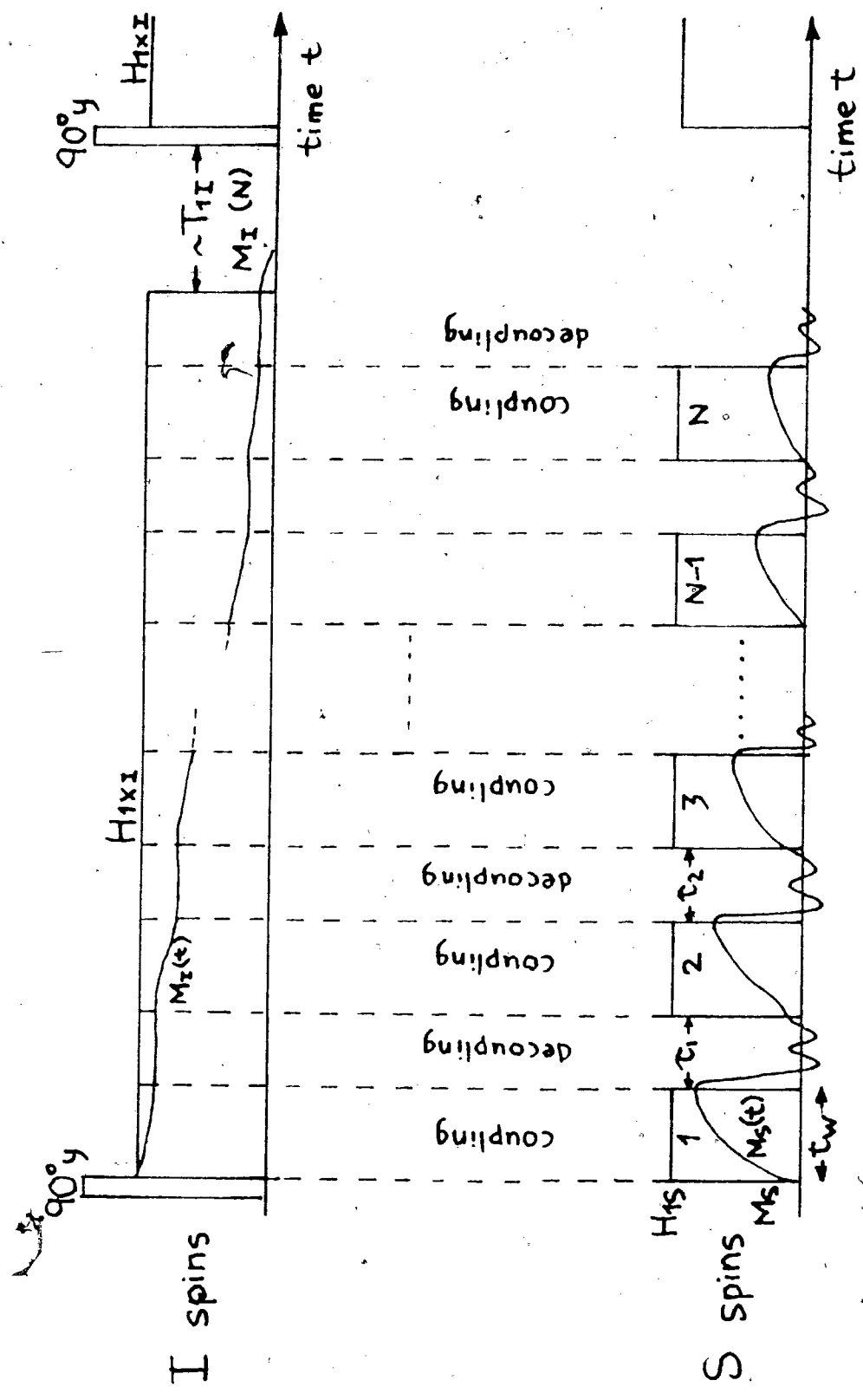
a very small number of the order of  $N_S/N_I$ , one may write  $1/(1+\epsilon) \cong 1-\epsilon$  i.e. according to eqns. [20] and [21], the I spin magnetization does not decrease very much in a single contact, however, the S spin magnetization may have been increased if  $\delta_I/\delta_S > 1$ .

In order to achieve a noticeable destruction of the I spin magnetization, multiple contacts (6,86,87,93) have to be performed, as demonstrated in Figure 3.5. The I spins are spin-locked in the field  $H_{Iz}$ , whereas, the S spins become polarized in the field  $H_{Is}$  which may be an effective field in the rotating frame. The pulsed  $H_{Is}$  field is of duration  $t_w$  with a spacing  $\tau_c$ . Coupling between the I and S spins is achieved, when the  $H_{Is}$  field is turned on and the I and S spins are decoupled consecutively, then  $H_{Is}$  is turned off. A free precession of the S spins can be observed during this time.

However, it should be pointed out that the multiple contact technique is not suitable to the study of surfaces. The proton spin-lattice relaxation time in the rotating frame ( $T_{1\rho}$ ) of adsorbed species is usually short, thus the spin-locking period cannot be held infinitely long for multiple contact to be effective. In some of our experiments,  $^{13}\text{C}$  enriched adsorbates are used, thus multiple-contact (for S spin magnetization enhancement) is really unnecessary.



Figure 3.5 Pulse timing of a typical double resonance experiment in the rotating frame.



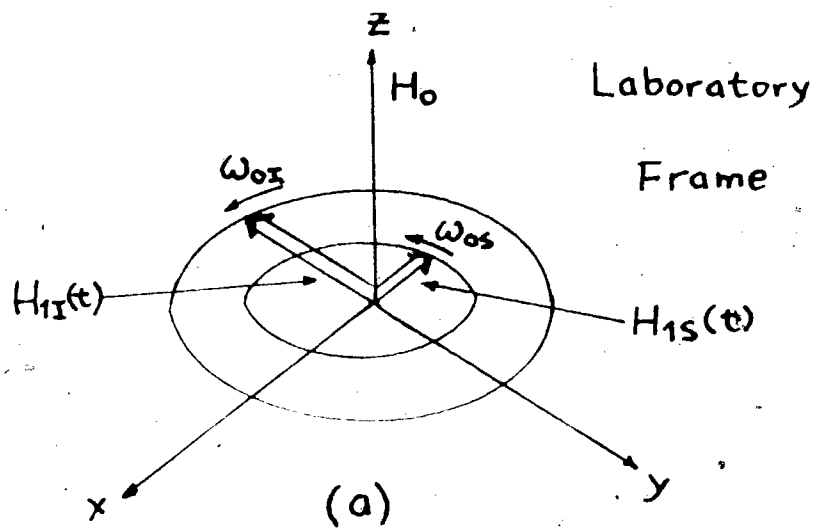
### 3.B.II Cross-Polarization of Dilute Spins

Pines, Gibby and Waugh (6,87) have designed a technique utilizing the double-resonance concept, to obtain high resolution spectra of rare spins in solids. The technique is called "Proton-Enhanced NMR of Dilute Spins in Solids". The timing of this technique is shown schematically in Figure 3.5.

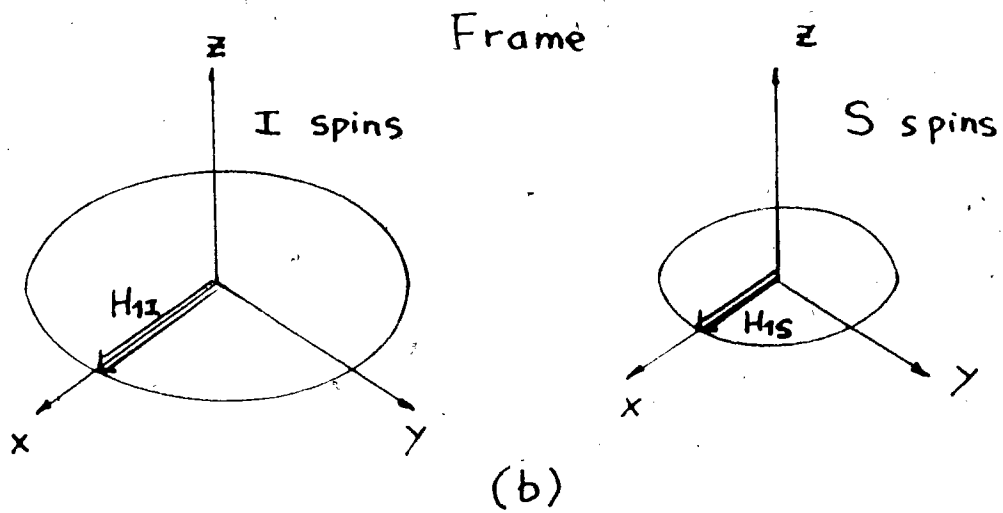
After polarization of the I spins in ca.  $T_{1I}$ , the I magnetization is spin-locked at resonance along  $H_{IX}$  in the I rotating frame (as in Figure 3.6). The S spins are brought into contact with the I reservoir by applying a resonant  $H_{IS}$  such that the Hartmann-Hahn condition (eqn.[10]) is satisfied. The spin systems come rapidly to equilibrium causing a small decrease in  $M_I$  and a growth of  $M_S$  along their  $H_I$  fields. This is indicated schematically in Figure 3.5 by the curves inside the  $H_I$  irradiation blocks. The  $H_{IS}$  field is then removed and the S free induction decay (f.i.d.) observed while continuing the I irradiation for spin decoupling. The pulse spacing  $\tau$  is large to allow the S spin magnetization to decrease fully to zero. The S spin magnetization between the pulses is observed and successive S spins f.i.d. are accumulated in an on-line computer and Fourier transformed to obtain the S spin spectrum. Since the I-field  $H_{IX}$  is kept on during the S spin f.i.d., the abundant I spins are decoupled, resulting a high resolution spectrum of the S spins.

Figure 3.6 Double-rotating frame transformation.

In the laboratory frame (a) the rotating components of the I and S rf have amplitudes  $H_{1I}$ ,  $H_{1S}$  and angular frequencies  $\omega_I$ ,  $\omega_S$ . A rotating frame transformation  $R = \exp[-it(\omega_{0I}I_z + \omega_{0S}S_z)]$  is then performed which rotates the I spins at  $\omega_I$  and the S spins at  $\omega_S$  about the Z axis. In this frame (b) we can imagine the I spins in their rotating frame experiencing a static field  $H_{1I}$  along  $x$  and the S spins in their rotating frame experiencing  $H_{1S}$  along  $x$ . The effects of  $H_{1S}$  on I spins and  $H_{1I}$  on S spins can be reflected if  $\omega_I - \omega_S$  is much longer than the S and I spectral widths, as is normally the case.



Double Rotating



The S spin magnetization after the k-th contact can be expressed as (6-8,85-87,93a):

$$[22] \quad M_S^{(k)} = \frac{\delta_I}{\delta_S} (1-\epsilon)^k M_{0S} \simeq \frac{\delta_I}{\delta_S} e^{-k\epsilon} M_{0S} \quad \cdot \quad k\epsilon \ll 1$$

since the Hartmann-Hahn condition is satisfied in this experiment. The contact time,  $t_w$  is in the order of milli-seconds, whereas,  $\tau$  may be on the order of a few hundred milliseconds, depending on the desired spectral resolution, the total co-added magnetization after N contacts may be expressed as:

$$[23] \quad M_S^{(N)} = \frac{\delta_I}{\delta_S} M_{0S} \sum_{k=1}^N e^{-k\epsilon}$$

We can now estimate the sensitivity of the single-contact cross-polarization experiment (6). The first step is to assume that the quality factor of the probe Q, filling factor and detector bandwidth can be represented by a constant K. Therefore, the signal voltage at the beginning of the non-equilibrium S-spin f.i.d. is  $K \cdot M_{0S}$ . The accumulated voltage after N cross-polarization is then, from eqn. [23].

$$[24] \quad V_S(N) = K \cdot \left( \frac{\delta_I}{\delta_S} \right) M_{0S} \sum_{k=1}^N e^{-k\epsilon}$$

This signal is, of course, maximized by making  $N \rightarrow \infty$ , however, successive signals decrease in amplitude in the presence of constant noise. If the rms noise voltage in the

bandwidth of the detector is  $V_{ns}$ , the accumulated signal to noise is (6):

$$[25] \quad (S/N)_{CP} = \left( \frac{\delta_I}{\delta_S} \cdot \frac{K \cdot M_{0S}}{V_{ns}} \right)^2 \frac{1}{N} \left( \sum_{k=1}^N e^{-k\epsilon} \right)^2$$

This is maximized for

$$[26] \quad N \cdot \epsilon \equiv \lambda \sim 1.3$$

for which

$$[27] \quad (S/N)_{CP} = 0.41 \left( \frac{\delta_I}{\delta_S} \right)^2 \epsilon^{-1} \left( \frac{K \cdot M_{0S}}{V_{ns}} \right)^2$$

For a single-contact cross-polarization experiment, each cycle of cross-polarization and signal recording requires a time of the order of  $T_{IS} + T_{2S}^*$ , where  $T_{2S}^*$  is the decay time corresponding to the obtainable frequency resolution  $\delta_S$  ( $\delta_S \cdot T_{2S}^* \geq 1$ ). Since  $T_{IS}$  is usually very short, it can be neglected in comparison to  $T_{2S}^*$ . Another practical problem that may arise is that the I-spin magnetization decays with a characteristic spin-lattice relaxation time in the rotating frame  $T_{1\rho I}$  ( $\leq T_{1I}$ ) irrespective of the desired loss to the S system. When this is the case, it is necessary to replace  $\epsilon$  in eqn. [23] by  $T_{2S}^*/T_{1\rho I}$ .

The cycle can now be repeated, only after a time ca.  $T_{1\rho I}$ , so that the I spins can become repolarized.

(N.B.  $T_{1T}^{\dagger} \sim \frac{5}{4} T_{1X}$  to obtain optimum signal (94)). The efficiency of the cross-polarization experiment can then be discussed in terms of a figure of merit  $Q_{cp}$  which measures the overall rate at which signal energy climbs out of the noise:

$$[28] \quad Q_{cp} = (T_{1T}^{\dagger})^{-1} (S/N)_{cp}$$

Now we are in the position to make a direct comparison between the efficiencies of the cross-polarization experiment and the ordinary equilibrium f.i.d. (Bloch decay), since the time dependences of the recorded signals are identical. As above, we can write

$$[29] \quad (S/N)_{fid} = \left( \frac{K \cdot M_{os}}{V_{ns}} \right)^2$$

Since this experiment requires a time ca.  $T_{1S}$  between repetitions, we can define

$$[30] \quad Q_{fid} = (T_{1S})^{-1} (S/N)_{fid}$$

On the basis of the above, we can define a gain in sensitivity resulting from use of the cross-polarization technique of

$$[31] \quad G_{cp} = Q_{cp} / Q_{fid} = (0.41) \left( \frac{\delta_I}{\delta_S} \right)^2 \left( \frac{T_{1S} T_{1T}^{\dagger}}{T_{1S}^* T_{1T}^{\dagger}} \right)$$



Choosing  $^1\text{H}$  as I spins and  $^{13}\text{C}$  as S spins, we can then estimate the four time constants.  $T_{2s}^*$  is about 0.01 second,  $T_{IS}$  is usually much longer than  $T_{II}^{\dagger}$ , which in turn is usually longer than or equal to  $T_{IEI}$ . Given this and  $\delta_I/\delta_S = 4$ , we could see that  $G_{CP}$  could become quite large especially if  $T_{II}^{\dagger} \rightarrow T_{IEI}$  through appropriate off-resonance irradiation (95).

A point of interest to note is that in the case of a multiple-contact cross-polarization experiment, the gain in sensitivity is much higher. This arises because the cross-polarization is repeated until the I-spin magnetization has been largely or fully transferred to the S-system. In doing so, the  $H_{II}$  has to be left on for periods of several seconds, which requires that  $T_{IEI}$  be relatively long. The gain in sensitivity in a multiple-contact cross-polarization experiment will then be (6):

$$[32] \quad G_{CP}' = (0.41) \epsilon^{-1} \left( \frac{\delta_I}{\delta_S} \right)^2 \left( \frac{T_{IS}}{T_{II}^{\dagger}} \right)$$

Using the same  $^1\text{H}$  and  $^{13}\text{C}$  systems as examples, where  $\epsilon = N_S/N_I \sim 1/150$ ,  $G_{CP}'$  is in the order of  $10^3$  even in the case of  $T_{II}^{\dagger} \sim T_{IS}$ . In fact  $T_{IS} \gg T_{II}^{\dagger}$ , and will become more so if paramagnetic doping is employed to speed relaxation, since there is more efficient diffusion of spin energy among the I spins.

### 3.B.III Cross-Polarization Dynamics

In our experiments on surfaces utilizing cross-polarization, the I spins are cooled by the spin-locking method. Therefore, in this section which describes the variation of the inverse spin temperatures  $\beta_I$  and  $\beta_S$  of the I spins and S spins respectively in the "mixing" part of the cross-polarization experiment, only the spin-locking case will be discussed. The other basic cross-polarization experiment using ADRF is excellently discussed in references (6,82).

As shown in Figure 3.4, for the initial S spin-temperature, we assume  $\beta_S = 0$ , and the I spin-temperature is described according to Section 3.B.I. For the spin-locking case,  $H_{IX} \gg H'_{LI}$  ideally

$$[33] \quad \beta_I = \beta_L \frac{H_0}{H_{IX}}$$

If we invoke energy conservation in the rotating frame, we can write

$$[34] \quad \frac{d}{dt} \beta_I + \epsilon' \frac{d}{dt} \beta_S = 0$$

where 
$$\epsilon' = \frac{N_S S(S+1)}{N_I I(I+1)} \alpha^2 = \epsilon \alpha^2$$

with 
$$\alpha = \frac{\delta_S H_{IS}}{\delta_I H_{IX}} = \frac{\omega_{es}}{\omega_{eI}}$$

The S spin-temperature  $\beta_S$  is relaxed with the time constant  $T_{IS}$  towards the instantaneous I spin-temperature which results in the following coupled differential eqn. (91):

$$[35a] \quad \frac{d}{dt} \beta_S = - \frac{1}{T_{IS}} (\beta_S - \beta_I)$$

$$[35b] \quad \frac{d}{dt} \beta_I = - \frac{\epsilon'}{T_{IS}} (\beta_I - \beta_S) - \frac{1}{T_{IeI}} \beta_I$$

The nature of  $T_{IS}$  and its dependence on  $H_{IS}$  will be discussed in more detail later. Notice, however, that an expression for  $1/T_{IS}$  has been quoted already in eqn. [12]. These coupled differential equations [35] are straight forwardly solved under the initial conditions:

$$\beta_S(0) = 0 \quad \beta_I(0) = \beta_{I0}$$

$$[36a] \quad \beta_S(t) = \beta_{I0} \left( \frac{1}{a_+ - a_-} \right) (e^{-a_- t / T_{IS}} - e^{-a_+ t / T_{IS}})$$

$$[36b] \quad \beta_I(t) = \beta_{I0} \left( \frac{1}{a_+ - a_-} \right) \left[ (1 - a_-) e^{-a_- t / T_{IS}} - (1 - a_+) e^{-a_+ t / T_{IS}} \right]$$

where 
$$a_{\pm} = \frac{1}{2} \left( 1 + \epsilon \alpha^2 + \frac{T_{IS}}{T_{IeI}} \right) \left[ 1 \pm \left( 1 - \frac{4 T_{IS} / T_{IeI}}{1 + \epsilon \alpha^2 + T_{IS} / T_{IeI}} \right)^{\frac{1}{2}} \right]$$

The variation of the magnetization  $M_S(t)$  of the S spins with the coupling time is

$$[37a] \quad \frac{M_S(t)}{M_{S0}} = \frac{\beta_S(t) H_{IS}}{\beta_L H_0} = \alpha \frac{\delta_I \beta_S(t)}{\delta_S \beta_{I0}}$$

where  $\beta_S(t)/\beta_{I0}$  must be inserted according to eqn. [37a].

The S spin magnetization reaches a maximum at time

$$[37b] \quad t_m = \frac{T_{IS}}{a_+ - a_-} \ln \left( \frac{a_+}{a_-} \right)$$

Notice, that for large values of  $T_{IEI}/T_{IS}$ , one has to wait a long time compared with  $T_{IS}$  for the S spin signal to reach its maximum. However, remember that already 95% of the maximum signal is reached after  $3T_{IS}$ . We turn now to the maximum S spin magnetization  $M_S$  obtainable at time  $t_m$  for a given value of  $\alpha$ . Applying eqns. [37], we obtain

$$[38] \quad t = t_m : \frac{M_S}{M_{S0}} = \alpha \frac{\delta_I}{\delta_S} \left( \frac{1}{a_+ - a_-} \right) \left[ \left( \frac{a_-}{a_+} \right)^{\frac{a_-}{a_+ - a_-}} - \left( \frac{a_-}{a_+} \right)^{\frac{a_+}{a_+ - a_-}} \right]$$

In the case of negligible I spin relaxation ( $T_{IS}/T_{IEI} \ll 1$ ;  $t_m = \infty$ ) we obtain

$$[39] \quad \frac{M_{S00}}{M_{S0}} = \frac{\beta_f H_{IS}}{\beta_L H_0} = \frac{\delta_I \alpha}{\delta_S (1 + \epsilon \alpha^2)}$$

However, in practice, for large rf fields at the S spin

resonance ( $\alpha \gg 1$ ), the cross-relaxation time  $T_{IS}$  becomes comparable to the I spin relaxation time in the rotating frame  $T_{I\tau}$  and eqns. [37a,38] have to be applied.

We can now discuss some special cases of eqn. [36]:

(i)  $\epsilon = 0$ ;  $T_{IS}/T_{I\tau} = 0$ , i.e. vanishing heat capacity of the S spins; negligible  $T_{I\tau}$  relaxation of the I spins.

$$[40a] \quad \beta_S(t) = (1 - e^{-t/T_{IS}}) \beta_{I0}$$

$$\beta_I(t) = \beta_{I0}$$

(ii)  $\epsilon = 0$ ;  $T_{IS}/T_{I\tau} \neq 0$ , i.e. same as (i) but  $T_{I\tau}$  relaxation of the I spins non-negligible.

$$[40b] \quad \beta_S(t) = \frac{1}{1-\lambda} (1 - e^{-(1-\lambda)t/T_{IS}}) e^{-t/T_{I\tau}} \cdot \beta_{I0}$$

$$\beta_I(t) = (e^{-t/T_{I\tau}}) \beta_{I0}$$

where  $\lambda = T_{IS}/T_{I\tau}$

This case is usually met under extreme dilution of the S spins and with matched Hartmann-Hahn condition ( $\alpha = 1$ ), but with short  $T_{I\tau}$  relaxation time.

(iii)  $\epsilon \neq 0$   $\lambda = 0$ , i.e. non-negligible heat capacity of the S spins, but negligible  $T_{I\tau}$  relaxation.

$$[41a] \quad \beta_S(t) = \frac{1}{1+\epsilon'} (1 - e^{-(1+\epsilon')t/T_{1S}}) \beta_{I0}$$

$$[41b] \quad \beta_I(t) = \frac{1}{1+\epsilon'} (1 + \epsilon' e^{-(1+\epsilon')t/T_{1S}}) \beta_{I0}$$

This case is usually met, no matter if the Hartmann-Hahn condition is matched or unmatched, as long as  $T_{1S} \ll T_{1I}$  —

In the single-contact cross-polarization experiment,  $\epsilon'$  usually becomes large and if the Hartmann-Hahn condition is not matched ( $\alpha \gg 1$ ),  $T_{1S}$  is comparable with  $T_{1I}$  or  $\lambda = 1$  i.e. eqn. [36] has to be used. This has been demonstrated by the study on adamantane by Pines (96) and on  $CF_3COOAg$  by Mehring (97).

### 3.C.I. Magic-angle Spinning (MAS) Technique (75)

It is well established that the rapid rotation of solid specimens narrows their NMR spectra, if the axis of rotation is well chosen and the speed of rotation is fast enough, the anisotropic broadening interactions are largely removed from the central spectrum. The rotation of solid specimens at high speed was first used by Andrew, Bradbury and Eades (73a) to study motional narrowing effects in the dipolar broadened NMR spectra of solids and to test the principle of second moment invariance with respect to rotation. It will be shown later that the central region of such a spectrum is narrowed by a factor  $|\frac{1}{2}(3\cos^2\theta - 1)|$ , where  $\theta$  is the angle between the

direction of the axis of specimen rotation and the direction of the laboratory magnetic field,  $H_0$ . It was independently recognized by Andrew (98) and by Lowe (99) that when  $\theta$  is chosen to have the special value, often called the "magic" angle,  $\cos^{-1}(1/\sqrt{3})$  or  $54^\circ 44'$ , the reduction factor is zero, and the dipolar broadening may largely be removed, as experiments confirmed (99, 100). Subsequently, it was shown by Andrew and Eades (101) that high speed rotation about the magic axis should be similarly effective in removing spectral broadening arising from anisotropy of the chemical shift in polycrystalline or amorphous specimens. Resolution of chemical shift fine structures by this technique was provided by Andrew and Wynn (73b).

### 3.C.II. Basic Theory of MAS Technique (75)

The total Hamiltonian which describes the NMR spectrum of a diamagnetic solid may be written as the sum of five terms:

$$[42] \quad \mathcal{H} = \mathcal{H}_z + \mathcal{H}_c + \mathcal{H}_D + \mathcal{H}_J + \mathcal{H}_Q$$

which are respectively the Zeeman, chemical shift, magnetic dipolar, indirect electron-coupled, and electric quadrupolar interactions of the nuclei. To the interest of this section, only the last four terms will be discussed.

The chemical shift term  $\mathcal{H}_c$  is the modification to the Zeeman interaction caused by the electron screening of the

nuclei, which in general, is anisotropic, and is given by

$$[43] \quad \mathcal{H}_c/h = \frac{1}{2\pi} \sum_i \delta_i \vec{I}_i \cdot \hat{\sigma}_i \cdot \vec{I}_j \cdot H_0$$

where  $\hat{\sigma}_i$  is the screening tensor of nucleus  $i$ .  $\mathcal{H}_D$  is the truncated magnetic dipolar interaction between the nuclei:

$$[44] \quad \mathcal{H}_D/h = \frac{1}{2\pi} \sum_{i < j} \vec{I}_i \cdot \hat{D}_{ij} \cdot \vec{I}_j \\ = \sum_{i < j} \sum_{\frac{h}{8\pi^2}} \delta_i \delta_j r_{ij}^{-3} (3 \cos^2 \theta - 1) (\vec{I}_i \cdot \vec{I}_j - 3 I_{iz} I_{jz})$$

$\hat{D}_{ij}$  being the truncated dipolar interaction tensor.  $\mathcal{H}_J$  is the indirect electron-coupled nuclear spin interaction, which in general is anisotropic:

$$[45] \quad \mathcal{H}_J/h = \sum_{i < j} \vec{I}_i \cdot \hat{J}_{ij} \cdot \vec{I}_j$$

where  $\hat{J}_{ij}$  is the electron-coupled nuclear spin interaction tensor. Both  $\hat{D}_{ij}$  and  $\hat{J}_{ij}$  represent bilinear interactions between the spins, however,  $\hat{D}_{ij}$  is an axially symmetric traceless tensor,  $\hat{J}_{ij}$  is not necessarily axially symmetric, nor is it traceless.  $\mathcal{H}_Q$  is only non-zero for nuclei with spin number greater than 1/2 in a non-cubic environment, and is given by:

$$[46] \quad \mathcal{H}_Q/h = \sum_i \rho_i [3I_{iz}^2 - \vec{I}_i^2 + \eta_Q (I_{ix}^2 + I_{iy}^2)] / 4I(2I+1)$$



where  $\rho_i$  is the nuclear electric quadrupole coupling constant given by

$$[47] \quad \rho = e^2 Q q / h$$

$eQ$  is the nuclear electric quadrupolar moment,  $eq$  is the  $z'z'$  component of the electric field gradient tensor.  $\eta_Q$  is its asymmetry parameter, and  $x'$ ,  $y'$ ,  $z'$  are its principal axes.

Since in our study of surfaces, we did not study any spin  $> 1/2$ , we will delete the discussion on the quadrupolar interaction.

When the solid is rotated with uniform angular velocity  $\omega_r$  about an axis inclined at an angle  $\beta$  to  $H_0$ , all the anisotropic terms in  $\mathcal{H}$  become time-dependent with periodicity  $\omega_r$ . Thus the Zeeman term is not affected by the motion, but in general, all the other four are affected, and can be treated as perturbations (since they are small compared with the Zeeman term) and the time-dependent Hamiltonian  $\mathcal{H}'(t)$  is

$$[48] \quad \mathcal{H}'(t) = \mathcal{H}_c(t) + \mathcal{H}_D(t) + \mathcal{H}_J(t) + \mathcal{H}_Q(t)$$

The individual effect upon the specimen can now be considered (75). Since the chemical shift tensor components are small compared with unity, we need only retain  $\sigma_{zz}$  (defined later).

$$[49] \quad \mathcal{H}_c/h = \sum_i \frac{1}{2\pi} \delta_i \sigma_{i33} H_0 I_z$$

The chemical shift tensor  $\widehat{\sigma}_i$  may be divided into a symmetric tensor  $\widehat{\sigma}_i^*$  and an antisymmetric tensor  $\widehat{\sigma}_i^\dagger$  where

$$[50] \quad \widehat{\sigma}_i^* = \frac{1}{2} (\widehat{\sigma}_i + \widehat{\sigma}_i') \quad ; \quad \widehat{\sigma}_i^\dagger = \frac{1}{2} (\widehat{\sigma}_i - \widehat{\sigma}_i')$$

in which  $\widehat{\sigma}_i'$  is the transpose of  $\widehat{\sigma}_i$ . If the principal values of  $\widehat{\sigma}_i^*$  are  $\sigma_{i1}$ ,  $\sigma_{i2}$ ,  $\sigma_{i3}$  and the direction cosines of its principal axes with respect to  $H_0$  are  $\lambda_{i1}$ ,  $\lambda_{i2}$ ,  $\lambda_{i3}$  then

$$[51] \quad \sigma_{i33} = \lambda_{i1}^2 \sigma_{i1} + \lambda_{i2}^2 \sigma_{i2} + \lambda_{i3}^2 \sigma_{i3}$$

Since the isotropic average of each  $\lambda^2$  is  $1/3$ , the average value of  $\sigma_{i33}$  in a normal fluid is

$$[52] \quad \overline{\sigma_{i33}} = \frac{1}{3} \text{Tr} \{ \widehat{\sigma}_i \} = \sigma_i$$

where  $\sigma_i$  is the scalar chemical shift encountered in high-resolution NMR spectra of fluids. When the rigid array of nuclei in a solid is rotated with angular velocity  $\omega_r$  about an axis inclined at an angle  $\beta$  to  $H_0$ , and at angles

$\chi_{i1}$ ,  $\chi_{i2}$ ,  $\chi_{i3}$  to the principal axes of  $\widehat{\sigma}_i^*$ ,

we have

$$[53] \quad \lambda_{ip} = \cos \beta \cos \chi_{ip} + \sin \beta \sin \chi_{ip} \cos(\omega t + \psi_{ip})$$

where  $\psi_{ip}$  is the azimuth angle of the  $p$ th principal axis of  $\hat{\sigma}_i$  at  $t = 0$ . Substituting eqns. [53] and [51] and taking the time average, we have

$$[54] \quad \overline{\sigma_{izz}} = \frac{1}{2} \sin^2 \beta \operatorname{Tr} \{ \hat{\sigma}_i \} + \frac{1}{2} (3 \cos^2 \beta - 1) \sum_p \sigma_{ip} \cos^2 \psi_{ip}$$

Consequently, when  $\beta$  is the magic angle  $\sec^{-1} \sqrt{3}$ , the time-averaged value reduces to

$$[55] \quad \overline{\sigma_{izz}} = \frac{1}{3} \operatorname{Tr} \{ \hat{\sigma}_i \} = \sigma_i$$

which is the same as for a liquid, and in this case the mean value of  $\mathcal{H}_c$  becomes

$$[56] \quad \overline{\mathcal{H}_c/h} = \frac{1}{2\pi} \sum_i \delta_i \cdot \sigma_i \cdot I_{iz} \cdot H_0$$

The time-average of  $\mathcal{H}_D$  for an isotropic fluid is zero since the isotropic average of  $\cos^2(\theta_{ij})$  is  $1/3$ ; for this reason, the magnetic dipolar interaction makes little contribution to the NMR spectra of fluids and is usually ignored. For solids, rotation imparts a time-dependence to  $\cos \theta_{ij}$ , which may be expressed as

$$[57] \quad \cos \theta_{ij}(t) = \cos \beta \cos \beta'_{ij} + \sin \beta \sin \beta'_{ij} \cos(\omega t + \phi_{ij})$$

where  $\beta'_{ij}$  is the angle between the axis of rotation and  $\vec{r}_{ij}$ , and  $\phi_{ij}$  is the azimuth angle of  $\vec{r}_{ij}$  at  $t = 0$ . Thus the time average of  $\cos^2 \theta_{ij}(t)$  is

$$[58] \quad \overline{\cos^2 \theta_{ij}(t)} = \cos^2 \beta \cos^2 \beta'_{ij} + \frac{1}{2} \sin^2 \beta \sin^2 \beta'_{ij} \\ = \frac{1}{6} (3 \cos^2 \beta - 1)(3 \cos^2 \beta'_{ij} - 1) + \frac{1}{3}$$

Thus the time-average value of  $\mathcal{H}_D$  is, from [58] and [44],

$$[59] \quad \overline{\mathcal{H}_D}/h = \frac{1}{2} (3 \cos^2 \beta - 1) \sum_{i < j} \frac{h}{8\pi^2} \delta_i \delta_j r_{ij}^{-3} (3 \cos^2 \beta'_{ij} - 1) (\vec{I}_i \cdot \vec{I}_j - 3 I_{iz} I_{jz})$$

In particular, when  $\beta$  is the magic angle, we see then  $\mathcal{H}_D$  is zero.

When considering the electron-coupled nuclear-spin interaction  $\mathcal{H}_J$ , it is convenient to divide the coupling tensor  $\hat{\mathcal{J}}$  into three parts

$$[60a] \quad \hat{\mathcal{J}} = J \hat{1} + \hat{\mathcal{J}}^* + \hat{\mathcal{J}}^\dagger, \quad \text{where}$$

$$[60b] \quad J = \frac{1}{3} \text{Tr} \{ \hat{\mathcal{J}} \}, \quad \text{and}$$

$$[60c] \quad \hat{\mathcal{J}}^* = \frac{1}{2} (\hat{\mathcal{J}}_+ + \hat{\mathcal{J}}_-) - J \hat{1}$$

$$[60d] \quad \hat{\mathcal{J}}^\dagger = \frac{1}{2} (\hat{\mathcal{J}} - \hat{\mathcal{J}}_-)$$

in which  $\hat{J}$  is the transpose of  $\hat{J}$ . The suffixes  $i, j$  have been omitted for clarity since  $\hat{J}$  is in general different for each nuclear pair  $i, j$ . The term  $J\hat{1}$  in [60a] gives rise in [44] to the familiar interaction  $J_{ij} \hat{I}_i \cdot \hat{I}_j$ , expressing the scalar coupling between the nuclei. Clearly  $\hat{J}^*$  is traceless and symmetric while  $\hat{J}^\dagger$  is antisymmetric and traceless. Thus the isotropic average of  $\hat{J}$  is  $\bar{J} = \frac{1}{3} \text{Tr}\{\hat{J}\} = J$ , where  $J$  is the scalar coupling constant encountered in high resolution NMR spectroscopy of liquids. The contribution of this term to is therefore  $\sum_{i,j} J_{ij} \hat{I}_i \cdot \hat{I}_j$ .

Rotation of the solid specimen only affects  $\hat{J}^*$  and  $\hat{J}^\dagger$ . The symmetric component  $\hat{J}^*$  differs from the dipolar term in that it is not necessarily an axially symmetric tensor. For one particular nuclear pair this component of the interaction  $\mathcal{H}_J/h$  is

$$[61] \quad \hat{I}_i \cdot \hat{J}^* \hat{I}_j = \sum_{\alpha, \beta} J_{\alpha\beta} I_{i\alpha} I_{j\beta} = C_{\alpha n} C_{\beta n} J_n I_{i\alpha} I_{j\beta}$$

where  $J_n$  are the principal values of the tensor  $\hat{J}^*$  and  $C_{\alpha n}$ ,  $C_{\beta n}$  are the direction cosines of the principal axes of  $\hat{J}^*$  with respect to the laboratory axes  $\alpha$ ,  $\beta$  referring to the  $x, y, z$  in turn. Rearranging eqn. [61] and truncating as for the dipolar interaction by omitting spin products which do not contribute to the observed spectrum in first order, only the

following are left:

$$[62] \quad \vec{I}_i \cdot \widehat{J}^* \vec{I}_j = -\frac{1}{4} J_3 \{ (3C_{33}^2 - 1) + \eta_J (C_{32}^2 - C_{31}^2) \} \{ \vec{I}_1 \cdot \vec{I}_2 - 3I_{13}I_{23} \}$$

where the asymmetry parameter  $\eta_J$  is defined as

$$[63] \quad \eta_J = (J_2 - J_1) / J_3$$

taking  $J_3 > J_2 > J_1$ . When the solid is rotated, the direction cosines  $C_{3n}$  become time-dependent and the average values of their squares is

$$[64] \quad \overline{C_{3n}^2} = \frac{1}{6} (3\cos^2\beta - 1)(3\cos^2\mu_n - 1) + \frac{1}{3}$$

where  $\mu_n$  are the angles between the axis of rotation and the three principal axes of  $\widehat{J}^*$ . The result follows in the same manner as in eqn. [58]. When  $\beta$  is the magic angle,  $\overline{C_{3n}^2}$  is  $1/3$  for all values of  $n$ , and the time-averaged value of [62] is zero.

With the antisymmetric part  $\widehat{J}^\dagger$  of the tensor  $\widehat{J}$ , for one particular nuclear spin, this interaction from eqns. [45] and [60a] is

$$[65] \quad J_{\alpha\beta}^\dagger I_{1\alpha} I_{2\beta} = (C_{\alpha\alpha} C_{\beta\beta} - C_{\alpha\beta} - C_{\beta\alpha}) J_{\alpha\beta}^\dagger I_{1\alpha} I_{2\beta}$$

where  $\alpha$ ,  $\beta$  refer to the laboratory axes  $x, y, z$  and  $a, b$  refer to any convenient set of axes in the molecules  $x', y', z'$ , e.g. the principal axes of  $\hat{J}^*$ . Truncating as before, and taking the time-average of the cosine products, the average antisymmetric interaction for one nuclear pair in eqn. [45] is

$$[66] \quad \overline{J_{\alpha\beta}^{\dagger} I_{1\alpha} I_{2\beta}} = A_{12} (I_{1x} I_{2y} - I_{1y} I_{2x})$$

where  $A_{12}$  is a scalar antisymmetric coupling constant between nuclei 1 and 2 given by:

$$[67] \quad A_{12} = \frac{1}{2} J_{ab}^{\dagger} \sin \alpha_1 \sin \alpha_2 \sin \xi_a \sin \xi_b \{ \cos(\epsilon_{1a} - \epsilon_{2b}) - \cos(\epsilon_{1b} - \epsilon_{2a}) \}$$

where  $\alpha_1$ ,  $\alpha_2$  are the angles between the rotating axis and laboratory axis  $x, y$  respectively,  $\xi_a$ ,  $\xi_b$  are the angles between the rotation axis and the molecular axes  $a, b$  respectively.  $\epsilon_{aa}$  is the azimuth angle at  $t = 0$  of molecular axes  $a$  relative to the plane containing the axis of rotation and the laboratory axis  $\alpha$ . When  $\beta$  is the magic angle, eqns. [66] and [67] are not necessarily zero, and rotation about the magic axis does not in general remove the contribution of any antisymmetric part of  $\hat{J}$  from  $\mathcal{H}$ .

In summary, when  $\beta$  is the magic angle, the dipolar term  $\mathcal{H}_D$  and the quadrupolar term  $\mathcal{H}_Q$  vanish, leaving

$$\begin{aligned}
 [68] \quad \mathcal{H}/h &= (\mathcal{H}_z + \mathcal{H}_c + \mathcal{H}_J)/h \\
 &= -\frac{1}{2\pi} \sum_i \delta_i (1-\delta_i) I_{iz} H_0 + \sum_{i < j} \sum J_{ij} \vec{I}_i \cdot \vec{I}_j + A_{H_2} (I_{1x} I_{2y} - I_{1y} I_{2x})
 \end{aligned}$$

Considering the time-dependent part of the Hamiltonian  $\mathcal{H}'(t)$  and taking the component  $\mathcal{H}'_D(t)$  in [48] as example, from eqns. [44] and [58] the time-dependent part of the truncated dipolar interaction is

$$\begin{aligned}
 [69] \quad \mathcal{H}'_D(t)/h &= \sum_{i < j} \frac{3h}{16\pi^2} \delta_i \delta_j r_{ij}^{-3} (\vec{I}_i \cdot \vec{I}_j - 3I_{iz} I_{jz}) \{ \sin 2\beta \sin 2\beta'_{ij} \\
 &\quad \times \cos(\omega_r t + \phi'_{ij}) + \sin^2 \beta \sin^2 \beta'_{ij} \cos 2(\omega_r t + \phi'_{ij}) \}
 \end{aligned}$$

This perturbation thus consists of two terms periodic in  $\omega_r$  and in  $2\omega_r$ , and in a similar way, it could be shown that all four components of  $\mathcal{H}'(t)$  have terms periodic in  $\omega_r$  and in  $2\omega_r$ . By a variety of approaches, it has been shown (99, 102-107) that these time-dependent perturbations generate satellite spectra set on either side of the central resonance spectrum at integral multiples of  $\omega_r/2\pi$ . Such satellites are observed and are resolved when the frequency of rotation is comparable with the original linewidth.

### 3.D.I. MAS Combined with Proton-Enhanced NMR (CP/MAS)

So far one has studied how high-resolution NMR can be applied to solids. Proton-enhanced NMR removes the dipolar broadening, leaving a rich source of information, (e.g. chemical



shift anisotropy) for crystals. In polycrystalline or amorphous substances, this creates a problem, since the powder patterns arising from non-equivalent rare spins overlap, preventing resolution and interpretation of the individual resonances.

However, it has been shown (108) that the powder patterns can be collapsed to sharp lines by spinning the sample about the magic axis at a frequency  $\omega_r$  which exceeds the anisotropy linewidths  $\Delta\omega_0$  but is still too low to remove the dipolar broadening directly.

A possible conflict seems to arise between the requirement of line narrowing by rotation and those of the spin-exchange process by which the rare spins are polarized: the latter depends on an effectively static dipole-dipole interaction  $\mathcal{H}_{IS}$  between rare and abundant spins, and the sample rotation can render this interaction oscillatory. This feature is unimportant when  $|\mathcal{H}_{II}| \gg \hbar\Delta\omega_0$ . This is true since the modulation of  $\mathcal{H}_{IS}$  by I-I dipolar fluctuations overwhelms the additional coherent modulations by relatively slow spinning. However, sometimes when  $\hbar\omega_r \gg |\mathcal{H}_{II}|$ , then there is an interplay between the sample rotation and the conditions necessary for transfer of polarization.

### 3.D.II Theory of the CP/MAS Technique(109)

Transfer of polarization between rare (S) and abundant (I) spins is mediated by the dipole-dipole interactions. The

only part of these which remains secular or nearly so when averaged over the rapid precession induced by the static field  $H_0$  and by the resonant radiofrequency fields is (7,72,84):

$$[70] \quad \mathcal{H}_{II} = -\frac{1}{2} \sum_{k < l} \sum b_{kl} (\bar{I}_k - \bar{I}_l - 3J_{3k} I_{3l})$$

$$[71a] \quad \mathcal{H}_{IS} = V_{IS} \cos \Delta t + V'_{IS} \sin \Delta t$$

$$[71b] \quad V_{IS} = -\sum_n \sum_k b_{nk} (I_{xk} S_{xn} + I_{yk} S_{yn})$$

$$[71c] \quad V'_{IS} = -\sum_n \sum_k b_{nk} (I_{xk} S_{yn} - I_{yk} S_{xn})$$

with  $\Delta = \omega_{II} - \omega_{IS}$  the deviation from Hartmann-Hahn matching condition (7) and

$$[71d] \quad b_{ij} = \gamma_i \gamma_j \hbar r_{ij}^{-3} P_2(\cos \theta_{ij})$$

The coordinate system for eqns. [70] and [71] is the double rotating frame (110) in which the z-axes for both species are parallel to the respective rotating fields. The observable of interest is  $\langle S_z \rangle$ , the spin-locked rare spin polarization acquired at the expense of the abundant I spin neighbours.

For an S spin with a single neighbour, eqn. [71a] would lead to an oscillatory behaviour of  $\langle S_z(t) \rangle$ . With many neighbours present, oscillations at an enormous number of frequencies interfere and  $\langle S_z(t) \rangle$  quickly takes on the

character of an exponential approach to a final equilibrium value determined by the initial temperature of the I-system. (This is also aided by the I-I spin-flips induced by the  $\mathcal{H}_{II}$ ).

The secular transfer of polarization requires that  $\mathcal{H}_{IS}$  of [71a], as modified by  $\mathcal{H}_{II}$  have a time-independent part, that is, the explicit oscillation of the experimentally variable frequency  $\Delta$  must be effectively cancelled by some corresponding Fourier component hidden in  $V_{IS}$ . In a stationary sample having no  $V_{II}$  (defined similarly as for  $V_{IS}$ , except that it is between like abundant spins), no such additional time dependence exists, and secular transfer would occur only for  $\Delta = 0$ . The effect of  $V_{II}$  is to produce "dipolar fluctuations" (91) of near-neighbour moments  $I_k$  on account of their mutual flips with more distant neighbours expressed by terms of the type  $I_{\pm k} = I_{\mp k}$  embodied in [70]. Such fluctuations, impressed on  $V_{IS}$  through [71], have characteristic frequency  $\alpha' b_{k\ell}$ , the factor  $\alpha' (< 1$ , and with  $k\ell$  indices suppressed) being a recognition of (i) the reduction factor 1/2 in [70], and (ii) the fact that not all of  $\mathcal{H}_{II}$  is effective in causing spin flips which modulate  $V_{IS}$  (91). Secular IS transfer now occurs for  $\Delta \pm \alpha' b_{k\ell} \approx 0$ . The presence of many neighbours results in a dense spectrum  $f(\Delta)$  centered at  $\Delta = 0$  and having characteristic  $\alpha' b_{k\ell}$ .

The effect of sample spinning is to introduce additional oscillatory dependences to  $\mathcal{H}_{II}$  and  $\mathcal{H}_{IS}$ . For spinning about the magic angle at frequency  $\omega_r$ ,

$$[72] \quad b_{ij}(t) = \beta_{ij}^{(1)} \cos(\omega_r t - \delta_{ij}) + \beta_{ij}^{(2)} \cos(2\omega_r t - 2\delta_{ij})$$

with

$$[73a] \quad \beta_{ij}^{(1)} = \sqrt{2} \delta_i \delta_j \hbar r_{ij}^{-3} \sin \delta_{ij} \cos \delta_{ij}$$

$$[73b] \quad \beta_{ij}^{(2)} = \delta_i \delta_j \hbar r_{ij}^{-3} \sin^2 \delta_{ij}$$

Here  $\delta_{ij}$  is the angle between  $\vec{r}_{ij}$  and the spinning axis and  $\delta_{ij}$  is an initial azimuth of  $\vec{r}_{ij}$  about the axis.

The direct effect of [72] on  $\mathcal{H}_{IS}$  through the  $b_{IK}$  is clear:  $\mathcal{H}_{IS}$  becomes 100% amplitude modulated (with center band suppression) so that secular IS transfer occurs in the neighbourhood of  $\Delta = \pm \omega_r$ ;  $\pm 2\omega_r$  but not around  $\Delta = 0$ . This is true regardless of the size of  $\mathcal{H}_{IS}$ . The relative amplitudes of cross-relaxation peaks  $f(\pm 2\omega_r) : f(\pm \omega_r)$  depend on structures, e.g. for  $\vec{r}_{IK}$  perpendicular to the spinning axis  $f(\pm \Delta\omega_r) = 0$ .

The other effect of [72] is to modulate the characteristic frequencies  $\alpha \cdot b_{IK}$  which  $\mathcal{H}_{II}$  imposes on  $\mathcal{H}_{IS}$ . Each of the peaks  $f(\pm \omega_r)$ ,  $f(\pm 2\omega_r)$  mentioned above is split into FM sidebands at multiples of  $\omega_r$ , with modulation

indices of the type  $Z_{ij} = \beta_{ij}^{(1)}/\omega_r ; \beta_{ij}^{(2)}/2\omega_r$ . A qualitative feature of importance is that these sidebands, and the I-I interactions in which they originate, are required to restore secular transfer for  $\Delta = 0$ .

The relative amplitudes of the AM sidebands are estimated from the rms values of  $\beta^{(1)}$  and  $\beta^{(2)}$  of [73] over an isotropic powder distribution:  $\langle \beta_{rms}^{(2)} \rangle / \langle \beta_{rms}^{(1)} \rangle = 1/\sqrt{2}$ . The single effective modulative index  $Z = \alpha \cdot b / \omega_r$  can be obtained from the cross-relaxation spectrum of the static sample.

We can understand why MAS has so little effect on cross-polarization transfer rates on systems with strong I-I dipolar interactions (108). Such systems have an  $f(\Delta)$  with a width substantially greater than the practical spinning speeds. Thus the AM associated with spinning produces sidebands which for the most part fall completely within  $f(\Delta)$ , while the FM has such a high modulation index that no additional sidebands of significant intensity are produced outside of  $f(\Delta)$ . The net effect is an  $f(\Delta)$  which is substantially the same, whether spinning or non-spinning. This behaviour has been confirmed experimentally for a wide variety of solid polymers (108). In these systems, the full I-I interaction is of the order of 25 kHz, so that a full width at half-height of  $f(\Delta)$  of about 6 kHz is likely. Magic angle spinning at 3 kHz produces sufficiently little modulation of  $f(\Delta)$  that the observed

cross-polarization transfer rates (for both protonated and non-protonated carbons) change much less than a factor of 2, with no indication of a strong dependence on small Hartmann-Hahn mismatches.

An interesting case arises when  $H_{II}$  is small ( $\hbar\omega_r \gg |H_{II}|$ ). This was illustrated by Steiskal et al (109) in the study of adamantane. It was found that there is an interplay between the sample rotation and the conditions necessary for transfer of polarization, especially when the Hartmann-Hahn condition is not met. The magic-angle spinning has a tendency to redistribute the overall rate of polarization (instead of changing it), and intermolecular cross-polarization is possible.

## CHAPTER 4

4.A. Apparatus - General description

This section describes the necessary modifications of a commercial high-resolution NMR spectrometer so that  $^1\text{H}$ - $^{13}\text{C}$  solid-state cross-polarization (CP) experiments could be performed (111). The spectrometer used was a TT-14 from Transform Technology Inc., which is actually a hybrid device, comprising a Varian HA-60 magnet, a slightly modified Bruker WP-60 console and a Nicolet 1080 computer, with probes and interfacing logic provided by Transform Technology Inc. This spectrometer by itself provides 50 watt power at 15 MHz for  $^{13}\text{C}$ , a 15 watt  $^1\text{H}$  decoupler which can be pulsed, and a pulsed deuterium lock.

4.A.I. Probe

It is desirable to have a large volume probe since this modification has the intention of providing facility to study dilute spin systems, surface-adsorbed species in our case. For compatibility with other instrumentation existing in our laboratory, we decided to use 12 mm sample tubes. Since it was known that surface species would have short proton  $T_1$  values (66, 112-114), it was desirable that a high duty cycle be achieved to take full advantage. However, this implies possible problems with radiofrequency power dissipation in the probe, particularly for the necessary high field decoupler. Power dissipation may be kept within reasonable bounds by use of a

single coil for both observe and decoupling frequencies. This in turn generates isolation problems, but there exist designs (115, 116) of single coil probe which overcome this problem by the use of resonant cables. Of the two, we have chosen the design by Stoll, Vega and Vaughan (115).

The designed sample coil is 1.3 cm in diameter and 2 cm long wound on a thin-wall pyrex glass tube which accomodates a 12 mm sample tube. The coil is comprised of 7 turns of (2.5 mm x  $\emptyset$ .24 mm) silver strip. This is connected and double-tuned as described in (115). Computer simulation of this circuit, including explicitly the effects of the quarter-wave cable at both frequencies, showed that it is possible to select nearly correct capacitor values, and to achieve tuning with very little trial-and-error adjustment. It showed further, as did initial experiments, that the performance of this probe design is critically dependent upon losses in the capacitors and quarter-wave cable. We have therefore used low-loss cable (117) together with high Q fixed porcelain (118) and variable teflon (119) capacitors. With these components, we estimate that the major power loss is in the cable, and comprises 20-25% of the input power at each frequency.

The coil is cooled by a flow of air at ambient temperature, which impinges radially on the coil from a series of orifices. Normally, a flow of 0.7 litre/sec is used.



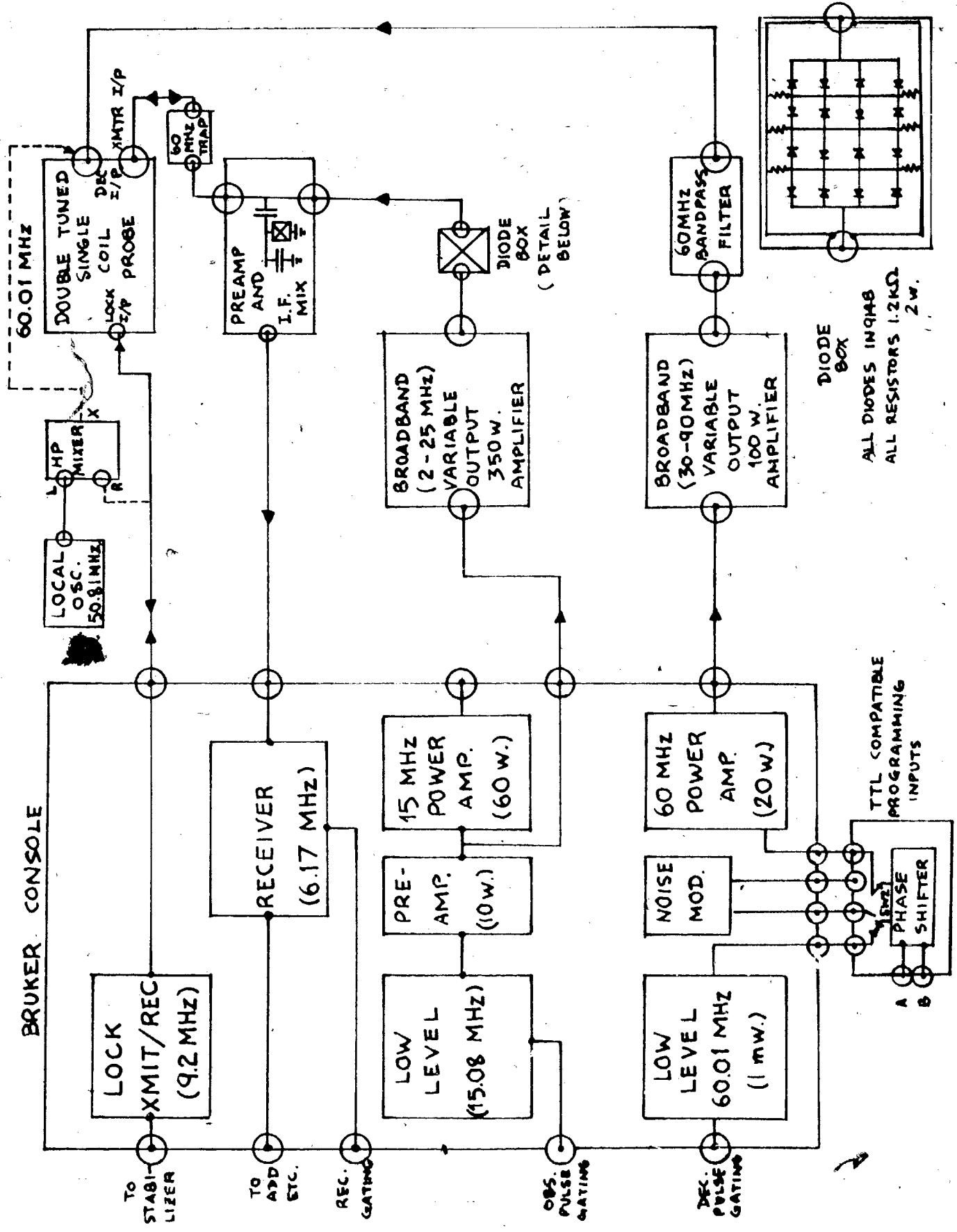
In addition, a small air flow passes axially between the sample tube and the coil support.

The probe is fitted with an external deuterium lock. This consists of a 5 mm tube containing  $D_2O$  (doped with  $CuSO_4$ ) which is wound with a coil. The coil is tuned to 9.2 MHz, matched to 50 ohms and connected to the pulsed lock circuit of the spectrometer. Use of an external lock precludes field shimming by maximizing the lock signal meter reading. We have restored this facility by locking, for shim purposes only, on the protons in a liquid sample (usually benzene). This is accomplished by mixing the lock transmitter output, with a 50.81 MHz local oscillator, and feeding the resultant sum to the proton channel of the probe, as indicated in Figure 4.1. The resultant nuclear resonance signal is mixed down to 9.2 MHz in the same mixer and activates the spectrometer lock circuitry in normal fashion. The signal from neat protonic liquids is sufficiently large that the losses on two passes through the mixer are not important.

#### 4.A.II. R.F. Power

With the above probe, the Bruker power amplifiers will produce fields of about 30 kHz ( $\gamma H_i / 2\pi$ ) at both 15 and 60 MHz, which are minimally adequate for solid-state work. However, there are drawbacks which make external power amplification necessary. First, although the  $^{13}C$  field has the above value when judged by the  $\pi/2$  pulse length, the amplitude

Figure 4.1 Block diagram of the modified spectrometer. Original components are enclosed in block at left.



of this field falls by about a factor of 3 over a pulse time of 1 ms. This, of course, is intolerable for cross-polarization experiments, in which the Hartmann-Hahn condition should be met for times of this order. The effect is undoubtedly due to insufficient power supply capacity to the 50 watt amplifier. Our solution is to extract the 15 MHz signal at the 10 watt level (see Figure 4.1) where droop is slight, and to provide external amplification.

In the case of the 60 MHz decoupler, there are no droop problems, provided it is operated at full power. However, an attempt to establish the Hartmann-Hahn condition using the decoupler output level control is unsuccessful. This is because the control uses a feedback circuit which senses the r.f. output level, and which has a time constant of about 5 msec. Thus, when the decoupler is pulsed on, the initial output is full power, decaying with the above time constant to the level determined by the control setting. Since we require a higher field in any case, we operate the decoupler at full output, and employ an external amplifier.

The power amplifiers used are home built broad-band amplifiers based on power VFET devices (120). The 15 MHz amplifier uses four VN646A transistors, and can provide 350 watt output with 10 watt input. The 60 MHz amplifier uses two BF50-35 devices, and provides 80 watt output with 10 watt input. Each amplifier is provided with a power supply having high

current capacity and large output capacitance, to give less than 5% amplitude droop with typical pulse lengths. Our practice is to establish the matching condition by operating the 60 MHz amplifier at full power, and varying the d.c. input to the 15 MHz amplifier to achieve matching. Our r.f. fields are typically 70 kHz at each frequency.

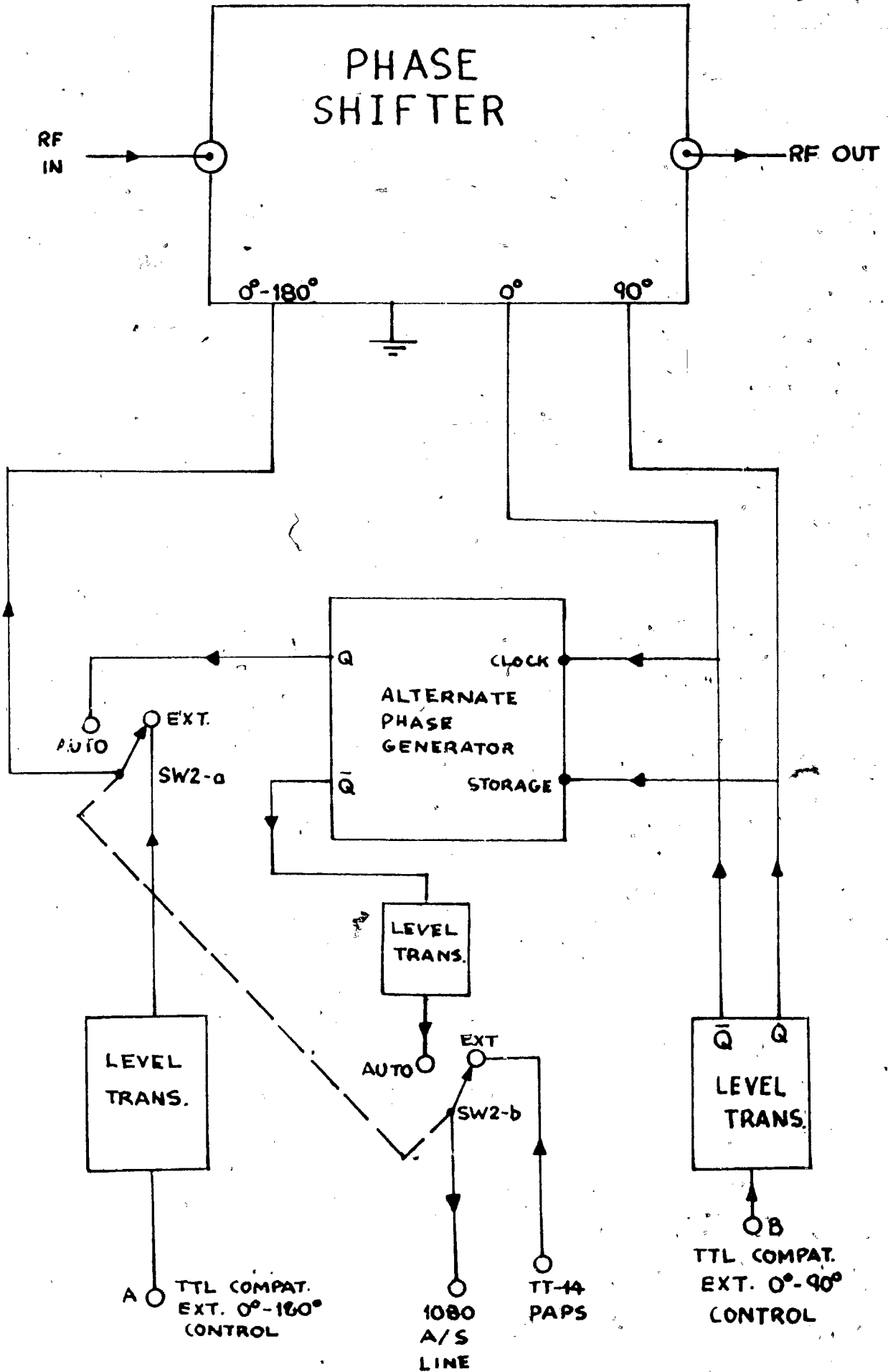
An additional pair of crossed diodes was added in parallel with the existing pair in the receiver input circuit. These are probably unnecessary, as we have had no problems here with pulse length up to 20 msec at full power. The Bruker diode box in the transmitter lead was destroyed at an early stage of this project, and was replaced by the diode network shown in Figure 4.1.

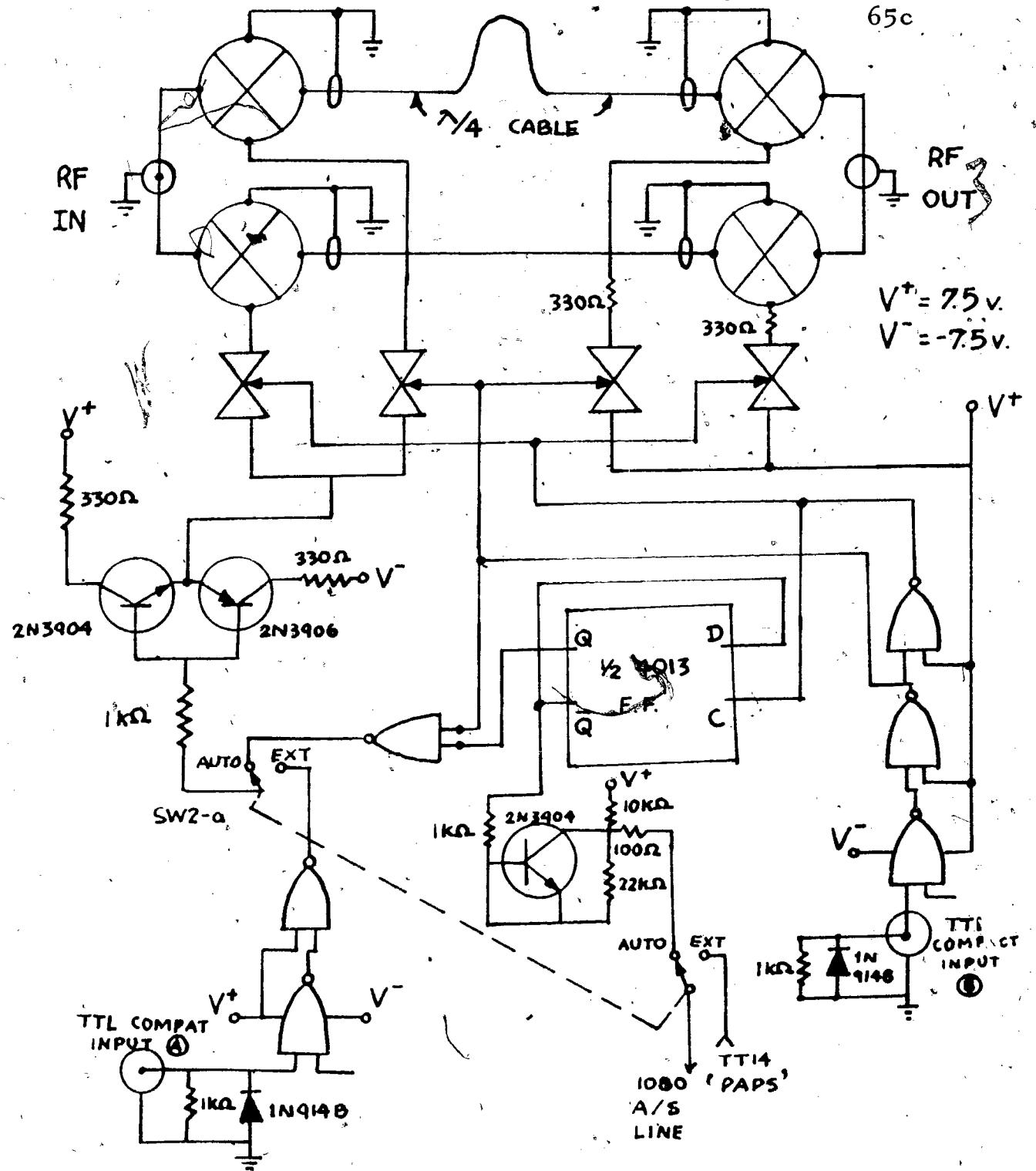
#### 4.A.III Decoupler Phase Control

The minimum requirement is for  $\pi/2$  phase shifting on the decoupler to provide spin-locking. In addition, it is highly desirable to provide an additional  $\pi$  phase shift so that "spin-temperature reversal" (110) may be performed on alternate polarizations. These shifts are provided by the unit shown in Figures 4.2 and 4.3. Doubled-balanced mixers (121) are used to provide  $\pi$  phase shift by polarity reversal, and  $\pi/2$  shift by switching in a quarter-wave cable as required. This unit is incorporated in the low power 60 MHz system as shown in Figure 4.1. Switch S1 disconnects the noise modulator, and substitutes the phase control unit in its place.

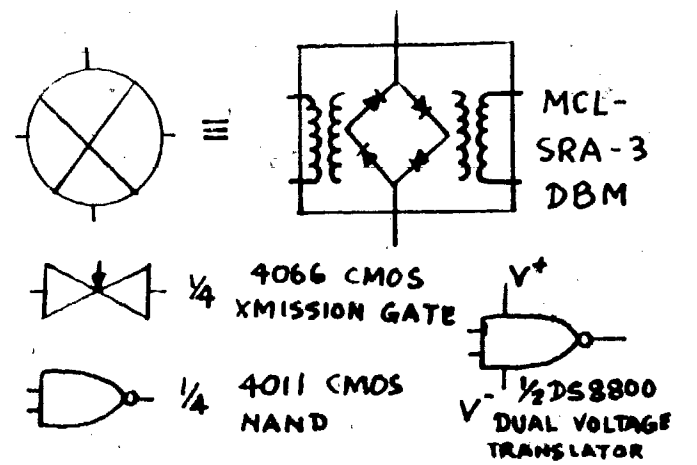
Figure 4.2 Block diagram of the phase shifter logic.

Figure 4.3 Phase shifter schematic.





TRUTH TABLE			TRUTH TABLE		
SW2	EXT	POS	SW2	AUTO	POS
A	B	∅	A	B	∅
1	0	0°	X	1	90°
1	1	90°	X	0	0°
0	0	180°	X	1	270°
0	1	270°	X	0	0°





Spin-temperature reversal is selected by operating switch S2. In this mode, the phase of the proton  $\pi/2$  pulse is changed by 180 degrees on alternate scans, and the computer Add/Subtract line alternated high and low respectively. This has the effect (110) of accumulating signals which originate from proton polarization, and cancelling all others. This is nearly imperative when studying polycrystalline samples of high anisotropy, since the high-Q probe gives a spurious ringing for about 100  $\mu$ sec which can otherwise cause severe baseline distortion.

#### 4.A.IV Control Logic

The spectrometer is normally controlled by a Nicolet 293 pulse controller. This is basically a series of six programmable timers, which can be controlled by the computer, together with some associated logic gates. A patch panel is provided to permit variable interconnections of these components. Our aim was to implement cross-polarization experiments with no changes to the Nicolet software (NTCFT version 1002) and with minimum repatching of the 293 patch panel, so that reversion to the standard configuration could be simply achieved.

These six timers are adequate for routine use only i.e. in normal single-contact or multi-contact cross-polarizations, proton  $T_1$ , and proton  $T_{1\rho}$  measurements. For carrying out

complicated pulse sequences e.g.  $^{13}\text{C}$   $T_1$  measurement, delayed decoupled experiment etc., we have built a programmable pulse generator in conjunction with the Nicolet 1080 computer to replace the Nicolet 293. The pulse generator is capable of producing almost any conceivable pulse sequence.

#### 4.B. Magic Angle Spinner (MAS)

In the later part of this project, a magic angle spinner for vacuum-sealed samples was built in this laboratory. The details of this design have been published (18) and won't be elaborated here. This spinner permits reliable spinning, up to 3 kHz of samples sealed in glass tubes. The glass tubes used are the Wilmad grade 507-PP NMR tubing.

#### 4.C. Preparation of Catalysts

##### 4.C.I MgO

Four kinds of MgO were prepared. MgO-(1) was made from  $\text{MgCO}_3 \cdot 3\text{H}_2\text{O}$  prepared by the co-precipitation of solutions of 3.6 M  $\text{Mg}(\text{NO}_3)_2 \cdot 6\text{H}_2\text{O}$  and 0.8 M  $\text{NaHCO}_3$  (123). The carbonate was then washed, dried and decomposed in vacuum at  $500^\circ\text{C}$  in a thin bed. The MgO-(1) so prepared has a surface area of  $115 \text{ m}^2/\text{g}$  and a bulk density of  $0.3 \text{ gm/cm}^3$ .

MgO-(2) was a  $\text{Ni}^{++}$ -doped MgO, so that the proton spin-lattice relaxation time ( $T_{1H}$ ) of the MgO-alcohol system would be shortened as the  $\text{Ni}^{++}$  act as paramagnetic centers. The MgO-(1) prepared above was soaked in a solution containing

$\text{Ni}(\text{NO}_3)_2 \cdot 6\text{H}_2\text{O}$  to provide a concentration of 10 ppm of  $\text{Ni}^{++}$  on  $\text{MgO}$ . This  $\text{MgO}$ -(2) was then dried in an oven at  $110^\circ\text{C}$  with constant stirring, and then calcined at  $500^\circ\text{C}$  for 20 hours in air. The  $\text{MgO}$ -(2) has a surface area of  $115 \text{ m}^2/\text{g}$  and a bulk density of  $0.2 \text{ gm/cm}^3$ .

$\text{MgO}$ -(3) was prepared from the decomposition of  $\text{Mg}(\text{OH})_2$  (reagent grade from Matheson, Coleman and Bell) in vacuum at  $300^\circ\text{C}$  for 20 hours in a thin bed.  $\text{MgO}$ -(3) has a surface area of  $220 \text{ m}^2/\text{g}$  and a bulk density of  $0.6 \text{ gm/cm}^3$ .

$\text{MgO}$ -(4) was prepared from  $\text{MgC}_2\text{O}_4 \cdot 2\text{H}_2\text{O}$ , obtained from the co-precipitation of solutions of  $0.5 \text{ M}$   $(\text{NH}_4)_2\text{C}_2\text{O}_4 \cdot \text{H}_2\text{O}$  and  $3.5 \text{ M}$   $\text{Mg}(\text{NO}_3)_2 \cdot 6\text{H}_2\text{O}$ . The oxalate was dried and then decomposed at  $300^\circ\text{C}$  in vacuum, after which it was further heated at  $400^\circ\text{C}$  in air. This further calcination was deemed necessary when one batch of  $\text{MgO}$ -(4) was found contaminated with some un-decomposed impurities.  $\text{MgO}$ -(4) has a surface area of  $200 \text{ m}^2/\text{g}$  and a bulk density of  $0.6 \text{ gm/cm}^3$ .

#### 4.C.II $\text{WO}_3$

There exist several commercial specimens and laboratory preparations of  $\text{WO}_3$ . The usual preparations of  $\text{WO}_3$  consist of calcination of ammonium paratungstate at  $500^\circ\text{C}$  (62, 63), decomposition of tungstic acid gel (122) etc. We have adopted Davis' method of obtaining  $\text{WO}_3$  (65).

To a 0.63 M solution of ammonium metatungstate (Koch-Light 99.9%) was added dropwise concentrated hydrochloric acid until precipitation was complete. The yellow tungtic acid was washed with water ten times and filtered, then dried at 110°C. This was then followed by decomposition at 300°C in a thin bed under vacuum for 4 hours. The  $WO_3$  thus prepared was bright yellow with a surface area of 33m<sup>2</sup>/g and a bulk density of 1.2 gm/cm<sup>3</sup>. We have tried other ammonium tungstates (e.g. ammonium paratungstate from Matheson, Coleman and Bell), or using concentrated nitric acid in this preparation. Either the tungstates have low solubility in water, or the prepared  $WO_3$  has a very low surface area (<10 m<sup>2</sup>/g), which is not suitable for surface studies, utilizing NMR.

The  $WO_3$  prepared above tended to turn green upon storage, so we treated the  $WO_3$  in  $O_2$  at 300°C for 2 hours and then degassed before introduction of the absorbate. The  $WO_3$  so treated always returned to the original yellow color.

#### 4.D.I. Experiments

All surface area determinations were done by the BET method using  $N_2$  at 77°K.

Samples of the different kinds of MgO and  $WO_3$  for static studies were loaded into 12 mm o.d. NMR tubes to a height of about 2 cm. For the MgO samples, they were slowly heated to

500°C in vacuum for 22 hours, for out-gassing and removal of surface water. Measured amounts of the desired adsorbate were then allowed to adsorb onto the oxide from gas phase at room temperature. The samples were then sealed off and allowed to stand for several days at room temperature before NMR measurements. Some samples were re-run after a period of 2-3 months to check for reproducibility which was always found to be excellent. Samples for magic-angle spinning were of about 1.5 cm in depth in a 5 mm o.d. NMR tube, and were treated in the same manner. In the case of alcohols having less than 20 mmHg vapor pressure at room temperature, a different technique was used. Measured samples of adsorbent and adsorbate were degassed and sealed in opposite ends of a two compartment tube. The two compartments were then brought into communication by breaking a breakseal, and the whole apparatus placed in an oven at a temperature (usually 50 - 110°C) at which the adsorbate had a vapor pressure of 10 to 100 mmHg. The apparatus was left in the oven for some hours and then allowed to cool. In no case was any liquid alcohol visible after this treatment, and since the amount of gas phase alcohol would be negligible, even at the vapor pressure of the liquid, we assume that essentially all of the alcohols were adsorbed on the solid sample.

The  $WO_3$  samples were prepared the same way except in the pre-treatment procedure. Two degassing time periods were used:  $WO_3$ -(1) for 2 hours and  $WO_3$ -(2) for 19 hours, both were out-gassed at 300°C. After the degassing procedure, both

WO<sub>3</sub>-(1) and WO<sub>3</sub>-(2) were activated with O<sub>2</sub> (ca. 200 mmHg) at 300°C, for 2.5 hours. Samples were then degassed again for 0.5 hour at the same temperature and then the desired adsorbate introduced.

In order to investigate the conversion products of alcohols on MgO and WO<sub>3</sub>, another series of experiments with the same samples were undertaken. At least three samples having different coverages of alcohols on MgO and WO<sub>3</sub> from each preparation were raised to successively higher temperatures. This was done by placing the sealed NMR sample tubes inside a tube furnace (170-180°C, 300-320°C, 485-500°C) for three hours. They were then cooled and left at room temperature for several days before NMR measurements.

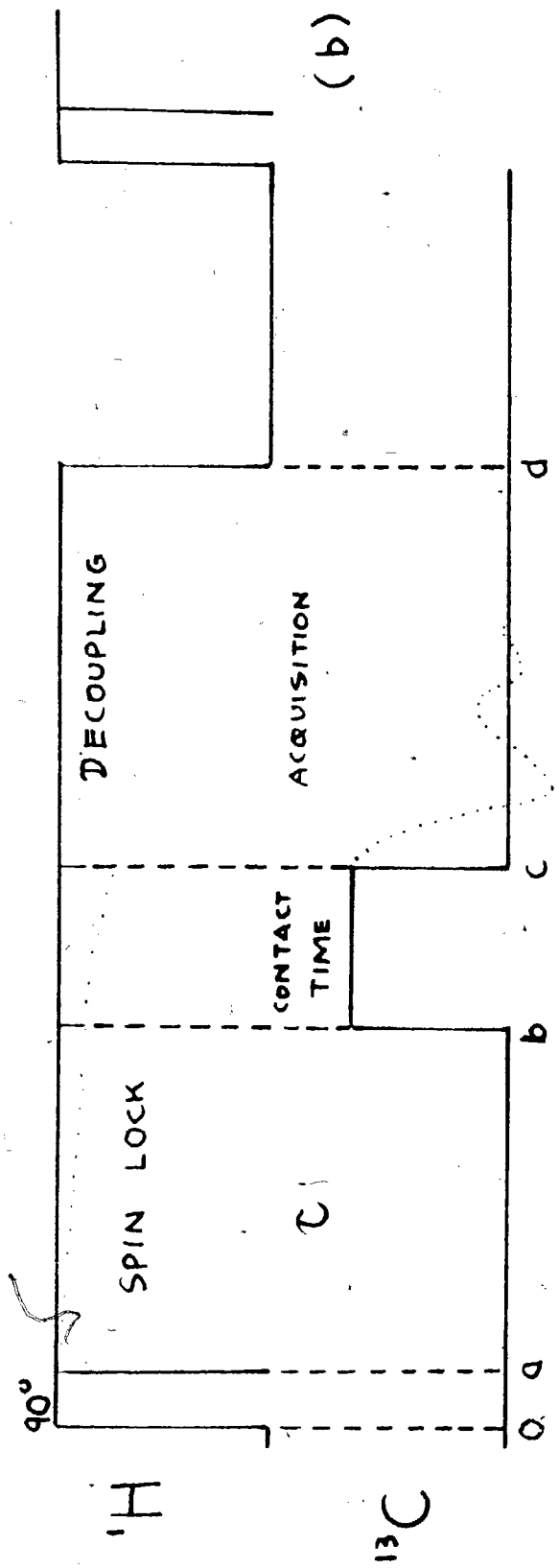
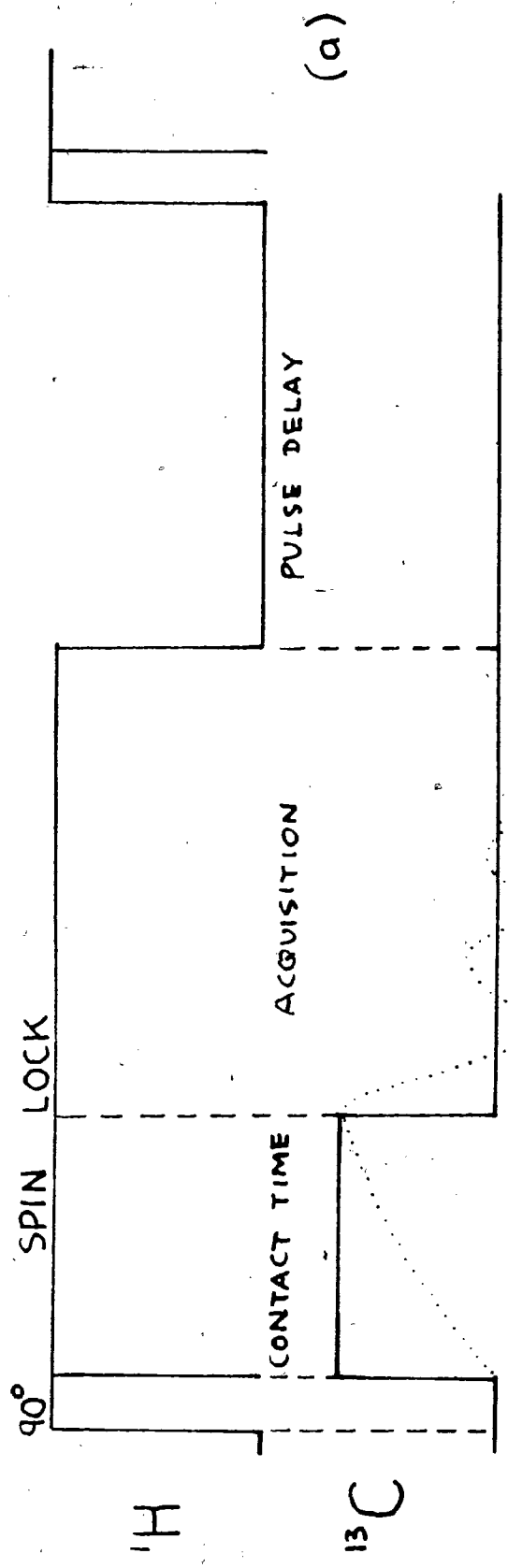
#### 4.D.II NMR Measurements

All <sup>13</sup>C NMR spectra (single-pulse, CP, MAS-CP) were measured at 15.08 MHz on the modified TT-14 spectrometer described earlier. Single-contact Hartmann-Hahn cross-polarization was used with radiofrequency field strengths ranging from 40 KHz ( $\delta H_1/2\pi$ ) to 70 KHz. "Spin-temperature reversal" was used on alternate polarization, so that observed signals arise only via cross-polarization from protons.

The pulse sequence used was shown in Figure 4.4. The proton pulse is typically 5  $\mu$ sec to 7.5  $\mu$ sec at field strengths varying from 70 KHz to 40 KHz. Contact time is either

Figure 4.4 Pulse Sequence.

- (a) Pulse diagram of the single-contact cross-polarization experiment.
- (b) Pulse diagram for the proton  $T_{1\rho}$  relaxation experiment.





1.5 or 2 msec. Proton  $T_1$  were measured for all the MgO-methanol systems and for some treated at elevated temperatures. Proton  $T_1$  was also measured for some ethanol-MgO systems. These were measured by the conventional  $180^\circ - \tau - 90^\circ$  sequence at 70 kHz field strength. The pulse delay in the single-contact cross-polarization experiment was then set at about  $1.5 T_{1H}$ . For systems with extremely short  $T_{1H}$ , we set the pulse delay at about 0.3 sec, so that no damage may occur to the probe. The same procedures were applied to alcohol- $WO_3$  systems.

Proton spin-lattice relaxation times in the rotating frame ( $T_{1\rho}$ ) were measured for some selected methanol MgO samples in which 60%  $^{13}C$ -enriched methanol was used. The pulse sequence for these experiments was shown in Figure 4.4. In the sequence shown, one sees that a relaxation period (a to b) of length  $\tau$  is inserted between the beginning of  $^1H$  spin-lock condition (at a) and the beginning of the contact period (at b) (at which time the Hartmann-Hahn condition is established). During the period  $\tau$  rotating-frame  $^1H$  spin-lattice relaxation occurs, hence, by observing the  $^{13}C$  intensity at the end of the contact period as a function of  $\tau$ , one can obtain a measure of  $T_{1\rho}$ , for those protons involved in cross-polarization with  $^{13}C$ .

The cross-polarization times ( $T_{CH}$ ) were measured for the same samples for which the proton  $T_{1\rho}$  were measured. This was

done by observing the resulting  $^{13}\text{C}$  signal when the contact times were varied.

U Some of the spectra shown in this dissertation were hand-traced from the original. Usually, free induction decay signals were stored on the Nicolet 294 disk accessory with Memorex hard disks, and spectra could be plotted on ordinary 8-1/2" x 11" papers after Fourier transformation. However, we suffered several disk-drive crashes and most of the disk memory was wiped out.

#### 4.E... Estimation of Errors and Experimental Difficulties

Sample preparations were carried out with a conventional mercury diffusion pumped vacuum line. The sample preparation area had a gas burette calibrated by weighing empty and full of distilled water. The manometer was of volume compensating type and allowed for a measurable change in volume of  $30\text{cm}^3$ . The manometer was mercury filled. Height differences in the manometer were measured with a meter ruler and accurate to  $\pm 0.3\text{mm}$ . Pressure readings were then accurate to  $\pm 0.6\text{mm}$  of Hg.

Volumes of those parts of the vacuum rack calibrated by helium and nitrogen expansion were accurate to  $\pm 0.1\%$ . Volumes of sample tubes were determined by nitrogen expansion to  $\pm 0.2\%$ . In order to save time in measuring the volume of each sample tube, several were made at once with the same external dimensions, then the volume was measured by nitrogen expansion.

The difference was found to be within  $0.1\text{cm}^3$  which was taken as the error in measurement in subsequent calculations. The amount of gas adsorbed on a sample was calculated from the pressure drop on allowing the gas into the sample tube containing the adsorbent. (All gases were assumed to be ideal.) Amounts of gas adsorbed were then accurate to about  $\pm 1\%$  for low coverages and  $< 10\%$  for high coverages.

Since the adsorbents ( $\text{MgO}$  and  $\text{WO}_3$ ) were not stored under an inert atmosphere inside a dessicator, surface area was measured for each individual sample after treatments (degassing or activating with oxygen). It was found that there was little variation in the surface area obtained even over a storage period of more than a year. The error in the surface area determination was estimated to be about  $\pm 1\%$ .

The proton relaxation data were measured by least squares fitting the amplitudes,  $A$  (F.I.D. intensity or the height of Fourier transformed spectrum) as a function of delay time  $\tau$ , according to:

$$[4.1] \quad A = a + b \exp(-\tau/T_1) \quad a, b = \text{constants}$$

Points to fit the eqn. [4.1] were measured with an error of from 5 to 15%, and usually 8 to 12 points were used to fit the exponential.

Standard deviations of fit were generally of the order of 5%, with the standard deviation of the slope of the line being of the same order.

The incurred error in the fit does not cause great problem in this dissertation because the purposes of these measurements are, (i) to obtain a general relaxation mechanism; (ii) to detect paramagnetic contribution to the relaxation; (iii) to obtain a rough estimate of the optimum repetition rate in the  $^{13}\text{C}$  CP experiments. All three purposes do not require an exact measurement of  $T_{1H}$ .

$T_{1F}$  and  $T_{CH}$  measurements are to ensure that the mixing time (of  $^1\text{H}$  or  $^{13}\text{C}$ ) is not too long or short respectively. Consequently they only serve as a guideline for the CP experiments, and exact values are not required.

Signal/noise problems were common in this study. The use of  $^{13}\text{C}$ -enriched adsorbates enhances the signal/noise ratio, however they make the edge of the chemical shift powder pattern less sharp. For ordinary adsorbates, the powder pattern obtained is sharper, but it requires a much longer time for data acquisition. Since the signal/noise ratio is proportional to the square root of number of contacts, it would take 4 times the number of contacts to obtain a signal that doubles the original signal/noise. One would encounter problems like field drifts

( $\pm 1$  ppm) and a subsequent loss of lock if the experiment was run too long (in excess of 24 hours).

For the chemical shift measurements in the  $^{13}\text{C}$  CP/MAS experiments, the error is estimated to be less than  $\pm 1$  ppm. The errors may arise from a slight field drift ( $< 1$  ppm), residual linewidth (ca. 1 ppm) (from magic-angle missetting or overlapping of resonances (18)).

#### 4.F. Reagents

The methanol used in these experiments was of spectroscopic grade from Fisher Scientific, and was stored over molecular sieve type 4A. The ethanol used was double distilled from 95% ethanol over magnesium and stored over molecular sieve types 3A and 4A. The isopropanol, n-butanol and acetone were from Fisher Scientific (suitable for electronic use), and were stored over molecular sieve types 3A and 4A. All the alkane-diols and acetaldehyde were from Matheson, Coleman and Bell. They were distilled at reduced pressure and stored over molecular sieve 4A prior to use. Carbon dioxide used in some experiments was from Canadian Liquid Air Ltd.

$^{13}\text{C}$ -enriched methanol and  $\text{CO}_2$  were obtained from Merck, Sharp and Dohme Isotopes and were vacuum distilled before use

Two 90%  $^{13}\text{C}$ -enriched ethanols, ethanol-1- $^{13}\text{C}$  and ethanol-2- $^{13}\text{C}$  were prepared from their respective 90%  $^{13}\text{C}$ -enriched sodium acetate precursor from MSD Isotopes, according to standard procedure (124).

### 5.A.1. Methanol and CO<sub>2</sub> Adsorption Isotherms

In order to observe the difference in the surface characteristics of the four preparations of MgO, adsorption isotherms were done for methanol and CO<sub>2</sub> at room temperature, as shown in Figures 5.1, 5.2 and 5.3. For those data in Figures 5.1 and 5.2, the MgO's were degassed at 500°C, but at 300°C for those in Figure 5.3.

Essentially, all isotherms show type II adsorption characteristics. The methanol adsorption isotherms are basically the same for all preparations of MgO. There is a slight deviation for MgO-(4) whose isotherm lies slightly higher than the others.

The CO<sub>2</sub> isotherms (Figures 5.2 and 5.3) show rather more variation with preparation and degassing conditions. For both methanol and CO<sub>2</sub>, a substantial chemisorbed population is achieved at lower pressure than one was able to use, and a more loosely-bound population is observed which increases with pressure.

Quantitatively, it can be concluded that the chemisorption level on MgO is 6-7  $\mu\text{mole}/\text{m}^2$  for methanol and 1-2  $\mu\text{mole}/\text{m}^2$  for CO<sub>2</sub>. Since CO<sub>2</sub> is slightly acidic, presumably it will adsorb on the basic sites on the MgO surface. Thus, if

Figure 5.1 Adsorption isotherms of methanol on all preparations of MgO at room temperature. Samples degassed at 500°C.

Figure 5.2 Adsorption isotherms of CO<sub>2</sub> on all preparations of MgO at room temperature. Samples degassed at 500°C.

Figure 5.3 Adsorption isotherms of CO<sub>2</sub> on all preparations of MgO at room temperature. Samples degassed at 300°C.

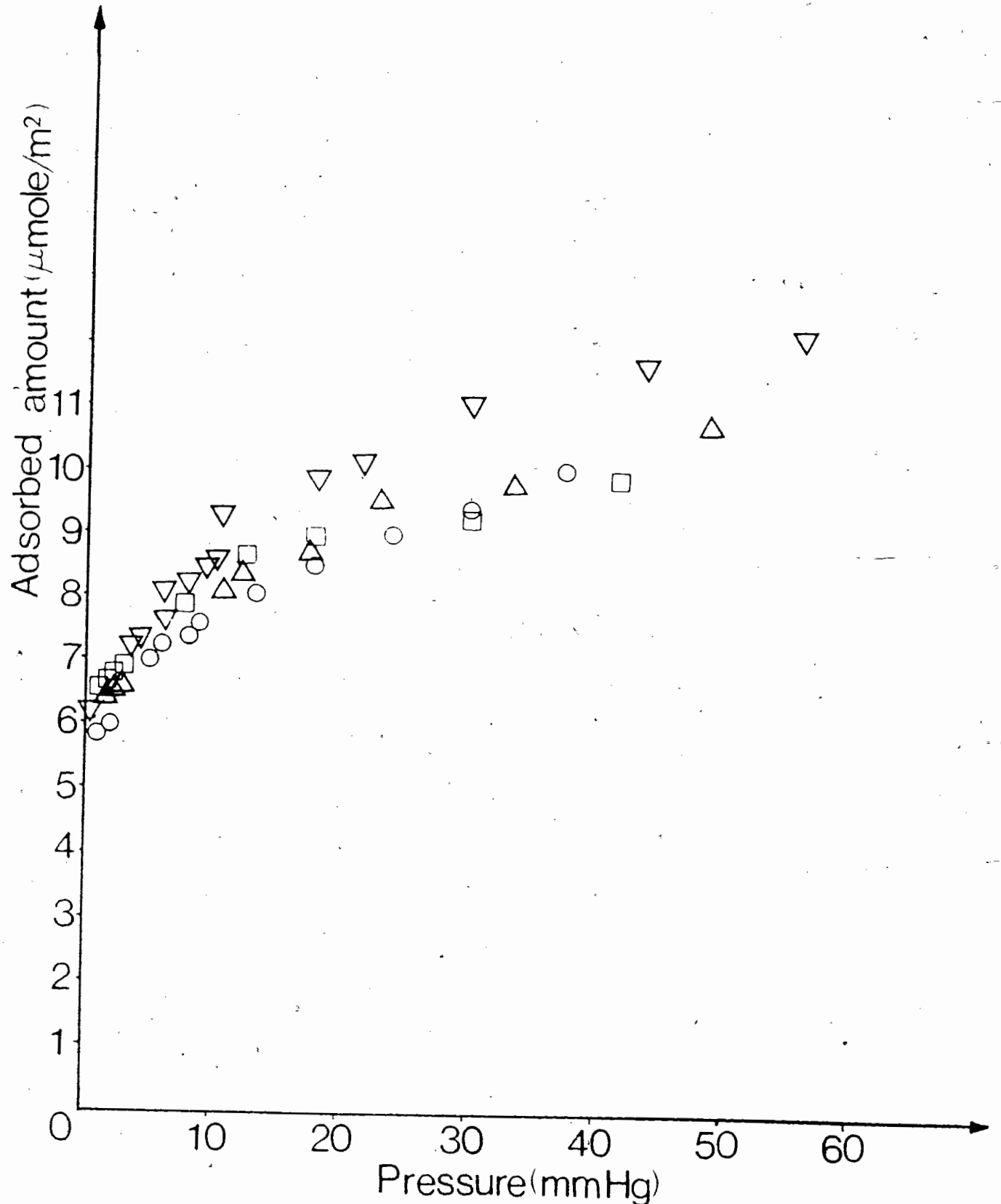
Legend: ○: MgO-(1)

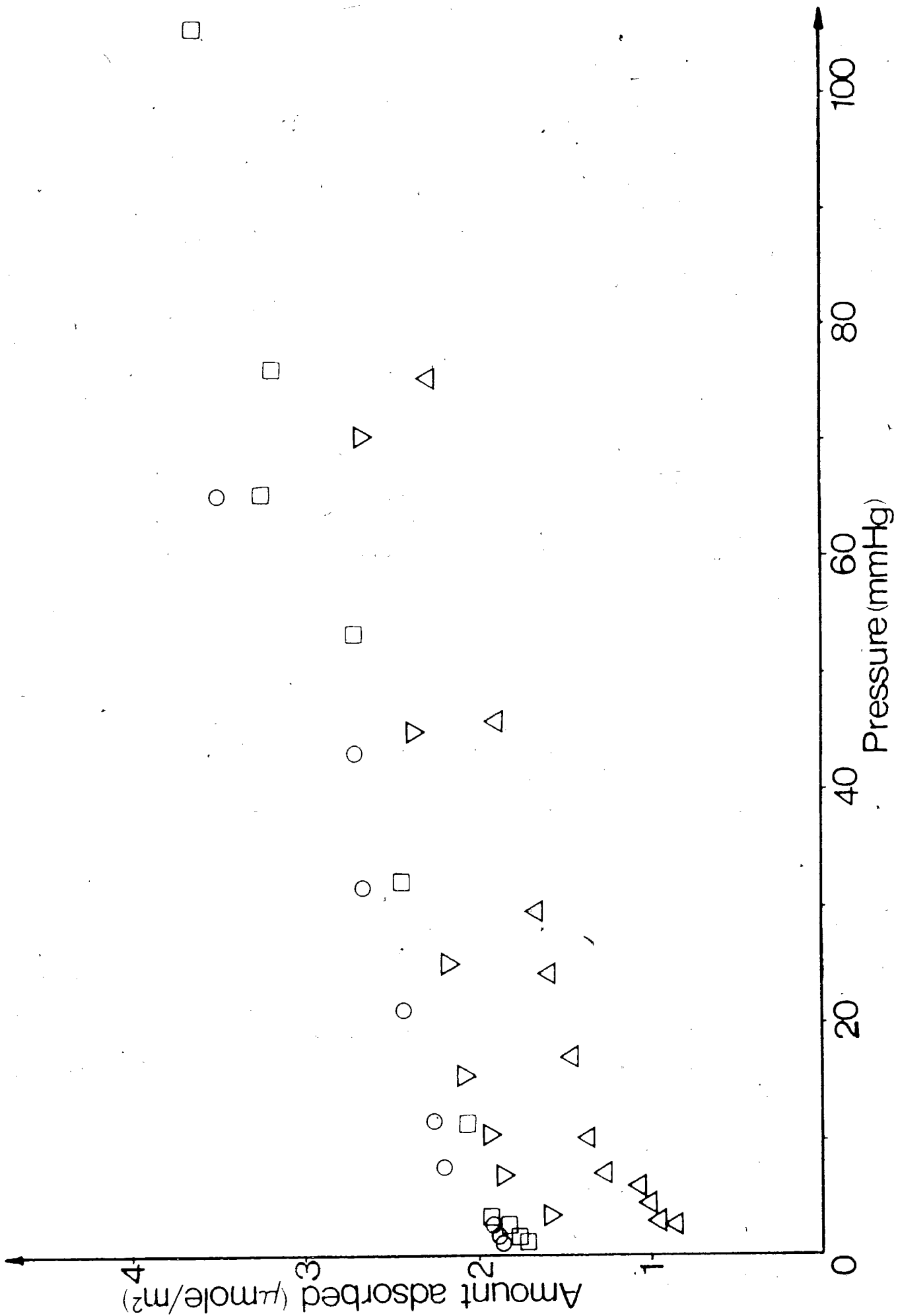
□: MgO-(2)

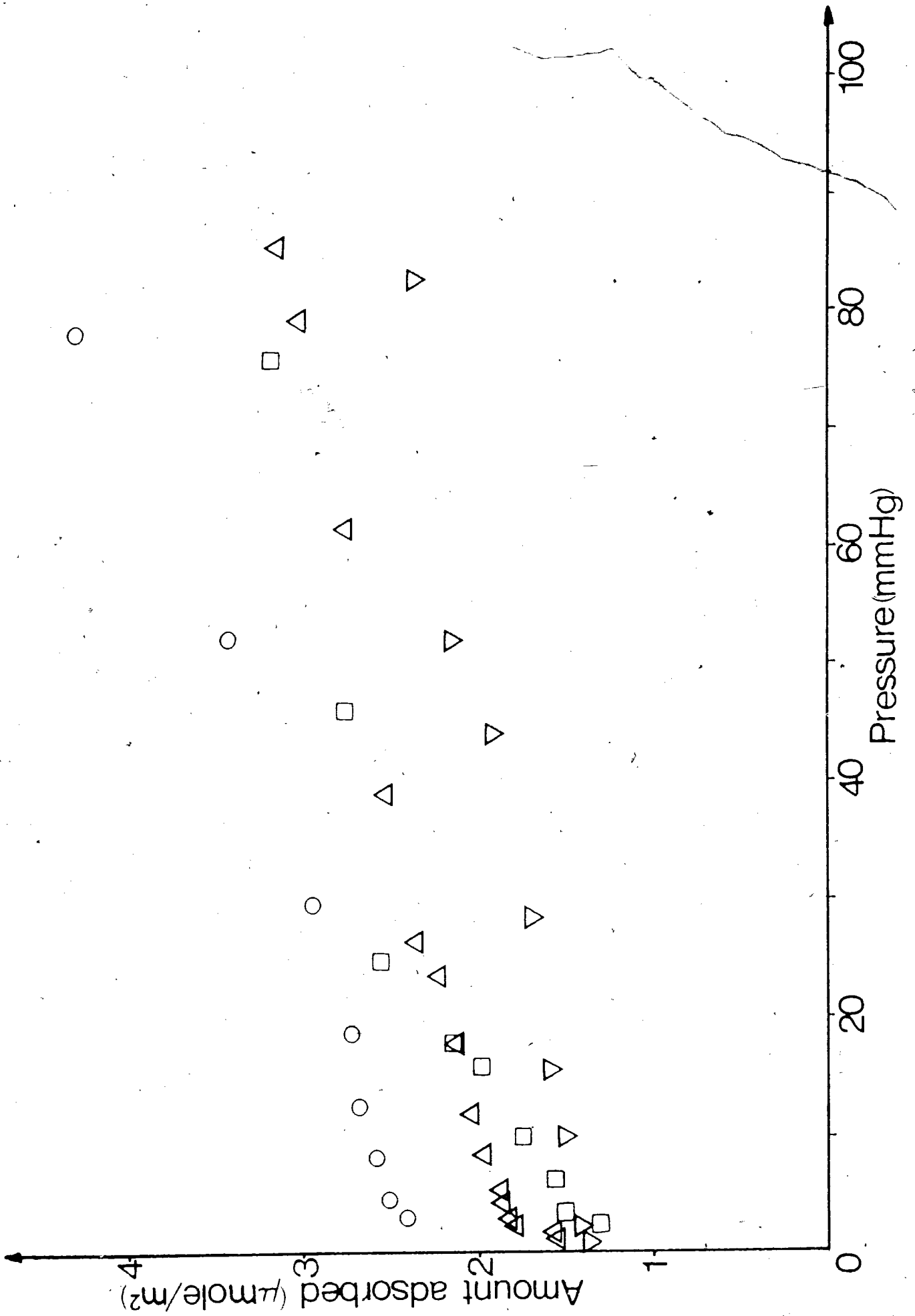
△: MgO-(3)

▽: MgO-(4)









methanol and  $\text{CO}_2$  both adsorb on the same site, then only one-quarter of the active sites are basic. However, this estimate of basic sites is 10 times bigger than that reported by indicator titration (32a). To investigate further into this aspect, the  $^{13}\text{C}$  NMR spectra were measured for 90%  $^{13}\text{C}$ -enriched  $\text{CO}_2$  adsorbed on all MgO's. The static  $^{13}\text{C}$  CP spectra are shown in Figure 5.4.

Magic-angle spinning (Figure 5.18) for  $\text{CO}_2$  on MgO-(3) reveals a single peak at an isotropic shift of 161.6 ppm. This is certainly consistent with a bicarbonate structure (or a carbonate species which is in close proximity to surface -OH groups). One finds, for example,  $\text{NH}_4\text{HCO}_3$  at 162.5 ppm and  $\text{BaCO}_3$  at 169.5 ppm.

MAS spectroscopy, using  $90^\circ$  pulses on  $^{13}\text{C}$  rather than cross-polarization yields a much weaker spectrum with the same chemical shift. This indicates that most of the adsorbed  $\text{CO}_2$  must be near enough to a surface proton for effective cross-polarization.

For bicarbonate formation on the surface the following mechanism is proposed:

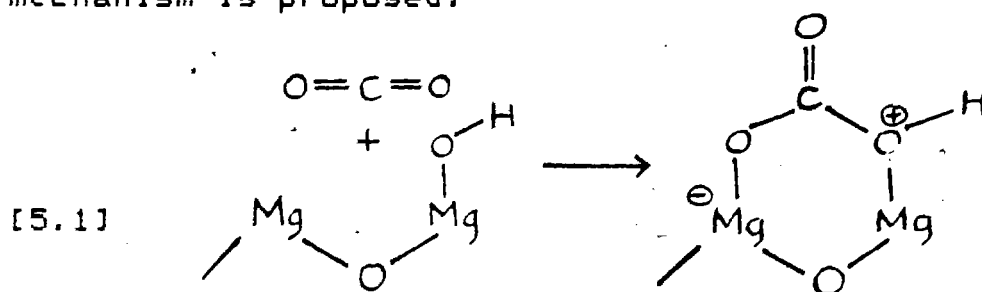
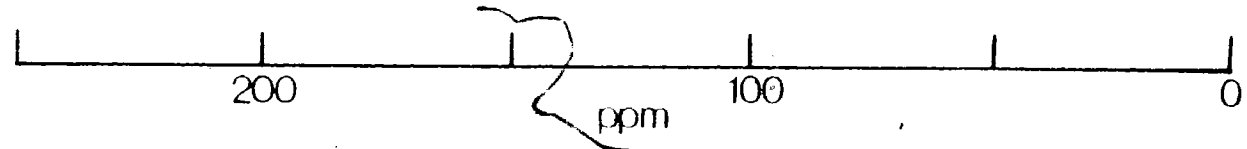
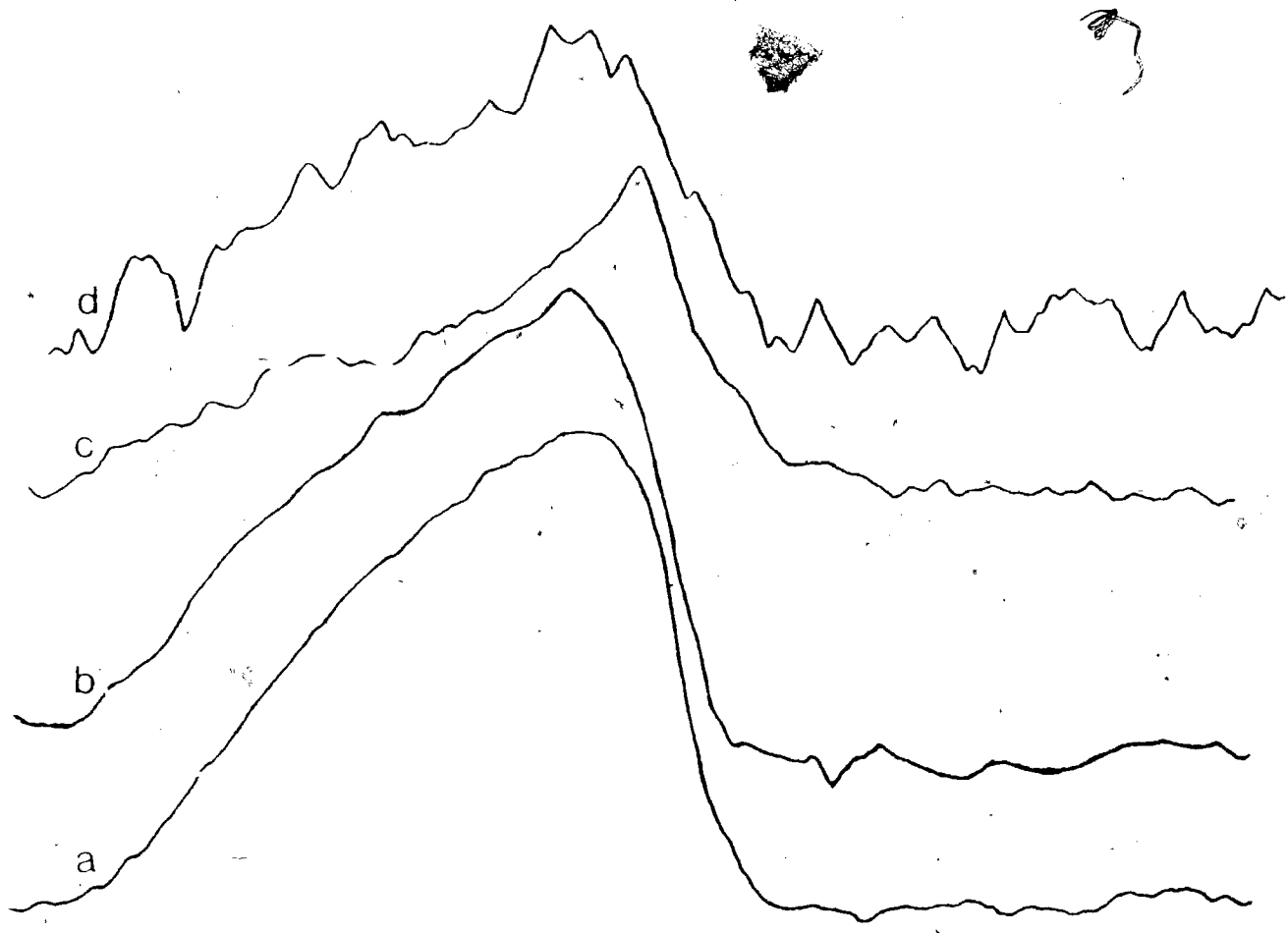


Figure 5.4  $^{13}\text{C}$  CP spectra of 90%  $^{13}\text{C}$ -enriched  $\text{CO}_2$  on all preparations of  $\text{MgO}$ .  
RF field = 40 kHz. Contact time = 2 msec.  
Repetition rate =  $1 \text{ sec}^{-1}$ . 10,000 contacts.  
(a)  $2.70 \mu\text{mole/m}^2$  of  $\text{CO}_2$  on  $\text{MgO}$ -(1)  
(b)  $2.46 \mu\text{mole/m}^2$  of  $\text{CO}_2$  on  $\text{MgO}$ -(2)  
(c)  $2.09 \mu\text{mole/m}^2$  of  $\text{CO}_2$  on  $\text{MgO}$ -(3)  
(d)  $2.98 \mu\text{mole/m}^2$  of  $\text{CO}_2$  on  $\text{MgO}$ -(4);  
95,000 contacts.  
All samples were degassed at  $500^\circ\text{C}$  for  
22 hours.



This simple mechanism would indicate that the  $\text{CO}_2$  adsorption occurs with participation of surface  $-\text{OH}$  groups. This would explain partly why the equilibrium adsorption level of methanol is 4 times bigger than that of  $\text{CO}_2$ . Since there are only  $3 \mu\text{mole}/\text{m}^2$  of surface  $-\text{OH}$  groups on  $\text{MgO}$  under the degassing conditions at  $500^\circ\text{C}$  (125), and there are about  $18 \mu\text{mole}/\text{m}^2$  of  $\text{Mg}^{2+}$  on the (100) plane of  $\text{MgO}$  surface, these will give ample sites where the methanol could adsorb. Therefore, it could be concluded that both methanol and  $\text{CO}_2$  adsorb onto the  $\text{Mg}^{2+}$  sites on the  $\text{MgO}$  surface, but  $\text{CO}_2$  requires an additional neighbouring surface  $-\text{OH}$  group.

As the degassing temperature is lowered to  $300^\circ\text{C}$ , one would expect the surface  $-\text{OH}$  groups to increase, thus the  $\text{CO}_2$  adsorption isotherm on  $\text{MgO}$ 's at room temperature would increase. However, this is the case only for  $\text{MgO}$ -(1) and  $\text{MgO}$ -(2), while  $\text{MgO}$ -(3) and -(4) show a decrease. This might indicate nearly complete coverage of the surface by  $-\text{OH}$  groups, for the  $\text{MgO}$ -(3) and -(4). This would inhibit  $\text{CO}_2$  adsorption if  $\text{CO}_2$  requires adjacent  $\text{Mg}$  and  $\text{MgOH}$  sites as proposed above.

#### 5.A.II. Measurements of Relaxation Times and Cross-Polarization Times

Proton spin-lattice relaxation times ( $T_{1H}$ ) were measured for all methanol- $\text{MgO}$  samples before  $^{13}\text{C}$  CP NMR spectra were taken. These data are important, as mentioned before, to

determine the optimum repetition period, which is about  $1.25 T_{1H}$ .  $T_{1H}$  were also measured for some selected samples with which higher temperature studies were done, as shown in Table 5.1. A consistent trend toward faster relaxation at high coverage is found. This is to be expected if dipole-dipole interaction is the major contribution to relaxation, as is the case for most adsorbed systems (66, 114, 126). The  $r^{-3}$  dependence of this dipolar interaction would obviously lead to faster relaxation at higher coverage. Possible changes in motional frequencies, however, preclude a quantitative assessment of this.

It will be noted that there is some variation of relaxation time between the various oxide preparations. This might arise either from varying levels of paramagnetic contaminants, or from variations in the motional state of the adsorbate, arising from differences in surface chemistry. The latter explanation is favored, as it is difficult to understand the coverage dependence of relaxation rate, if surface paramagnets determine the relaxation process.

In Table 5.2, the  $T_{1H}$  values are shown for some ethanol-MgO systems. The same trend is observed as in the methanol-MgO systems, i.e. faster relaxation at higher coverage. The same variation in relaxation times between the various MgO preparations is also observed. These observations can be



TABLE 5.1

$T_{1H}$  of all Methanol-MgO Systems  
and Selected Samples treated at Higher Temperature

	Coverage ( $\mu\text{mole}/\text{m}^2$ )	$T_{1H}$ (sec) RT	$T_{1H}$ (sec) 170°C	$T_{1H}$ (sec) 320°C	$T_{1H}$ (sec) 500°C
MgO-(1)	2.09*	0.55			
	3.63*	0.31			
	4.31*	0.50	0.56	0.51	0.38
	5.92	0.15	0.21	0.24	0.10
	7.04	0.16	0.25	0.19	0.13
	8.42	0.14	0.20	0.21	0.02
MgO-(2)	2.21*	0.15			
	3.37*	0.22	0.36	0.32	0.27
	4.48*	0.05			
	4.97*	0.12			
	6.23	0.05	0.06	0.10	0.02
	7.24	0.08			
	8.43	0.06	0.06	0.06	0.24
	9.44	0.06			
MgO-(3)	1.22*	0.39			
	2.79*	0.19			
	4.55*	0.07	0.12	0.18	0.07
	5.70	0.04	0.09	0.08	0.08
	7.73	0.04	0.08	0.07	0.11
	8.64	0.05			

Table 5.1 (continued)

MgO-(4)	2.99*	0.82
	4.11*	0.83
	4.98*	0.83
	6.21	0.68
	7.07	0.62
	8.18	0.51

\* denotes 60%  $^{13}\text{C}$ -enriched methanol was used

Table 5.2

Proton  $T_1$  Data of some Ethanol-MgO Systems

	Coverage ( $\mu\text{mole/m}^2$ )	Proton $T_1$ (sec)
MgO-(1)	4.21	0.25
	5.14	0.15
	5.88	0.18
	6.91	0.17
	8.01	0.14
MgO-(2)	4.92	0.06
	5.81	0.06
	6.14	0.11
	7.22	0.08
	8.23	0.10
MgO-(3)	4.19	0.10
	5.42	0.06
	6.11	0.09
	7.19	0.02
MgO-(4)	4.02	0.83
	4.93	0.83
	5.79	0.72
	8.00	0.60

attributed to the reasons given above (for the methanol-MgO systems).

In Table 5.3,  $T_{1H}$ ,  $T_{1\rho}$ , and  $T_{CH}$  are shown for some selected methanol-MgO systems in which 60%  $^{13}C$ -enriched methanol was used. These were measured at a field strength of 40 kHz for  $^1H$  and  $^{13}C$ . Proton  $T_{1\rho}$  in general is much shorter than the  $T_{1H}$  for the same system, except for one case in MgO-(1). For MgO-(1), the  $T_{1\rho}$  data show non-exponential relaxation, which can be resolved into a sum of two exponentials whose decay times are given in the table.

The general shortness of  $T_{1\rho}$ , relative to  $T_{1H}$  for the protons, indicates considerable low-frequency motion in the adsorbed layer. It cannot be accounted for by rapid methyl group rotation.

However, it should be noted that the measurement of proton  $T_{1H}$  and  $T_{1\rho}$  is not selective, and the measured value is the bulk value of the methyl protons of the methanol, and the protons on the surface -OH groups. The selectivity is masked because of the rapid spin-diffusions among protons during the contact time (in the order of msec). This is certainly the case when the paramagnetic contaminants on the surface are acting as a relaxation sink.

Table 5.3  
 $T_{1H}$ ,  $T_{1P}$  and  $T_{CH}$  for some  
 Selected Methanol-MgO Systems

	Coverage ( $\mu\text{mole/m}^2$ )	$T_{1H}$ (sec)	$T_{1P}$ (msec)	$T_{CH}$ (msec)
MgO-(1)	2.09	0.55	12,66	0.11
	3.63	0.31	13,380	0.13
MgO-(2)	2.21	0.15	47	0.12
	4.48	0.05	7	0.21
MgO-(3)	1.22	0.39	47	0.12
	2.79	0.19	21	0.11
MgO-(4)	2.99	0.82	25	0.14
	4.98	0.83	11	0.10

The cross-polarization times are short and relatively consistent for all samples. Clearly, this indicates a substantial static component of the intramolecular  $^1\text{H}$ - $^{13}\text{C}$  dipolar coupling.

Figures 5.5 show the  $^{13}\text{C}$  CP NMR spectra of a typical methanol-MgO system as the contact times are varied. At very short contact time, the  $^{13}\text{C}$  resonance is "split" in the middle showing that some of the adsorbed species for which the methyl rotation axis lies along the magic-angle do not receive adequate cross-polarization (127). Contact times are varied up to 2 msec, at which value the  $^{13}\text{C}$  CP experiments are usually performed. No dipolar oscillations (7, 92, 127, 128) were observed at short contact times. Plots of  $^{13}\text{C}$  signal intensity vs contact time are shown in Figures 5.6 to 5.9 for each preparation of MgO.

Generally, the contact times used in the  $^{13}\text{C}$  CP experiments (1.5 or 2 msec) are much greater than the longest  $T_{\text{CH}}$  in all the methanol-MgO systems, so that the carbons are cross-polarized to an equal extent. Also the contact time is much shorter than the  $T_{1\rho}$ , so that the spin-locked proton magnetization does not decay significantly within the contact period. This permits good quantitative  $^{13}\text{C}$  CP analysis of the methanol-MgO systems.

Figure 5.5  $^{13}\text{C}$  CP spectra of  $2.79 \mu\text{mole/m}^2$  of 60%  $^{13}\text{C}$ -enriched methanol on  $\text{MgO-(3)}$  at different contact times. R.F. field = 40 kHz. Repetition rate =  $2.5 \text{ sec}^{-1}$ . 512 contacts for all spectra. All spectra are normalized. Contact times ( $\mu\text{sec}$ ):

(a) 30; (b) 100; (c) 150; (d) 200;  
(e) 250; (f) 500; (g) 750; (h) 1000;  
(i) 1250; (j) 1500; (k) 1750; (l) 2000.

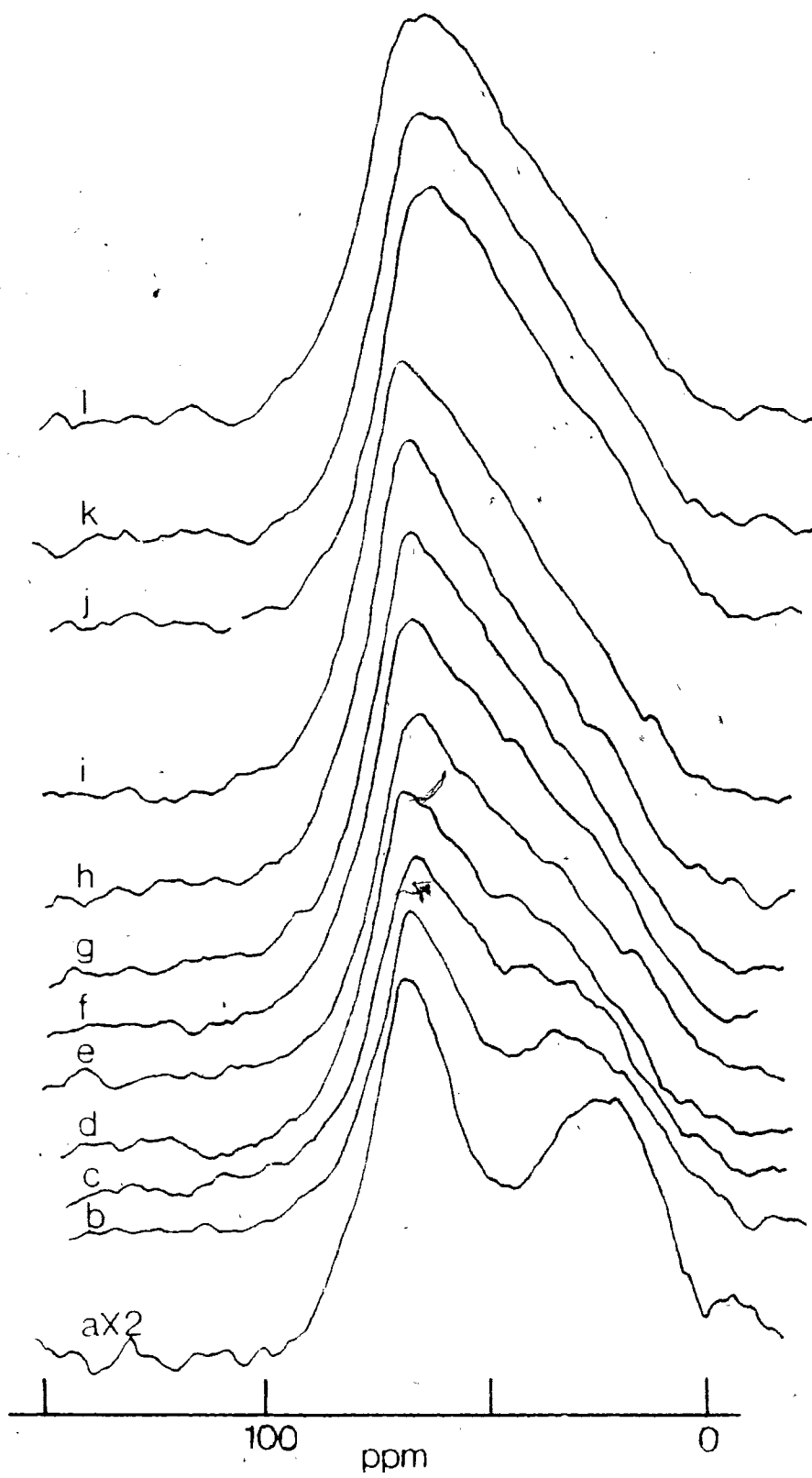


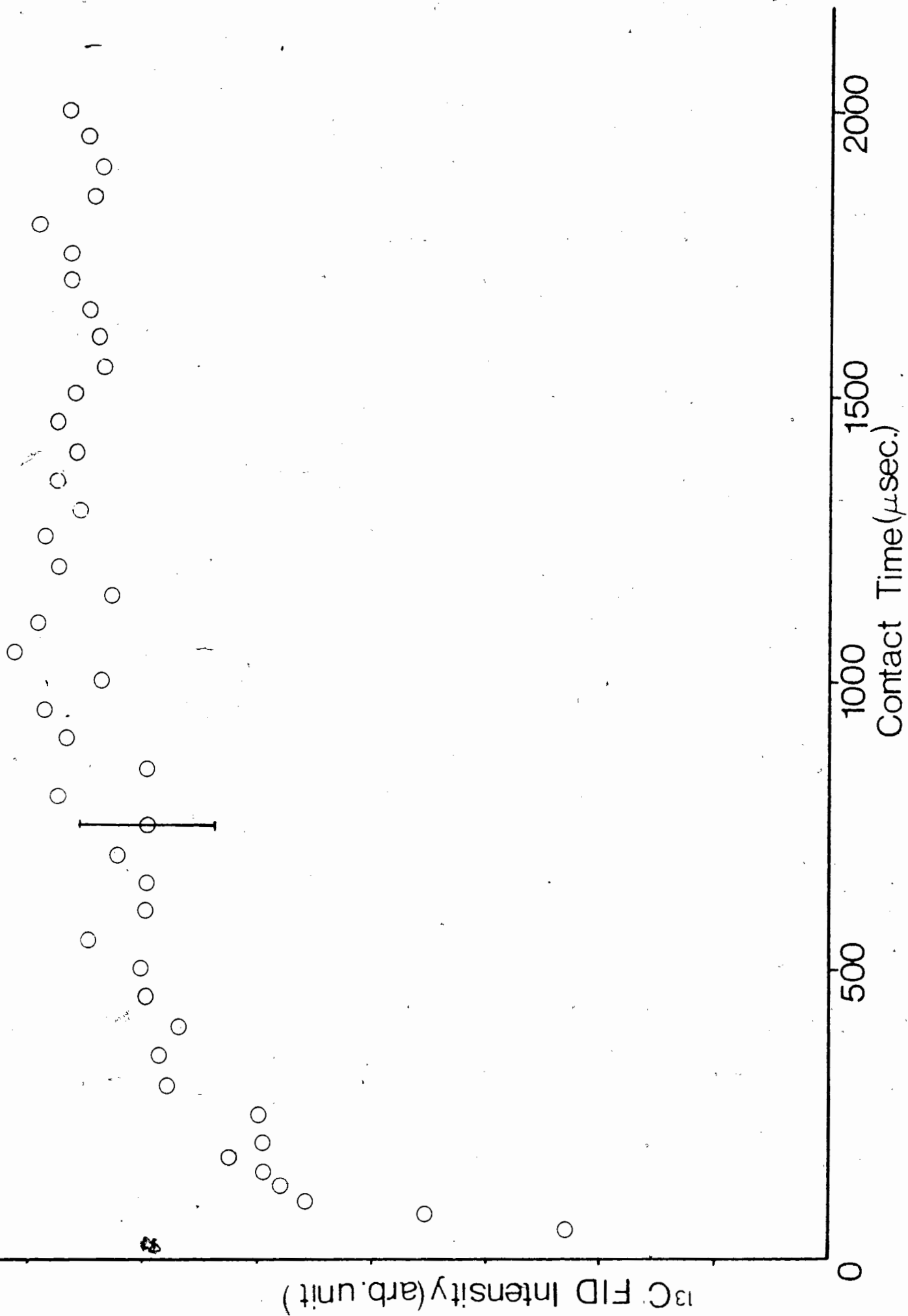


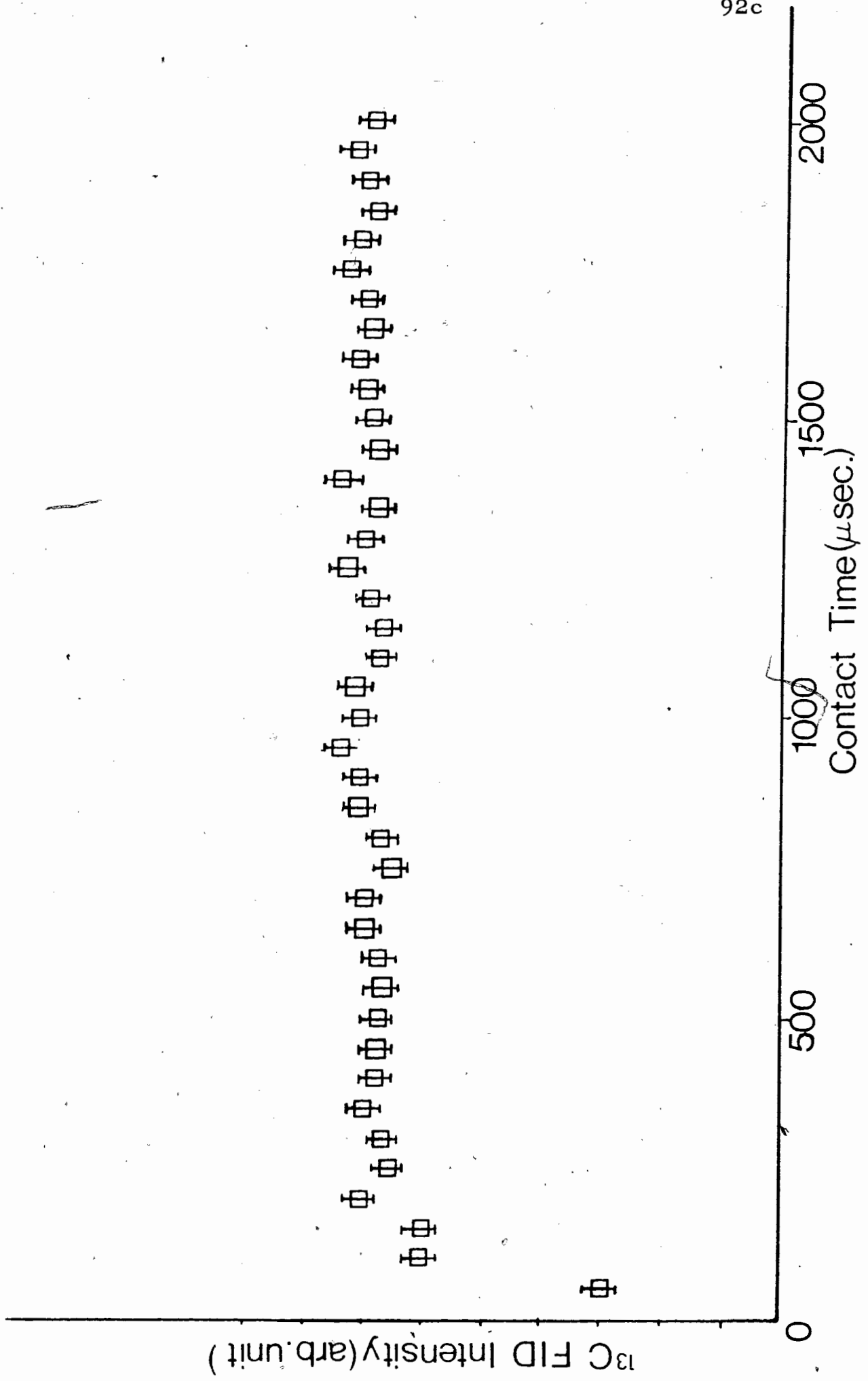
Figure 5.6 Plot of  $^{13}\text{C}$  FID signal vs contact times for the sample of  $2.09 \mu\text{mole}/\text{m}^2$  of 60%  $^{13}\text{C}$ -enriched methanol on MgO-(1). The error bar indicates the associated uncertainty.

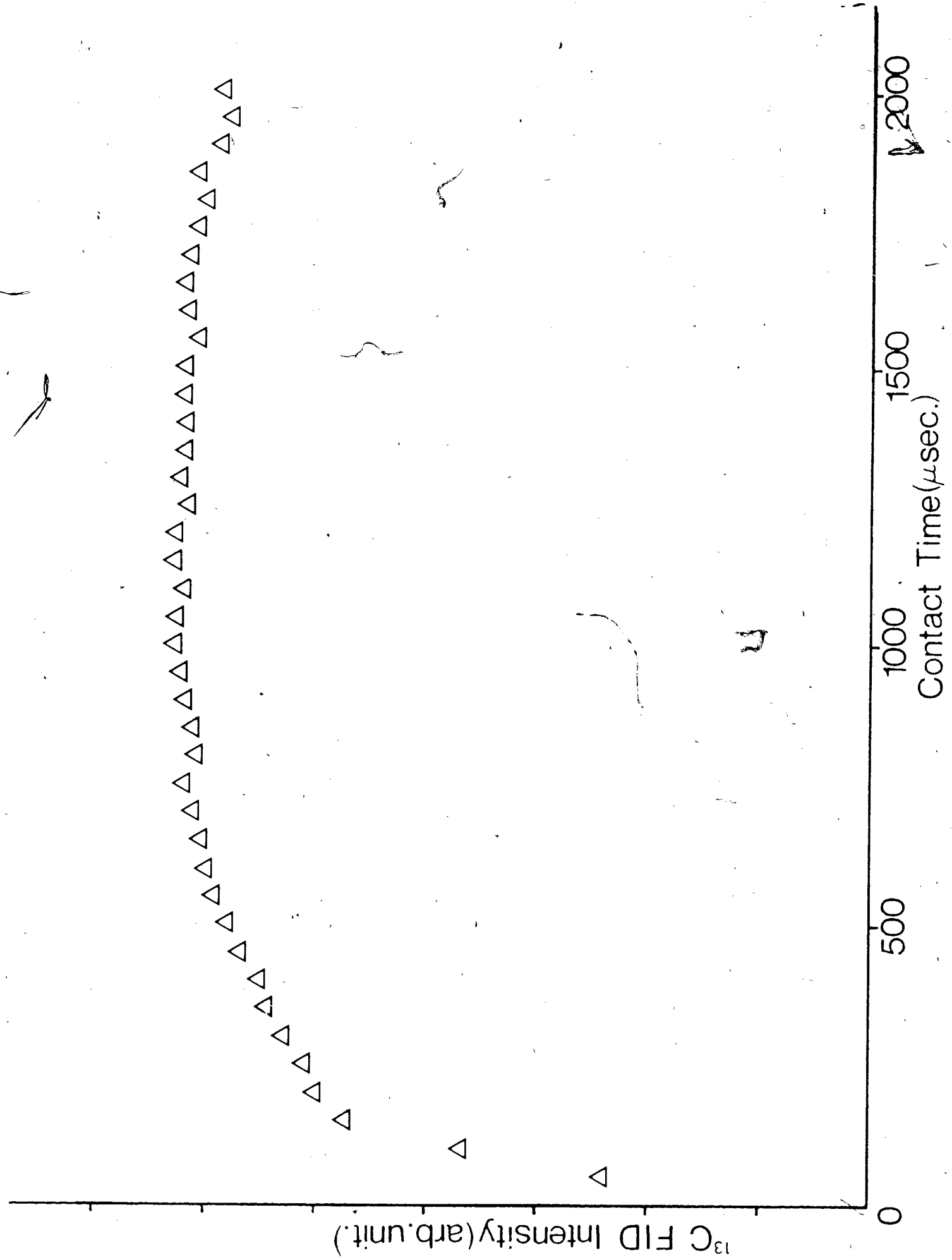
Figure 5.7 Plot of  $^{13}\text{C}$  FID signal vs contact times for the sample of  $2.21 \mu\text{mole}/\text{m}^2$  of 60%  $^{13}\text{C}$ -enriched methanol on MgO-(2). The error bar indicates the associated uncertainties.

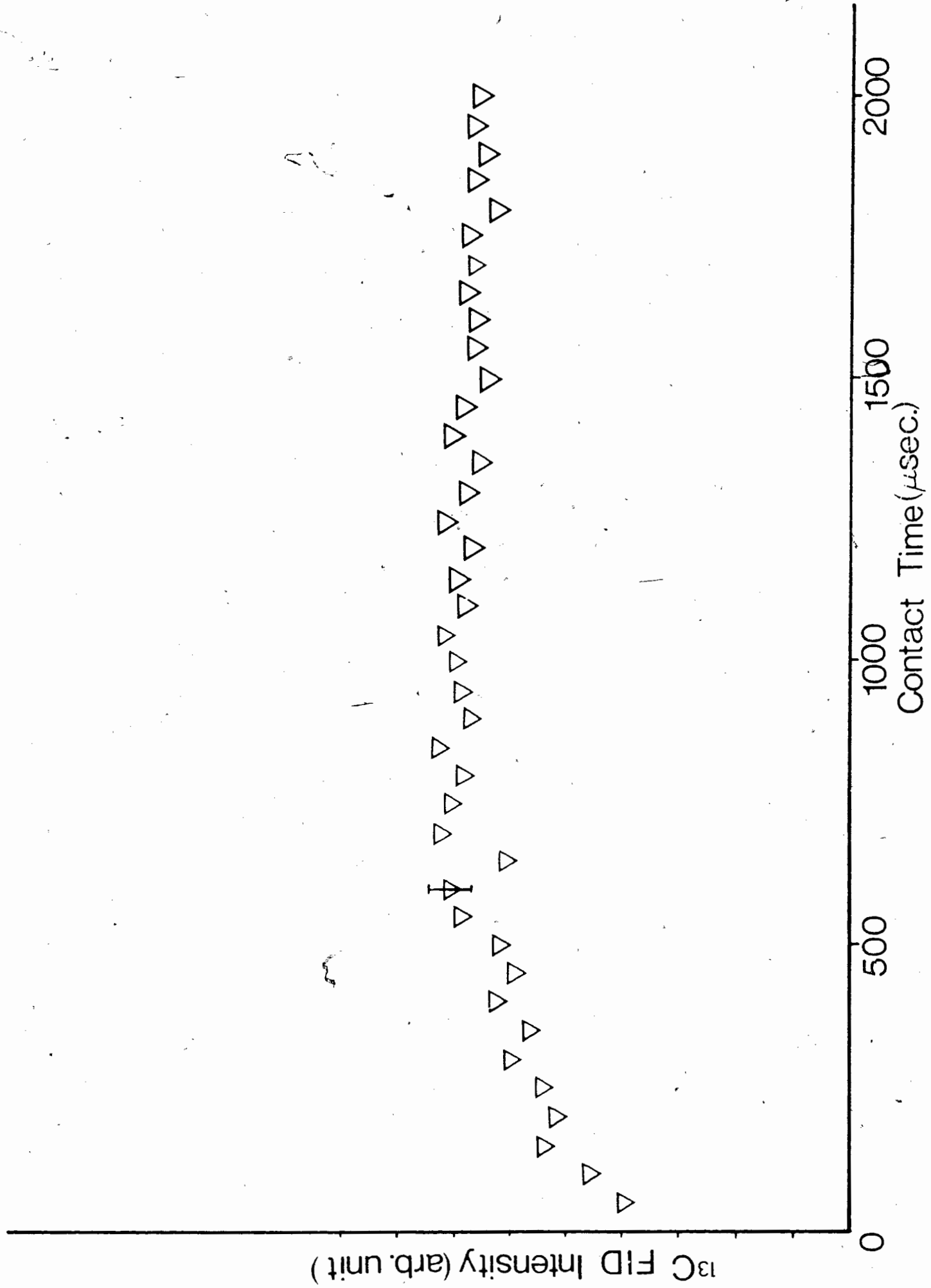
Figure 5.8 Plot of  $^{13}\text{C}$  FID signal vs contact times using data from Figure 5.5 ( $2.79 \mu\text{mole}/\text{m}^2$  of 60%  $^{13}\text{C}$ -enriched methanol on MgO-(3)). Associated error is included inside the  $\Delta$ .

Figure 5.9 Plot of  $^{13}\text{C}$  FID signal vs contact times for the sample of  $2.99 \mu\text{mole}/\text{m}^2$  of 60%  $^{13}\text{C}$ -enriched methanol on MgO-(4). The error bar indicates the associated uncertainty.









### 5.A.III Summary

It was established that there exist slight differences among the four MgO prepared differently. This was indicated by their methanol and CO<sub>2</sub> adsorption isotherms. Although they all showed type II characteristic, their adsorption levels varied. This implies a difference in the surface characteristics on the MgO from the four preparations e.g. surface morphologies and concentration of surface -OH groups.

Although there appeared variations in the T<sub>1H</sub> and proton T<sub>1ρ</sub> measured for each different preparation of MgO, a consistent trend of faster relaxation at higher coverage is found for both adsorbed methanol and ethanol. This indicates that a dipole-dipole interaction is the major contribution to relaxation. However a quantitative assessment of this is impossible due to possible change in motional frequencies.

The differences in the relaxation times between various MgO preparations could be attributed to varying levels of paramagnetic contaminants or from variations in the motional state of the adsorbate (due to the differences in surface morphologies). Thus, MgO-(2), which is Ni<sup>++</sup>-doped, is expected to have the shortest T<sub>1H</sub>. However, MgO-(3) which was prepared from the decomposition of Mg(OH)<sub>2</sub> (which has <0.01% of heavy metal, from manufacturer's specifications) showed the same

shortness in  $T_{1H}$ , this probably indicates some variations in motional state of the adsorbed methanol.

Also, noting that these  $T_{1H}$  and proton  $T_{1\rho}$  measurements are the bulk values (protons on the methoxide and those on the surface -OH groups) only, it is difficult to make any quantitative assessment of these.

Comparing the proton  $T_{1\rho}$  values obtained for MgO-(1) and -(2), the same trend is observed. This probably indicates considerable low-frequency motions in the adsorbed layer.

#### 5.B.I. $^{13}C$ Spectra of Adsorbed Methanol

Figures 5.10 to 5.13 show spectra of static samples, for various coverages, on each preparation of MgO. In general, for all cases, a broad powder pattern is observed in the region expected for a methoxide species. At low coverages, with which  $^{13}C$ -enriched methanol was used, it caused the edges of the pattern to be less sharp than previously reported (23). This is because the  $^{13}C$ - $^{13}C$  dipolar coupling amounts to a few hundred Hz for the enriched samples and gives a linewidth of this magnitude, convolved with the powder pattern.

On all samples, an isotropic peak appears near 50 ppm at high coverages. This presumably represents the appearance of loosely-bound methanol once the available chemisorption sites have been filled. It is well known that only in highly

Figure 5.10

$^{13}\text{C}$  CP spectra of methanol adsorbed on  $\text{MgO}$ -(1) at various coverages. R.F. field = 70 kHz. Contact time = 2 msec, except (a) which is 1.5 msec.

- (a)  $2.09^* \mu\text{mole}/\text{m}^2$ , rep rate =  $1.54 \text{ sec}^{-1}$ , 5,000 contacts
- (b)  $3.63^* \mu\text{mole}/\text{m}^2$ , rep rate =  $2.94 \text{ sec}^{-1}$ , 6,000 contacts
- (c)  $4.31^* \mu\text{mole}/\text{m}^2$ , rep rate =  $1.82 \text{ sec}^{-1}$ , 2,000 contacts
- (d)  $5.92 \mu\text{mole}/\text{m}^2$ , rep rate =  $5.56 \text{ sec}^{-1}$ , 285,000 contacts
- (e)  $7.04 \mu\text{mole}/\text{m}^2$ , rep rate =  $5.56 \text{ sec}^{-1}$ , 66,000 contacts
- (f)  $8.42 \mu\text{mole}/\text{m}^2$ , rep rate =  $6.25 \text{ sec}^{-1}$ , 90,000 contacts

\* indicates 60%  $^{13}\text{C}$ -enriched methanol used.



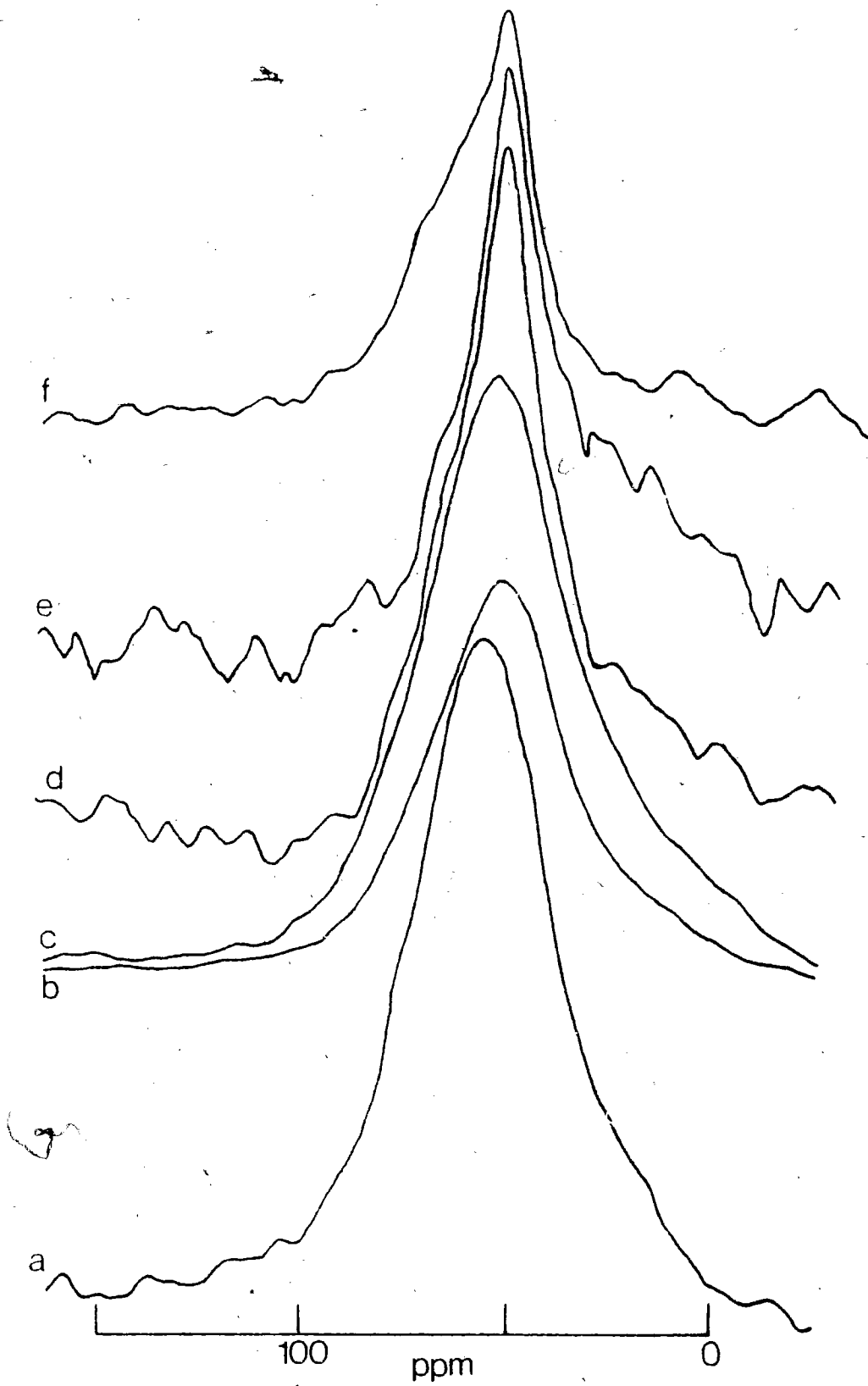


Figure 5.11

$^{13}\text{C}$  CP spectra of methanol adsorbed on MgO-(2) at different coverages. R.F. field = 70 kHz. Contact time = 1.5 sec.

- (a)  $2.21^* \mu\text{mole}/\text{m}^2$ , rep rate =  $5 \text{ sec}^{-1}$ , 6,000 contacts
- (b)  $3.37^* \mu\text{mole}/\text{m}^2$ , rep rate =  $8.33 \text{ sec}^{-1}$ , 6,000 contacts
- (c)  $4.97^* \mu\text{mole}/\text{m}^2$ , rep rate =  $10 \text{ sec}^{-1}$ , 2,000 contacts
- (d)  $6.23 \mu\text{mole}/\text{m}^2$ , rep rate =  $12.5 \text{ sec}^{-1}$ , 336,000 contacts
- (e)  $7.24 \mu\text{mole}/\text{m}^2$ , rep rate =  $12.5 \text{ sec}^{-1}$ , 480,000 contacts
- (f)  $8.43 \mu\text{mole}/\text{m}^2$ , rep rate =  $12.5 \text{ sec}^{-1}$ , 465,000 contacts

\* indicates 60%  $^{13}\text{C}$ -enriched methanol used.

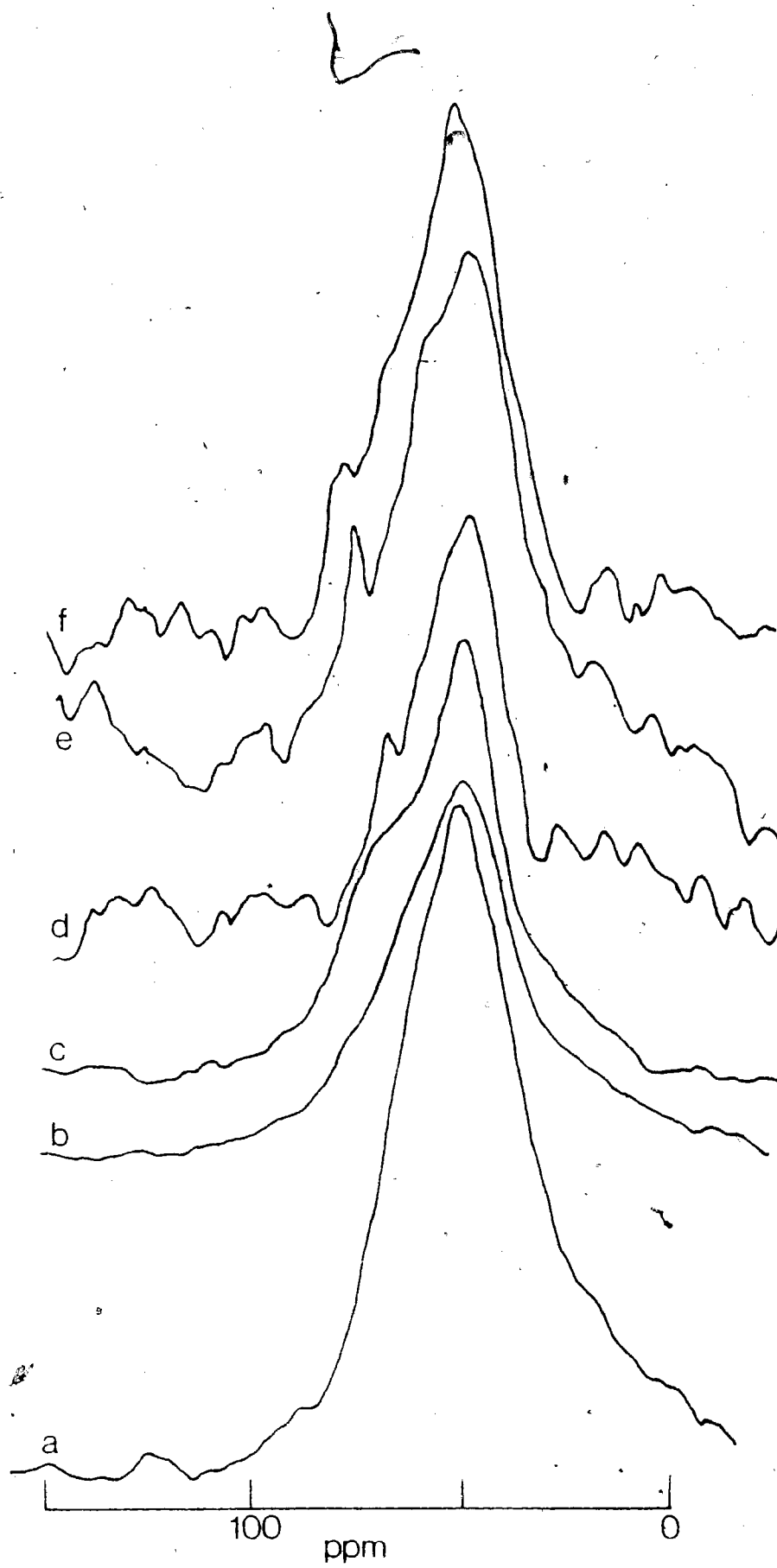


Figure 5.12

$^{13}\text{C}$  CP spectra of methanol adsorbed on  $\text{MgO-(3)}$  at different coverages. R.F. field = 70 kHz. Contact period = 1.5 msec, except (c), (d) and (e) which are 2 msec.

- (a)  $1.22^* \mu\text{mole/m}^2$ , rep rate =  $2.56 \text{ sec}^{-1}$ , 6,000 contacts
- (b)  $2.79^* \mu\text{mole/m}^2$ , rep rate =  $6.25 \text{ sec}^{-1}$ , 5,400 contacts
- (c)  $4.55^* \mu\text{mole/m}^2$ , rep rate =  $14.3 \text{ sec}^{-1}$ , 350 contacts
- (d)  $5.70 \mu\text{mole/m}^2$ , rep rate =  $14.3 \text{ sec}^{-1}$ , 39,600 contacts
- (e)  $7.70 \mu\text{mole/m}^2$ , rep rate =  $14.3 \text{ sec}^{-1}$ , 86,000 contacts
- (f)  $7.73 \mu\text{mole/m}^2$ , rep rate =  $12.5 \text{ sec}^{-1}$ , 430,000 contacts

\* indicates 60%  $^{13}\text{C}$ -enriched methanol used.

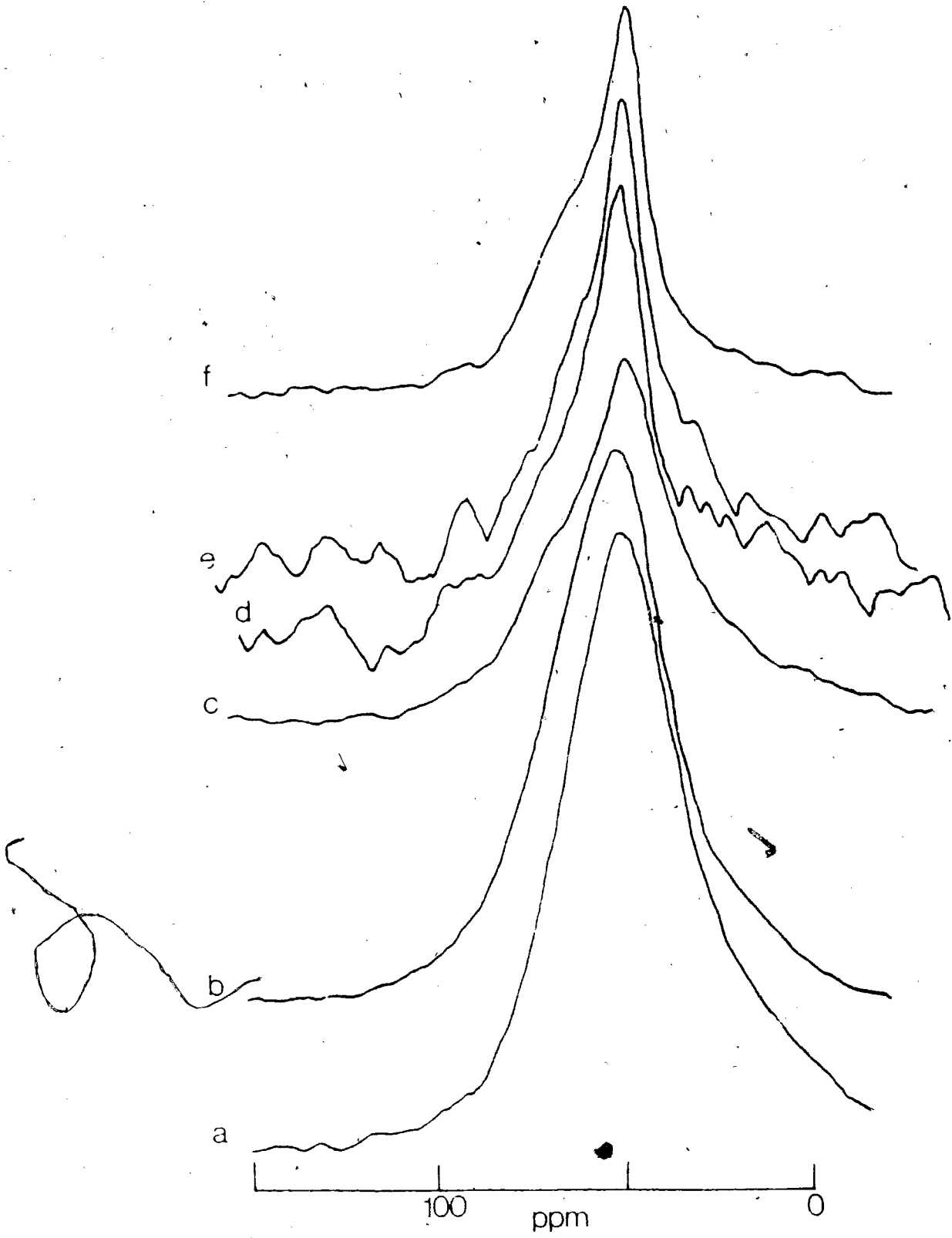


Figure 5.13

$^{13}\text{C}$  CP spectra of methanol adsorbed on  $\text{MgO}$ -(4) at different coverages. R.F. field = 40 kHz. Contact period = 2 msec. Rep rate =  $3.33 \text{ sec}^{-1}$ .

(a)  $2.99^* \mu\text{mole/m}^2$ , 14,400 contacts

(b)  $4.11^* \mu\text{mole/m}^2$ , 8192 contacts

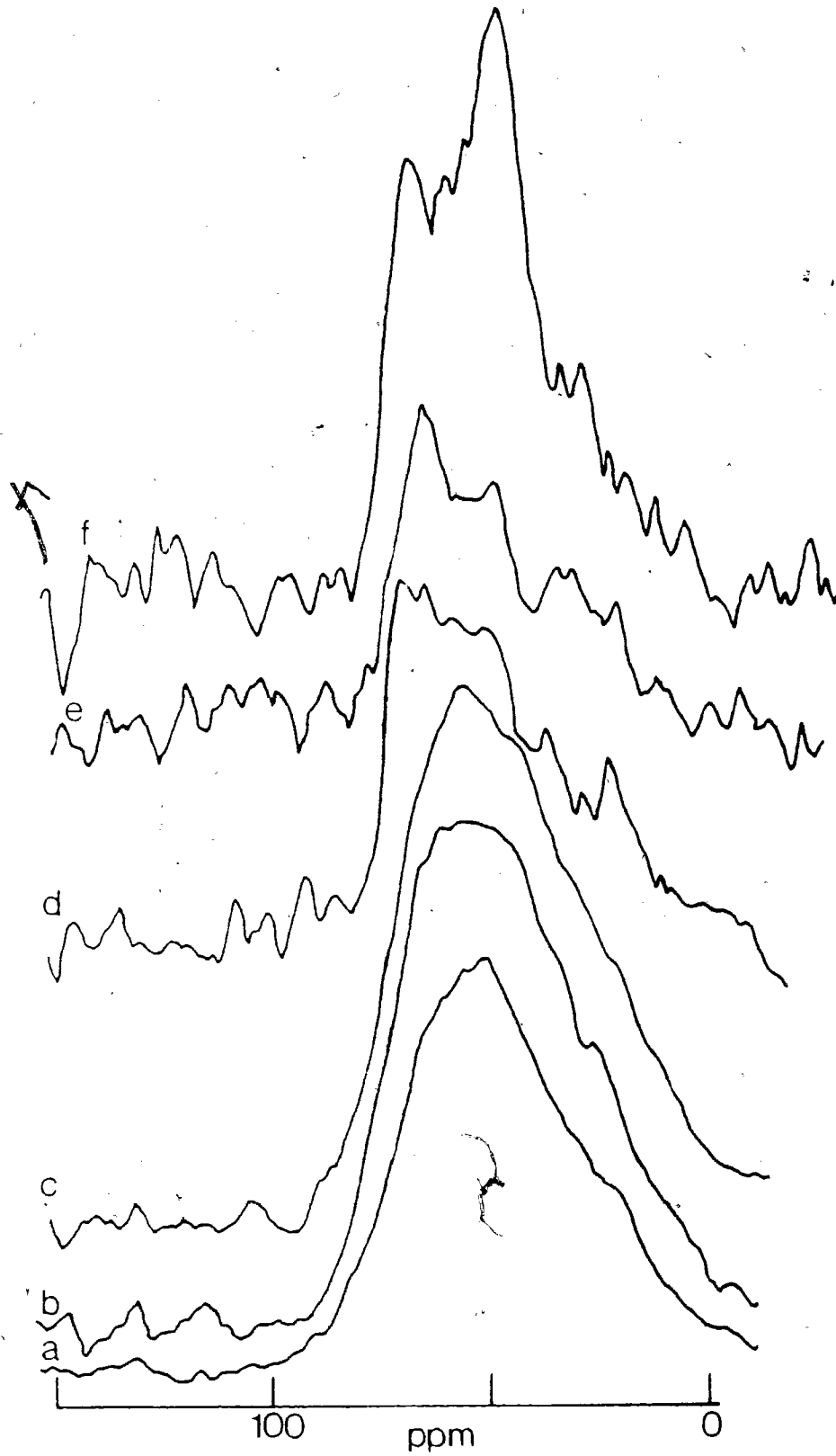
(c)  $4.98^* \mu\text{mole/m}^2$ , 8192 contacts

(d)  $6.21 \mu\text{mole/m}^2$ , 429,000 contacts

(e)  $7.07 \mu\text{mole/m}^2$ , 435,000 contacts

(f)  $8.18 \mu\text{mole/m}^2$ , 244,000 contacts

\* indicates 60%  $^{13}\text{C}$ -enriched methanol used.



symmetrical molecules e.g. adamantane, that narrow resonances are observed in the  $^{13}\text{C}$  CP spectra (109). Rotation about the O-C bond or the Mg-O bond in the surface methoxide species, even in the correct frequency range, the powder pattern would not collapse into a narrow resonance as the case here. This may indicate the presence of some methoxide species which possess accidental degeneracy in the chemical shift components due to special symmetry or motion, or both.

Magic-angle spectra have been obtained for a sample of methanol-MgO-(3) (Figure 5.18). These show a single peak having a width of 80 Hz. The position of this peak shifts from 49.3 ppm at  $1.3 \mu\text{mole}/\text{m}^2$  to 50.3 ppm at  $7.6 \mu\text{mole}/\text{m}^2$ .

All of these data are consistent with only two chemisorbed species on MgO at room temperature - a relatively rigid methoxide and a mobile species which appears at high coverages. The fairly minor differences among different preparations can be accounted for by varying populations of the two species and by motional differences. A change in number of chemisorption sites with preparation will of course vary the relative proportions of species at the higher coverages. Motional variations between preparations can be inferred at all coverages from the proton  $T_1$  data above. These will partially average the powder patterns from chemisorbed species, leading to



the small differences in the adsorbed layer if different preparations yield different local geometries for neighbouring adsorption sites.

#### 5.B.II. $^{13}\text{C}$ NMR Measurements of Adsorbed Methanol Treated at Elevated Temperatures

The  $^{13}\text{C}$  CP spectra of the methanol-MgO systems at room temperature and after heating (170, 320, 500°C) are shown in Figures 5.14 to 5.17. The spectra shown are those in which 60%  $^{13}\text{C}$ -enriched methanol was used.

Essentially, the spectra of the adsorbed species remained the same until being treated at 300°C. One striking feature is the gradual sharpening of the methoxide powder pattern as the temperature is raised. This is more pronounced for MgO-(2), -(3) and -(4) than for MgO-(1). This is perhaps due to the "recrystallization" of the adsorbed layer on heating and cooling. Possibly a more uniform layer is achieved by thermal crossing of activation barriers. A similar effect is observed in the magic-angle spectra on MgO-(3). The linewidth decreased from 80 to 40 Hz on heating to 300°C and re-cooling as seen in Figure 5.18.

The spectra of all methanol-MgO systems treated at 500°C showed a low field resonance with the complete disappearance of the methoxide species.

Figure 5.14

$^{13}\text{C}$  CP NMR spectra of  $4.31 \mu\text{mole}/\text{m}^2$  of methanol (60%  $^{13}\text{C}$ -enriched) on MgO-(1) treated at different temperatures. R.F. field = 70 kHz. Contact period = 2 msec, except (a) which is 1.5 msec.

- (a) Room temp., rep rate =  $1.82 \text{ sec}^{-1}$ , 2,000 contacts
- (b)  $170^\circ\text{C}$  (3 hrs), rep rate =  $1.43 \text{ sec}^{-1}$ , 7,600 contacts
- (c)  $300^\circ\text{C}$  (3 hrs), rep rate =  $1.72 \text{ sec}^{-1}$ , 5,900 contacts
- (d)  $500^\circ\text{C}$  (3 hrs), rep rate =  $4.17 \text{ sec}^{-1}$ , 38,800 contacts

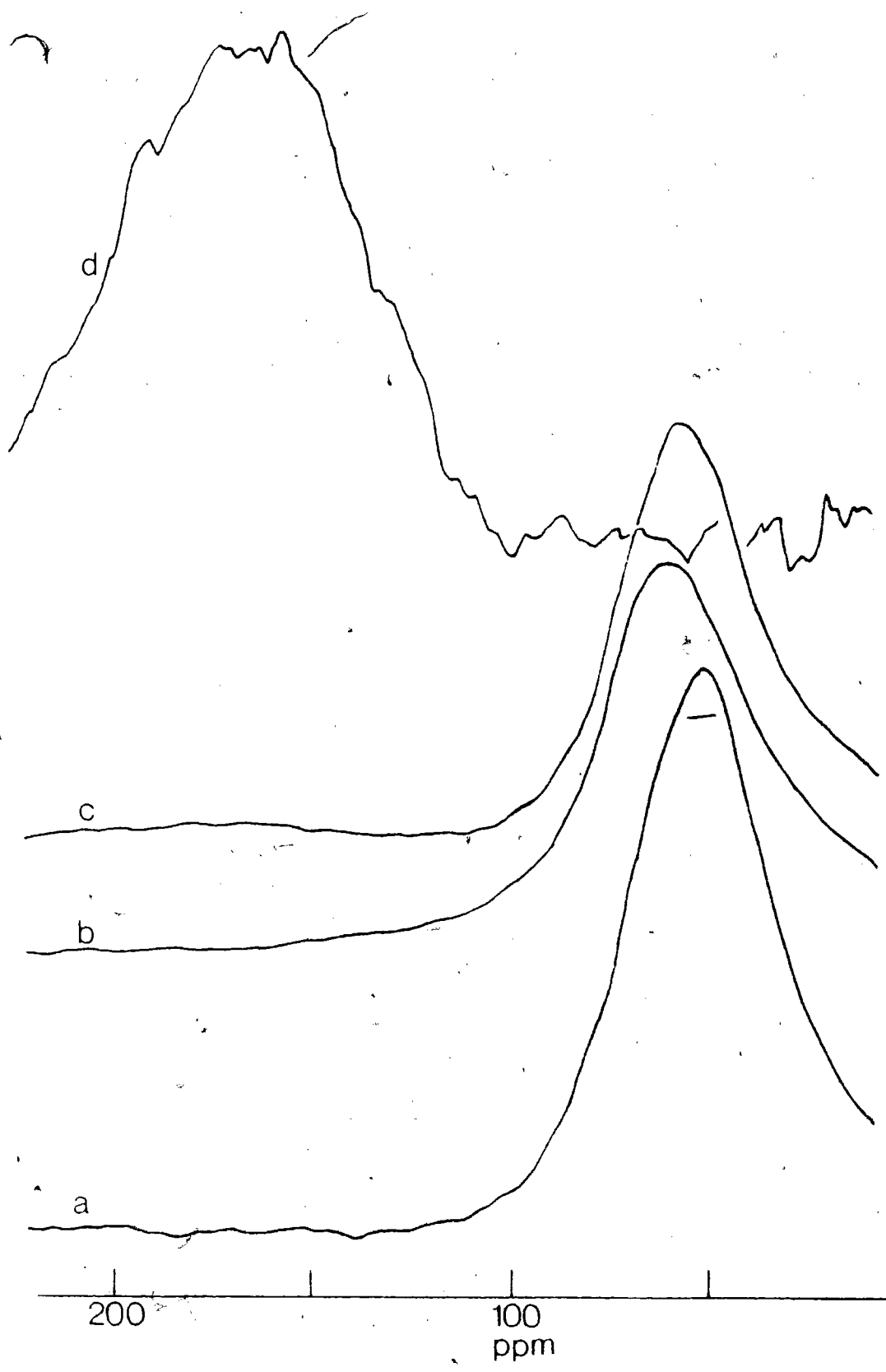
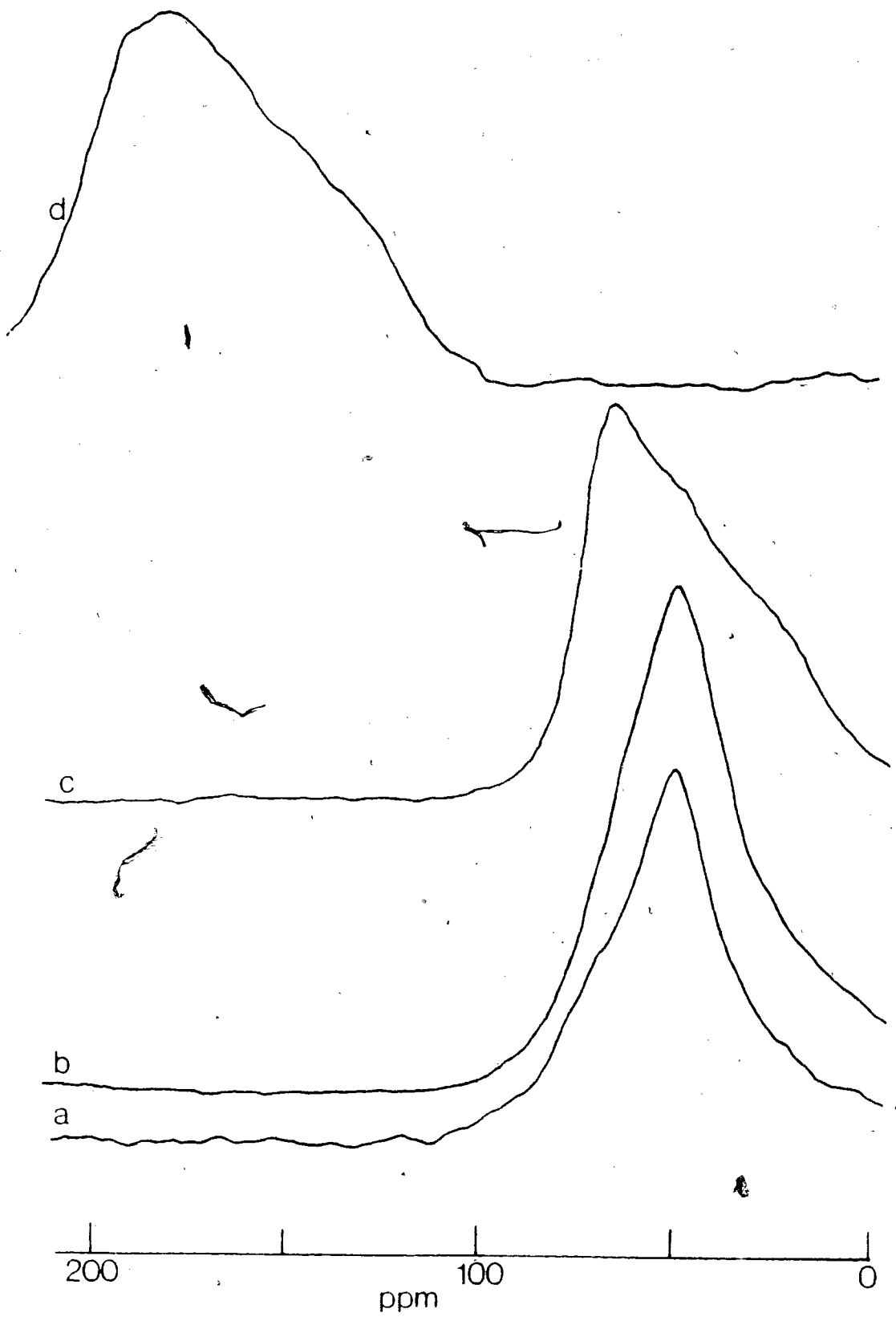


Figure 5.15

$^{13}\text{C}$  CP NMR spectra of  $4.97 \mu\text{mole/m}^2$  of methanol (60%  $^{13}\text{C}$ -enriched) on  $\text{MgO}$ -(2) treated at elevated temperatures. R.F. field = 40 kHz except (a) which is 70 kHz. Contact period = 2 msec except (a) which is 1.5 msec.

- (a) Room temp., rep rate =  $10 \text{ sec}^{-1}$ , 2,000 contacts
- (b)  $170^\circ\text{C}$  (~~5~~ hrs), rep rate =  $10 \text{ sec}^{-1}$ , 10,000 contacts
- (c)  $300^\circ\text{C}$  (3 hrs), rep rate =  $10 \text{ sec}^{-1}$ , 2,400 contacts
- (d)  $500^\circ\text{C}$  (3 hrs), rep rate =  $2 \text{ sec}^{-1}$ , 20,000 contacts



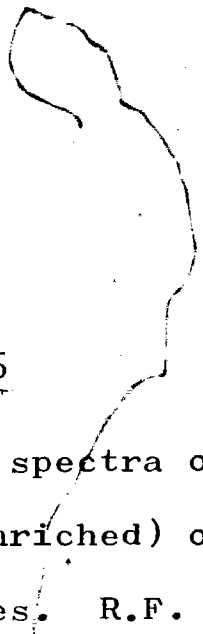


Figure 5.16

$^{13}\text{C}$  CP NMR spectra of  $3.55 \mu\text{mole}/\text{m}^2$  of methanol (60%  $^{13}\text{C}$ -enriched) on MgO-(3) treated at elevated temperatures. R.F. field = 70 kHz. Contact period = 1.5 msec.

- (a) room temp., rep rate =  $14.3 \text{ sec}^{-1}$ , 350 contacts
- (b)  $170^\circ$  (3 hrs), rep rate =  $6.67 \text{ sec}^{-1}$ , 6000 contacts
- (c)  $300^\circ$  (3 hrs), rep rate =  $10 \text{ sec}^{-1}$ , 3000 contacts
- (d)  $500^\circ$  (3 hrs), rep rate =  $10 \text{ sec}^{-1}$ , 26,000 contacts

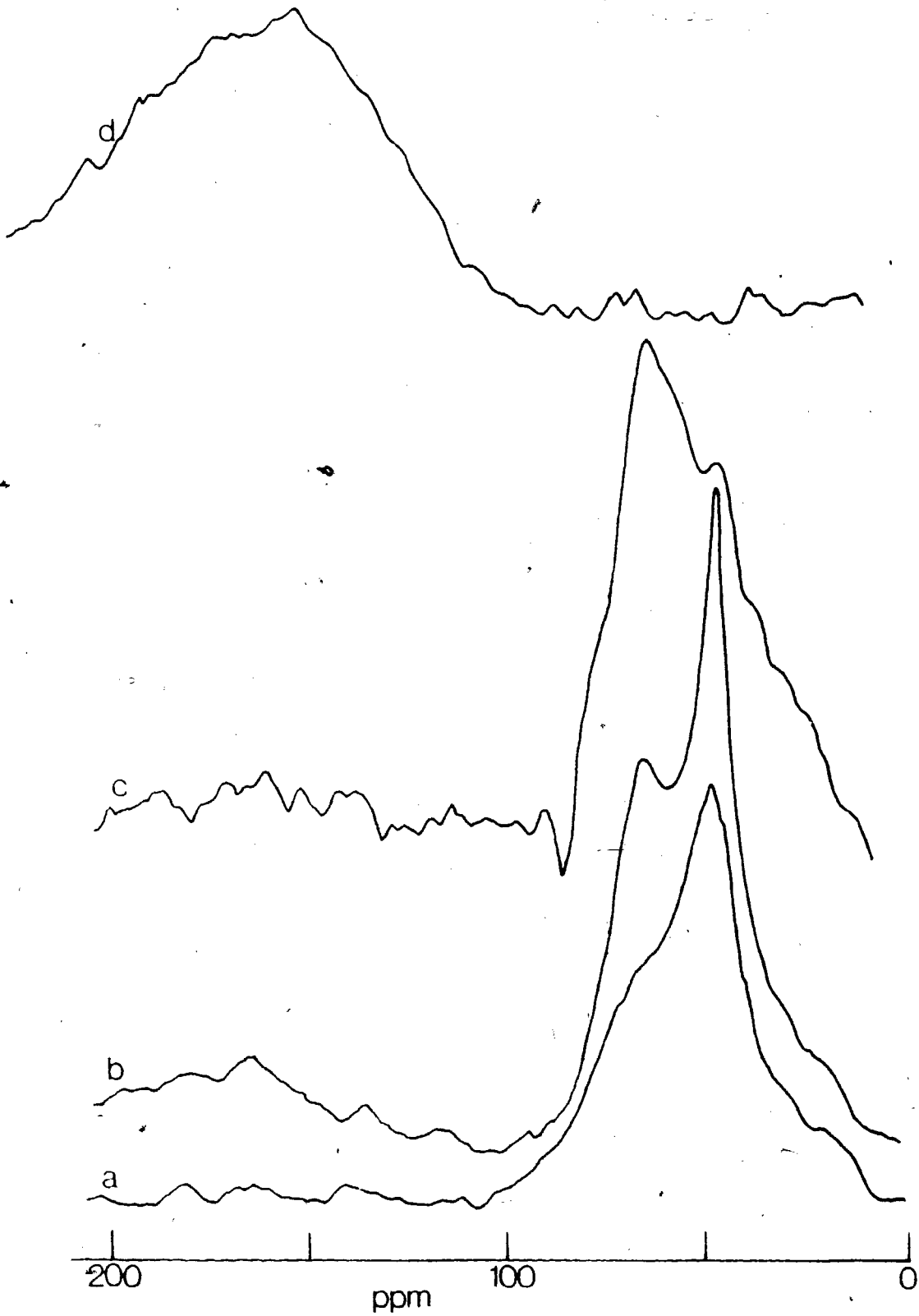


Figure 5.17

$^{13}\text{C}$  CP NMR spectra of  $4.11 \mu\text{mole}/\text{m}^2$  of methanol (60%  $^{13}\text{C}$ -enriched) on  $\text{MgO}$ -(4) treated at elevated temperatures. R.F. field = 40 kHz except (a) which is 70 kHz. Contact time = 2 msec.

- (a) Room temp., rep rate =  $3.33 \text{ sec}^{-1}$ , 8,192 contacts
- (b)  $170^\circ\text{C}$  (3 hrs), rep rate =  $0.83 \text{ sec}^{-1}$ , 2,347 contacts
- (c)  $300^\circ\text{C}$  (3 hrs), rep rate =  $0.83 \text{ sec}^{-1}$ , 78,357 contacts
- (d)  $500^\circ\text{C}$  (3 hrs), rep rate =  $0.83 \text{ sec}^{-1}$ , 103,100 contacts



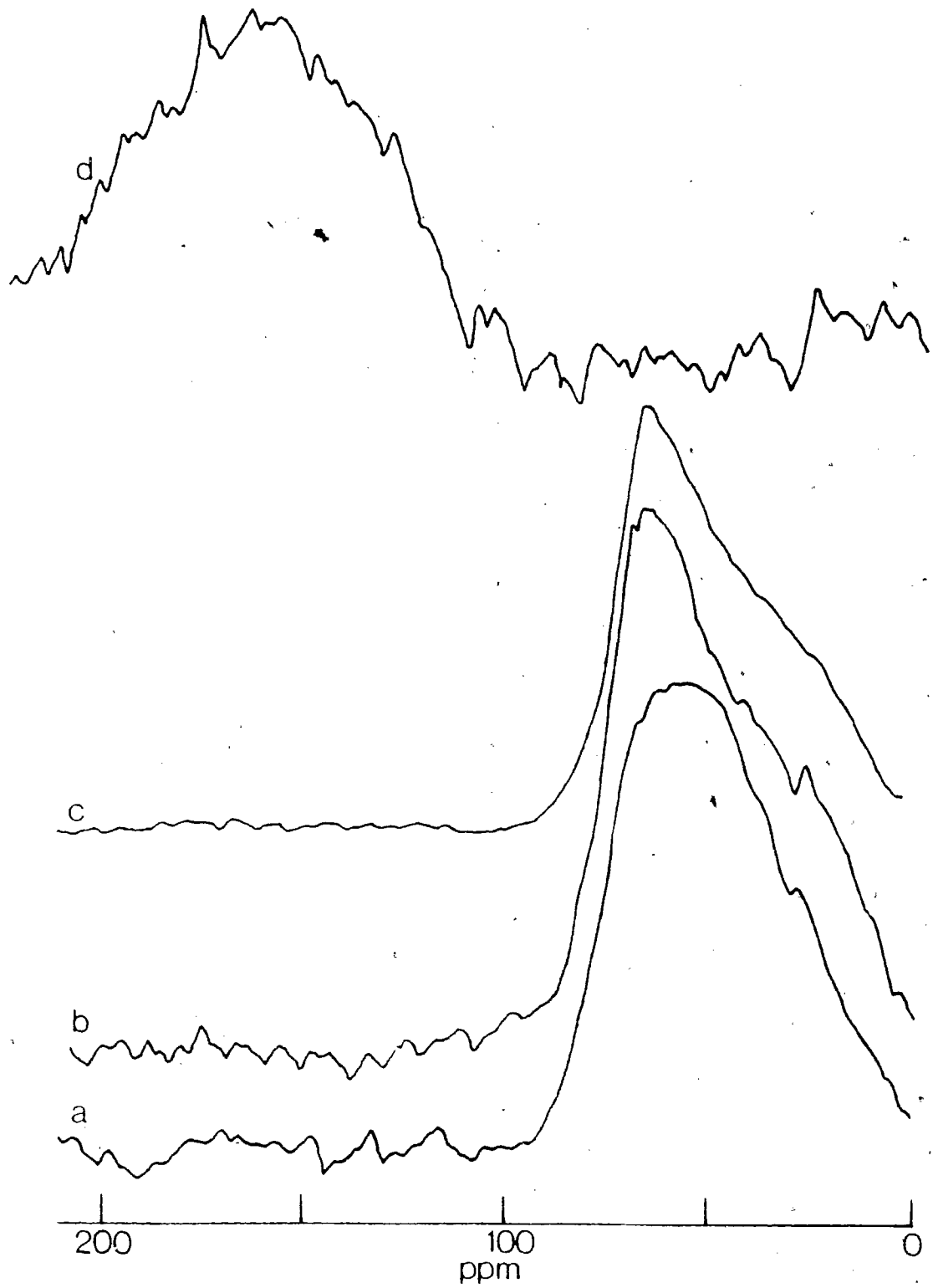
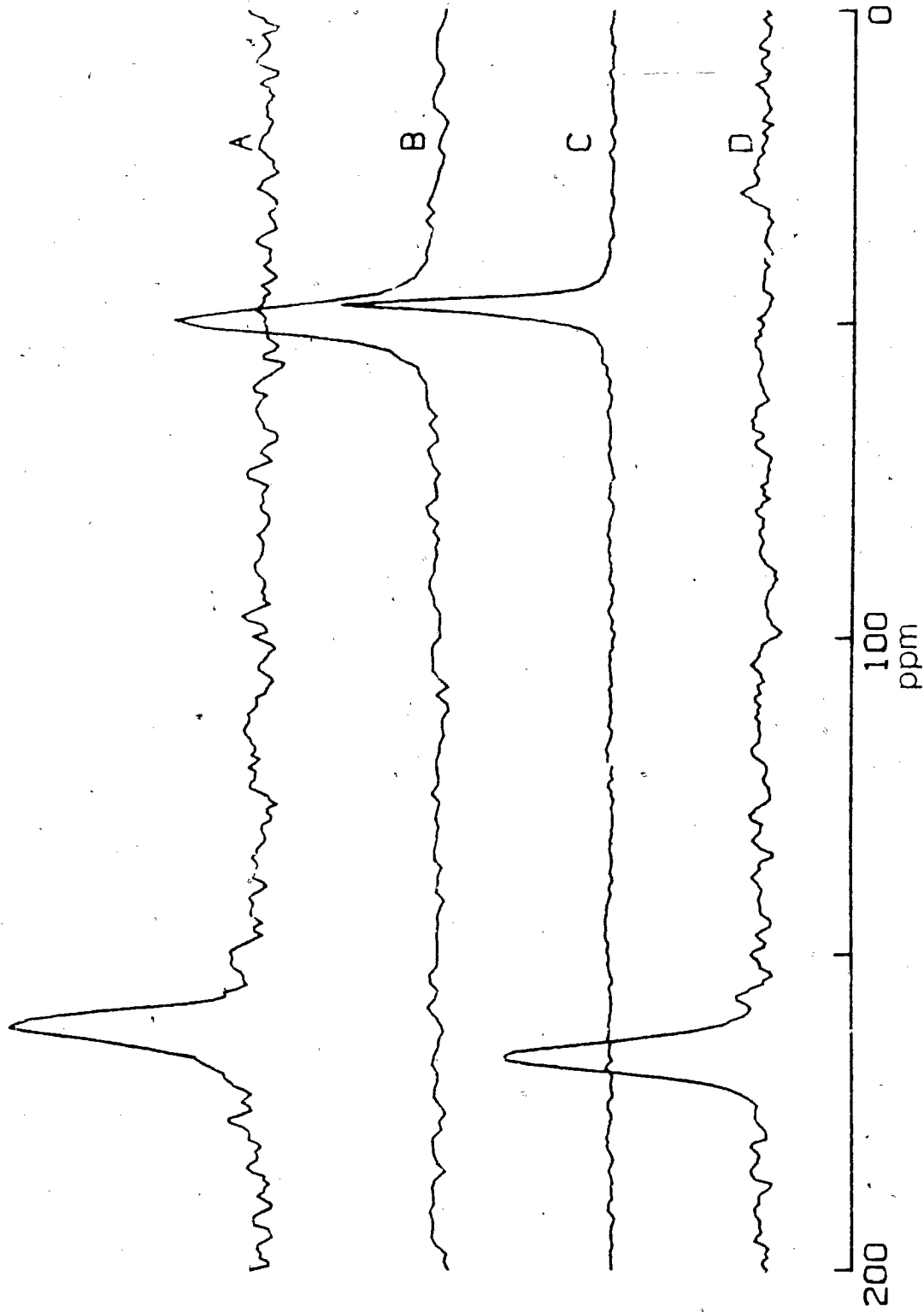


Figure 5.18  $^{13}\text{C}$  CP/MAS spectra of

- (A)  $\text{CO}_2$  (90%  $^{13}\text{C}$ -enriched) on  $\text{MgO}$ -(3).
- (B) Methanol (60%  $^{13}\text{C}$ -enriched) on  $\text{MgO}$ -(3).
- (C) Sample (B) heated to  $300^\circ\text{C}$  for 3 hours.
- (D) Sample (B) heated to  $500^\circ\text{C}$  for 3 hours.

Field strength = 60 kHz.

Contact time = 2 msec. Rep. rate = 2 sec<sup>-1</sup>.



From the position and anisotropy of this resonance, it clearly contains  $sp^2$  carbon and is presumably a carbonate or formate species. The magic-angle spectrum shows a single line at 167.4 ppm having a width of 110 Hz. With the MAS technique one was able to perform a delayed decoupling experiment (129, 130). The resonance intensity of this species is reduced to 50% by a decoupler delay of 200  $\mu$ sec. This strongly suggests a proton two bonds distant from the carbon (130). Given the chemical shift, bicarbonate is the obvious species. It is most unlikely that this is a formate species. A decoupler delay experiment on ammonium formate shows decay to 50% in 25  $\mu$ sec and to 5% in 60  $\mu$ sec. For the MgO surface species, the intensity is >95% after a 60  $\mu$ sec delay. These results clearly exclude the possibility of a surface formate.

It may appear that the chemical shift powder patterns which were attributed to surface bicarbonate species (spectrum (d) in Figures 5.14 to 5.17) are quite different from the chemical shift powder patterns shown for  $CO_2$  in Figure 5.4 (which were also attributed to bicarbonate species). It was demonstrated by Stejskal et al. (11a,b) that adsorbed  $CO_2$  shows different anisotropies at different loading levels on  $Na^+$ -mordenite. This may be the case for the present NMR observation, that due to different concentration or surface morphologies that different signs of the anisotropies were observed.

Conventional single-pulse  $^{13}\text{C}$  NMR spectroscopy done on some selected samples revealed a wide range of alkanes and alkenes and  $\text{CO}_2$  on MgO, when the methanol-MgO was heated to  $500^\circ\text{C}$  for 3 hours. The resolvable resonances, relative to TMS, are  $-10.6$  ( $\text{CH}_4$ ),  $4.2$  ( $\text{C}_2\text{H}_6$ ),  $11.6$ ,  $15.4$ ,  $23.6$ ,  $110.5$ ,  $117.5$ ,  $120.6$ ,  $133.8$ ,  $142.4$ ,  $158.3$ ,  $169.1$  ( $\text{CO}_3^{--}$ ) and  $183.9$  ( $\text{CO}$ ). These were not observed in the CP experiments, indicating them to be highly mobile species, probably no more than physisorbed in any case. Gas chromatography and mass spectrometer analysis of the gaseous products (or easily-desorbed surface species) reveal hydrocarbons ranging from  $\text{C}_1$  to  $\text{C}_4$  (both saturated and unsaturated) and large amounts of  $\text{CO}$  and  $\text{H}_2$ .

### 5.B.III. Summary

The  $^{13}\text{C}$  CP spectra indicate that the first monolayer of the methanol-MgO systems consists mainly of chemisorbed species - with a powder pattern similar to that obtained from magnesium methoxide. As the coverage increases, physisorbed methanol appears as an isotropic peak superimposed on the powder pattern. This isotropic peak has a  $^{13}\text{C}$  chemical shift of 49 ppm, very close to the  $^{13}\text{C}$  chemical shift of methanol in liquid form.

It is conjectured that the physisorbed methanol molecules reside on less active sites on the surface (i.e. sites with lower energy of adsorption). The force of interaction would be greater in magnitude than hydrogen-bonding or Van der

Waals forces, otherwise these physisorbed molecules would behave more like a "liquid" and not be observed by the  $^{13}\text{C}$  CP technique. It is further speculated that these physisorbed molecules either rotate very slowly (a few kHz) to average out the chemical shift anisotropies but not fast enough to average out the C-H dipolar coupling, or, intermolecular cross-polarization plays an important role in the  $^{13}\text{C}$  CP spectra (23).

The adsorbed methoxide species are stable up to  $300^\circ\text{C}$ . When the samples were treated to  $500^\circ\text{C}$ , a low-field resonance appeared on the  $^{13}\text{C}$  CP spectra, which was believed to be a bicarbonate species - the only chemisorbed species on the surface. Therefore, MgO from all preparations dehydrogenate the methanol to  $\text{CO}_2$  (precursor for the adsorbed bicarbonate species) and  $\text{H}_2$  (from gas-chromatography analysis). It was also found that a wide range of alkanes and alkenes plus carbon monoxide were produced as side-products. This probably involves some very complicated mechanism in their formation, especially in the initial C-C bond formation (19-21).

#### 5.C.I. $^{13}\text{C}$ Spectra of Adsorbed Ethanol on MgO

The study of adsorbed ethanol on MgO by conventional techniques has been scarce (31, 50-54, 57b, 131). The general consensus is that the ethanol chemisorbed on the MgO surface as an ethoxide species, which is stable up to  $150^\circ\text{C}$ . At about  $250^\circ\text{C}$ , dehydrogenation sets in to yield acetaldehyde and

hydrogen (53), along with ethene (probably from the dehydration of ethanol). At still higher temperatures, 1,3-butadiene is observed along with hydrogen. The formation of 1,3-butadiene probably arises from the reaction of 3-hydroxybutanal (self-condensation product of acetaldehyde) with another surface ethoxide, with water and another acetaldehyde as byproducts (132). Most of these products were identified via infrared spectroscopy, and by gas chromatography with mass spectrometer analysis.

Figures 5.19-5.22 show the static  $^{13}\text{C}$  CP spectra of ordinary ethanol adsorbed on the four different preparations of MgO at varying coverages. At low coverages, the observed powder patterns resemble those of magnesium ethoxide. In general, at coverages of  $6 \mu\text{mole}/\text{m}^2$  and up, there is a slight broadening of both the methyl and methylene chemical shift anisotropies. This we attribute to the possible existence of more than one chemisorbed ethanol species, which superimpose on each other due to the proximity of their chemical shifts.

The methylene carbon shows an antisymmetric powder pattern due to the lack of a symmetry axis, which is to be expected. Its powder pattern overlaps with that of the methyl resonance, thus the  $\delta_{33}$  (the high field component of the powder pattern) is obscured. On the other hand, the methyl resonance shows almost an isotropic pattern, probably due to

Figure 5.19

$^{13}\text{C}$  CP spectra of ethanol adsorbed on  $\text{MgO}$ -(1) at various coverages. Field strength = 70 kHz. Contact time = 2 msec.

- (a)  $4.21 \mu\text{mole}/\text{m}^2$ , rep rate =  $4 \text{ sec}^{-1}$ , 192,800 contacts
- (b)  $5.14 \mu\text{mole}/\text{m}^2$ , rep rate =  $5.3 \text{ sec}^{-1}$ , 252,100 contacts
- (c)  $5.88 \mu\text{mole}/\text{m}^2$ , rep rate =  $4.2 \text{ sec}^{-1}$ , 24,700 contacts
- (d)  $6.91 \mu\text{mole}/\text{m}^2$ , rep rate =  $5 \text{ sec}^{-1}$ , 30,969 contacts
- (e)  $8.01 \mu\text{mole}/\text{m}^2$ , rep rate =  $5 \text{ sec}^{-1}$ , 266,605 contacts



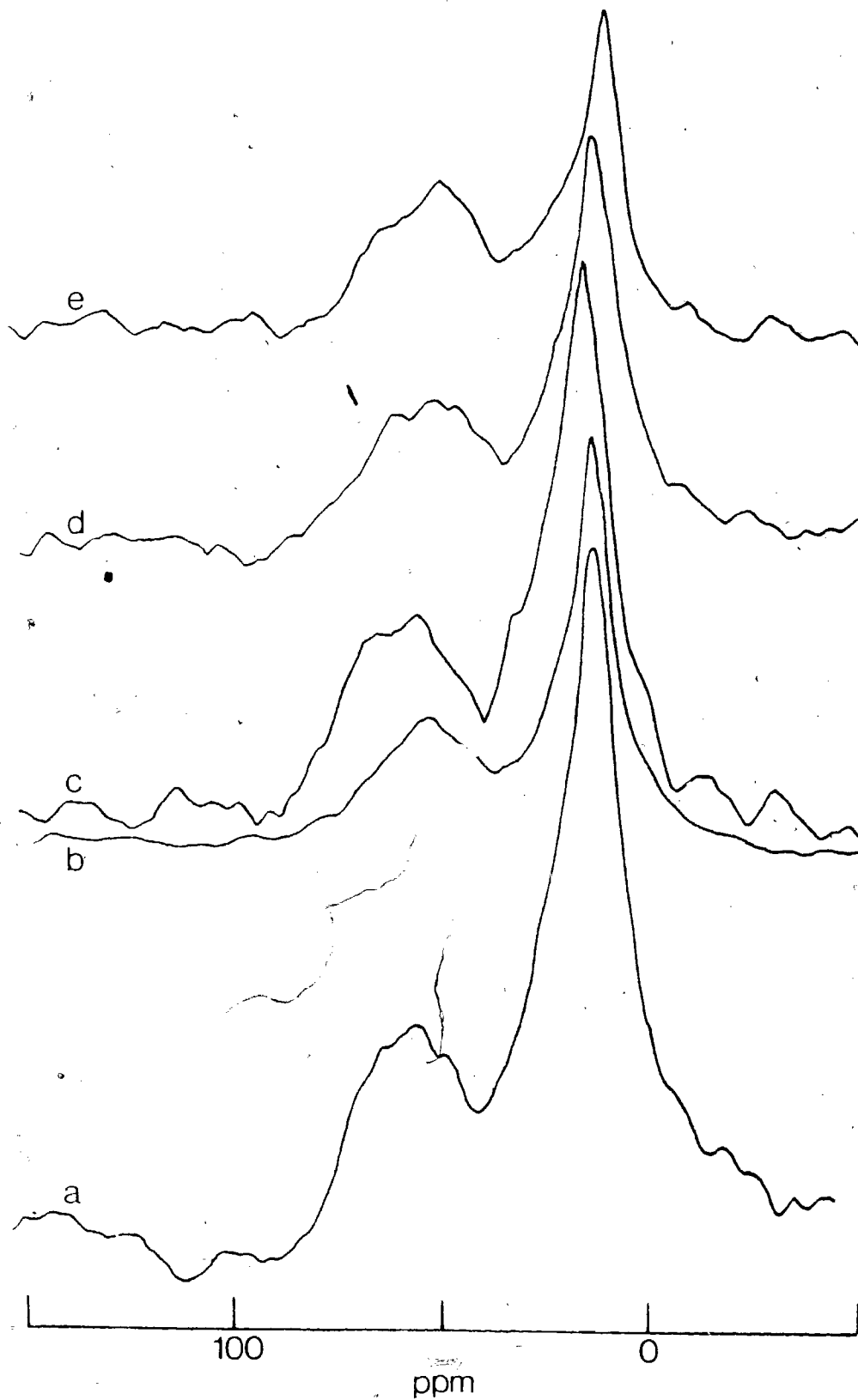


Figure 5.20

$^{13}\text{C}$  CP spectra of ethanol adsorbed on  $\text{MgO}$ -(2) at various coverages. Field strength = 70 kHz. Contact time = 2 msec.

- (a)  $4.92 \mu\text{mole}/\text{m}^2$ , rep rate =  $10 \text{ sec}^{-1}$ , 343,800 contacts
- (b)  $5.81 \mu\text{mole}/\text{m}^2$ , rep rate =  $10 \text{ sec}^{-1}$ , 140,100 contacts
- (c)  $6.14 \mu\text{mole}/\text{m}^2$ , rep rate =  $4.2 \text{ sec}^{-1}$ , 203,900 contacts
- (d)  $7.22 \mu\text{mole}/\text{m}^2$ , rep rate =  $10 \text{ sec}^{-1}$ , 129,000 contacts
- (e)  $8.23 \mu\text{mole}/\text{m}^2$ , rep rate =  $10 \text{ sec}^{-1}$ , 141,800 contacts

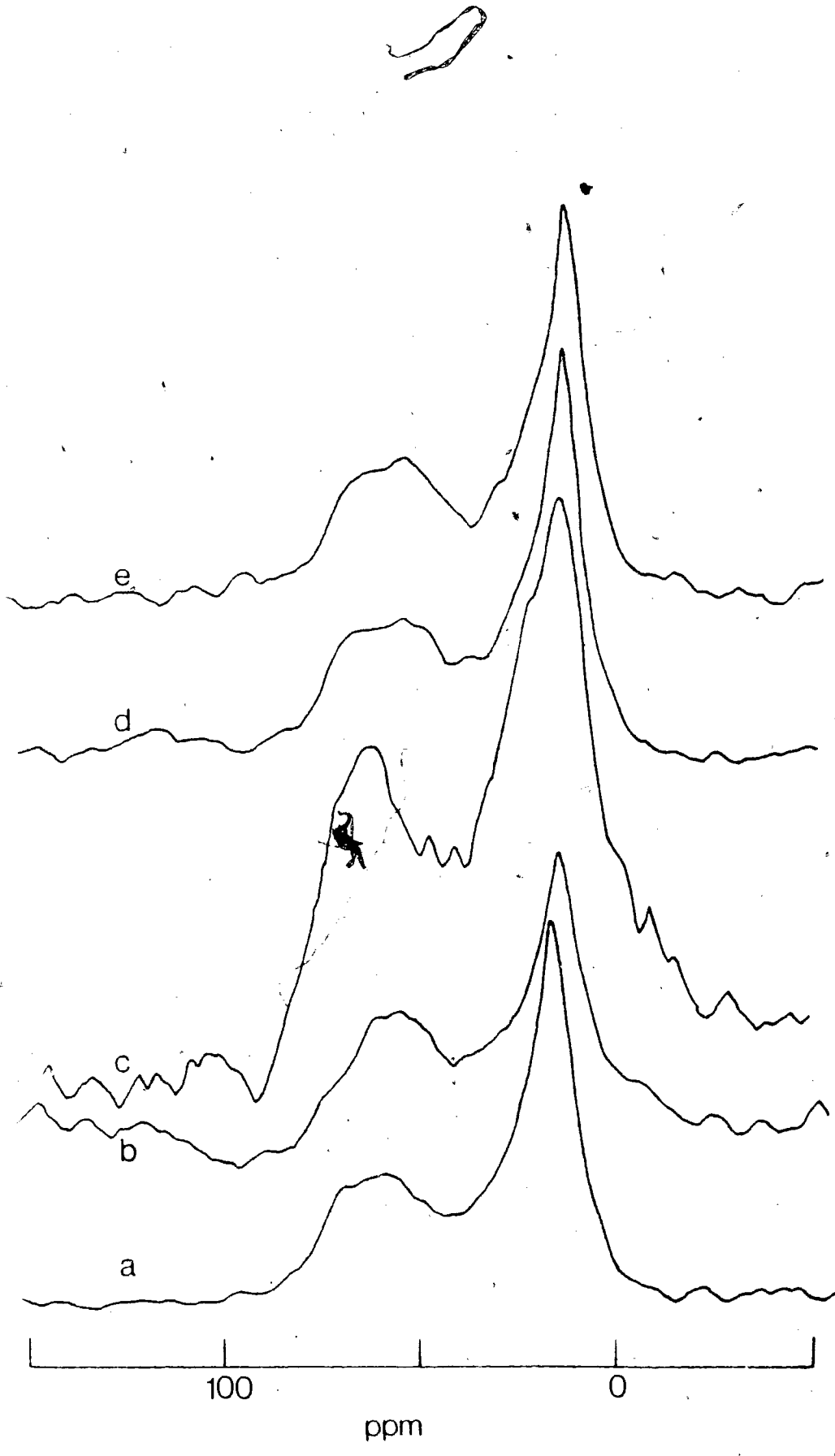


Figure 5.21

$^{13}\text{C}$  CP spectra of ethanol adsorbed on  $\text{MgO}(3)$  at various coverages. Field strength = 70 kHz.

Contact time = 1.5 msec. Rep. rate =  $10 \text{ sec}^{-1}$ , except (c) which is  $2.7 \text{ sec}^{-1}$ .

(a)  $4.19 \mu\text{mole/m}^2$ , 321,700 contacts

(b)  $5.42 \mu\text{mole/m}^2$ , 468,400 contacts

(c)  $6.11 \mu\text{mole/m}^2$ , 113,800 contacts

(d)  $7.19 \mu\text{mole/m}^2$ , 47,212 contacts

(e)  $8.92 \mu\text{mole/m}^2$ , 6,647 contacts

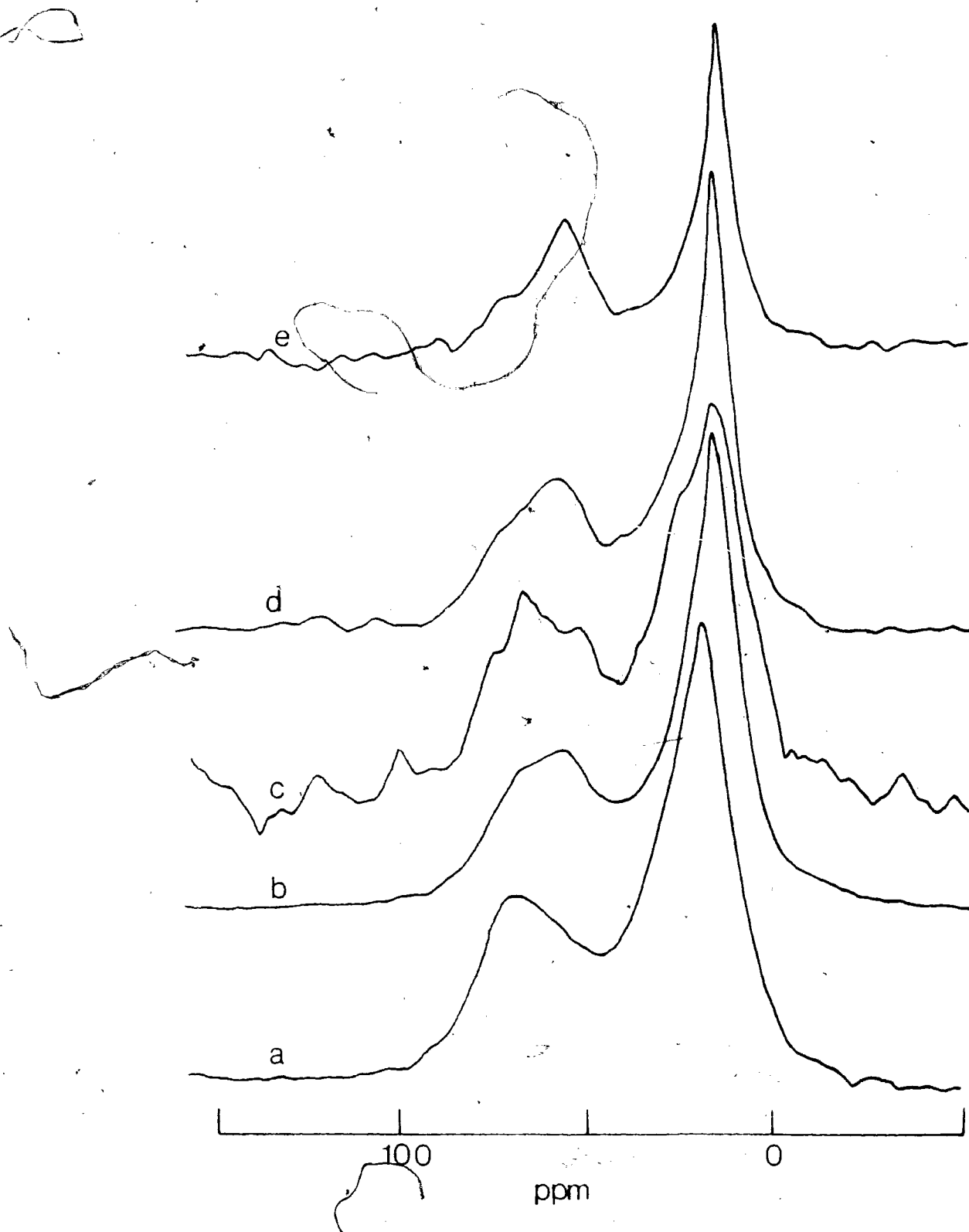
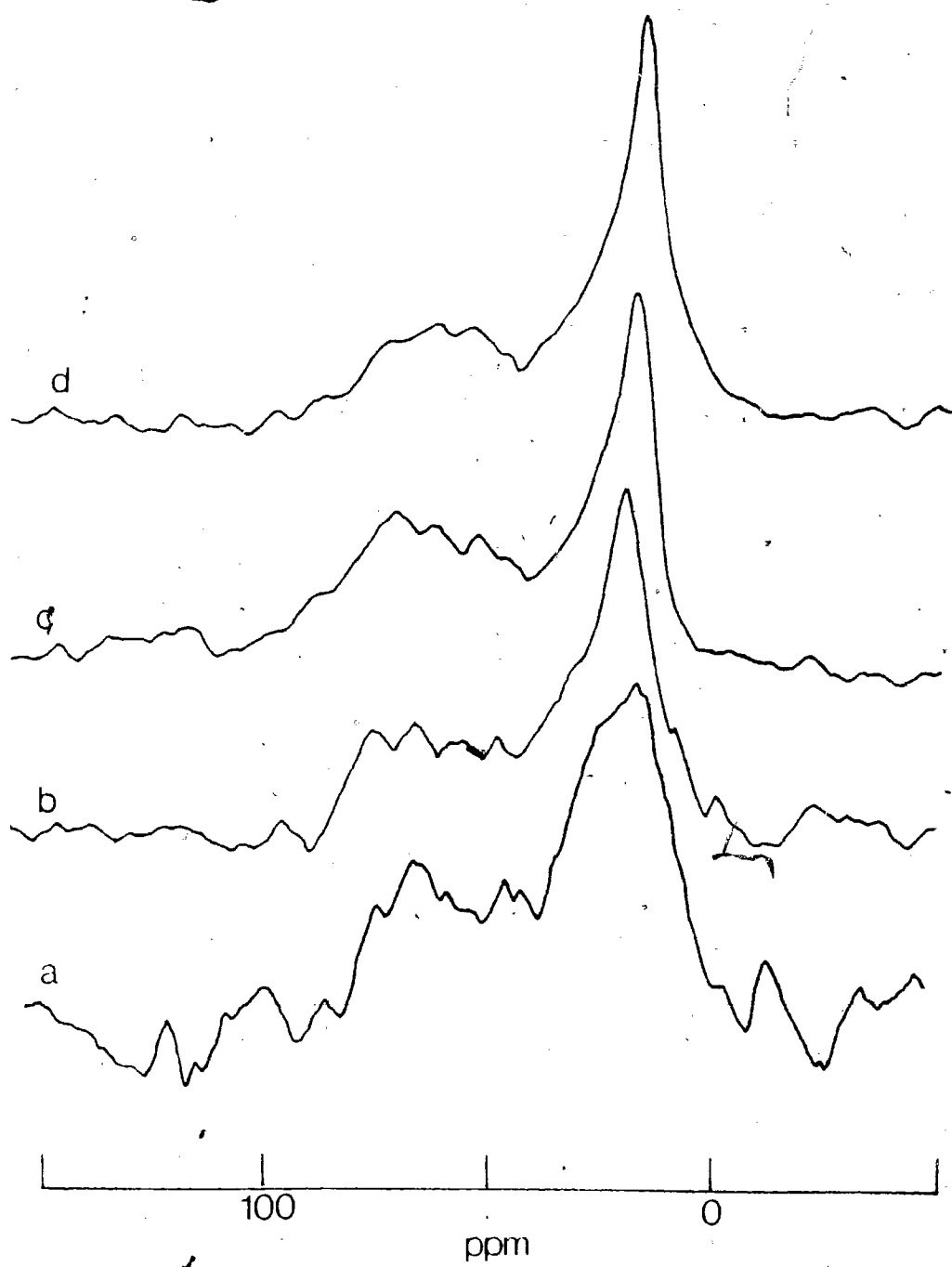


Figure 5.22

$^{13}\text{C}$  CP spectra of ethanol adsorbed on  $\text{MgO-(4)}$  at various coverages. Field strength = 40 kHz. Contact time = 2 msec. Rep. rate =  $2.5 \text{ sec}^{-1}$  except (d) which is  $3.3 \text{ sec}^{-1}$ .

- (a)  $4.02 \mu\text{mole/m}^2$ , 120,000 contacts
- (b)  $4.93 \mu\text{mole/m}^2$ , 143,400 contacts
- (c)  $5.79 \mu\text{mole/m}^2$ , 300,000 contacts
- (d)  $8.00 \mu\text{mole/m}^2$ , 222,400 contacts



some limited rotation about the C-C bond axis, but not fast enough, so that it could be observed in the CP spectrum.

5.C.II.  $^{13}\text{C}$  NMR Measurements of Adsorbed Ethanol Treated at Elevated Temperatures

Figures 5.23 to 5.26 show the static  $^{13}\text{C}$  CP spectra of one selected sample of ethanol-MgO system from each preparation of MgO when treated at elevated temperatures. At  $180^\circ$ , both carbon resonances in all spectra are broadened, probably due to the formation of more chemisorbed ethoxide species which overlap. As the samples were treated at  $300^\circ\text{C}$ , the spectra show a narrower methylene resonance, but a corresponding broader methyl resonance, for all samples.

If both anisotropies had narrowed, then they could be attributed to surface "recrystallization" on heating and cooling as was proposed for the similar situation in the methanol-MgO system, treated at  $300^\circ\text{C}$ .

In addition, there appears some feature in the  $\text{sp}^2$ -carbon region in all spectra from different samples. It is suspected that some of the surface ethoxide species may have decomposed at or below  $300^\circ\text{C}$  yielding other products. However, due to poor resolution in the spectra, these decomposed products cannot be identified.



Figure 5.23

$^{13}\text{C}$  CP spectra of  $8.01 \mu\text{mole/m}^2$  of ethanol adsorbed on MgO-(1) treated at elevated temperatures. Field strength = 40 kHz except (a) which is 70 kHz. Contact time = 2 msec except (a) which is 1.5 msec.

- (a) Room temp., rep rate =  $5 \text{ sec}^{-1}$ , 26,605 contacts
- (b)  $180^\circ\text{C}$  (3 hrs), rep rate =  $2.5 \text{ sec}^{-1}$ , 120,000 contacts
- (c)  $350^\circ\text{C}$  (3 hrs), rep rate =  $1.7 \text{ sec}^{-1}$ , 226,900 contacts
- (d)  $500^\circ\text{C}$  (3 hrs), rep rate =  $1 \text{ sec}^{-1}$ , 368,900 contacts
- (e) Same sample as in (d). Single-pulse  $^{13}\text{C}$  NMR spectrum, rep rate =  $0.67 \text{ sec}^{-1}$ , 16,695 scans.

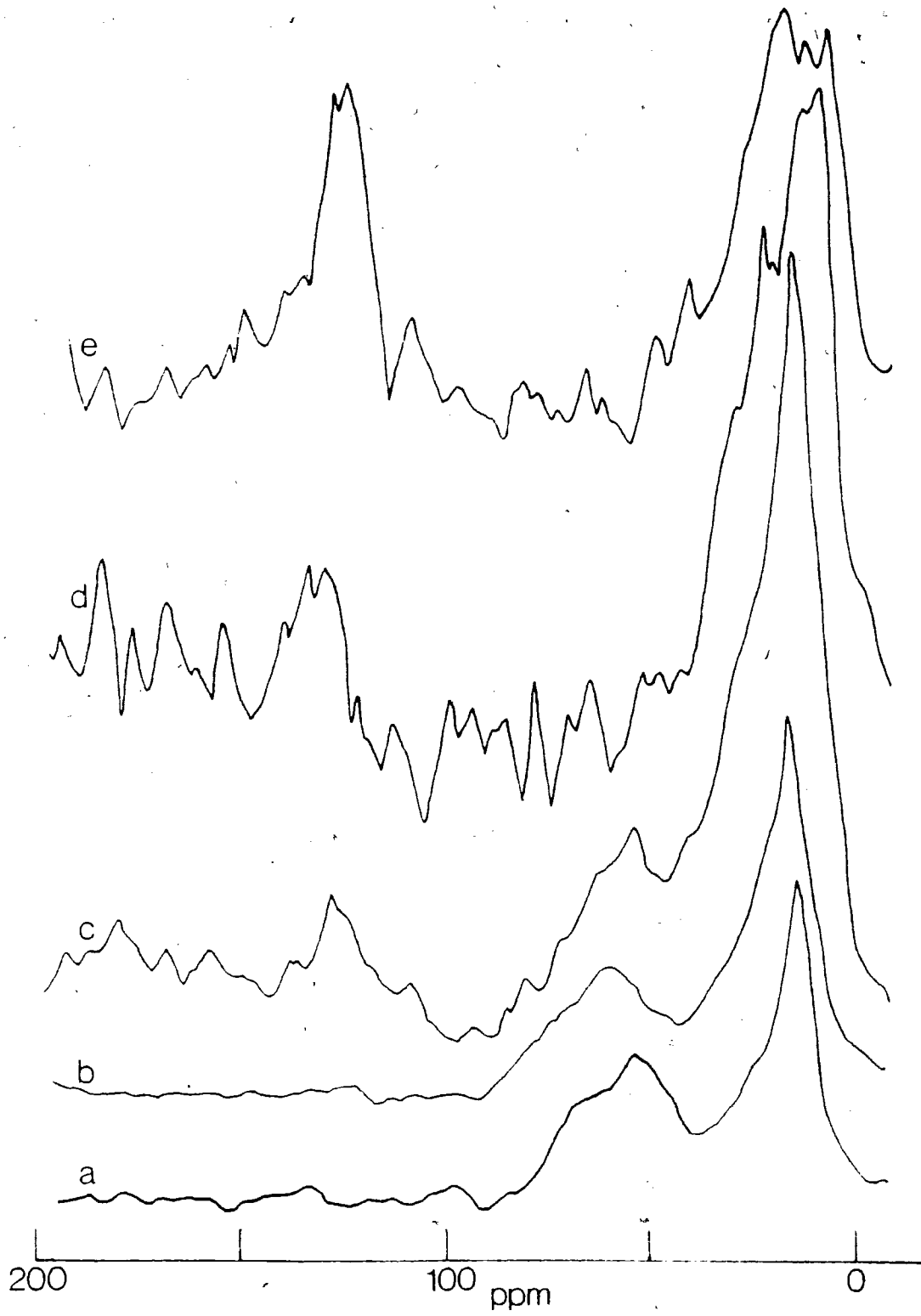


Figure 5.24

$^{13}\text{C}$  CP spectra of the sample of  $7.22 \mu\text{mole}/\text{m}^2$  of ethanol on  $\text{MgO}$ -(2) treated at elevated temperatures.

Field strength = 40 kHz except (a) which is 70 kHz.

Contact time = 2 msec, except (a) which is 1.5 msec.

(a) Room temp., rep rate =  $10.0 \text{ sec}^{-1}$ , 129,600 contacts

(b)  $180^\circ\text{C}$  (3 hrs), rep rate =  $5.0 \text{ sec}^{-1}$ , 293,400 contacts

(c)  $350^\circ\text{C}$  (3 hrs), rep rate =  $2.5 \text{ sec}^{-1}$ , 125,000 contacts

(d)  $500^\circ\text{C}$  (3 hrs), rep rate =  $3.3 \text{ sec}^{-1}$ , 444,600 contacts

(e) Same sample as in (d), but single-pulse  $^{13}\text{C}$  NMR, rep rate =  $2 \text{ sec}^{-1}$ , 64,626 scans.

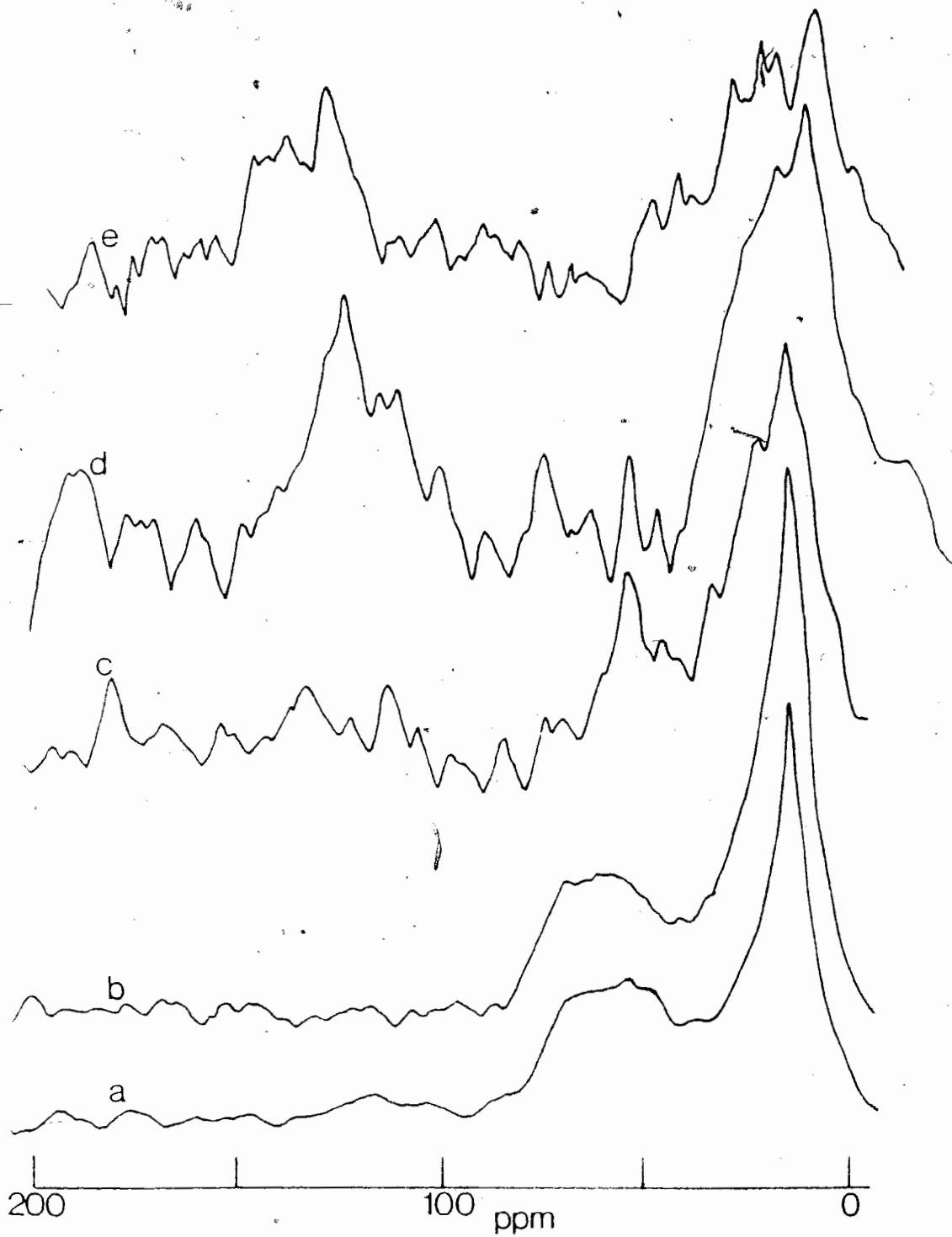


Figure 5.25

$^{13}\text{C}$  CP spectra of  $7.19 \mu\text{mole/m}^2$  of ethanol adsorbed on MgO-(3) treated at elevated temperatures. Field strength = 40 kHz except (a) which is 70 kHz. Contact time = 2 msec, except (a) which is 1.5 msec.

(a) Room temp., rep rate =  $10 \text{ sec}^{-1}$ , 47,212 contacts

(b)  $180^\circ\text{C}$  (3 hrs), rep rate =  $2.5 \text{ sec}^{-1}$ , 60,000 contacts

(c)  $350^\circ\text{C}$  (3 hrs), rep rate =  $2 \text{ sec}^{-1}$ , 114,600 contacts

(d)  $500^\circ\text{C}$  (3 hrs), rep rate =  $3.3 \text{ sec}^{-1}$ , 214,475 contacts

(e) Same sample as in (d). Single-pulse  $^{13}\text{C}$  NMR spectra at rep rate =  $3.3 \text{ sec}^{-1}$ , 66,620 scans.

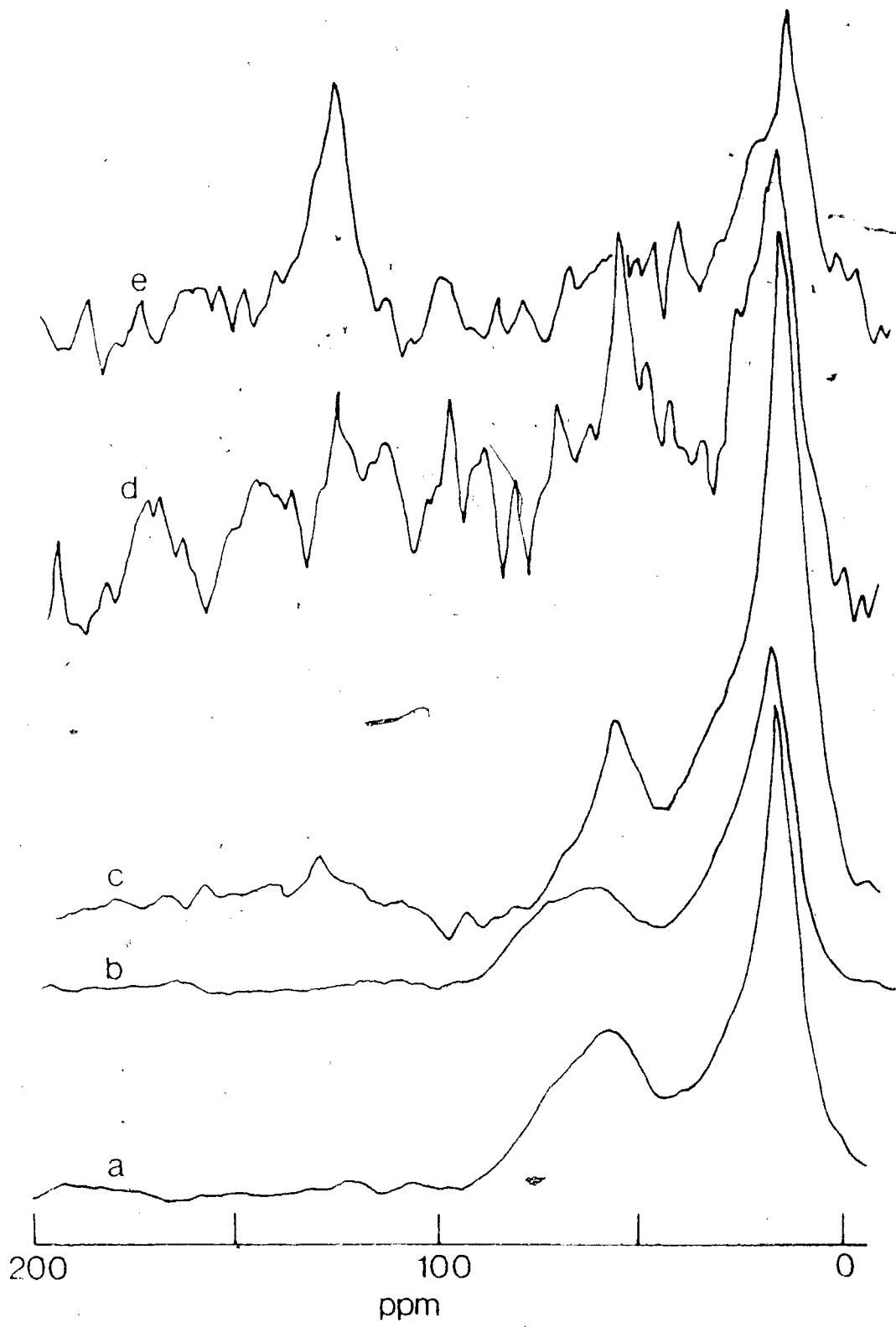


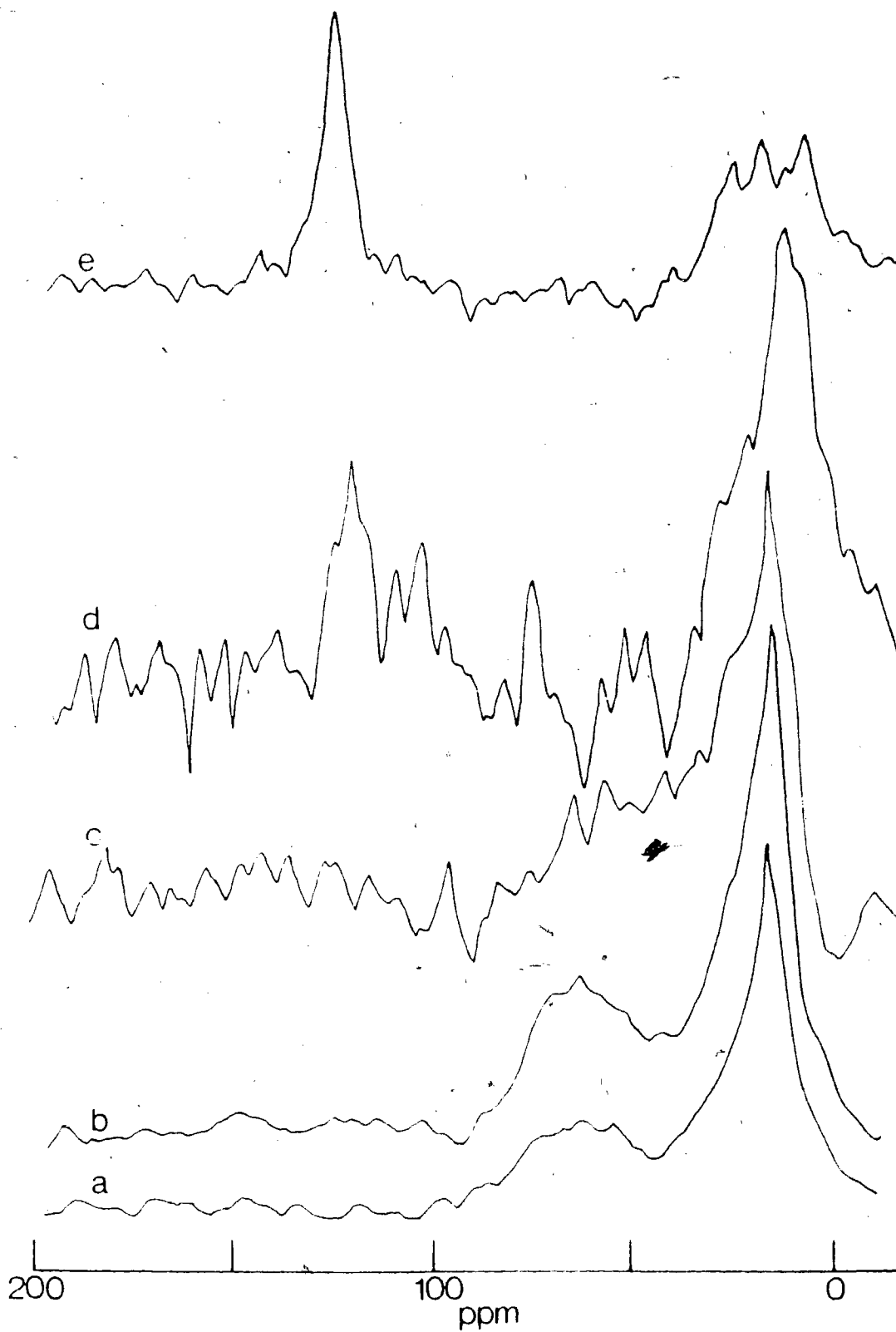
Figure 5.26

$^{13}\text{C}$  CP spectra of the sample of  $8.00 \mu\text{mole}/\text{m}^2$  of ethanol adsorbed on  $\text{MgO}$  (4) treated at elevated temperature.

Field strength = 40 kHz. Contact time = 2 msec.

- (a) Room temp., rep rate =  $3.3 \text{ sec}^{-1}$ , 222,400 contacts
- (b)  $180^\circ\text{C}$  (3 hrs), rep rate =  $1 \text{ sec}^{-1}$ , 78,369 contacts
- (c)  $350^\circ\text{C}$  (3 hrs), rep rate =  $0.6 \text{ sec}^{-1}$ , 37,298 contacts
- (d)  $500^\circ\text{C}$  (3 hrs), rep rate =  $2 \text{ sec}^{-1}$ , 749,000 contacts
- (e) Same sample as in (d). Single-pulse  $^{13}\text{C}$  NMR at rep rate of  $2 \text{ sec}^{-1}$  and 68,359 scans.







When treated at 500°C, all samples turned to a greyish color, distinctly different from the original white color of the MgO. The  $^{13}\text{C}$  CP spectra, in all cases, show two major resonances at 20 and 120 ppm respectively downfield from TMS, except for ethanol-MgO-(3) which reveals another resonance at 50 ppm downfield from TMS also. It appears that most of the original ethoxide species have decomposed, yielding mainly hydrocarbons (of both saturated and unsaturated categories), except for ethanol-MgO-(3) system, in which some alkoxide species (at  $\sim 60$  ppm) still remained. The single-pulse  $^{13}\text{C}$  NMR spectra (e) in all figures (for the same sample treated at 500°C) reveal the same resonances, indicating that the surface species have short carbon  $T_1$ , and they are probably hydrocarbons.

### 5.C.III. $^{13}\text{C}$ CP/MAS Studies of Adsorbed Ethanol on MgO

Two samples, each containing ca. 0.2 gm of MgO-(3) were tightly packed into 5 mm o.d. tubes, and  $4.3 \times 10^{-5}$  moles of either 90%  $^{13}\text{C}$ -enriched ethanol-1- $^{13}\text{C}$  or ethanol-2- $^{13}\text{C}$  was adsorbed onto the MgO (corresponding to a coverage of  $1.3 \mu\text{mole/m}^2$ ) from gas-phase at room temperature. The  $^{13}\text{C}$  CP/MAS spectra of these two samples at room temperature and after treatment at elevated temperatures are shown in Figures 5.27 and 5.28 respectively. Corresponding single-pulse  $^{13}\text{C}$  NMR/MAS spectra were also measured for the same samples at the various temperatures are shown in Figures 5.29 and 5.30.

Figure 5.27  $^{13}\text{C}$  CP/MAS spectra of 90%  $^{13}\text{C}$ -enriched ethanol-1- $^{13}\text{C}$  on MgO-(3), at room temperature and treated at elevated temperatures. Temperature is designated on the left-hand-side of the spectra, and the heating period was 3 hours, unless otherwise specified. All spectra were normalized for the number of contacts with respect to the spectrum recorded at room temperature. Field strength = 60 kHz. Rep. rate = 2 sec<sup>-1</sup>. Spinning rate = 1.8 kHz. Contact time = 2 msec.

8

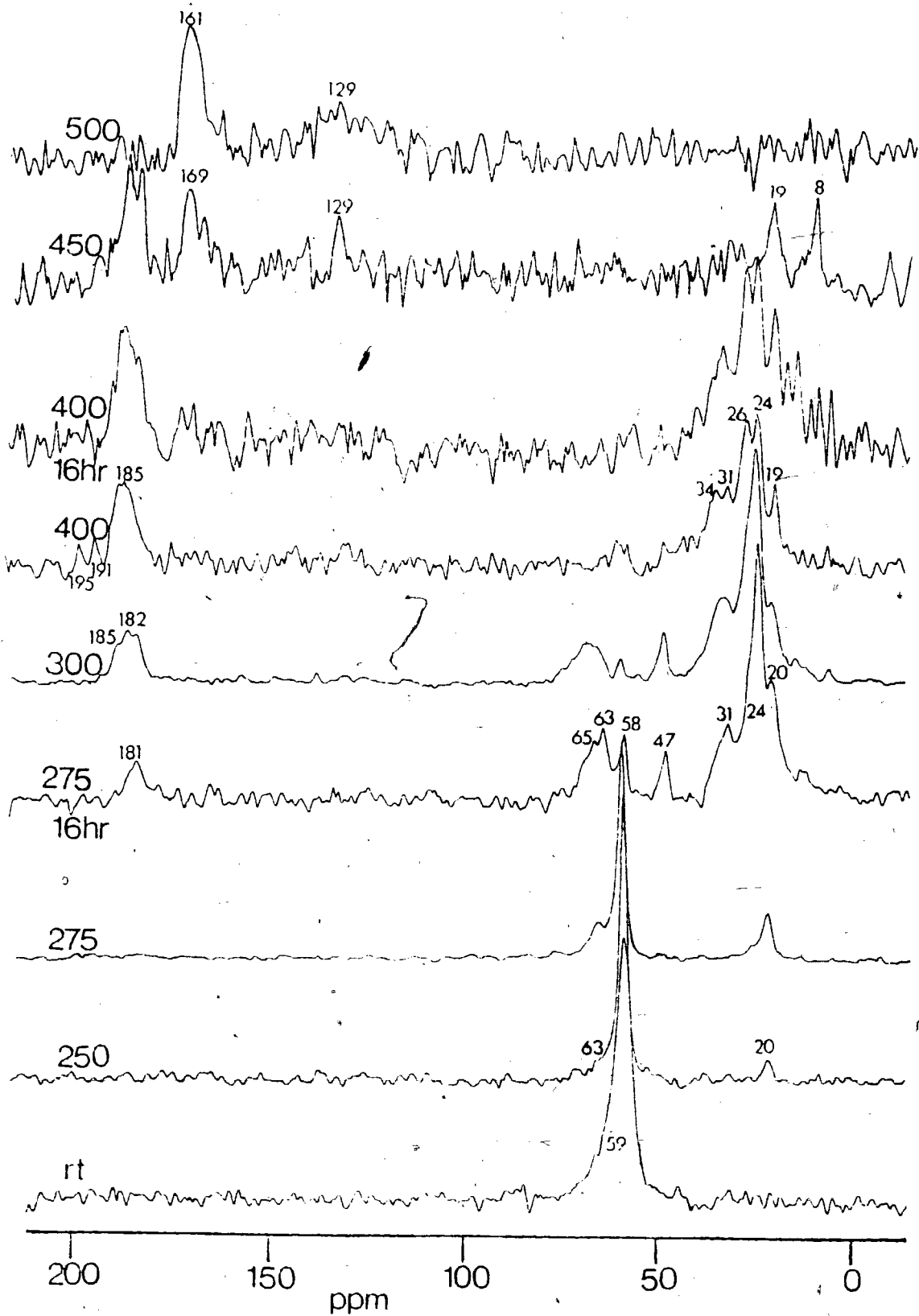


Figure 5.28  $^{13}\text{C}$  CP/MAS spectra of 90%  $^{13}\text{C}$ -enriched ethanol-2- $^{13}\text{C}$  on MgO-(3) at room temperature and treated at elevated temperatures. Designation and normalization same as in Figure 5.27.

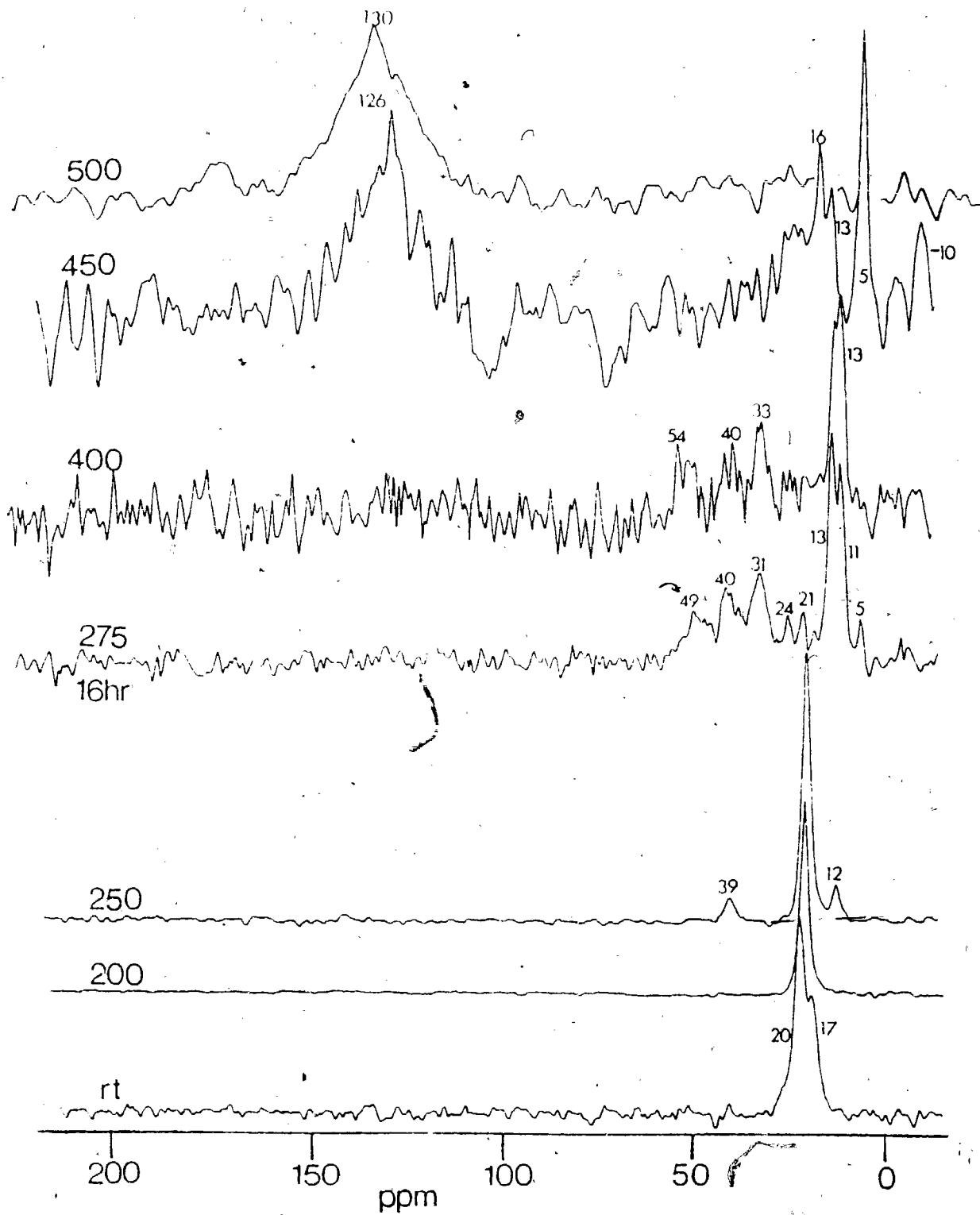


Figure 5.29 <sup>13</sup>C MAS NMR spectra of the same sample as in Figure 5.27 treated at elevated temperature. Designation and normalization same as in Figure 5.27. Rep. rate = 2 sec<sup>-1</sup>. Decoupler on during acquisition.

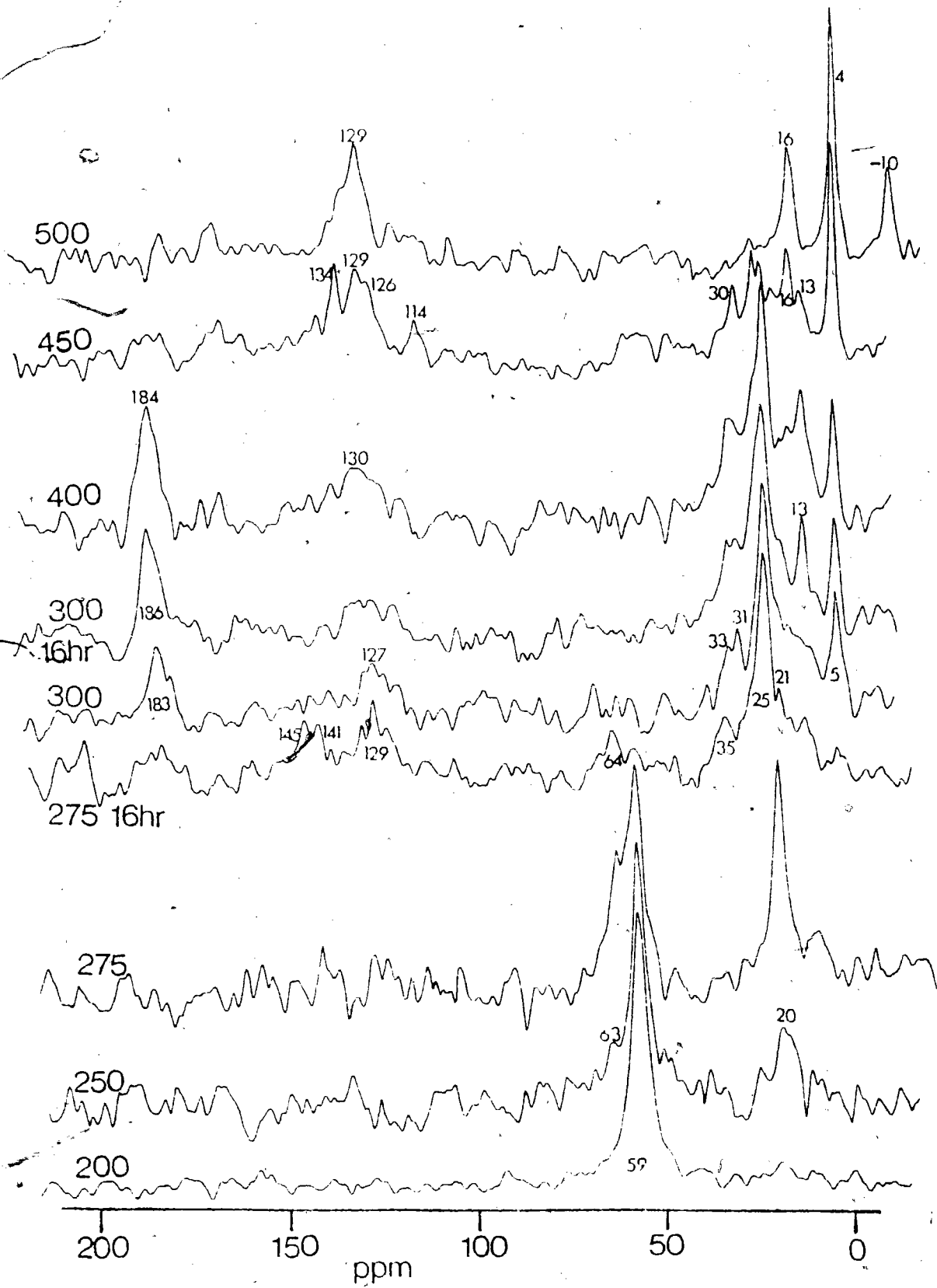
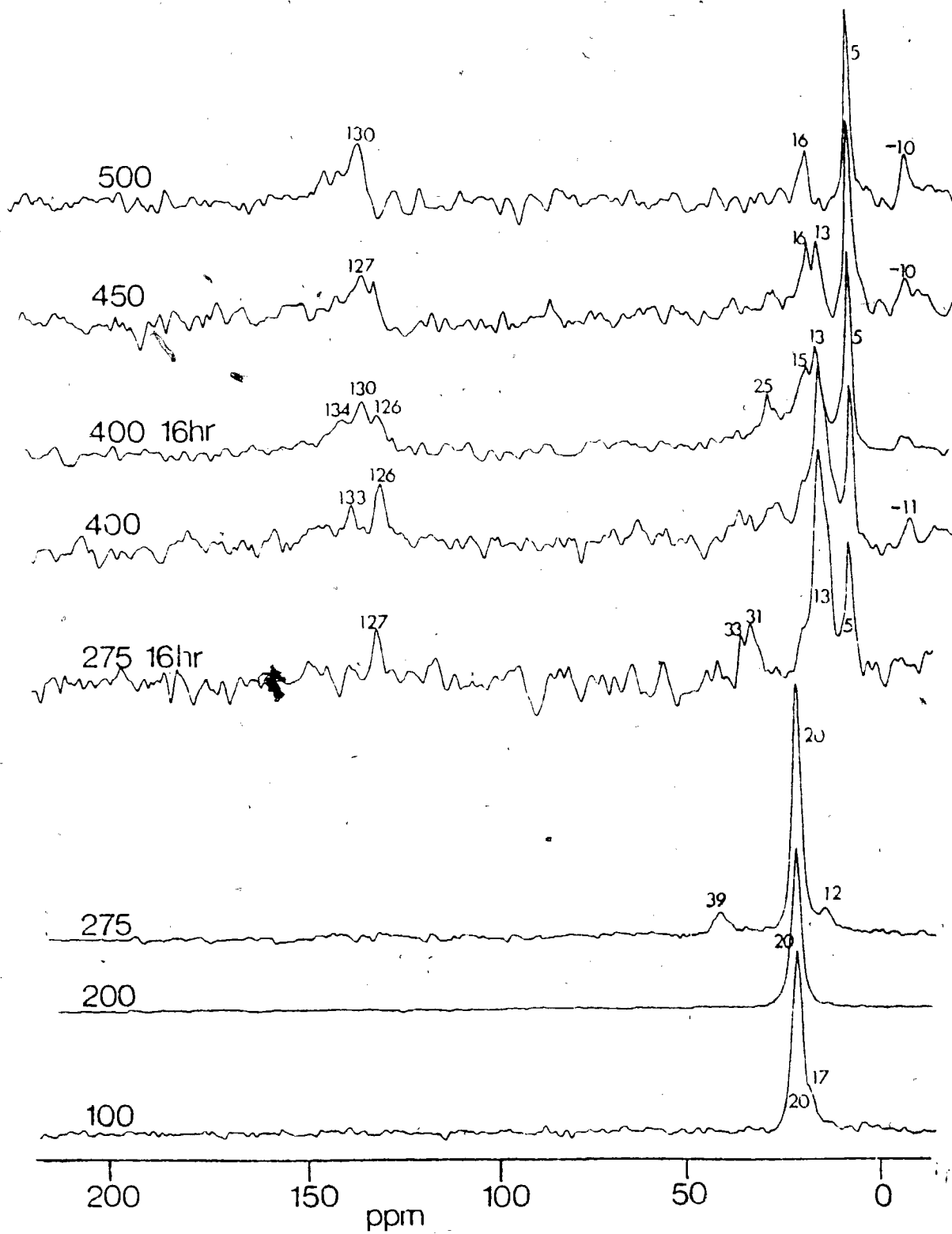


Figure 5.30  $^{13}\text{C}$  MAS NMR spectra of the same sample as in Figure 5.28 treated at elevated temperatures. Designation and normalization same as in Figure 5.28. Rep. rate =  $2 \text{ sec}^{-1}$ . Decoupler on during acquisition.





No change was observed at treatment temperatures below 250°C, so only one representative spectrum is shown in each figure. In general, temperature was raised in increments of 50°C, and the samples were heated at that temperature for three hours, except at 275°, 300° and 400°C, at which temperature, the samples were heated for another 16 hours, after the initial heating for 3 hours.

(i) Room Temperature to 200°C

From Figures 5.27 and 5.28, the resonance of the surface ethoxide species appear at 20 and 58 ppm downfield from TMS for the methyl and methylene carbon respectively. While there is a small difference in the chemical shift (ca. 1 ppm) for the methylene carbon, the chemical shift of the methyl resonance is significantly different from the methyl resonance at 22.5 ppm for magnesium ethoxide in the polymeric form (133), or the methyl resonance at 17.3 ppm for liquid ethanol (134). The downfield shift of 2.7 ppm for the methyl resonance of the surface magnesium ethoxide and the 5.2 ppm for the magnesium ethoxide polymer relative to the liquid ethanol is probably due to the spatial interaction of the -CH<sub>3</sub> group with the neighbouring Mg<sup>2+</sup> ions which serve to deshield the methyl resonance.

The picture of chemisorbed ethanol on MgO is then a tightly bound ethoxide species possessing characteristics between that of liquid-like ethanol and the magnesium ethoxide

polymer. It also implies that the  $-CH_3$  group of the adsorbed ethoxide species lies very close to the surface and more specifically in close proximity with immediate  $Mg^{2+}$  neighbours. This could occur by rotational hop about the  $Mg-O-C$  bond.

The resonance at 17 ppm in Figures 5.28 and 5.30 (on the high field shoulder of the 20 ppm resonance), is attributed to physisorbed ethanol molecules on the MgO surface. This resonance eventually disappeared when the sample was treated at  $200^\circ C$ , which probably indicates a complete conversion of the physisorbed ethanol to chemisorbed ethoxide species.

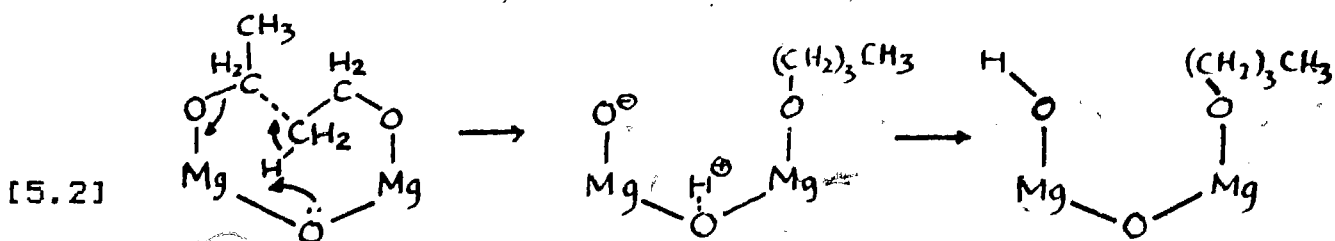
(ii)  $250^\circ C$ , 3 hours

New resonances appear in both spectra as shown in Figures 5.27 and 5.28. The  $-CH_2$  group gives rise to new resonances at 63 and 20 ppm (Figure 5.27), and the  $-CH_3$  group gives rise to new resonances at 39 and 12 ppm respectively (Figure 5.28). Note that in these two parallel experiments, only one carbon of the ethanol was enriched with 90%  $^{13}C$ , so it will be this carbon that was observed. Any new resonance(s) observed have to originate from this carbon, while the other carbon (containing only 1.1% natural abundant  $^{13}C$ ) will be obscured in the noise. Combining the two spectra would then imply that some of the chemisorbed ethoxide species are converted to one or more compounds having  $^{13}C$  resonances at 12, 20, 39 and 63 ppm downfield from TMS upon heating at  $250^\circ C$  for

3 hours. The surface ethoxide remains as the major species in the sample.

The identity of this intermediate is suggested to be an adsorbed n-butoxide species. The  $^{13}\text{C}$  chemical shifts have been measured for adsorbed n-butanol on  $\text{MgO}$  and they are 64.0, 41.3, 20.1 and 13.2 ppm downfield from TMS at a coverage of  $3.44 \mu\text{mole}/\text{m}^2$ . As the coverage is increased to  $7.26 \mu\text{mole}/\text{m}^2$ , there appears a new resonance at 36.4 ppm, while the original peak at 41.3 ppm appears as a low-field shoulder at 40.6 ppm. The chemical shifts of 64.0, 36.4, 20.1 and 14.1 ppm are very close to the literature values of 61.7, 35.3, 19.4 and 13.9 ppm reported for liquid n-butanol (134). This suggests that as the n-butanol is adsorbed on the  $\text{MgO}$  surface, both the  $\alpha$ - and  $\beta$ -carbons adjacent to the  $-\text{OH}$  group experience a deshielding effect from the surface  $\text{Mg}^{2+}$  ions, so that the resonances at 64.0, 41.3, 20.1 and 13.2 ppm are observed. As the coverage is increased, physisorbed n-butanol appear, yielding the extra resonance at 36.4 ppm for the  $\beta$ -carbon.

For the formation of this n-butoxide intermediate, the following mechanism involving two neighbouring adsorbed ethoxide species is proposed:



This mechanism is practical because : (a) it involves a six-membered ring intermediate which is stable, (b) MgO is known to be a dehydrogenation catalyst, and the lone pair of electrons on the O atom can abstract the acidic proton from the methyl group, (c) the observed  $^{13}\text{C}$  CP/MAS spectra agree with the given mechanism: when ethanol-1- $^{13}\text{C}$  is used, this will give rise to labels at the C-1 and C-3 carbons on the resulting n-butoxide species and resonances at 63 and 20 ppm respectively, and indeed this is observed in Figure 5.27. Conversely, when ethanol-2- $^{13}\text{C}$  is used, this will give rise to the C-2 and C-4 labels on the resulting n-butoxide and resonances at 41 and 13 ppm respectively, as shown in Figure 5.28.

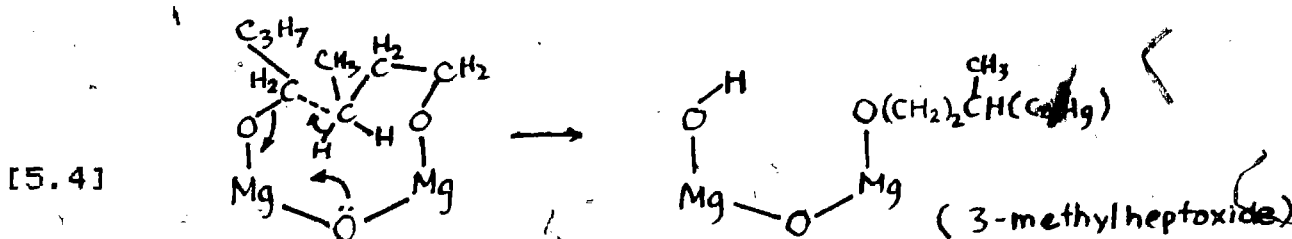
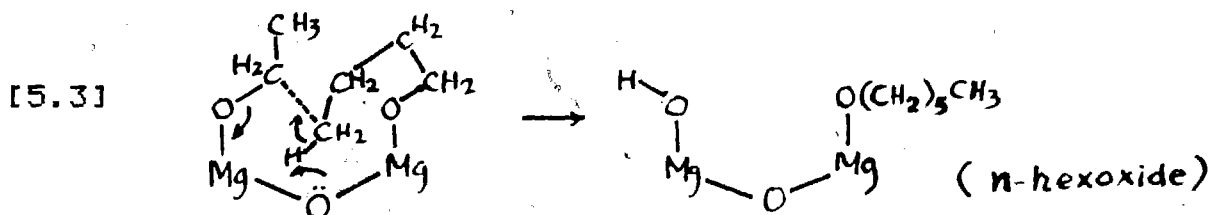
The single-pulse  $^{13}\text{C}$  NMR/MAS spectra in Figures 5.29 and 5.30 show essentially the same resonances as those in Figures 5.27 and 5.28.

(iii) 275°C, 16 hours

Further changes in the spectra in Figures 5.27 and 5.28 occurred when the samples were treated at 275°C for 16 hours. The resonances corresponding to the original surface ethoxide species (at 58 and 20 ppm), and the n-butanol species (at 63, 39, 20, 14 ppm) still persist in the spectra, although the resonances corresponding to the ethoxide species have gone down in intensity.

New resonances include one at 181 ppm and a series of peaks in the range from 24 to 65 ppm in Figure 5.27, and a series of resonances from 5 to 49 ppm in Figure 5.28. The resonances at 181 ppm (Figure 5.27) and the 24 ppm resonance (Figure 5.28) probably correspond to a surface acetate species. Magnesium acetate has isotropic shifts at 181 and 25 ppm, according to the study in this laboratory and that of Ganapathy et al. (135). However, present spectroscopic evidence is insufficient for a positive identification, although infrared data has strongly suggested the conversion of ethanol to an acetate species at 335°C (46).

The rest of the resonances in the spectra in Figures 5.27 and 5.28 are attributed to the products of reaction between ethoxide and butoxide, and between two butanol species on the MgO surface, to yield a mixture of straight-chain or branched-chain alcohols. The mechanism of formation would be similar to that for n-butoxide proposed above, for example:



In keeping with the six-membered ring intermediate, the following alcohols are possible reaction products: n-hexanol, n-octanol, 2-ethylbutanol, 3-methylpentanol, 3-methylheptanol and 2-ethylhexanol. Most of these alcohols do not have reported  $^{13}\text{C}$  chemical shift data, so they are calculated by the formulae from Eijchart (136) and Roberts et al. (137), with the chemical shift data from their respective alkane precursors (138). These data are listed in Table 5.4. From the broadness of the resonances observed, it is speculated that most (if not all) of the alcohols listed in Table 5.4 are present as reaction products, and their  $^{13}\text{C}$  resonances overlapped.

As was mentioned above, that both the  $\alpha$ - and  $\beta$ -carbons of the alcohols experience some deshielding effects upon adsorption on the surface, therefore, without the spectra of the appropriate reference alcohols on the MgO surface, it is impossible to identify all resonances on the spectra in Figures 5.27 and 5.28.

It is also suspected that some decomposition has set in to yield some hydrocarbons at this experimental condition. This arises from the observation of the resonance at 5 ppm (in Figures 5.28, 5.29 and 5.30). Only ethane has  $^{13}\text{C}$  chemical shifts so far upfield. This resonance is not observed in Figure 5.27, probably due to inadequate S/N and resolution.

TABLE 5.4

Calculated  $^{13}\text{C}$  Chemical Shifts of some Alcohols (a) pertinent to this work

	<u>C-1</u>	<u>C-2</u>	<u>C-3</u>	<u>C-4</u>	<u>C-5</u>	<u>C-6</u>	<u>C-7</u>	<u>C-8</u>
4 3 2 1 C-C-C-C-OH (b)	61.5	35.1	19.2	13.7				
6 5 4 3 2 1 C-C-C-C-C-OH (b)	62.0	32.9	25.9	32.1	22.9	14.3		
8 7 6 5 4 3 2 1 C-C-C-C-C-C-OH (b)	62.0	33.0	26.2	29.8	29.7	32.2	22.9	14.0
C   C								
C-C-C-C-OH 4 3 2 1	64.3	42.6	22.0	10.4 (c)				
C <sup>6</sup> 								
C-C-C-C-OH 5 4 3 2 1	60.8	39.4	30.8	29.4 (c)	10.8 (c)	18.7 (c)		



Table 5.4 (continued)

$  \begin{array}{c}  \text{C}^8 \\    \\  \text{C}-\text{C}-\text{C}-\text{C}-\text{C}-\text{C}-\text{C}-\text{OH} \\  7 \quad 6 \quad 5 \quad 4 \quad 3 \quad 2 \quad 1  \end{array}  $	60.2	39.9	29.1	36.6(c)	29.2(c)	22.9(c)	13.6(c)	20.1(c)
$  \begin{array}{c}  \text{C}^8 \\    \\  \text{C}^7 \\    \\  \text{C}-\text{C}-\text{C}-\text{C}-\text{C}-\text{C}-\text{OH} \\  6 \quad 5 \quad 4 \quad 3 \quad 2 \quad 1  \end{array}  $	64.6	41.0	29.2	29.1(c)	23.0(c)	13.6(c)		22.4

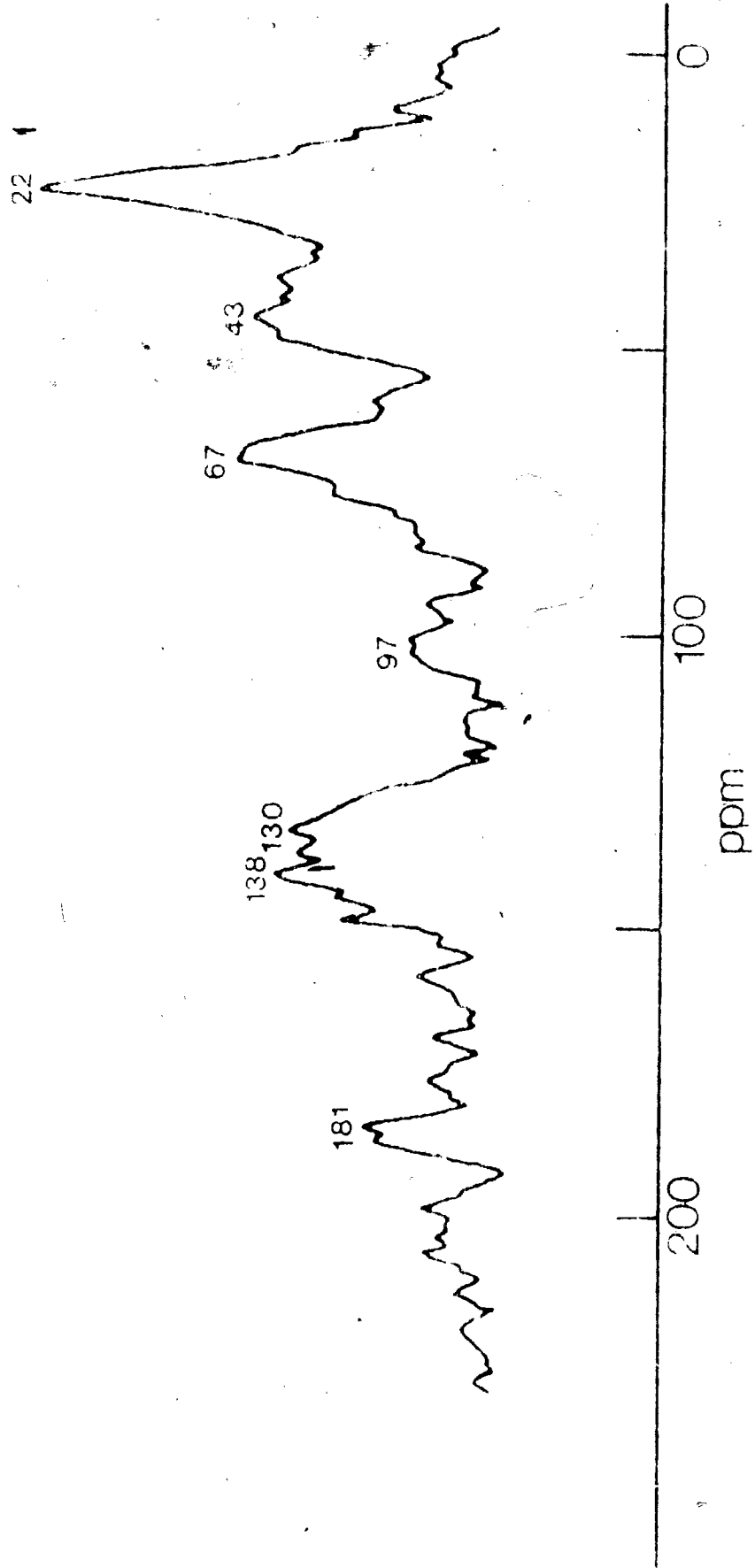
(a) all  $^{13}\text{C}$  chemical shift data are corrected to TMS scale

(b) data obtained from ref. 137

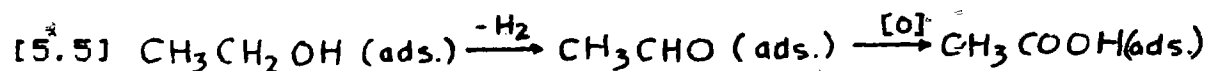
(c)  $\delta$ -effects are estimated from formula given in ref. 137. All other  $\alpha$ ,  $\beta$  and  $\gamma$  effects are estimated from parameters given by Eijchart (ref. 138)

For comparison, the  $^{13}\text{C}$  CP/MAS spectrum of adsorbed acetaldehyde on MgO at room temperature was measured. The resonances at 30 and 199 ppm corresponding to free acetaldehyde (124) are missing in the spectrum (see Figure 5.31). A rather complicated spectrum is observed, with major peaks at 22, 43, 67, 93, 130, 138 and 181 ppm downfield from TMS. It was suspected that acetaldehyde has probably undergone some reaction on the surface. The resonances at 22 and 97 ppm probably indicate the formation of aldoxan (the trimer of acetaldehyde) (139). The same resonance at 181 ppm observed earlier is also present in this spectrum. Two explanations can be proposed, first, that the carbonyl carbon on acetaldehyde experiences a chemical shift change of 18 ppm upfield (!), and second, that the acetaldehyde is oxidized to an acetate species upon adsorption on the MgO surface (while the methyl resonance of this acetate species is obscured under the 22 ppm resonance). The second explanation is favored in view of the complexity of the spectrum, which indicates polymerization (to aldoxan), dehydrogenation (to yield olefinic compounds with resonances in the 130-138 ppm region), reduction to alcohols, indicated by the resonance at 67 ppm) and probably some oxidation (to the acetate species at 181 ppm).

Returning to the present system of adsorbed species treated at 275°C for 16 hours, if some of the adsorbed ethoxide species were oxidized to the acetate species, some acetaldehyde intermediates would have been observed, that is, via the



following mechanism:



For the discussion given above to be correct, either the concentration of the surface acetaldehyde species has to be very low (below detection level), or the half-life of this acetaldehyde species has to be very short (unobservable beyond 16 hours). Since the reaction condition is quite vigorous (275°C for 16 hours), the second explanation seems to be reasonable.

The  $^{13}\text{C}$  single-pulse NMR/MAS spectra shown in Figures 5.29 and 5.30 exhibit little resemblance to the  $^{13}\text{C}$  CP/MAS spectra shown in Figures 5.27 and 5.28. The obvious difference is the presence of the resonances in the 120-150 ppm region (corresponding to  $\text{sp}^2$  carbons). Obviously, this indicates the presence of some physisorbed olefins which possess relatively high frequency motions (compared to the chemisorbed species). We propose that some of the surface alkoxide species may have decomposed at the C-O bond to yield a variety of olefins such as ethene, 1-butene (from dehydration of n-butanol), cis and trans-2-butene (from isomerization of 1-butene), and other branched-chain alkenes (from their respective branched-chain alcohol precursors). The resonances at 141 and 145 ppm are attributed to olefinic carbons with alkyl group substituents (139). These alkenes may have arisen from the decomposition of

the branched-chain alcohols listed in Table 5.4. The resonance at 5 ppm (which was attributed to ethane earlier) gives additional evidence that decomposition has taken place on the surface at this experimental conditions. However, the possibility of these  $sp^2$  carbons being aromatics could not be ruled out, although the mechanisms of formation would be very complicated.

The complete identification of all the resonances in both spectra is hampered by the inadequate resolution and the lack of reference materials. However, from the relative decrease in intensity (or the absence) of the resonances in the 40-70 ppm region in Figure 5.29 and in the 35-50 ppm region in Figure 5.30, it can be concluded that most of the physisorbed alcohols have been reacted, or converted to chemisorbed species (observed only in the  $^{13}C$  CP/MAS spectra).

(iv) 300°C, 16 hours

Although no spectra are shown, there is a complete disappearance of the resonance at 58 ppm (in Figure 5.27) and at 20 ppm (in Figure 5.28), implying that all surface ethoxide species have been converted. No new resonances are observed.

(v) 400°C, 3 hours

Both samples turned a slight greyish color after the heat treatment. The two resonances at 191 and 195 ppm

in the spectrum in Figure 5.27 indicate the presence of ketones. This could arise from the further oxidation of the alkoxide species on the surface. Note that this ketone species would have to be quite inert on the MgO surface. The  $^{13}\text{C}$  CP/MAS spectrum of adsorbed acetone is shown in Figure 5.42. From the complexity of this spectrum, it is suspected that acetone probably undergoes some reaction on the MgO surface yielding a variety of products. From this experience, the proposed "ketone" species probably contains bulky alkyl groups as protecting groups.

The possibility of these resonances belonging to an ester species is ruled out. The  $^{13}\text{C}$  chemical shifts of most esters lie between 160 to 180 ppm (134), and a downfield shift of ca. 20 ppm (to yield resonances at 190 ppm in the present spectrum) is unthinkable.

A complex of the type Mg-CO (terminal carbonyl) could not be excluded although it was found that carbon monoxide does not adsorb on the MgO surface in any appreciable amount, and no  $^{13}\text{C}$  CP spectrum could be obtained. Metal carbonyls have anisotropies of about 400 ppm (18). The spinning rate (ca. 1.8 kHz) used in this experiment is not fast enough to average out the whole anisotropy, and one would observe the first sidebands at about 120 ppm on either side of the resonance at ca. 190 ppm (if it was a Mg-CO species). Since these sidebands are not

observed in the present spectrum, the possibility of a Mg-CO species could be ruled out.

The resonances which were originally assigned as the  $\alpha$  -carbons of the surface alkoxide species in Figure 5.27 have all disappeared after treatment at 400°C for 3 hours. However, the resonances which were attributed to the other carbons on the aliphatic alcohols still persist in the 20-35 ppm region, with an additional peak at 26 ppm. One could suggest that the decomposition of the surface alkoxide species is complete at this stage. This is also supported by the huge increase in the intensity of the resonance at 185 ppm (the acetate species).

Resonances corresponding to olefinic hydrocarbons or aromatics are still observed in the spectra in Figures 5.29 and 5.30 (no such resonances in Figures 5.27 and 5.28). The  $^{13}\text{C}$  MAS/NMR spectrum in Figure 5.30 indicates the presence of methane at 11 ppm upfield from TMS.

(vi) 450°C, 3 hours

There are significant changes in both  $^{13}\text{C}$  CP/MAS spectra as shown in Figures 5.27 and 5.28. In Figure 5.27, only the acetate resonance at 182 ppm remains the same. The new resonance at 169 ppm probably corresponds to a carbonate species next to a surface -OH group, or a bicarbonate species, which arises from the decomposition of the acetate species. The rest of the resonances at 129, 29, 27, 19 and 8 ppm are probably a

mixture of saturated and unsaturated hydrocarbons.

In Figure 5.28, a very broad peak in the olefinic region (110-140 ppm) appears in the spectrum. Coupled with the other resonances below 50 ppm, this probably indicates a wide range of unsaturated and saturated hydrocarbons, as in the case in Figure 5.27.

There are no essential changes in the  $^{13}\text{C}$  NMR/MAS spectra in Figures 5.29 and 5.30.

(vii) 500°C, 3 hours

Both samples turned a dark grey color after this treatment. In Figure 5.27, the resonance at 161 ppm probably corresponds to a bicarbonate species, originating from the carbonate species discussed earlier. The broad patterns (centered at 129 ppm) are probably the remnants of olefins (or aromatics) which are still quite tightly bound on the surface. In Figure 5.28, only a broad resonance centered at 130 ppm remains. It is speculated that the previously tightly-bound hydrocarbons are either distilled off or they became physisorbed on the MgO surface.

The broad resonance centered at 130 ppm raises some speculation.  $^{13}\text{C}$  CP/MAS studies on coal (147-149) showed two broad resonances, in the aromatic region (110-150 ppm) and the aliphatic region (10-50 ppm). Inspection of the coal spectra



and the present spectrum show close resemblance in the aromatic region. The aliphatic region resonance is absent in the present spectrum. This tends to suggest a graphite type species in the MgO sample. However,  $^{13}\text{C}$  NMR study on graphite (150, 151) revealed two broad resonances centered at ca. 170 ppm downfield and ca. 50 ppm upfield from TMS respectively. FWHM of each resonance is about 70 to 100 ppm wide. This leads to the speculation that the black color in the MgO samples (developing into an overall greyish color with the MgO) are due to condensed aromatics, on the way to become graphite.

The single pulse  $^{13}\text{C}$  MAS/NMR spectra in Figures 5.29 and 5.30 show three distinct resonances, at 16 and 5 ppm downfield from TMS, and 10 ppm upfield from TMS. They probably correspond to propane, ethane and methane respectively.

#### 5.C.IV. Summary

All the room temperature  $^{13}\text{C}$  CP spectra of the ethanol-MgO systems show a narrow resonance for the methyl group and a relatively broad methylene resonance. The  $^{13}\text{C}$  CP spectra of the ethanol-MgO samples treated at higher temperatures are not very informative. This is because of the broadness of the anisotropies which obscure any changes.

However, employing the CP/MAS technique and selectively  $^{13}\text{C}$  enriched ethanol enable one to investigate the mode of adsorption of ethanol on MgO, and identify some of the

intermediates as the ethanol-MgO system was treated to successively higher temperatures.

It is found that the chemisorbed ethanol on MgO behaves somewhere between liquid ethanol and solid magnesium ethoxide polymer. This is substantiated by the chemical shift change of the  $-CH_3$  resonance of ethanol upon adsorption on MgO. This chemisorbed ethoxide species is stable on the MgO surface up to 250°C. At this treatment temperature, a n-butoxide species is observed on the surface.

At slightly higher temperature and a longer duration (275°C, 16 hours), the spectra become very complicated and overlapping resonances are observed. It is postulated that these resonances at high field are products of cross-reaction between the surface ethoxide and n-butoxide species. A low field resonance is also observed, this is attributed to a surface acetate species. The mechanism of its formation is uncertain, since no acetaldehyde intermediate was observed (probably below detection limit).

The  $^{13}C$  MAS/NMR spectra of these samples show some resonances in the  $sp^2$ -carbon region (120-150 ppm region). This could be attributed to some physisorbed unsaturated hydrocarbons, or aromatics.

All the adsorbed ethanol (chemisorbed or otherwise)

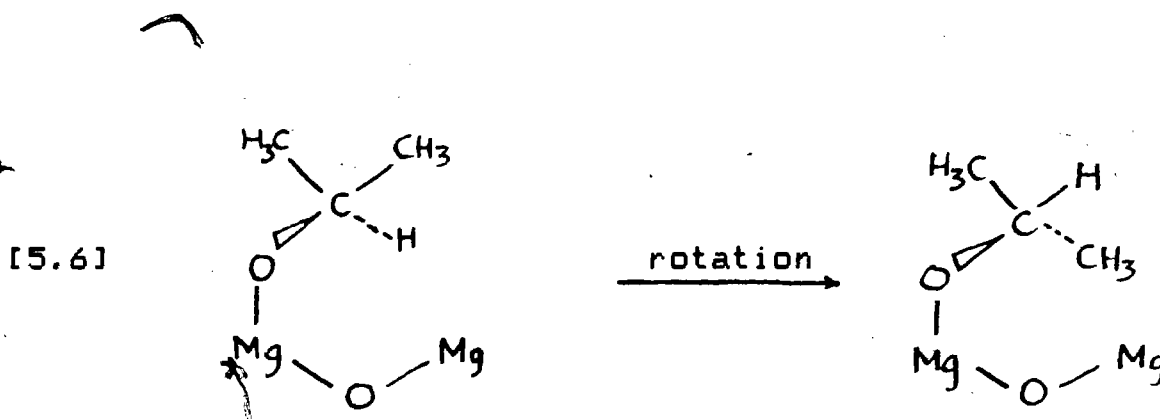
disappears when the samples were treated at 300°C. At this stage, the conversion products (from ethanol) are mainly some higher alcohols (C<sub>2</sub>-C<sub>6</sub>), acetates and some unsaturated hydrocarbons (olefins or aromatics).

At 400°C, all surface alkoxides have decomposed, yielding a variety of hydrocarbons (in fragmented or polymeric form). Small molecular weight hydrocarbons (e.g. CH<sub>4</sub>, C<sub>2</sub>H<sub>6</sub>) are also observed. Beyond this temperature, decomposition of all surface species has been completed. Major species consist of small molecular weight hydrocarbons (methane, ethane, propane), bicarbonate species (from surface acetate species) and some aromatics on the way to become graphite.

It should be pointed out that isotope scrambling is not observed in all the spectra shown (Figure 5.27 to 5.30). This probably rules out any carbocation intermediates in the decomposition of ethanol on the MgO surface. Following the transformation of the C-1 of the adsorbed ethanol, it clearly indicates that this carbon remains on the Mg-O-C bond viz. ethoxide, higher molecular weight alkoxides, acetate and bicarbonate (or carbonate) species. This probably demonstrates that the decomposition of ethanol on MgO is mainly a surface reaction, or the reversible re-adsorption of gaseous species (after distilling off) does not occur.

### 5.D.I. Adsorption of Isopropanol on MgO

The  $^{13}\text{C}$  CP static spectra of isopropanol adsorbed on all four preparations of MgO at different coverages are shown in Figures 5.32 to 5.35. All spectra showed a methyl carbon in the 0-50 ppm region and a methine resonance in the 50-80 ppm region, downfield from TMS. The methyl resonance is very sharp and narrow ( $\Delta\sigma \sim 10$  ppm) at low coverage for MgO-(1), -(2) and -(3), but wider for MgO-(4). The chemical shielding anisotropy for this resonance is consistent with the methyl resonances in ethanol and diethylether (82). Isopropanol adsorbed on MgO surface as an isopropoxide species, is depicted below:



Depending on the degree of rotation along the O-C bond axis, the two methyl groups may not be equivalent due to the interaction with the surface. It is speculated that this gives rise to the difference between MgO-(4) and the rest of the MgO. Due to the difference in surface morphology on MgO-(4), there may be a hindered rotation along this O-C bond, thus the observed methyl resonance is actually a combination of two methyl resonances of slightly different chemical shift.

Figure 5.32

$^{13}\text{C}$  CP static spectra of isopropanol adsorbed on MgO-(1) at various coverages. Field strength = 60 kHz except (b) and (d) which are 40 kHz. Contact period = 2 msec.

- (a)  $4.08 \mu\text{mole}/\text{m}^2$ , rep rate =  $5 \text{ sec}^{-1}$ , 222,700 contacts
- (b)  $5.28 \mu\text{mole}/\text{m}^2$ , rep rate =  $2.5 \text{ sec}^{-1}$ , 5,987 contacts
- (c)  $6.92 \mu\text{mole}/\text{m}^2$ , rep rate =  $4 \text{ sec}^{-1}$ , 164,560 contacts
- (d)  $8.36 \mu\text{mole}/\text{m}^2$ , rep rate =  $0.8 \text{ sec}^{-1}$ , 5,941 contacts

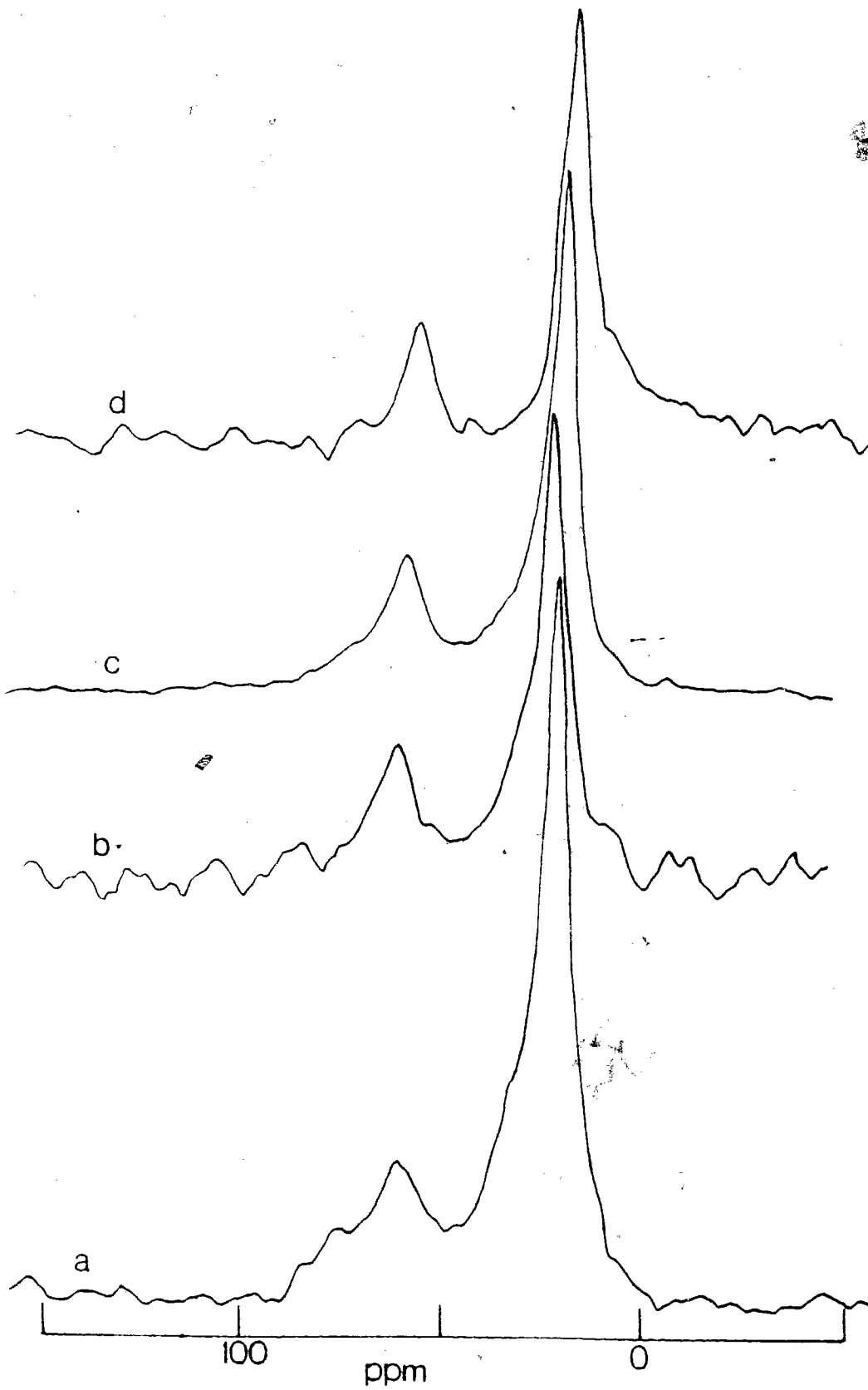


Figure 5.33

$^{13}\text{C}$  CP static spectra of isopropanol adsorbed on MgO-(2) at various coverages. Field strength = 40 kHz.

Contact period = 2 msec.

- (a)  $3.83 \mu\text{mole}/\text{m}^2$ , rep rate =  $3.3 \text{ sec}^{-1}$ , 410,100 contacts
- (b)  $5.07 \mu\text{mole}/\text{m}^2$ , rep rate =  $3.3 \text{ sec}^{-1}$ , 218,600 contacts
- (c)  $5.85 \mu\text{mole}/\text{m}^2$ , rep rate =  $4 \text{ sec}^{-1}$ , 171,300 contacts
- (d)  $8.03 \mu\text{mole}/\text{m}^2$ , rep rate =  $3.3 \text{ sec}^{-1}$ , 28,118 contacts.

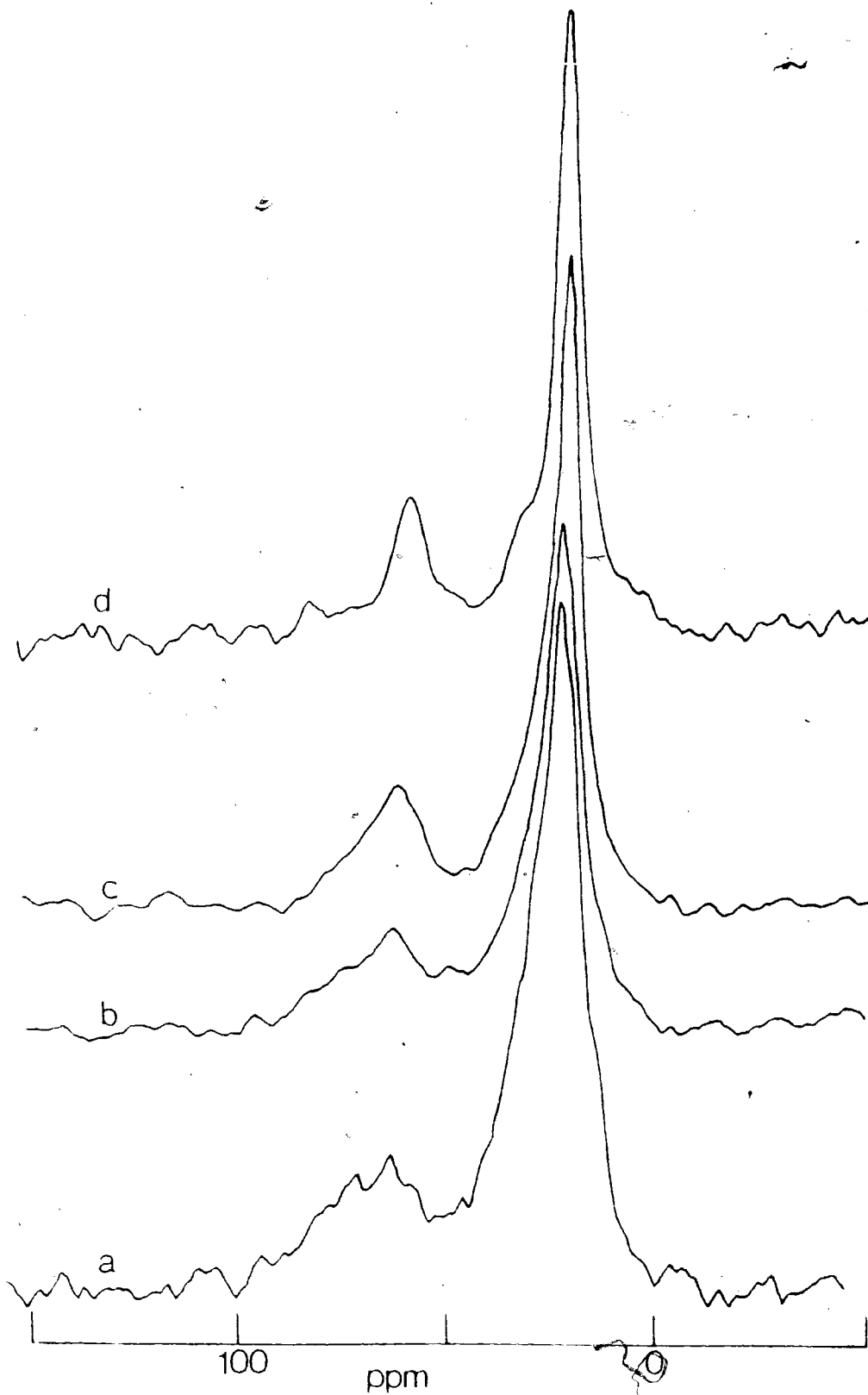




Figure 5.34

$^{13}\text{C}$  CP static spectra of isopropanol adsorbed on  $\text{MgO-(3)}$  at various coverages. Field strength = 40 kHz. Contact period = 2 msec. Spectra are not normalized for the different number of contacts.

- (a)  $3.60 \mu\text{mole/m}^2$ , rep rate =  $1.7 \text{ sec}^{-1}$ , 47,376 contacts
- (b)  $4.38 \mu\text{mole/m}^2$ , rep rate =  $3.3 \text{ sec}^{-1}$ , 33,003 contacts
- (c)  $6.05 \mu\text{mole/m}^2$ , rep rate =  $2.5 \text{ sec}^{-1}$ , 37,452 contacts
- (d)  $7.12 \mu\text{mole/m}^2$ , rep rate =  $0.8 \text{ sec}^{-1}$ , 7649 contacts
- (e)  $8.18 \mu\text{mole/m}^2$ , rep rate =  $0.8 \text{ sec}^{-1}$ , 20,000 contacts

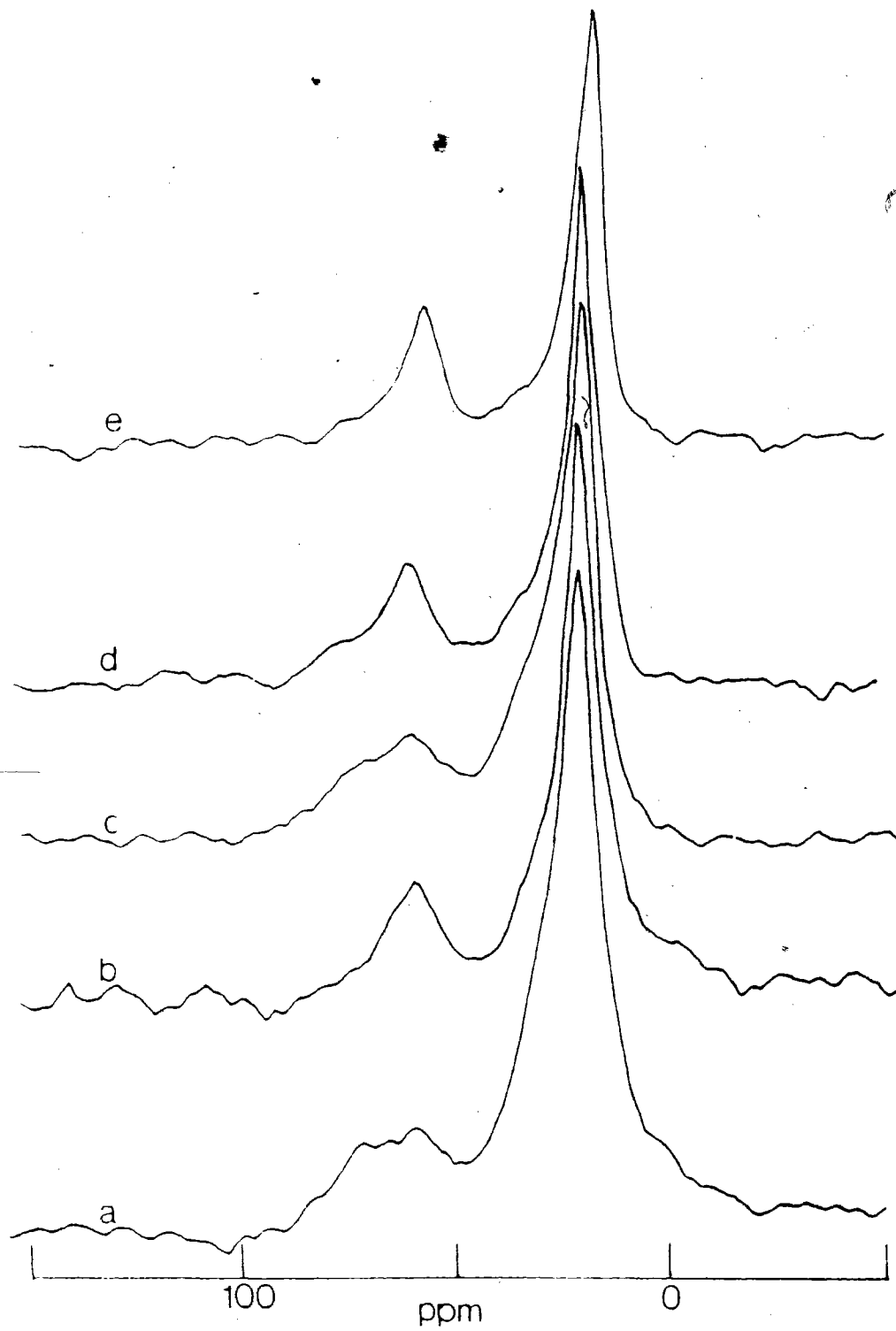


Figure 5.35

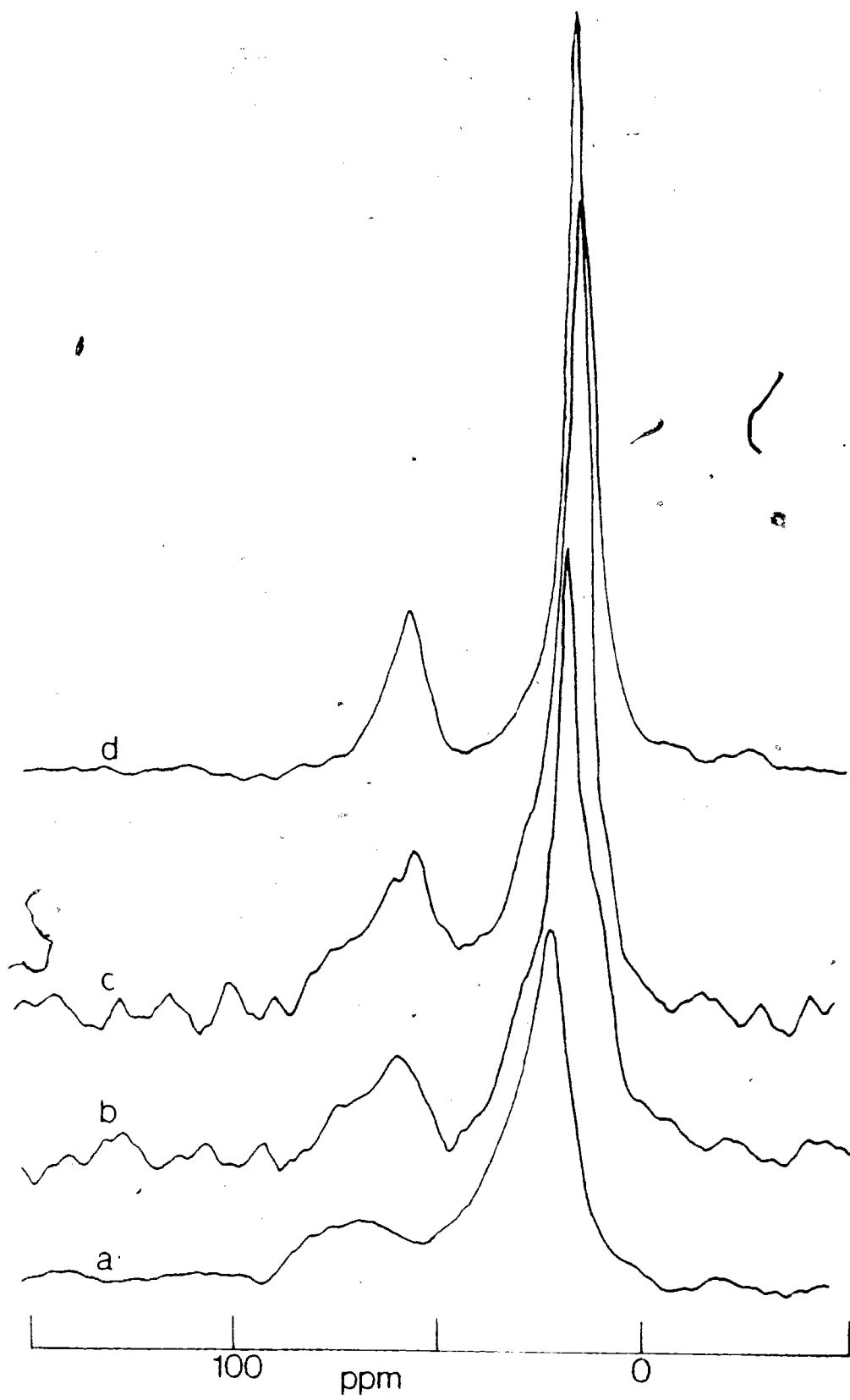
$^{13}\text{C}$  CP static spectra of isopropanol adsorbed on MgO-(4) at various coverages. Field strength = 40 kHz. Contact period = 2 msec. Spectra are not normalized to the different number of contacts. Repetition rate =  $2.5 \text{ sec}^{-1}$ .

(a)  $4.16 \mu\text{mole/m}^2$ , 148,400 contacts

(b)  $5.15 \mu\text{mole/m}^2$ , 117,700 contacts

(c)  $6.07 \mu\text{mole/m}^2$ , 120,000 contacts

(d)  $7.02 \mu\text{mole/m}^2$ , 115,100 contacts



The methine carbon resonance is partially overlapped with the methyl resonance, so that the high-field component,  $\sigma_{33}$  of the chemical shift anisotropy is not known. Since this methine carbon does not possess any axis of symmetry, we expect it to exhibit an asymmetric powder pattern (of a second-rank tensor interaction). The width of the anisotropy ( $\Delta\sigma$ ) of this methine carbon is ca. 30 ppm, comparable to that of the methine carbon in diammonium tartrate (140) as shown in Figure 5.36.

As the loading level of isopropanol increases the methine carbon appears to get narrower with no observable change in the methyl resonance. We attribute this narrowing of the methine carbon to the averaging between the several adsorbed isopropanol species on the MgO surface.

The  $^{13}\text{C}$  CP/MAS spectrum of 5.7  $\mu\text{mole}/\text{m}^2$  of ordinary isopropanol adsorbed on MgO-(3) (Figure 5.43) reveals two resonances at 26.8 and 63.5 downfield from TMS. These values are very close to the literature values of 25.4 and 63.7 ppm for liquid isopropanol (134). This observation is consistent with our previous result that the methoxide and liquid methanol have the same isotropic shift.

#### 5.D.II. $^{13}\text{C}$ NMR Measurements of Adsorbed Isopropanol

##### Treated at Elevated Temperatures

The  $^{13}\text{C}$  CP static spectra of the isopropanol-MgO


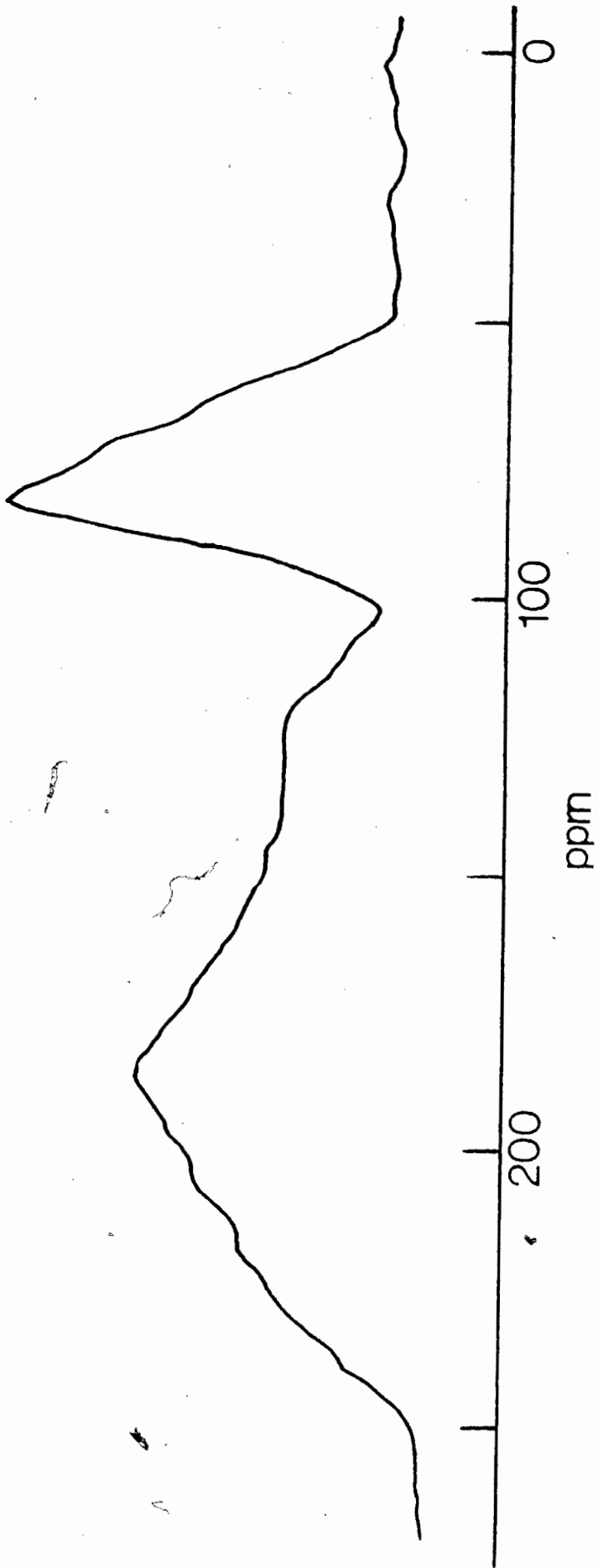


Figure 5.36  $^{13}\text{C}$  CP spectrum of ammonium tartronate.  
Field strength = 40 kHz. Contact  
time = 2 msec. Repetition rate = 1 sec<sup>-1</sup>.  
7,000 contacts.



systems at room temperature and after heating (170, 300, 400°C) are shown in Figures 5.37 to 5.40.

Essentially, the spectra of the adsorbed isopropanol remained the same until 300°C.

At 300°C, the spectra for MgO-(1) and-(2) were quite similar, containing a broad resonance at 10-40 ppm region and a broad resonance in the  $sp^2$ -carbon region with a sharp peak at 127 ppm downfield from TMS. The width of anisotropy of this resonance is comparable to that in spectra for MgO-(3) and MgO-(4), but the latter spectra showed very poor resolution and sensitivity. Although we do not observe any resonances downfield from 180 ppm, this does not exclude the presence of acetone on the surface.

$^{13}C$  CP spectra of adsorbed acetone on MgO-(3) are shown in Figure 5.42 with and without MAS. While the static spectrum showed no particular feature except a broad resonance in the 10-60 ppm region, the MAS spectrum revealed some fine features. The absence of peaks downfield from 180 ppm indicates that acetone molecules do not adsorb in the free form. It is speculated that acetone adsorbs via an enolate intermediate, i.e.

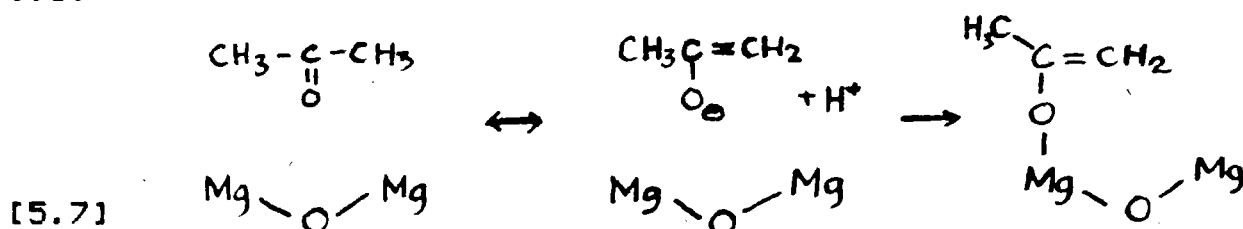




Figure 5.37

$^{13}\text{C}$  CP spectra of  $6.92 \mu\text{mole}/\text{m}^2$  of isopropanol on MgO-(1) treated at elevated temperatures. Field strength = 40 kHz except (a) which is 60 kHz.

Contact period = 2 msec.

- (a) Room temp., rep rate =  $4 \text{ sec}^{-1}$ , 164,600 contacts
- (b)  $170^\circ\text{C}$ , rep rate =  $1.6 \text{ sec}^{-1}$ , 20,641 contacts
- (c)  $300^\circ\text{C}$ , rep rate =  $2 \text{ sec}^{-1}$ , 120,900 contacts
- (d)  $400^\circ\text{C}$ , rep rate =  $2.5 \text{ sec}^{-1}$ , 309,307 contacts

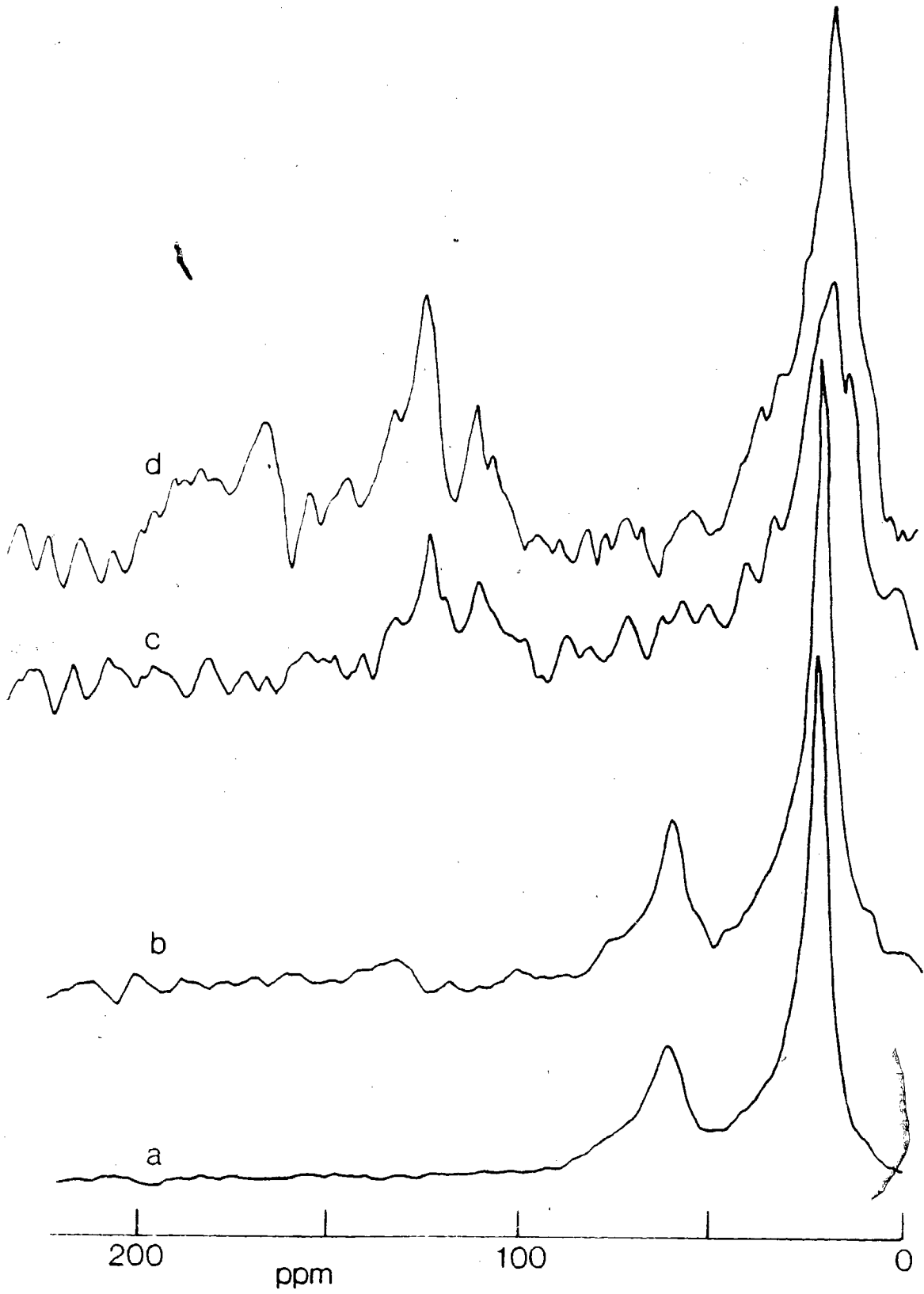


Figure 5.38

$^{13}\text{C}$  CP static spectra of  $5.85 \mu\text{mole}/\text{m}^2$  of isopropanol on  $\text{MgO}$ -(2) treated at elevated temperatures. Field strength = 40 kHz. Contact period = 2 msec.

- (a) Room temp., rep rate =  $4 \text{ sec}^{-1}$ , 171,300 contacts
- (b)  $170^\circ\text{C}$ , rep rate =  $3.3 \text{ sec}^{-1}$ , 100,000 contacts
- (c)  $300^\circ\text{C}$ , rep rate =  $3.3 \text{ sec}^{-1}$ , 378,905 contacts
- (d)  $400^\circ\text{C}$ , rep rate =  $3 \text{ sec}^{-1}$ , 190,630 contacts

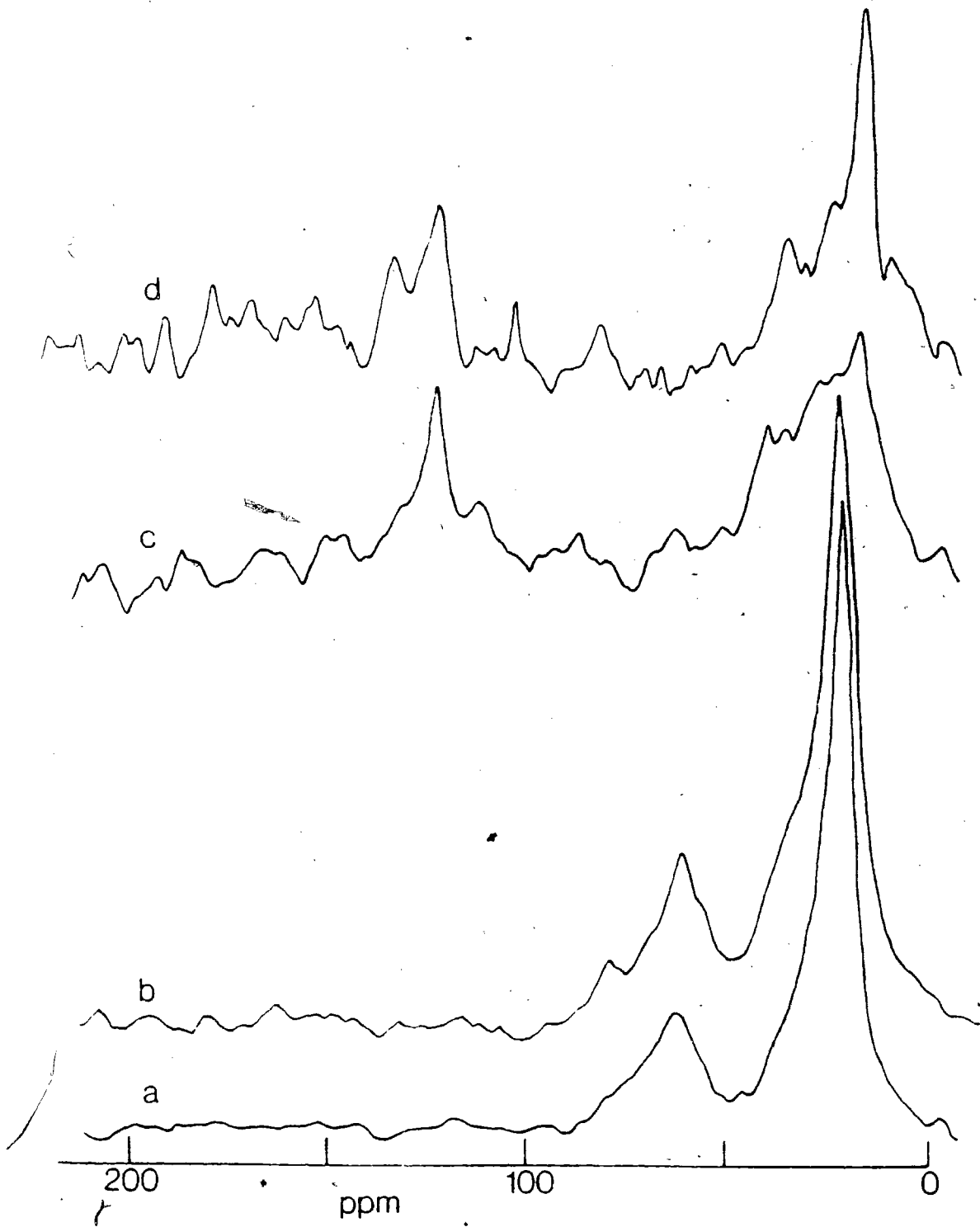


Figure 5.39

$^{13}\text{C}$  CP static spectra of  $6.05 \mu\text{mole}/\text{m}^2$  of isopropanol on  $\text{MgO-(3)}$  treated at elevated temperatures. Field strength = 40 kHz. Contact period = 2 msec.

- (a) Room temp., rep rate =  $2.5 \text{ sec}^{-1}$ , 37,452 contacts
- (b)  $170^\circ\text{C}$ , rep rate =  $2 \text{ sec}^{-1}$ , 14,105 contacts
- (c)  $300^\circ\text{C}$ , rep rate =  $2.5 \text{ sec}^{-1}$ , 219,610 contacts
- (d)  $400^\circ\text{C}$ , rep rate =  $1.7 \text{ sec}^{-1}$ , 133,528 contacts

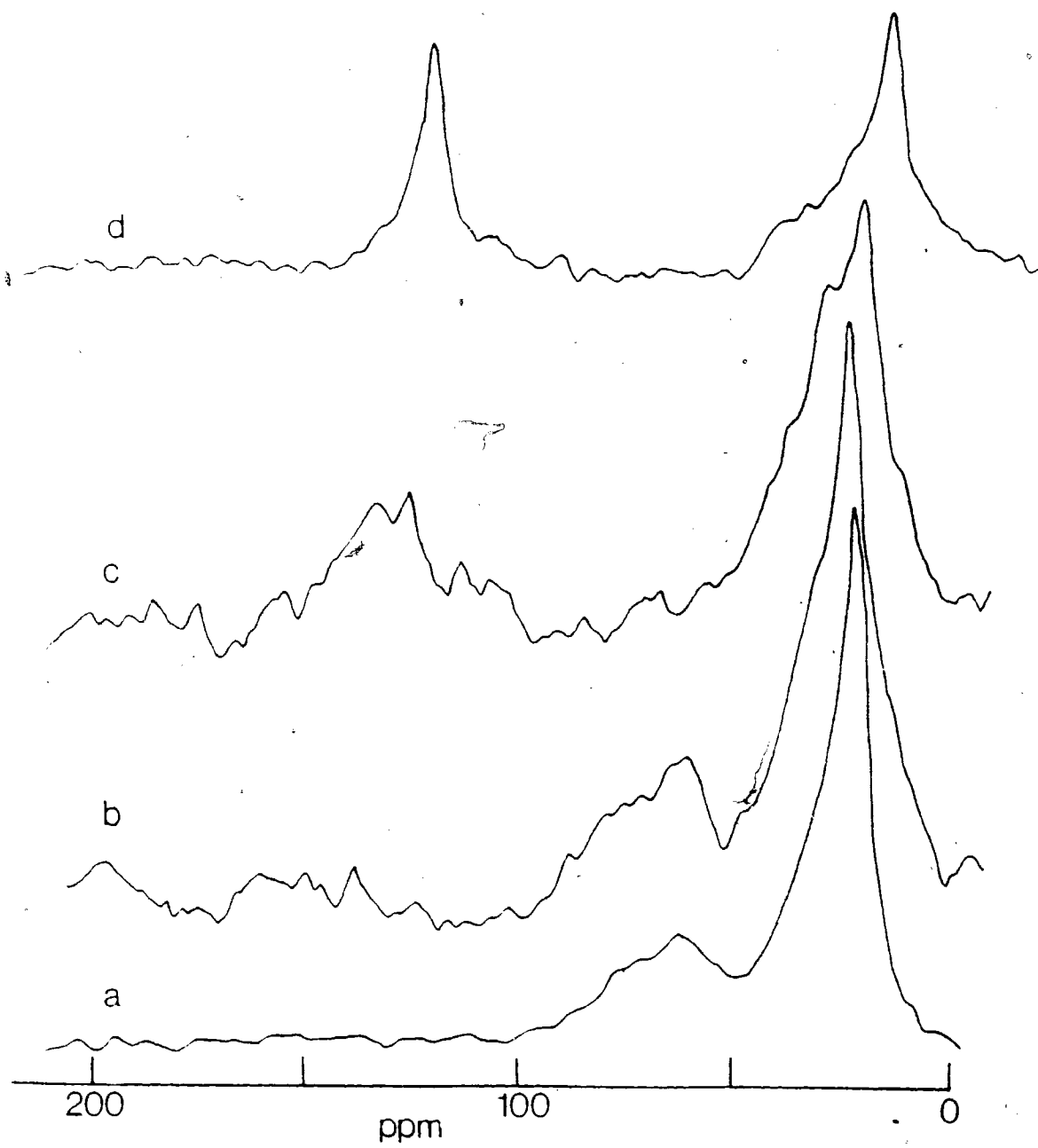


Figure 5.40

$^{13}\text{C}$  CP static spectra of  $7.02 \mu\text{mole}/\text{m}^2$  of isopropanol on MgO-(4) treated at elevated temperatures. Field strength = 40 kHz. Contact period = 2 msec.

- (a) Room temp., rep rate =  $2.5 \text{ sec}^{-1}$ , 115,100 contacts
- (b)  $170^\circ\text{C}$ , rep rate =  $1 \text{ sec}^{-1}$ , 15,704 contacts
- (c)  $300^\circ\text{C}$ , rep rate =  $3 \text{ sec}^{-1}$ , 115,000 contacts
- (d)  $400^\circ\text{C}$ , rep rate =  $1.7 \text{ sec}^{-1}$ , 119,003 contacts

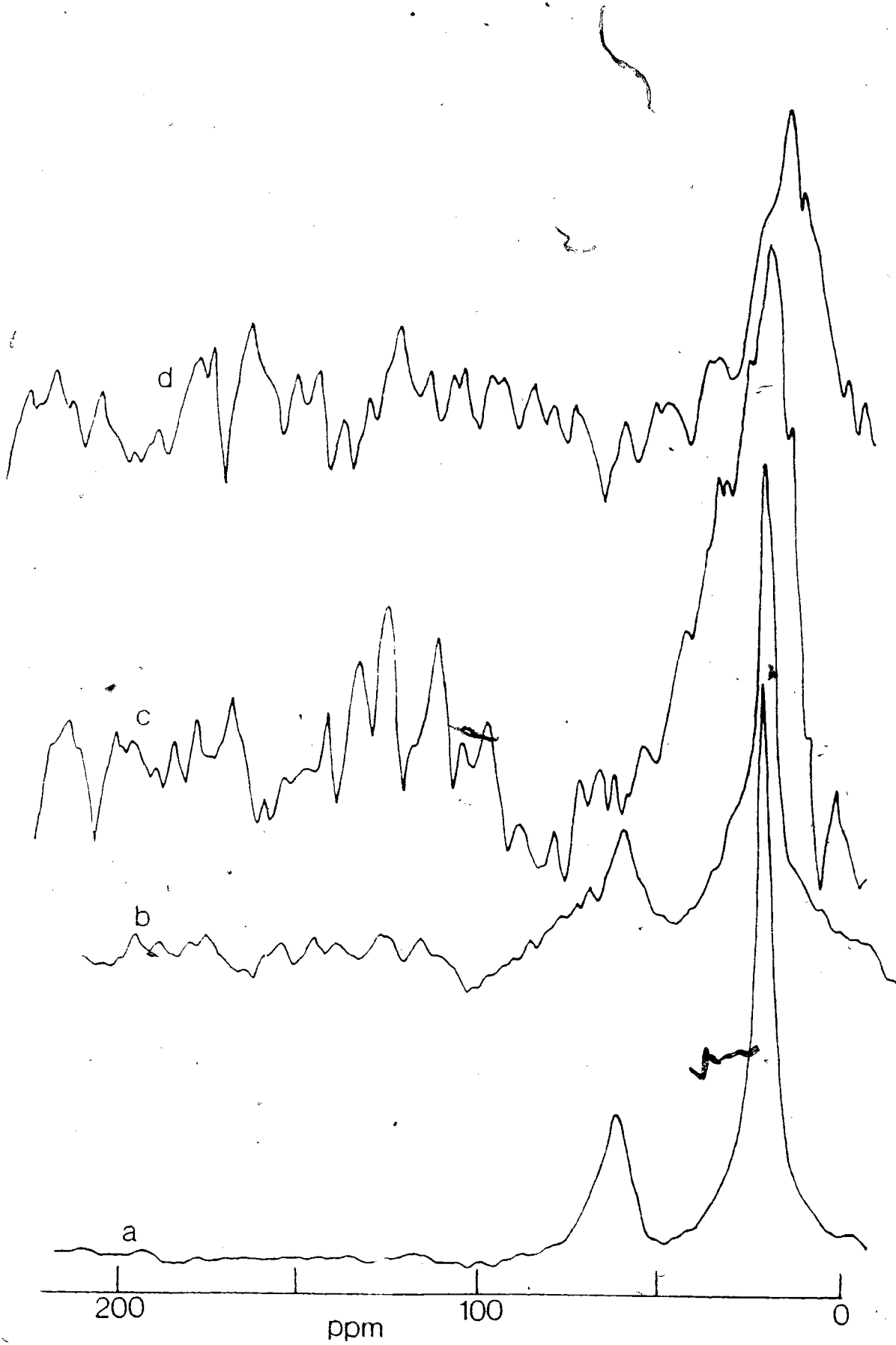




Figure 5.41 Single-pulse  $^{13}\text{C}$  NMR spectra of  
6.92  $\mu\text{mole}/\text{m}^2$  of isopropanol on MgO-(1)  
treated at 300 and 400°C, at 15.08 MHz.  
(a) 300°C, 55,695 scans at 1  $\text{sec}^{-1}$   
(b) 400°C, 144,289 scans at 1  $\text{sec}^{-1}$

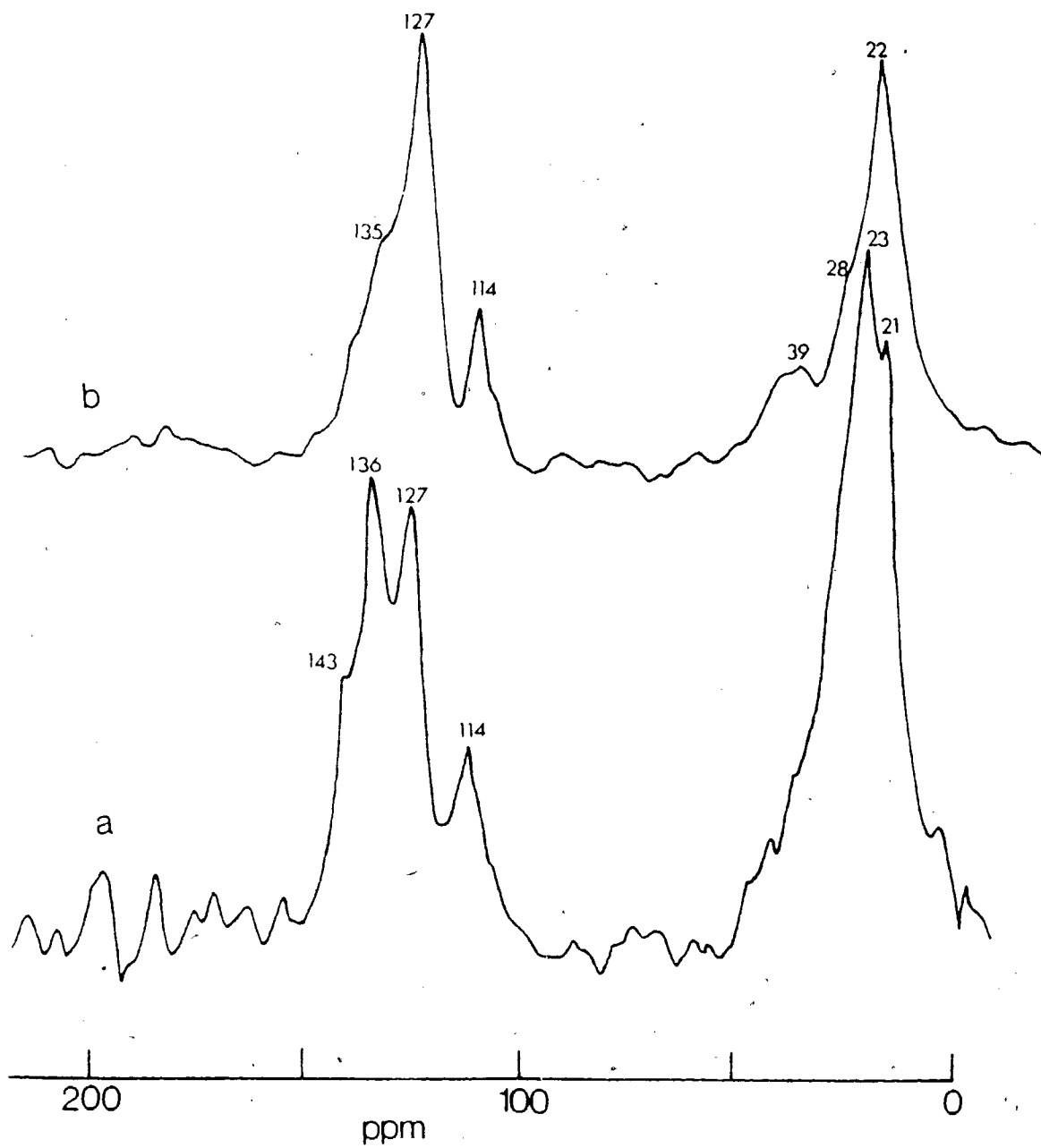


Figure 5.42

$^{13}\text{C}$  spectra of acetone adsorbed  
on MgO-(3).

(a) CP static. Field strength = 40 kHz.

Contact period = 2 msec.

Rep. rate = 1 sec<sup>-1</sup>.

62,946 contacts.

Concentration = 7.25  $\mu\text{mole}/\text{m}^2$ .

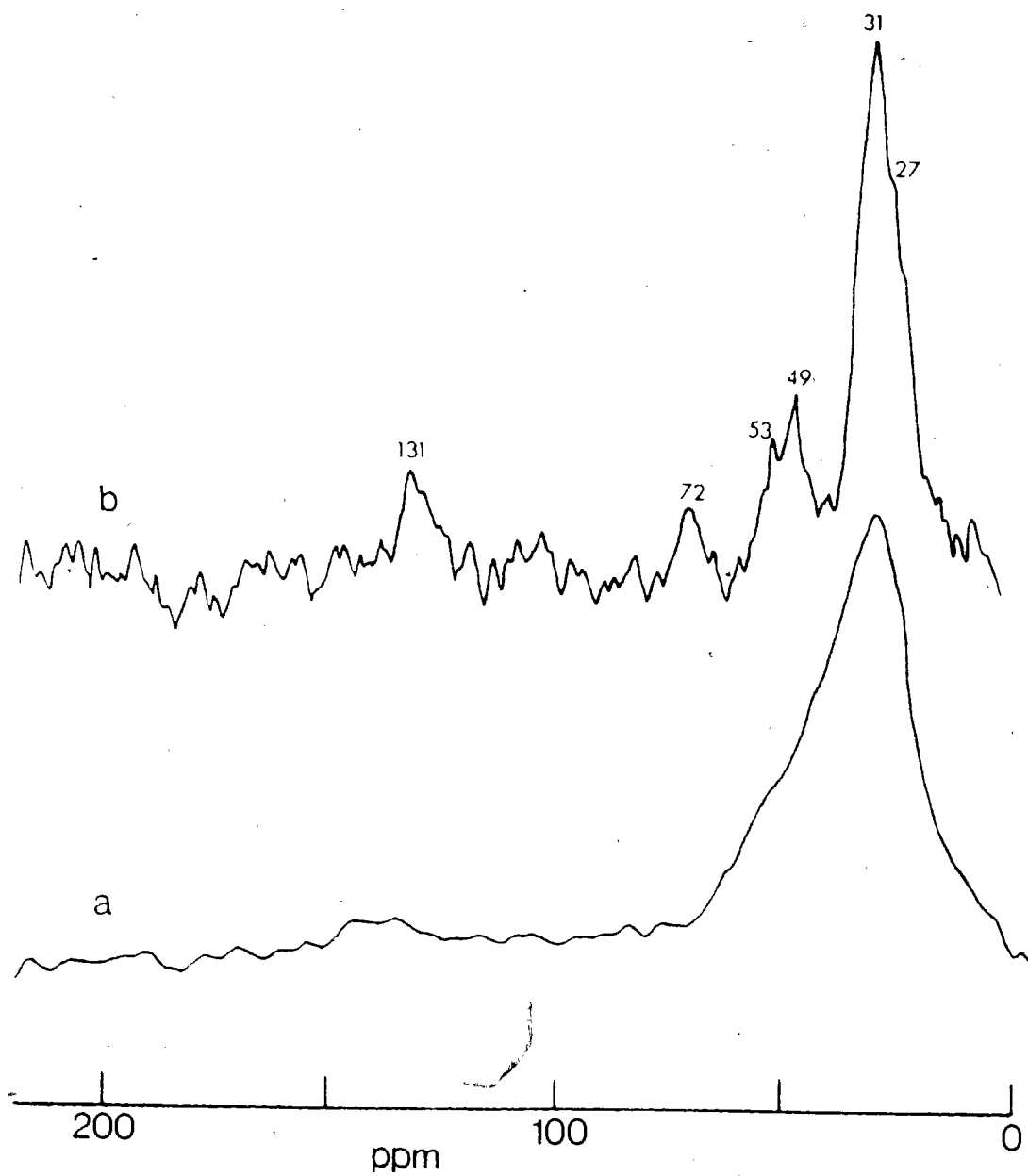
(b) CP/MAS. Field strength = 70 kHz.

Contact period = 2 msec.

Rep. rate = 3.3 sec<sup>-1</sup>.

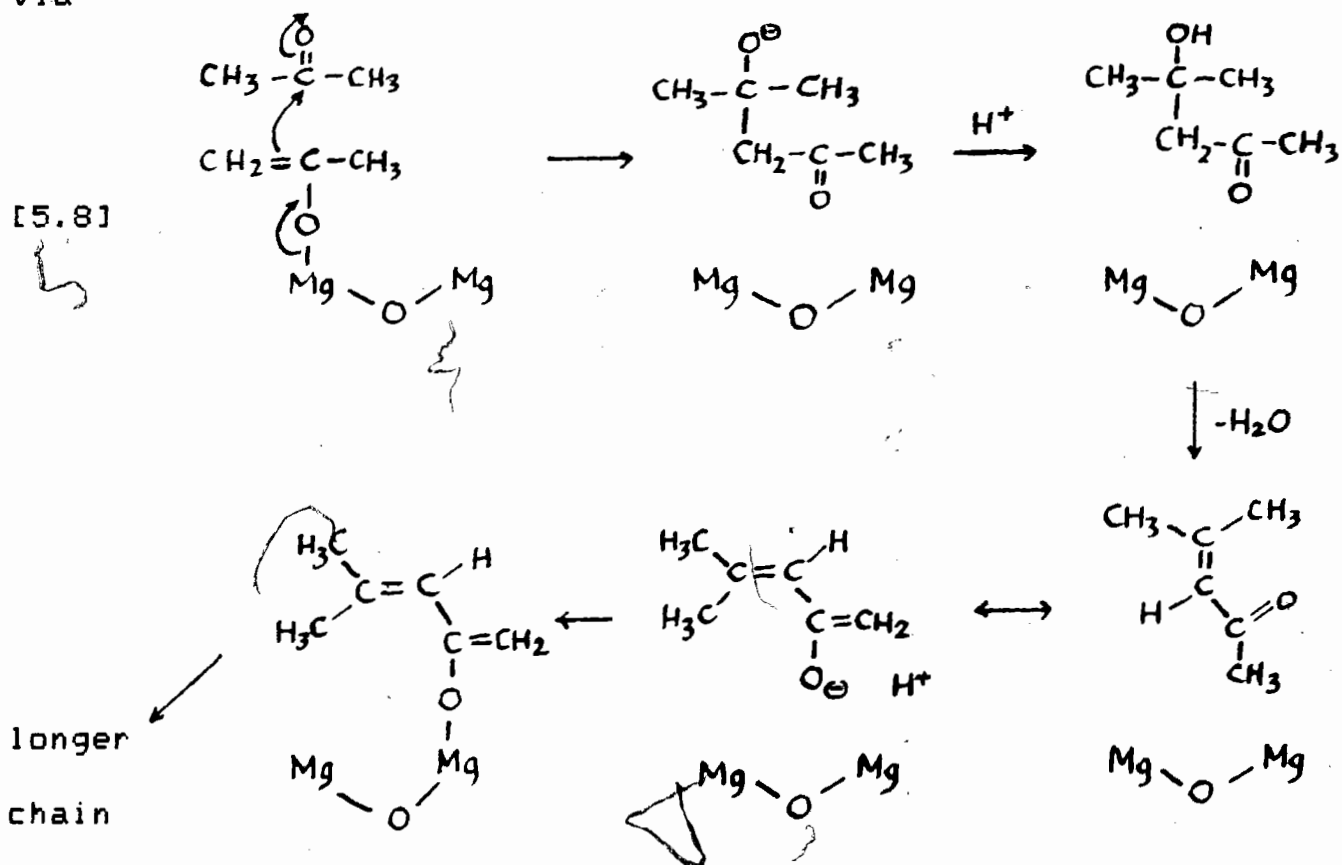
156,460 contacts.

Concentration = 9.60  $\mu\text{mole}/\text{m}^2$ .



The vinyl carbons in methylvinyl ether have chemical shifts at 85 and 153 ppm downfield from TMS respectively (139). It is expected that the same applies to the vinyl carbons of the enolate. The 72 and 131 ppm resonances measured in the  $^{13}\text{C}$  CP/MAS spectrum could be attributed to the shielding effects of the  $\text{O}^-$  ion and the methyl group on the enolate. Noting the intensities of these two resonances, and comparing them to the huge resonance at ca. 30 ppm, it is apparent that the enolate is not the only surface species present.

It is possible that a polymeric species could result from the reaction of an enolate with another acetone molecule via



Notice that the mechanism would project a propagation of the chain as long as there is any presence of acetone. This would partly explain the absence of a ketone resonance in the spectrum. The identity of the other resonances in the spectrum could not be ascertained. However, it is very possible that decomposition may have set in, yielding fragmented hydrocarbon species, thus giving rise to these resonances.

It is apparent then the adsorbed species on the surface of the isopropanol-MgO systems after treatment at 300°C could be the enol form of acetone or the polymeric form mentioned above. However, the spectroscopic evidence is not as concrete as one wants it to be.

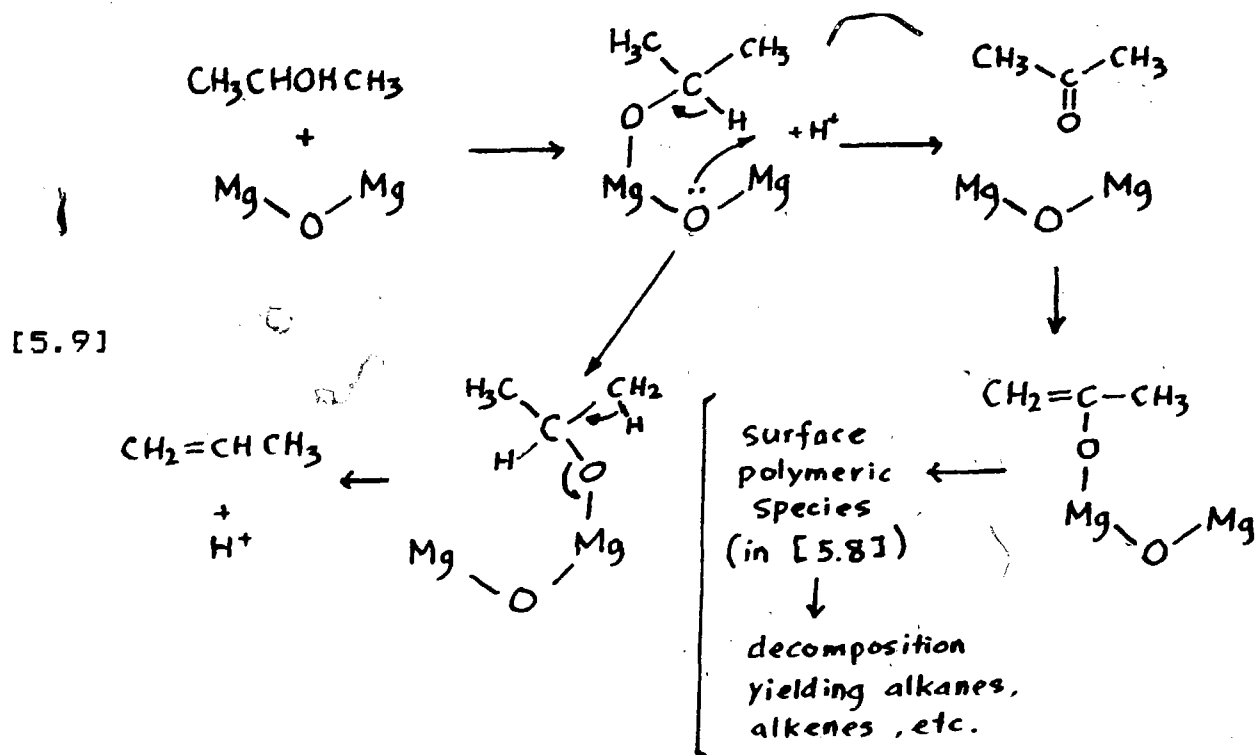
The single-pulse  $^{13}\text{C}$  NMR spectra have also been measured for the isopropanol-MgO systems treated at 300°. Both  $^{13}\text{C}$  NMR and  $^{13}\text{C}$  CP spectra appear to be very similar. The representative  $^{13}\text{C}$  NMR spectra of isopropanol-MgO-(1) treated at 300 and 400°C are shown in Figure 5.41. At 300°C, the isopropanol-MgO systems seemed to consist of a range of linear alkanes and alkenes as loosely-bound species on the surface. The resonances at 21, 114 and 136 ppm downfield from TMS seemed to indicate the presence of propene (the dehydration product of

isopropanol). The rest of the resonances may indicate the decomposition products of the polymeric species on the surface.

At 400°C, the  $^{13}\text{C}$  CP static spectra of the isopropanol-MgO systems appeared to be identical with those treated at 300°C. The interesting feature seems to be the sharpening of the peak at 22 ppm from the broad resonance between 10 and 50 ppm region. This may be due to the "recrystallization" of the surface due to the heating and cooling, thus resulting a more uniform layer of adsorbed species on the surface, or maybe the disappearance of overlapping species. The  $^{13}\text{C}$  single-pulse NMR spectrum appears to be quite different. The resonance at 136 ppm had gone down in intensity (appearing as a shoulder on the downfield side of the 127 ppm resonance), probably indicating some isomerization of the alkenes (from decomposition of the polymers) present at 300°C. The aliphatic region shows a sharpening of the resonance at 22 ppm, and a "hump" at 39 ppm which may indicate some branching of the alkane(s) present.

With the present observations one could suggest the following mechanism for the isopropanol adsorption and

decomposition:



It is apparent then, that MgO act both as a dehydrogenation and dehydration catalyst, yielding acetone and propene respectively, from adsorbed isopropanol beyond 300°C. Previous studies (50, 54) indicated that only the dehydration product, namely propene, was observed, while the dehydrogenation products were below detection limit, employing the technique of temperature programmed desorption.

It was noted by Krylov (58) that in general the activation energy is lower in magnitude in dehydrogenation compared to dehydration of isopropanol on various metal oxides catalysts. This observation may be applied to the system of isopropanol-MgO treated at elevated temperatures. Dehydrogenation to acetone occurs first at 300°C because of lower activation energy. Subsequent dehydration (to propene, etc.)



occurs much later, and at higher temperatures.

### 5.D.III. $^{13}\text{C}$ CP/MAS Study of Adsorbed Isopropanol on MgO

We have prepared a sample of adsorbed isopropanol on MgO-(3) at a coverage of  $5.70 \mu\text{mole}/\text{m}^2$  for the further investigation into the decomposition products at higher temperatures, by the  $^{13}\text{C}$  CP/MAS and  $^{13}\text{C}$  NMR/MAS techniques.

At room temperature, only two resonances at 64 ppm (methine carbon) and at 27 ppm (methyl groups) are observed. There are no observable changes in the spectra until treatment at  $300^\circ\text{C}$ .

At  $300^\circ\text{C}$  (spectrum (b), Figure 5.43) the high-field resonance with the highest peak at 23 ppm is very broad, probably containing a wide range of methyl and methylene carbons. There is another broad resonance in the  $\text{sp}^2$ -carbon region centred at 132 ppm. On closer inspection, this spectrum is very similar to the spectrum corresponding to adsorbed acetone on MgO-(3) shown in Figure 5.42. This certainly indicates that the adsorbed isopropanol dehydrogenates on MgO to yield acetone, at  $300^\circ\text{C}$ .

The observed spectrum showed little difference as the sample was treated to  $350^\circ\text{C}$ , except that the resonance at 68 ppm disappears and the olefinic resonances split to two major resonances at 138 and 128 ppm. It is suspected that this is due



Figure 5.43

$^{13}\text{C}$  CP/MAS spectra of  $5.70 \mu\text{mole/m}^2$  of isopropanol on MgO-(3), at room temperature and after heating to elevated temperatures. Field strength = 60 kHz. Contact time = 2 msec. Repetition rate =  $2 \text{ sec}^{-1}$ .

(a) Room temp., 106,296 contacts

(b)  $300^\circ\text{C}$  (3 hrs), 120,064 contacts

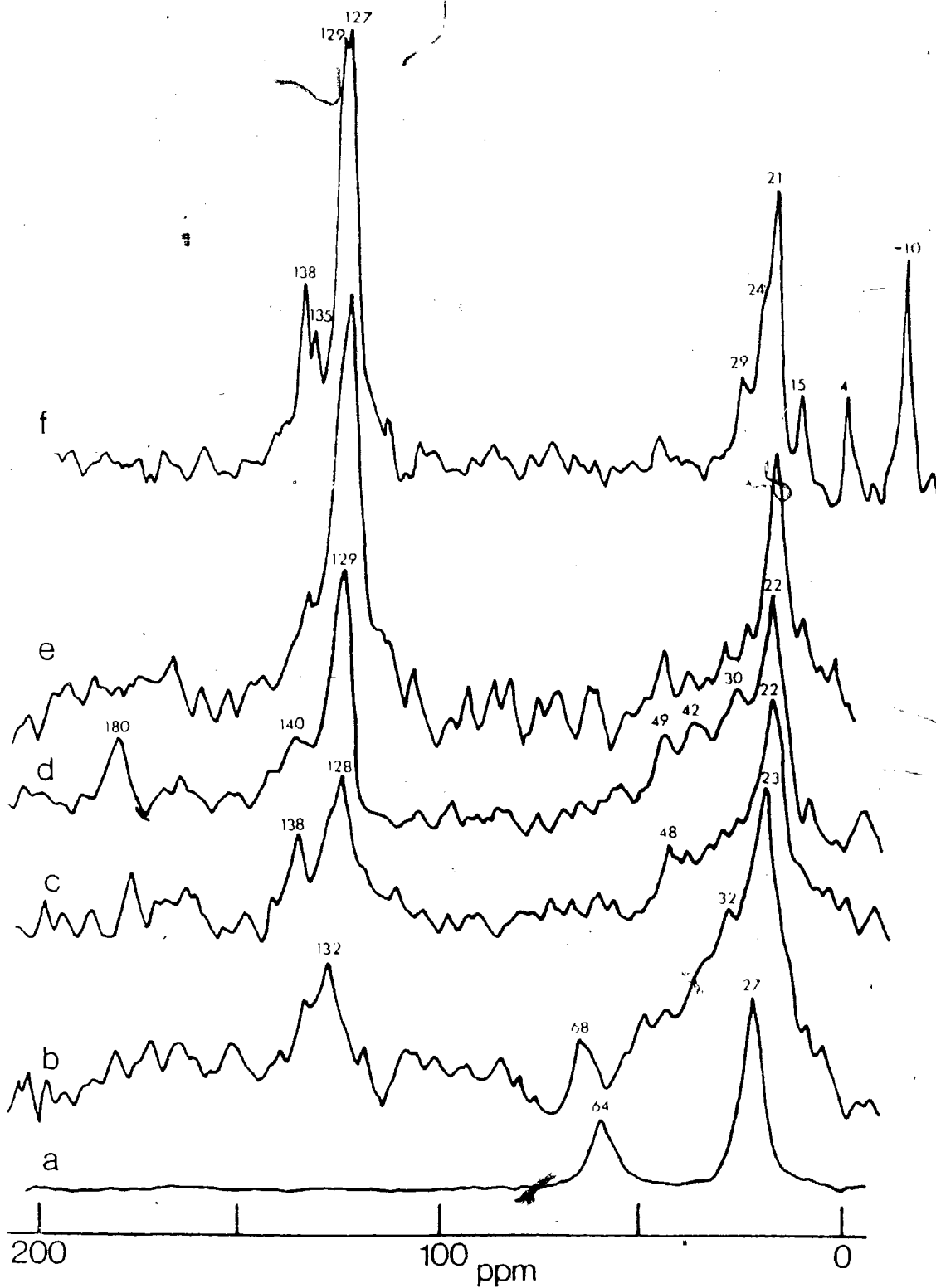
(c)  $350^\circ\text{C}$  (3 hrs), 93,944 contacts

(d)  $400^\circ\text{C}$  (3 hrs), 288,795 contacts

(e)  $450^\circ\text{C}$  (3 hrs), 233,580 contacts

(f)  $500^\circ\text{C}$  (3 hrs), Single-pulse  $^{13}\text{C}$  MAS/NMR,

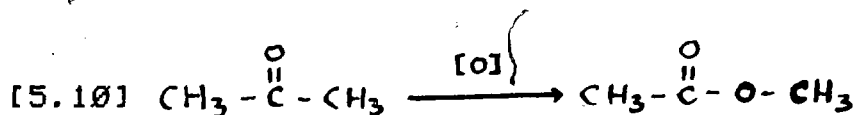
rep. rate =  $2 \text{ sec}^{-1}$ , 167,967 scans.



to surface recrystallization after the heating and cooling, so that the resonances sharpened up.

Up to this temperature, all the measured  $^{13}\text{C}$  NMR/MAS spectra resemble closely with their counterpart  $^{13}\text{C}$  CP/MAS spectra.

When the sample was treated to  $400^\circ\text{C}$ , there is an extra resonance at  $180$  ppm (spectrum (d) in Figure 5.43), no such peak was observed in the  $^{13}\text{C}$  NMR/MAS spectrum. It is suspected that some of the acetone may have oxidized to a methyl acetate species via:



However, this kind of oxidation requires a very strong oxidizing reagent (e.g. peracids), and it is not certain if this mechanism is correct. The absence of this peak in the corresponding  $^{13}\text{C}$  MAS/NMR spectrum clearly indicates that this is not a CO species. This peak at  $180$  ppm eventually disappeared when the sample was treated at  $450^\circ\text{C}$ , probably being decomposed to yield  $\text{CO}_2$  and  $\text{CH}_4$ .

The  $^{13}\text{C}$  CP/MAS spectrum ((e) in Figure 5.43) of the sample after treatment at  $450^\circ\text{C}$ , reveals a huge increase in the intensity of the resonance at  $129$  ppm. At the same time, the isopropanol-MgO sample started to turn greyish. This probably

indicates the formation of some aromatics, on the way to become graphite.

The  $^{13}\text{C}$  CP/MAS spectrum of the sample after treatment at  $500^\circ\text{C}$  is not shown because of poor S/N even after  $>100,000$  contacts. This probably indicates that the concentration of surface species is minimal (probably distilled off the surface). However, the  $^{13}\text{C}$  MAS/NMR spectrum reveals a lot of information for the same experimental condition. The resonances at -10, 4, 15 ppm downfield from TMS probably correspond to methane, ethane and propane respectively. The rest of the resonances probably correspond to a wide range of alkane and alkenes. Since there are no observable resonances in the 110-115 ppm region, it is suspected that simple alkenes e.g. propene, 1-butene are not present. Since most of the olefinic resonances lie in the 127-138 ppm region, one would incline to identify them as substituted alkenes (134), and aromatics.

#### 5.D.IV. Summary

It is established in this short study that isopropanol adsorbed on MgO as an isopropoxide species, which is stable up to  $300^\circ\text{C}$ .

At  $300^\circ\text{C}$ , the surface  $\text{O}^-$  ion extracts an hydrogen from the adsorbed isopropoxide species to yield an acetone species via a 5-membered ring intermediate. This acetone species readsorbs on the MgO surface in the enolate form. The

enolate is suspected to undergo further aldol condensation to yield other higher molecular weight vinyl alcohols. This is the basic reaction containing both dehydrogenation and dehydration.

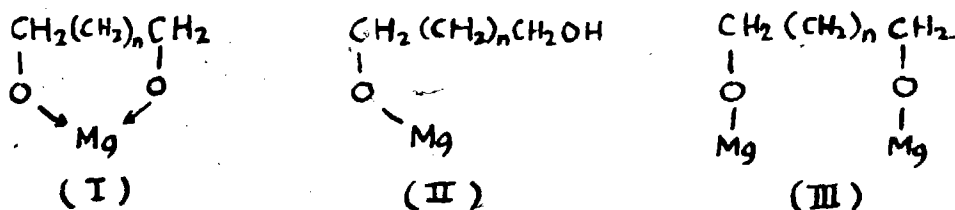
Under the same condition (300°C), some dehydration of the isopropoxide to propene is also suspected, this was indicated by the single-pulse  $^{13}\text{C}$  NMR evidence.

At higher temperatures, dehydration becomes more important, and the previously assigned enolate species and its aldol condensation polymeric products dehydrate to yield a variety of olefinic products. Some decomposition may have set in yielding some alkanes.

#### 5.E. $^{13}\text{C}$ CP NMR of Adsorbed Alkanediols on MgO

The purposes of this investigation into the adsorption of alkanediols on MgO are three-fold. First, having established that aliphatic alcohols adsorb on MgO as alkoxides, it will be pertinent to check if alkanediols behave likewise when adsorbed on MgO (as a chemisorbed species). Second, the picture of adsorbed alcohols on MgO is an 1:1 adsorption (i.e. one alcohol molecule to one Mg ion on the MgO surface). This view may be drastically changed for the adsorption of alkanediols on MgO. There are three possible modes of adsorption for alkanediols on MgO, viz:

[5.11]



(n = 0 to 2 in our case)

Adsorption modes I and III would yield similar  $^{13}\text{C}$  CP spectra because the terminal  $-\text{CH}_2\text{OH}$  groups are attached to the  $\text{Mg}^{2+}$  ions on the  $\text{MgO}$  surface (though they may have slightly different chemical shifts due to the deshielding effect of one or two  $\text{Mg}^{2+}$  ions). On the other hand, adsorption mode II would permit motions (e.g. rotation along C-C bond) on the whole molecule, except the one  $-\text{CH}_2\text{OH}$  group which is bonded to the surface. Depending on the chemical shift changes, adsorption mode II may yield a completely different  $^{13}\text{C}$  CP spectrum.

Third, 1,3-butadiene is very important industrially in the manufacturing of synthetic rubber, it would be interesting to test if 1,3-butadiene could be produced from the thermal decomposition of 1,4-butanediol adsorbed on  $\text{MgO}$ .

For the present investigation,  $^{13}\text{C}$  CP static spectra have been measured for three adsorbed alkanediols:

1,2-ethanediol, 1,3-propanediol and 1,4-butanediol on  $\text{MgO}$ -(3). Their respective  $^{13}\text{C}$  CP spectra at various coverages are shown in Figures 5.44 to 5.46.

Figure 5.44

$^{13}\text{C}$  CP static spectra of 1,2-ethanediol adsorbed on MgO-(3) at various coverages. Contact period = 2 msec. Field strength = 40 kHz. Rep. rate =  $3.3 \text{ sec}^{-1}$  except (a), which is  $1 \text{ sec}^{-1}$ , and (d) which is  $2 \text{ sec}^{-1}$ .

(a)  $4.14 \mu\text{mole/m}^2$ , 260,000 contacts

(b)  $5.58 \mu\text{mole/m}^2$ , 184,500 contacts

(c)  $8.40 \mu\text{mole/m}^2$ , 75,086 contacts

(d)  $10.83 \mu\text{mole/m}^2$ , 13,722 contacts



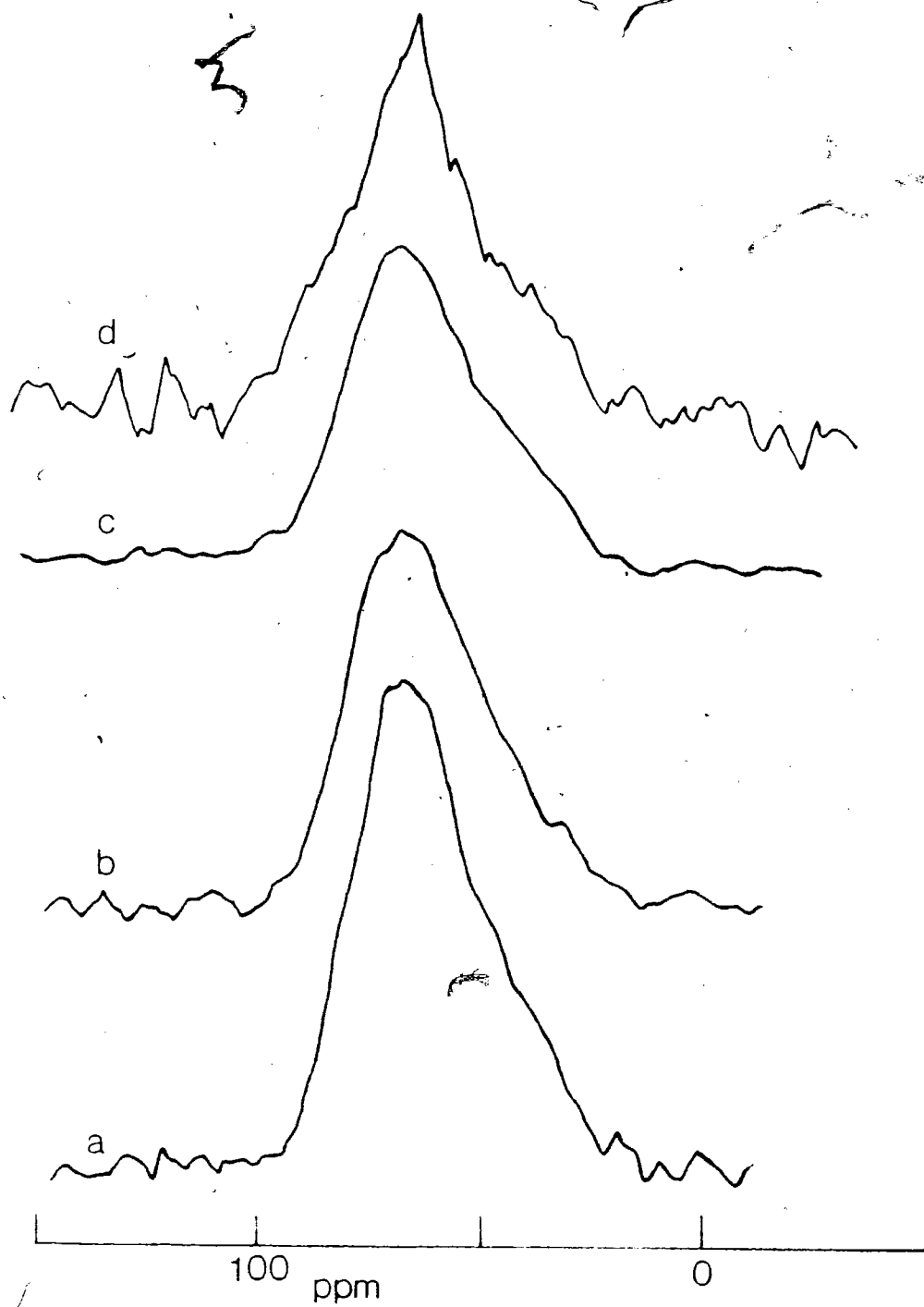


Figure 5.45

$^{13}\text{C}$  CP static spectra of 1,3-propanediol adsorbed on MgO-(3) at different coverages. Field strength = 40 kHz.

Contact period = 2 msec, except (b) which is 0.5 msec.

Rep. rate =  $3.3 \text{ sec}^{-1}$ , except (c) which is  $0.5 \text{ sec}^{-1}$ .

(a)  $5.62 \mu\text{mole/m}^2$ , 35,130 contacts

(b)  $7.70 \mu\text{mole/m}^2$ , 218,000 contacts

(c)  $9.46 \mu\text{mole/m}^2$ , 92,000 contacts

Spectra are not normalized to the different number of contacts.

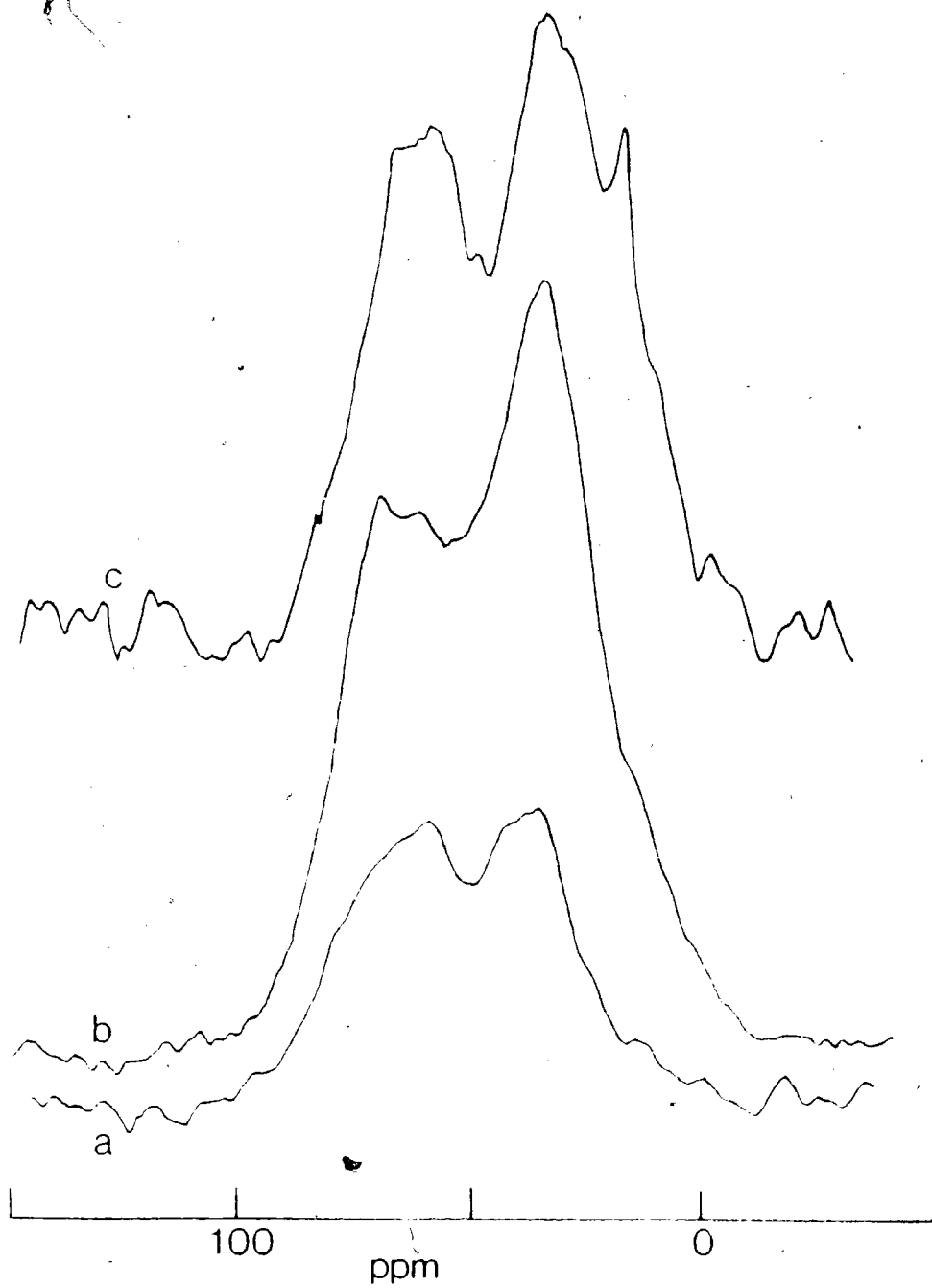


Figure 5.46

$^{13}\text{C}$  CP static spectra of 1,4-butanediol adsorbed on MgO-(3) at different coverages. Field strength = 40 kHz.

Contact period = 2 msec.

(a)  $4.12 \mu\text{mole/m}^2$ , rep rate =  $1 \text{ sec}^{-1}$ , 76,226 contacts

(b)  $6.22 \mu\text{mole/m}^2$ , rep rate =  $3.3 \text{ sec}^{-1}$ , 75,018 contacts

(c)  $8.14 \mu\text{mole/m}^2$ , rep rate =  $3.3 \text{ sec}^{-1}$ , 35,419 contacts

Spectra are not normalized for the different number of contacts.

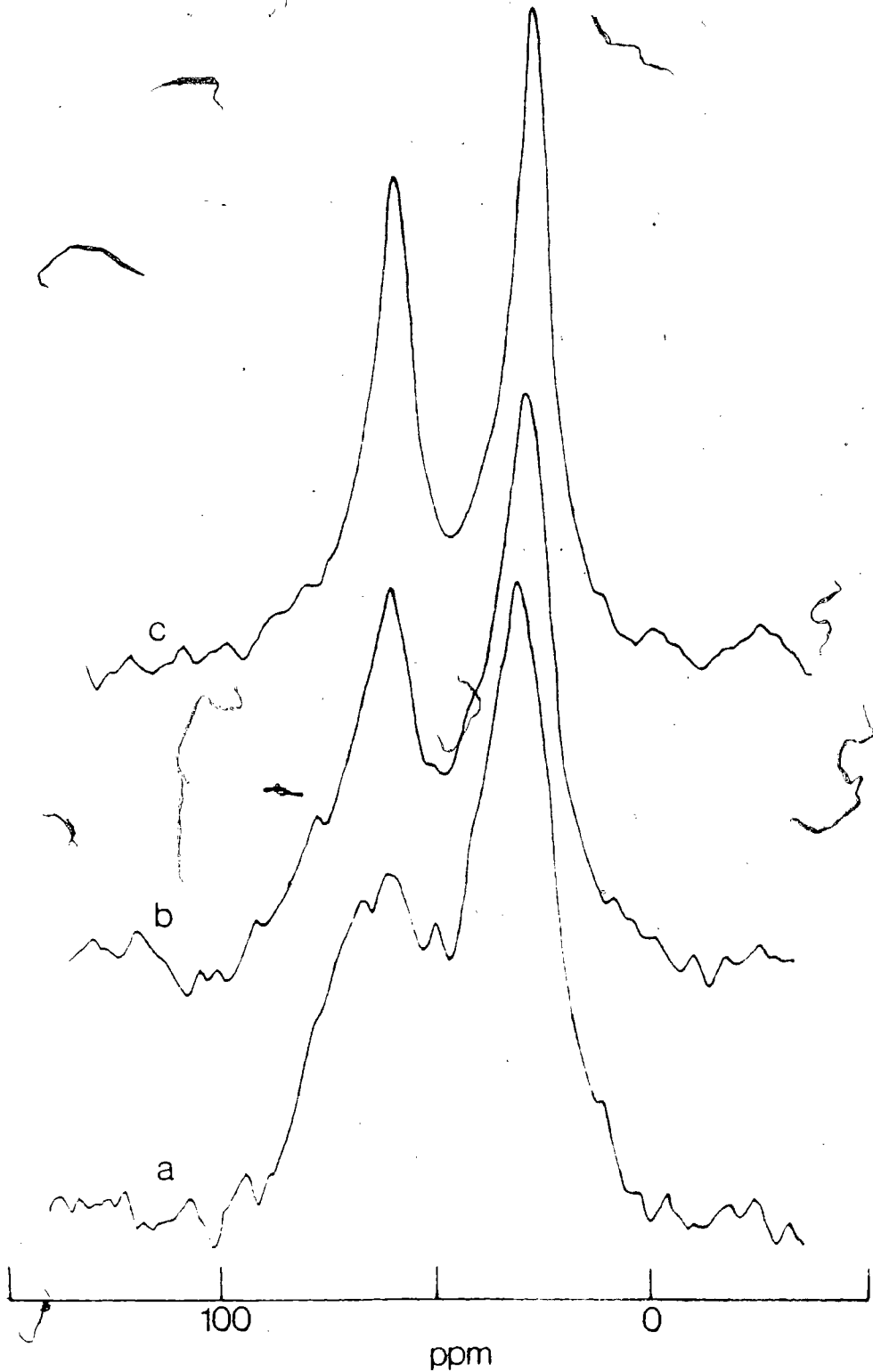


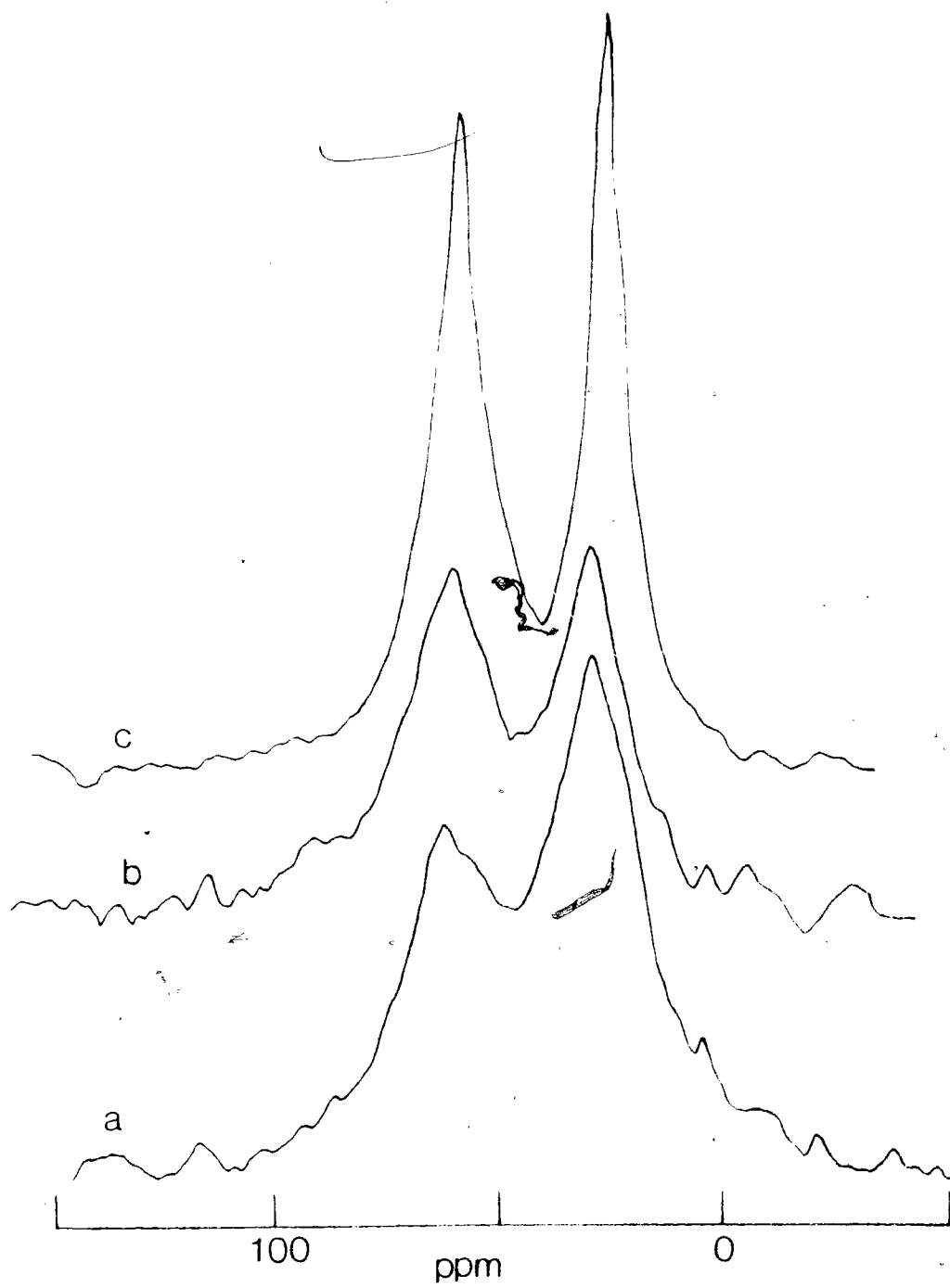
Figure 5.47

Single-pulse  $^{13}\text{C}$  NMR spectra of 1,4-butanediol adsorbed on MgO-(3) at different coverages (same samples as in Figure 5.46).

(a)  $4.12 \mu\text{mole}/\text{m}^2$ , rep rate =  $1 \text{ sec}^{-1}$ , 43,000 scans

(b)  $6.22 \mu\text{mole}/\text{m}^2$ , rep rate =  $1 \text{ sec}^{-1}$ , 15,081 scans

(c)  $8.14 \mu\text{mole}/\text{m}^2$ , rep rate =  $2 \text{ sec}^{-1}$ , 13,758 scans



### 5.E.I. Adsorbed 1,2-ethanediol

For 1,2-ethanediol, the  $^{13}\text{C}$  CP static spectra (Figure 5.44) reveal an axially symmetric powder pattern, with a width of about 50 ppm. The spectra remain essentially the same as the coverage increases. No isotropic peak at 63.4 ppm downfield from TMS (corresponding to physisorbed 1,2-ethanediol) was observed superimposed on this powder pattern.

It seems quite improbable to obtain a strongly-held chemisorbed species with the first mode of adsorption (I) because the distance between the two hydroxyl groups is too large for them to attach to the same  $\text{Mg}^{2+}$  ion on the surface. The third mode of adsorption (III), at first glance, seems to be quite different from mode (II) of adsorption, however, spectral evidence reveals otherwise.

The concentration of  $\text{Mg}^{2+}$  ions on the  $\text{MgO}$  (100) plane is about  $18 \mu\text{mole}/\text{m}^2$ . This surface would provide sufficient active sites for adsorption at loading level below about  $9 \mu\text{mole}/\text{m}^2$  of 1,2-ethanediol in the adsorption mode (III). At coverages above this limit, we would expect a certain population of the adsorbates to be physisorbed or be converted to adsorption mode (II). This abrupt change should be reflected in the chemical shift anisotropies we observed in the  $^{13}\text{C}$  CP spectrum. However, the spectrum (d) in Figure 5.44 (which contains  $10.83 \mu\text{mole}/\text{m}^2$  of 1,2-ethanediol) is almost the same as other spectra at lower coverages.



The explanation for this "no-observable change" lies in two directions: (i) The adsorption mode (II) is the dominant mode for the adsorption of 1,2-ethanediol on the MgO surface. The reason we don't observe any physisorbed species (as in the methanol case) is that they are obscured inside the observed powder pattern of the chemisorbed species. This also applies to the other carbon which is not actively attached to the surface. (ii) There exists an equilibrium between the two modes of adsorption (that is, the active sites on the MgO surface are susceptible to both types of adsorption modes), and the chemical shift powder patterns are the same for both. However, both explanations given above do not adequately answer the question why we would have observed an axially symmetric powder pattern for the adsorbed 1,2-ethanediol (axially symmetric powder pattern usually implies at least a  $C_3$  axis of symmetry).

The  $^{13}\text{C}$  CP/MAS spectra (Figure 5.48) were also measured 1,2-ethanediol on MgO at two coverages. The spectra show a single peak at 63 ppm downfield from TMS.

#### 5.E.II. Adsorbed 1,3-propanediol

For the adsorption of 1,3-propanediol on MgO, the  $^{13}\text{C}$  CP static spectra (Figure 5.45) show two overlapping methylene carbon resonances. At low coverage, the two overlapping powder patterns are featureless. At intermediate coverage ( $7.70 \mu\text{mole/m}^2$ ), the observed powder patterns are

Figure 5.48

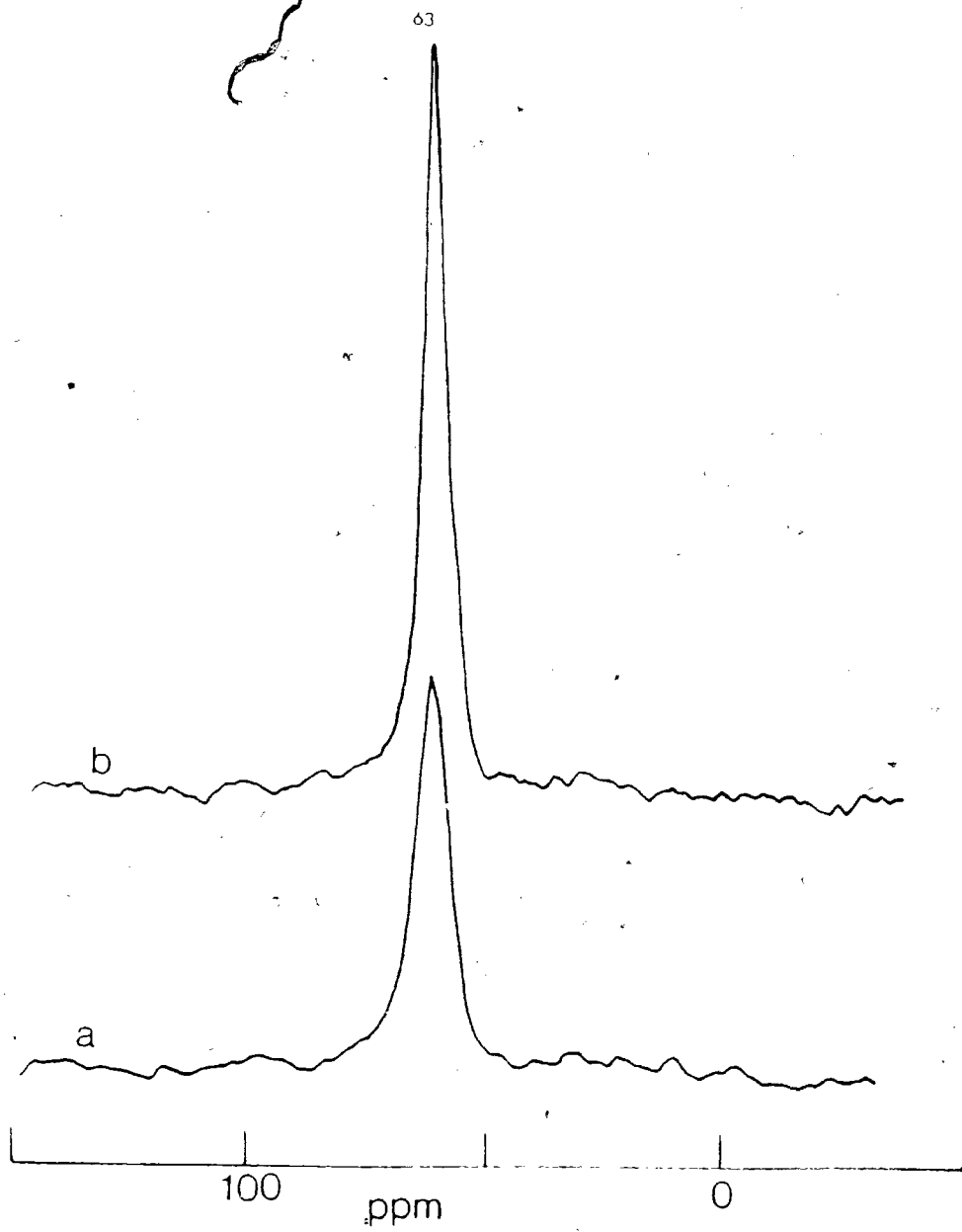
$^{13}\text{C}$  CP/MAS spectra of 1,2-ethanediol on  $\text{MgO-(3)}$  at two coverages. Field strength = 60 kHz.

(a)  $5.20 \mu\text{mole/m}^2$ , contact time = 2 msec,

rep rate =  $1 \text{ sec}^{-1}$ , 60,372 contacts

(b)  $9.40 \mu\text{mole/m}^2$ , contact time = 1.5 msec,

rep rate =  $2 \text{ sec}^{-1}$ , 99,066 contacts



compatible with those of the computer simulated spectrum: an axially symmetric powder pattern corresponding to C-1 (at 71.4, 71.4 and 34.8 ppm downfield from TMS), and an asymmetric C-2 powder pattern (at 62.2, 37.6, 7.8 ppm downfield from TMS). The isotropic shifts are remarkably close to the chemical shifts of liquid 1,3-propanediol (134). At even higher coverage ( $9.46 \times 10^{-6}$  mole/m<sup>2</sup>), a new peak is observed on the high field side of the C-2 powder pattern at 19 ppm downfield from TMS. It is suspected that it is an artifact (a glitch), since it is not plausible that any reaction could have occurred at the experimental condition. (Since 1,3-propanediol has a very low vapor pressure at room temperature, it is practical to warm up both the MgO sample and 1,3-propanediol to about 110°C for vapor phase adsorption). Since only methyl resonances appear in this range of chemical shift, decomposition (to produce a species with terminal methyl group) must have set in for this peak at 19 ppm to be real. However, previous experience with adsorbed alcohols on MgO show that 110°C is too low a temperature for any reaction to occur on the surface.

The <sup>13</sup>C CP/MAS shown in Figure 5.49 reveal more variations. Neat 1,3-propanediol has <sup>13</sup>C chemical shift at 35.4 and 59.2 ppm downfield from TMS (134). In the spectra, the major <sup>13</sup>C resonances occur at 38 and 65 ppm downfield from TMS respectively. This shift to low field is probably caused by the strong deshielding effect from the surface Mg<sup>2+</sup> ions, indicating a very strongly-held chemisorbed species.

Figure 5.49

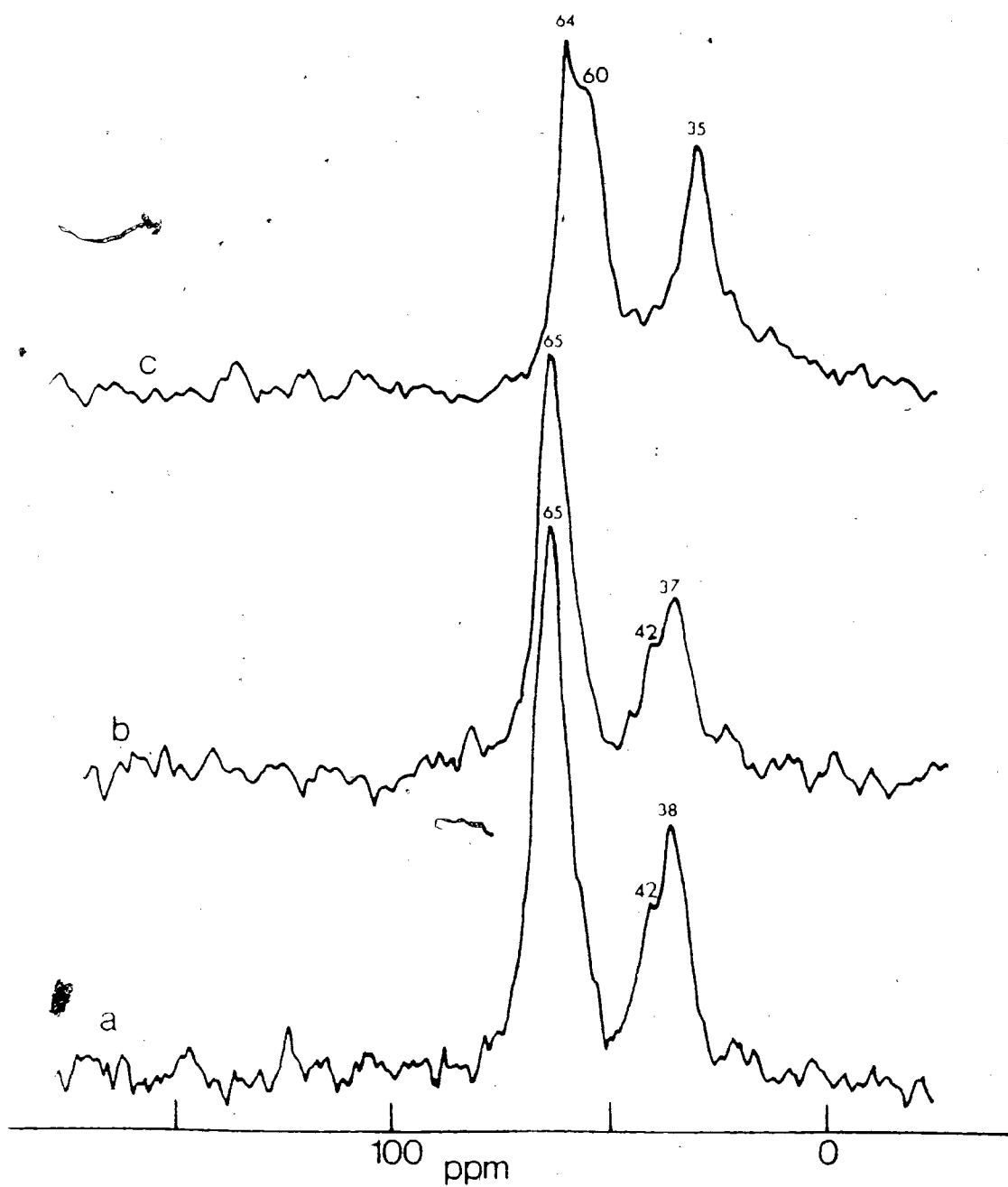
$^{13}\text{C}$  CP/MAS spectra of 1,3-propanediol on  $\text{MgO-(3)}$  at various coverages. Field strength = 65 kHz. Contact period = 2 msec. Repetition rate =  $3.3 \text{ sec}^{-1}$  except

(a) which is  $2 \text{ sec}^{-1}$ .

(a)  $3.77 \mu\text{mole/m}^2$ , 353,400 contacts

(b)  $7.84 \mu\text{mole/m}^2$ , 178,451 contacts

(c)  $9.69 \mu\text{mole/m}^2$ , 132,027 contacts



Most adsorbed alcohols on MgO discussed in this dissertation do not show such a large downfield shift (5 ppm for C-1 and 3 ppm for C-2) except ethanol, which exhibits a large downfield shift for the C-2 carbon only. The huge downfield shift for C-2 probably indicates that it lies very close to the surface (so that it could be deshielded). This rules out the possibility that 1,3-propanediol may adsorb on the surface in the adsorption mode (I) because with such a mode of adsorption, the C-2 carbon would be the furthest away from the surface.

Adsorption mode (III) would lead to a surface structure which has the C-2 carbon lying very close to the surface, and this is probably the preferred mode of adsorption.

Another point of interest in the low-coverage spectra is the smaller peak at 42 ppm (on the low-field shoulder of the resonance at 38 ppm). It is speculated that this peak arises from the stronger interaction with a  $Mg^{2+}$  ion on the surface (which deshields the C-2 carbon more), or some kind of configurational effect.

At high coverage ( $9.69 \mu\text{mole}/\text{m}^2$ ), a peak at 60 ppm (on the high-field shoulder of the 64 ppm resonance) is observed. This is also accompanied by the upfield shift of the high-field resonance to 35 ppm. This probably corresponds to the increase in the population of physisorbed 1,3-propanediol, or a

conversion of the chemisorbed species to the adsorption mode (II). Note that in the adsorption mode (II), there are two carbons on the 1,3-propanediol molecule which are not in close proximity to the surface, and thus not experiencing the deshielding effect from the surface. The resonance at 64 ppm would indicate that there is still a high population of chemisorbed species in adsorption mode (III).

### 5.E.III. Adsorbed 1,4-butanediol

The  $^{13}\text{C}$  CP static spectra of 1,4-butanediol adsorbed on MgO (Figure 5.46) are quite similar to those of 1,3-propanediol on MgO. Basically, the spectra consist of two powder patterns overlapping with each other. The powder patterns seem to get narrower and sharper, as coverage increases, especially for the methylene resonance corresponding to the C-2 and C-3 carbons. At coverage of about  $8.14 \mu\text{mole}/\text{m}^2$ , both resonances are quite narrow, and the linewidths are comparable to those obtained by  $^{13}\text{C}$  CP/MAS technique, as shown in Figure 5.50 (ca. 15 ppm wide).

This narrowing effect is not quite understood. It is plausible that there exists a high population of physisorbed 1,4-butanediol molecules which rapidly exchange with the chemisorbed species. The single-pulse  $^{13}\text{C}$  NMR/MAS measurements of the same samples as those in Figure 5.46 (shown in Figure 5.47) show almost the same spectra. It is apparent then that



there exists quite a population of physisorbed 1,4-butanediol molecules on the MgO surface.

The  $^{13}\text{C}$  CP/MAS spectra shown in Figure 5.50 reveal more variations. At low coverages, the S/N is poor, probably due to insufficient number of cross-polarization contacts.

As the coverage is increased to  $7.83 \mu\text{mole/m}^2$ , two resonances at 35 and 64 ppm are observed (spectrum b). Noticing that liquid 1,4-butanediol has isotropic shifts at 29.4 and 62.1 ppm respectively (134), the adsorbed 1,4-butanediol obviously shows a strong deshielding effect at the C-2 and C-3 carbons.

If the hypothesis about the deshielding effect as arising from the  $\text{Mg}^{2+}$  ions on the surface is correct, then these two carbons (C-2 and C-3) would lie very close to the surface. This would eliminate the possibility that 1,4-butanediol adsorbs on the MgO surface via adsorption mode (I), because in this mode, the C-2 and C-3 carbons would lie furthest from the surface. By the same token, adsorption mode (III) would be the most likely model of adsorption, because in this mode, all four carbons are "fixed" and lie very close to the surface. Adsorption mode (II) would have at least three carbons "hanging around" and behave almost like a physisorbed species.

Figure 5.50

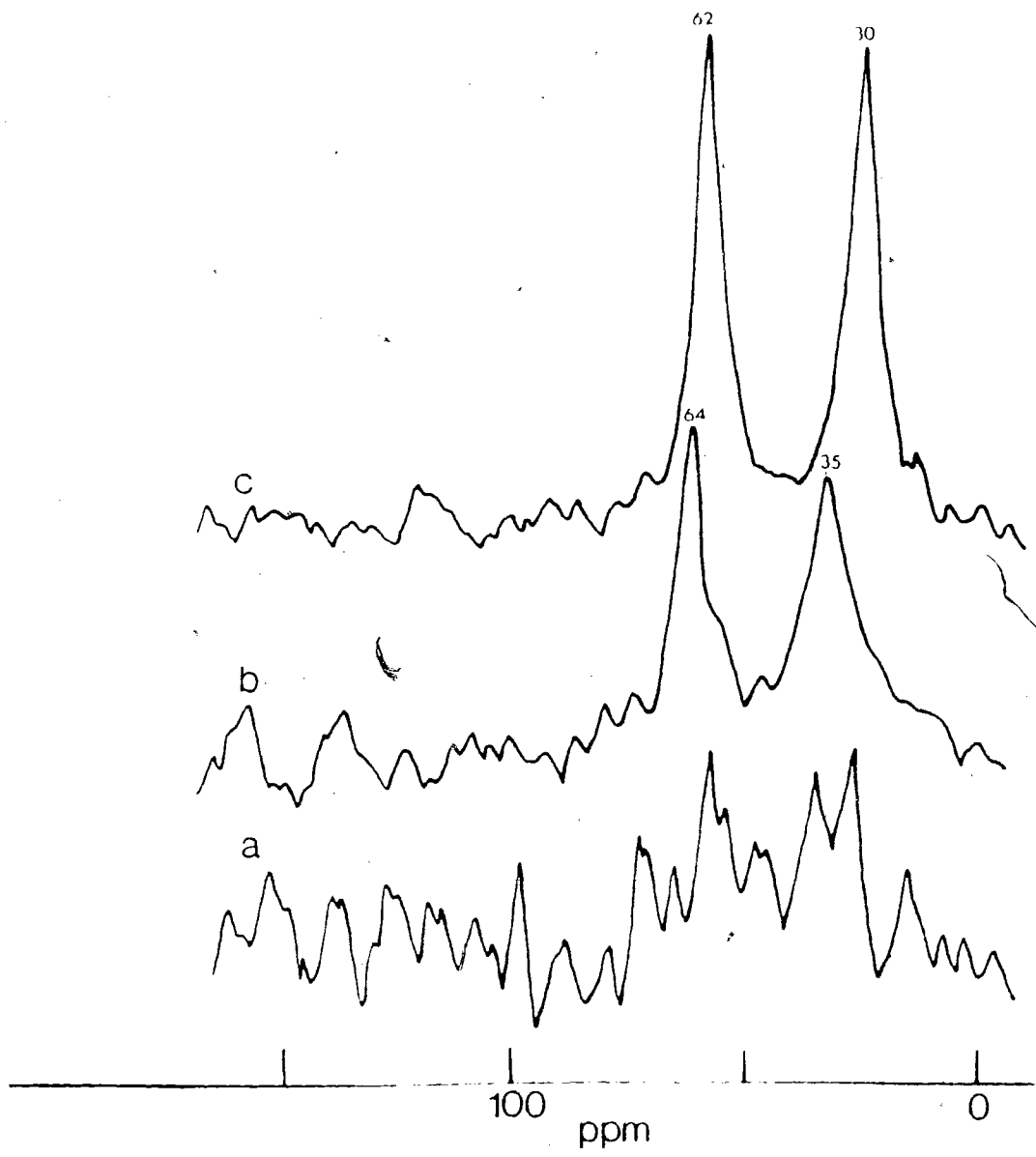
$^{13}\text{C}$  CP/MAS spectra of 1,4-butanediol adsorbed on MgO at various coverages. Field strength = 60 kHz. Contact time = 0.5 msec, except (c) which is 2 msec.

Rep. rate =  $2 \text{ sec}^{-1}$ , except (b) which is  $3.3 \text{ sec}^{-1}$ .

(a)  $4.44 \mu\text{mole/m}^2$ , 110,086 contacts

(b)  $7.83 \mu\text{mole/m}^2$ , 194,871 contacts

(c)  $9.52 \mu\text{mole/m}^2$ , 24,904 contacts



5.E.IV  $^{13}\text{C}$  CP/MAS Study of Adsorbed 1,4-butanediol on MgO Treated at Elevated Temperatures

The sample of  $7.83 \mu\text{mole/m}^2$  of 1,4-butanediol on MgO-(3) was treated to higher temperatures. The  $^{13}\text{C}$  CP/MAS spectra recording all the changes are shown in Figure 5.51. There is no observable change until treatment at  $300^\circ\text{C}$ . At this temperature, there appears a sharp resonance at low-field centered at 184 ppm, which probably indicates the formation of some carboxylate species. The high-field resonances are very broad with major resonances at 66, 48, 37 and 32 ppm. The resonance at 66 ppm probably corresponds to some not yet decomposed alkoxide species on the surface.

It is suspected that there could be the formation of some branched-chain alcohols on the surface following the mechanism (equation [5.2]) proposed for the formation of n-butanol. The resonance at 48 ppm would then probably correspond to the  $\beta$ -substituted carbons on these highly-branched alcohols.

At  $400^\circ\text{C}$ , the low-field resonance at 183 ppm has grown in intensity. This is accompanied by the appearance of peaks at 167 ppm (bicarbonate) and a broad resonance centered at 128 ppm (probably a wide range of olefinic carbons). The high-field resonance is centered between 10-40 ppm, indicating the complete decomposition of the surface alkoxide species, and

Figure 5.51

$^{13}\text{C}$  CP/MAS spectra of the sample of  $7.83 \mu\text{mole/m}^2$   
1,4-butanediol on MgO treated at elevated temperatures.

Field strength = 65 kHz. Contact time = 2 msec,

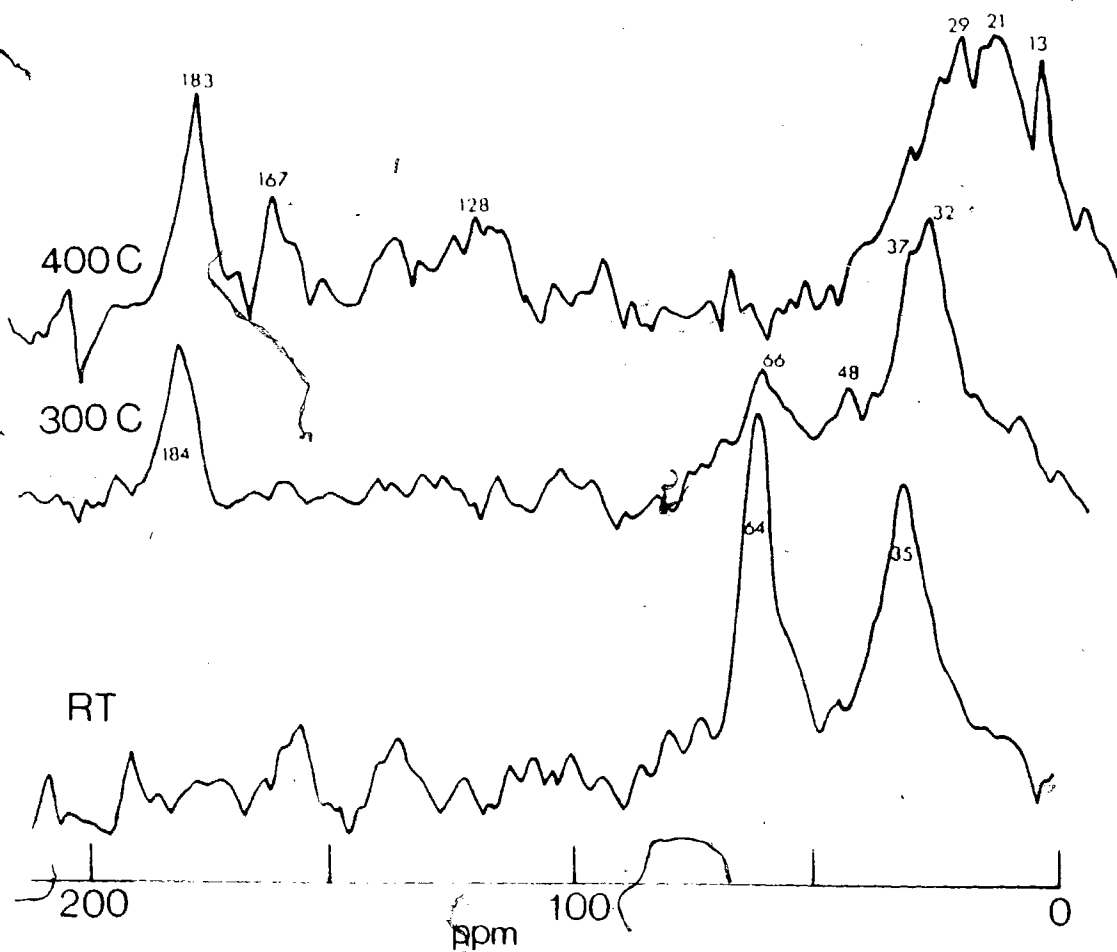
except (a), which is 0.5 msec. Repetition

rate =  $2 \text{ sec}^{-1}$ , except (a) which is  $3.3 \text{ sec}^{-1}$ .

(a) Room temp., 194,871 contacts

(b)  $300^\circ\text{C}$  (3 hrs), 88,117 contacts

(c)  $400^\circ\text{C}$ , 150,150 contacts



leaving a wide range of alkanes and alkenes. However, the present resolution precludes any identification of these surface species.

No surface species could be detected when the sample was treated above  $400^{\circ}\text{C}$ . The only observable resonance is at 128 ppm (probably some aromatics), but it is very broad.

#### 5.E.V. Adsorbed 1,3-butanediol

Notice that so far in the study of adsorbed alkanediols on MgO, only molecularly symmetric compounds were chosen. The reason is simple: the more carbon resonances the compound has, the more complex the spectrum is, and overlapped resonances may occur leading to poor resolution).

To conclude this chapter, the  $^{13}\text{C}$  CP/MAS of adsorbed 1,3-butanediol on MgO has been measured (Figure 5.52). At low coverage, four major resonances at 70, 64, 44 and 24 ppm are observed. Liquid 1,3-butanediol has  $^{13}\text{C}$  chemical shifts at 59.0 (C-1), 41.2 (C-2), 64.9 (C-3) and 23.3 (C-4) (141). It is probably then that both carbons bearing the -OH groups (C-1 and C-3) experience a deshielding effect (to 64 and 70 ppm from 59 and 65 ppm respectively). The C-2 carbon also suffers some deshielding (from 41 to 44 ppm downfield from TMS), this probably indicates that this carbon also lies very close to the surface.

Figure 5.52

$^{13}\text{C}$  CP/MAS spectra of 1,3-butanediol on  $\text{MgO}$ -(3) at various coverages. Field strength = 46 kHz except

(a) which is 60 kHz. Contact time = 2 msec.

Repetition time = ~~1~~  $\text{sec}^{-1}$  except (b) which is

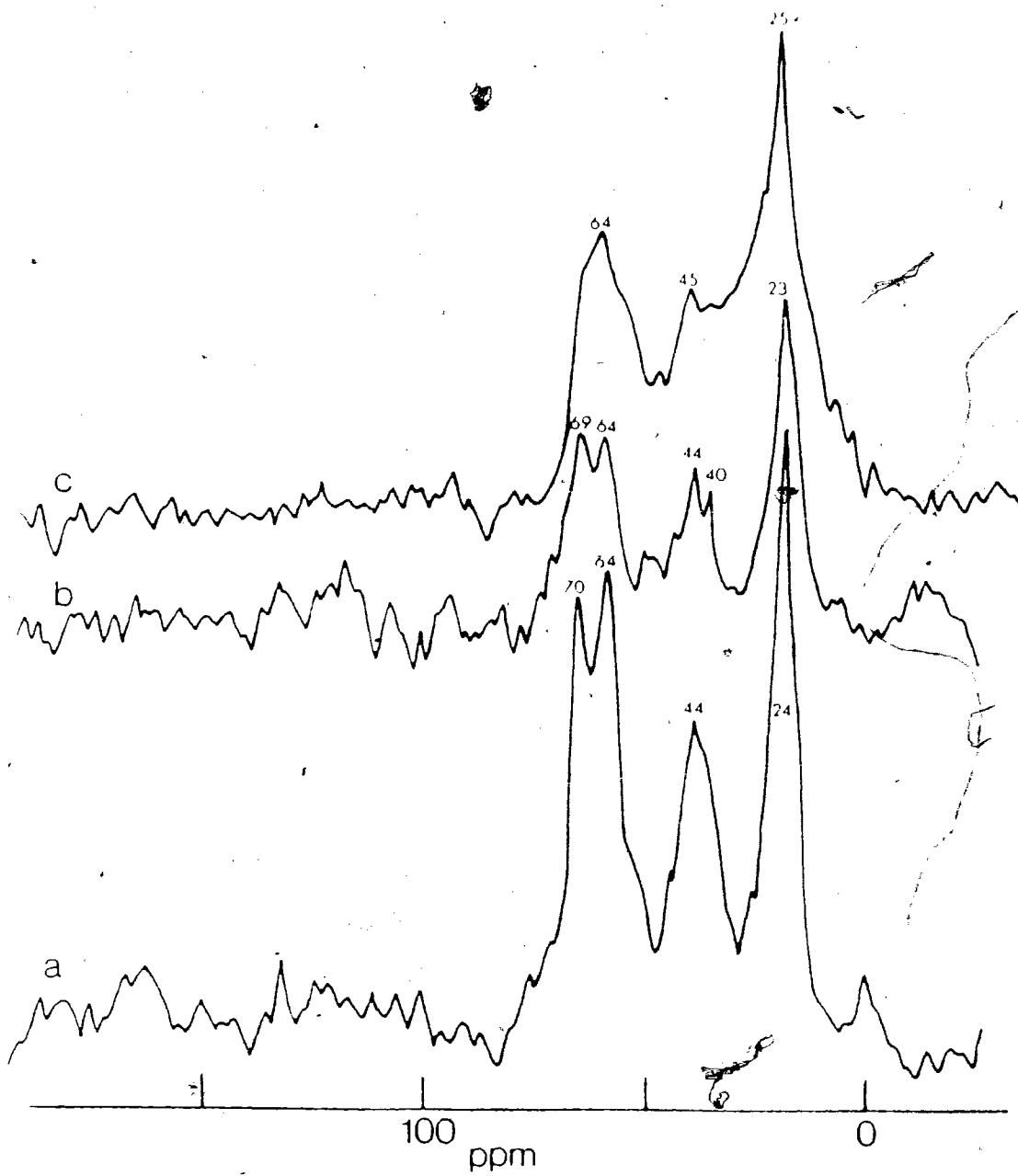
$2 \text{ sec}^{-1}$ . All spectra are not normalized for the different number of contacts.

(a)  $4.66 \mu\text{mole}/\text{m}^2$ , 54,600 contacts

(b)  $7.43 \mu\text{mole}/\text{m}^2$ , 266,730 contacts

(c)  $9.15 \mu\text{mole}/\text{m}^2$ , 68,905 contacts





This observation confirms that alkanediols adsorb on MgO surface in adsorption mode (III), i.e. both -OH groups are bonded to the surface. This similar effect is also observed for the adsorbed 1,3-propanediol on MgO surface, which is not surprising since the structures of 1,3-propanediol and 1,3-butanediol are very similar.

As the coverage is increased to  $7.43 \mu\text{mole}/\text{m}^2$ , there is a new resonance at 40 ppm, which was probably obscured in the previous spectrum by the resonance at 44 ppm. From this observation, there may be a definite population of the adsorbed species which behaves like physisorbed molecules, or adsorbing in adsorption mode (II).

As the coverage is increased to  $9.15 \mu\text{mole}/\text{m}^2$ , the resonance at 70 ppm appears only as a low-field shoulder on the major peak at 64 ppm. The previous resolved peaks at 44 and 24 ppm are now overlapped. The loss in resolution is probably due to the appearance of more adsorbed species, or the 1,3-butanediol starts to adsorb in other modes of adsorption due to crowding. It is also possible that the line broadening may be due to motions at the spinner frequency.

#### 5.E.VI. Summary

It is shown that the two -OH groups on the alkanediols do not adsorb onto the same  $\text{Mg}^{2+}$  on the surface, even if the -OH groups are four-carbon length apart (as in the

case of 1,4-butanediol ). Therefore, it is established that the adsorption mode of alcohols on MgO is a 1:1 ratio, i.e. no more than one alcohol molecule per active site ( $Mg^{2+}$ ) on the surface. The downfield shift experienced by the  $\beta$ -carbon(s) on 1,3-propanediol and 1,4-butanediol indicate that the  $\beta$ -carbon(s) lie very close to the surface. This further establishes that the two -OH groups on the alkanediols adsorb onto two different  $Mg^{2+}$  ions on the surface. It is found that there exists a substantial population of physisorbed 1,4-butanediol molecules on the MgO surface. This probably arises from crowding.

Preliminary study on the 1,4-butanediol-MgO system treated at elevated temperatures revealed little. No 1,3-butadiene was observed (probably below detection level). It is suspected that some branched-chain alcohols could be formed. Some dehydrogenation was observed - by the presence of a carboxylate species at ca. 183 ppm downfield from TMS. Treatment above 400°C revealed aromatics species (ca. 128 ppm) probably on the way to become graphite.

## CHAPTER 6

6.A. WO<sub>3</sub>

After the initial success with the alcohol-MgO systems utilizing CP technique, it is desirable to extend this technique to other catalytic systems. In continuation of this project, the study of the chemisorption of methanol on WO<sub>3</sub> has been undertaken.

As was mentioned earlier in Chapter 2, WO<sub>3</sub> has not been studied extensively, especially as an alcohol-dehydration catalyst. Most studies on WO<sub>3</sub> focus on its semi-conductor behaviour, rather than the dehydration activity. Studies of WO<sub>3</sub> also suffered because of the difficulty in preparation. Commercially available WO<sub>3</sub> does not have high surface area, which is a drawback in the study of surface chemistry and catalysis by NMR. My experience in the laboratory preparation of WO<sub>3</sub> is that the quality of the catalyst differed from batch to batch. This may be due to a slight change in the experimental conditions: simmering conditions for the tungstic acid gel, pumping speed in the dehydration of the tungstic acid etc. Also, the ammonium-metatungstates (precursor of tungstic acid) from different manufacturers are quite different.

### 6.A.I. Methanol Adsorption Isotherm

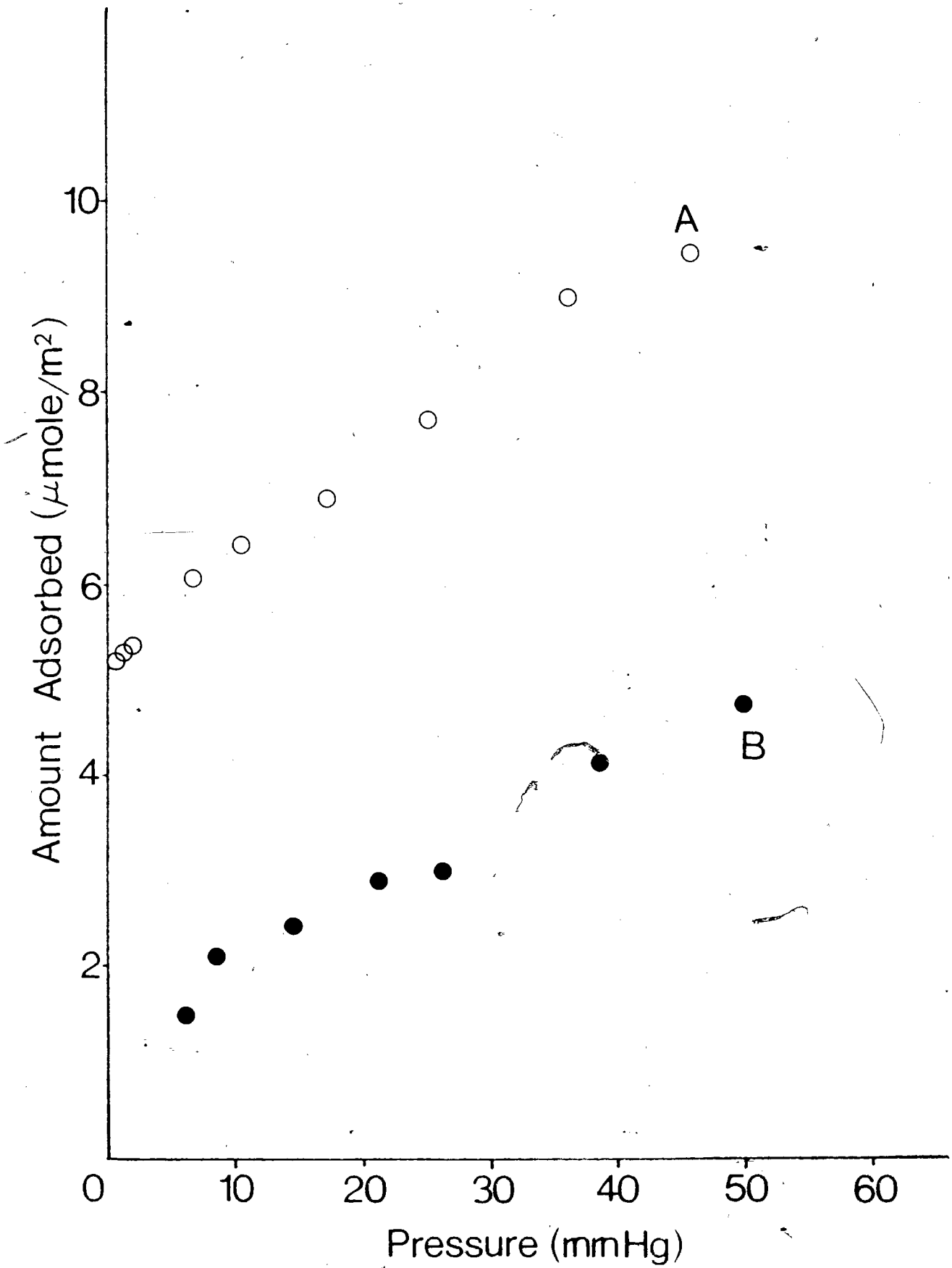
A batch of  $WO_3$  has been successfully prepared which has reasonable surface area, high density and general consistency from sample to sample as described in Chapter 4. Two different out-gassing procedures have been attempted:  $WO_3$ -(1) was degassed for 2 hours at  $300^\circ C$ , while  $WO_3$ -(2) was degassed at  $300^\circ C$  for 19 hours. Both types of  $WO_3$  were then treated with  $O_2$  at  $300^\circ C$  for 2 hours, then pumped out prior to the introduction of alcohols.

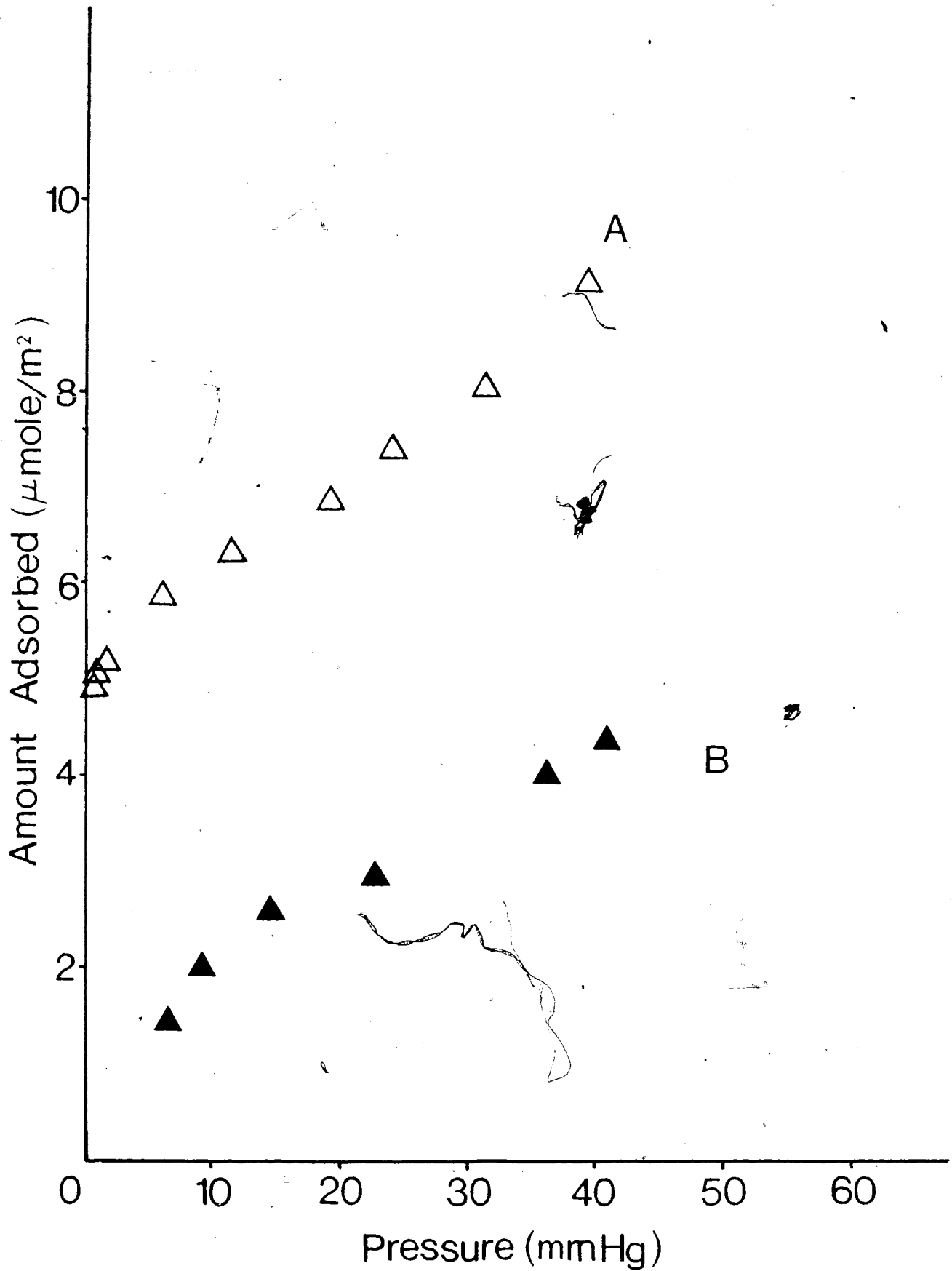
The methanol adsorption isotherms on  $WO_3$ -(1) and  $WO_3$ -(2) at room temperature are shown in the upper curves in Figures 6.1 and 6.2 respectively. The lower curves are the isotherms obtained after pumping for 2 hours at room temperature after the first isotherm. The methanol adsorption isotherms on both types of  $WO_3$  show essentially the same features. This probably indicates that the surface water molecules are essentially desorbed at  $300^\circ C$  in 2 hours. A further heating of 16 hours does not vary the concentration of surface  $-OH$  groups to any extent so that both types of  $WO_3$  show the same adsorption capacity for methanol.

On the other hand, both isotherms shown in the same figure are almost parallel within experimental error, and their difference,  $4.6 \mu\text{mole}/\text{m}^2$  is taken as a measure of the active sites on the  $WO_3$  surface. Assuming a first order desorption

Figure 6.1 Adsorption isotherm of methanol on  $WO_3$ -(1) at room temperature. (Upper Curve, A). Lower Curve B degassed at room temperature for 2 hours after A.

Figure 6.2 Adsorption isotherm of methanol on  $WO_3$ -(2) at room temperature. (Upper Curve (A)). Lower Curve (B), after degassing at room temperature for 2 hours after (A).







kinetics for methanol, the activation energy for desorption can then be estimated.

Assuming first order desorption kinetics for methanol, then in 2 hours of pumping, 75% of those molecules will be desorbed whose rate constant for desorption is  $2 \times 10^{-4} \text{ sec}^{-1}$ , and a higher fraction for those having a greater rate constant. Similarly, only 25% will be desorbed for a rate constant of  $4 \times 10^{-5} \text{ sec}^{-1}$  and lesser amounts for smaller rate constants. By approximating the rate constant as  $(kT/h)\exp(-E/RT)$  where  $k$  is the Boltzmann constant and  $h$  Planck's constant, it can be shown that the two rate constants above correspond to activation energies  $E$ , for desorption of 23 and 24 kcal/mole respectively. Thus at the present pumping conditions, methanol on sites with  $E < 23$  kcal/mole will be essentially all desorbed, while that with  $E > 24$  kcal/mole is essentially all retained. In these conditions, physically adsorbed and hydrogen-bonded methanol should be removed, while methanol bound to strong active sites is retained, and the amount reflected in the lower coverage observed for the subsequent isotherm.

#### 6.A.II. NMR Relaxation Parameters

Proton spin-lattice relaxation times  $T_{1H}$  were measured for methanol on  $WO_3$ -(1) and  $WO_3$ -(2), and are listed in Table 6.1. The following was observed: while there is no observable difference in  $T_{1H}$  between  $WO_3$ -(1) and  $WO_3$ -(2), there exists a trend towards faster relaxation at higher coverage. This is to

Table 6.1

Proton Spin-Lattice Relaxation Time ( $T_{1H}$ )for Methanol-WO<sub>3</sub> Samples

Coverage ( $\mu\text{mole/m}^2$ )	Degassing Time (hrs)	Degassing Temp( $^{\circ}\text{C}$ )	$T_{1H}$ (sec)	
4.69*	2	300	0.28	} WO <sub>3</sub> -(1)
5.78*	2	300	0.25	
6.26*	2	300	0.21	
6.41*	2	300	0.19	
7.55*	2	300	0.17	
8.58	2	300	0.11	
4.76*	19	300	0.24	} WO <sub>3</sub> -(2)
5.73*	19	300	0.25	
8.61	19	300	0.11	

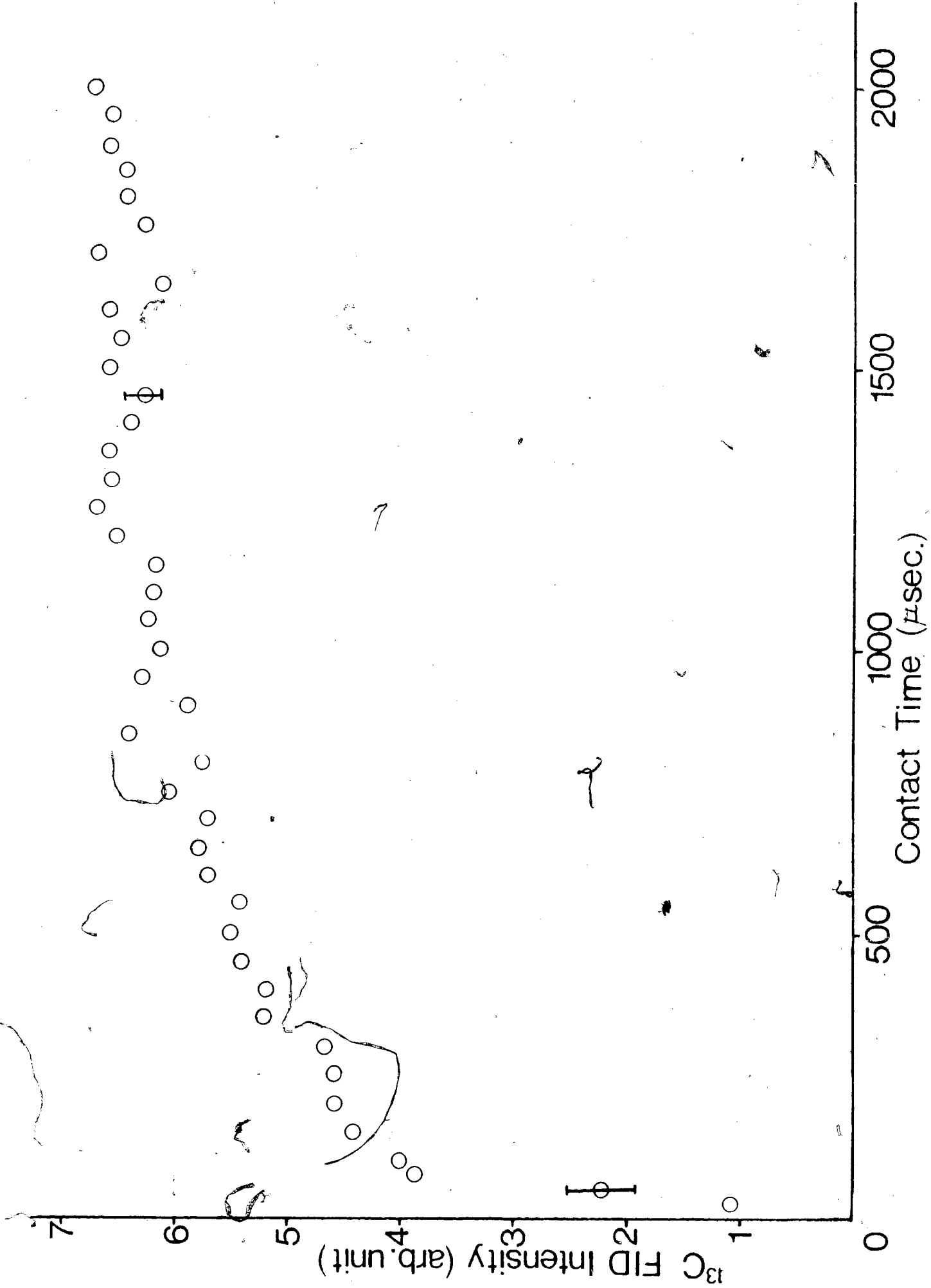
\* denotes 14% <sup>13</sup>C-enriched methanol used

be expected if the dipole-dipole interaction is the major contribution to relaxation. The  $r^{-3}$  dependence of the dipolar interaction would obviously lead to faster relaxation at higher coverage.

Comparing these  $T_{1H}$  values with those of  $Ni^{2+}$ -doped MgO, as in MgO-(2), the methanol- $WO_3$  systems clearly show longer relaxation times. Superficially, it may seem that the tungsten atoms in the  $WO_3$  exist in the highest oxidation state (W(VI)), so that they are not paramagnetic in nature.

The cross-polarization time ( $T_{CH}$ ) and the proton spin-lattice relaxation time in the rotating frame ( $T_{1\rho}$ ) were also measured for one sample: the  $5.78 \mu\text{mole}/\text{m}^2$  of 14%  $^{13}\text{C}$ -enriched methanol on  $WO_3$ -(1). A plot of  $^{13}\text{C}$ -signal intensity vs contact times is shown in Figure 6.3. The  $T_{CH}$  values is estimated to be 0.15 msec. The proton  $T_{1\rho}$  is measured to be 23 msec, by the technique mentioned in Chapter 4. These values are comparable to the relaxation data measured for the methanol-MgO systems. The cross-polarization time is short, indicating substantial static component of the intramolecular  $^1\text{H}$ - $^{13}\text{C}$  dipolar coupling. The shortness in proton  $T_{1\rho}$  relative to the proton  $T_1$  indicates considerable low-frequency motion in the adsorbed layer, i.e. tightly-bound methoxide species on the surface.

Figure 6.3 Plot of  $^{13}\text{C}$  free induction decay signal vs contact time for  $5.78 \mu\text{mole/m}^2$  of  $^{14}\text{C}$ -enriched methanol on  $\text{WO}_3$ -(1).



### 6.A.III. $^{13}\text{C}$ CP Static Spectra of Adsorbed Methanol

Figures 6.4 and 6.5 show the  $^{13}\text{C}$  CP spectra of static samples at various coverages of adsorbed methanol on  $\text{WO}_3$ -(1) and  $\text{WO}_3$ -(2) respectively. In general, for both preparations, a broad powder pattern is observed in the region expected for a methoxide species, with an isotropic peak at near 50 ppm downfield from TMS. The edges of the powder pattern were smoothed out for the spectra in which  $^{13}\text{C}$ -enriched methanol was used. This is probably due to the  $^{13}\text{C}$ - $^{13}\text{C}$  dipolar coupling (of the order of few hundred Hz) convolved with the powder pattern. The spectrum (f) in Figure 6.4 in which ordinary methanol was used, showed a typical methoxide species, with the low field component ( $\sigma_1$ ) at about 77 ppm, but the high field shielding component was not resolved.

The isotropic peak at 50 ppm could be attributed to the loosely-bound methanol on the  $\text{WO}_3$  surface. In spectra (a) and (b) in Figure 6.4, the intensity of the isotropic peak at ca. 50 ppm (loosely-bound species) seems to be larger than the powder pattern of the methoxide species. This seems to contradict with the observation from the adsorption isotherm shown in Figure 6.1, which indicates only a small population of the physisorbed molecules. No plausible explanation is obvious from present results.

The duration of the degassing period seems to have some effects on the  $^{13}\text{C}$  static spectra of methanol on  $\text{WO}_3$ . The

Figure 6.4

$^{13}\text{C}$  static CP spectra of methanol on  $\text{WO}_3$ -(1).  
 Field strength = 70 kHz. Rep. rate = 3  $\text{sec}^{-1}$ ,  
 except (d) and (e) which are 2  $\text{sec}^{-1}$ .

	Coverage ( $\mu\text{mole}/\text{m}^2$ )	Contact Time (msec)	Number of contacts
(a)	4.69*	1.5	10,110
(b)	5.78*	2	15,689 ✓
(c)	6.26*	2	25,341
(d)	6.41*	1	16,384
(e)	7.55*	1.5	16,384
(f)	8.58	2	193,300

\* denotes 14%  $^{13}\text{C}$ -enriched methanol was used.

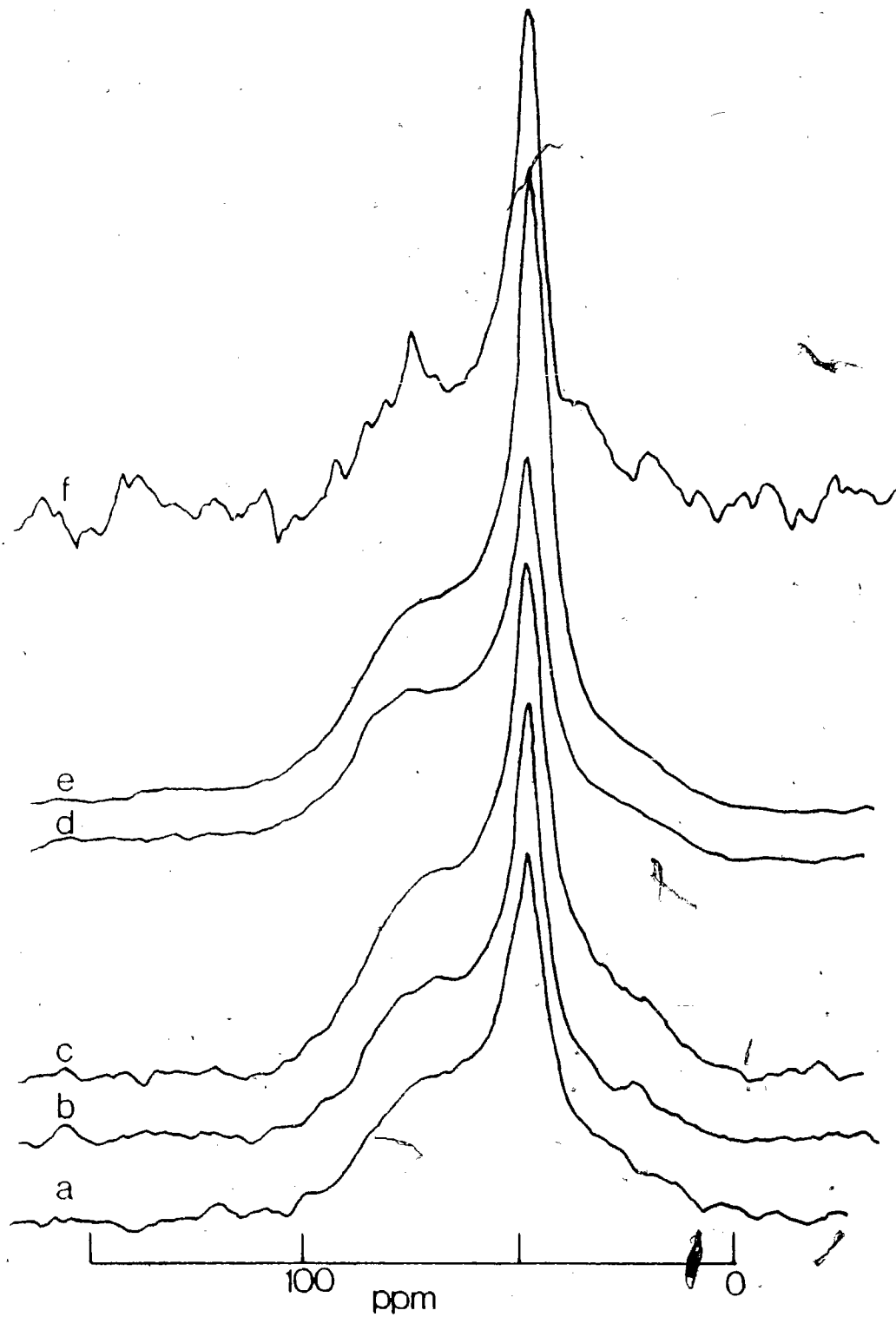


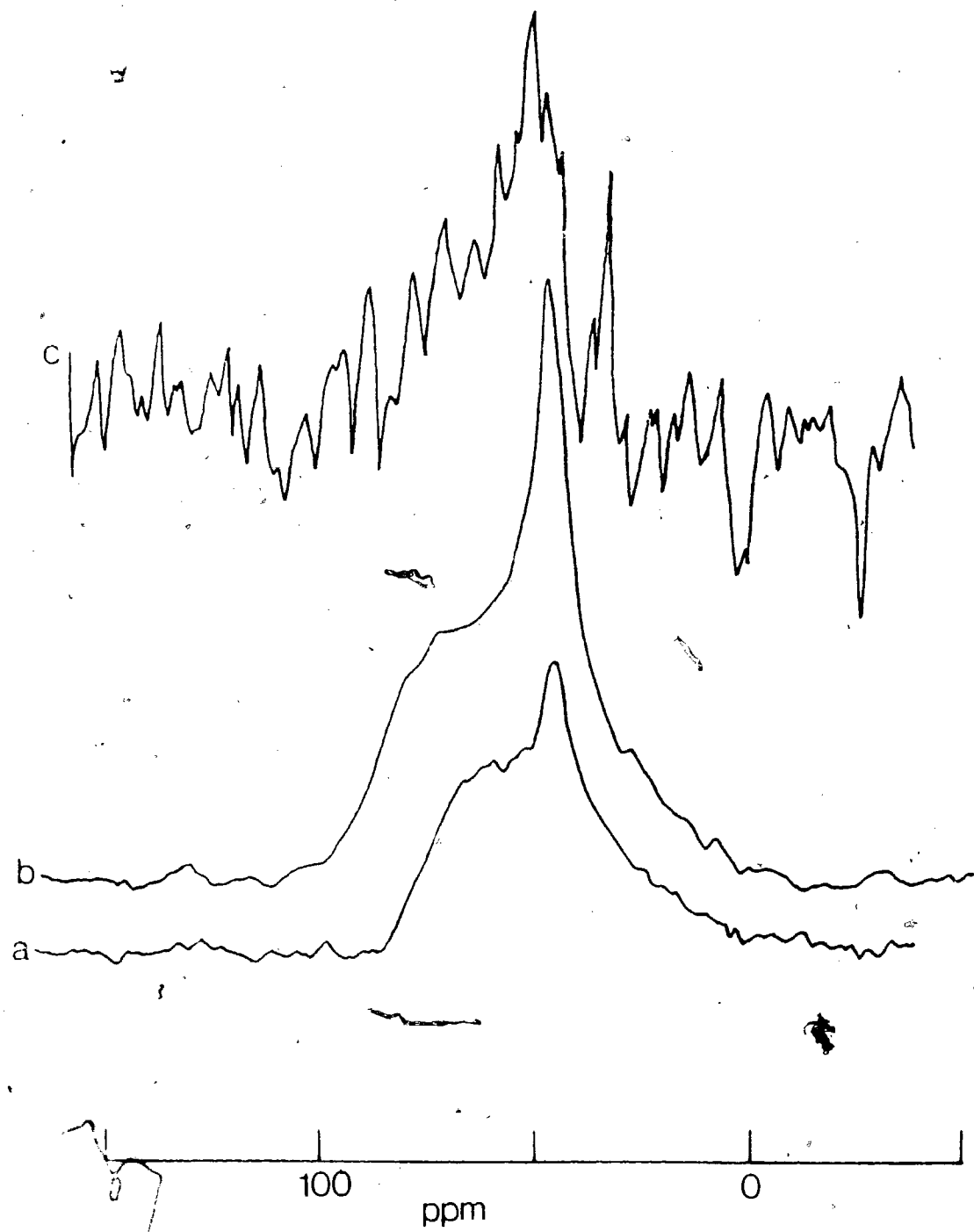


Figure 6.5

$^{13}\text{C}$  static CP spectra of methanol on  $\text{WO}_3$ -(2).  
Field strength = 40 kHz, except (b) which was  
70 kHz. Contact time = 2  $\mu\text{sec}$ . Repetition  
rate = 2  $\text{sec}^{-1}$ , except (b) which is 3.3  $\text{sec}^{-1}$ .

	Coverage ( $\mu\text{mole}/\text{m}^2$ )	Number of Contacts
(a)	4.76*	32,768
(b)	5.73*	29,522
(c)	8.61	81,920

\* denotes 14%  $^{13}\text{C}$ -enriched methanol was used.



low-field shielding component of the spectra in Figure 6.5 (except spectrum (c)) seemed to be sharper than the corresponding powder pattern observed in Figure 6.4 for the same coverage of methanol. This may imply a more rigid methoxide species on the surface, or the  $^{13}\text{C}$ - $^{13}\text{C}$  coupling did not convolve with the powder pattern. The latter explanation may indicate that the intermolecular interactions between the methoxide species are diminished, probably arising from the longer distance (due to surface morphology) between the chemisorbed methanol species.

It is also apparent that spectra (a) and (b) in Figure 6.5 look more like what one would expect, i.e. a much smaller isotropic peak at 50 ppm compared to the powder pattern of the methoxide species. This could be attributed to the redistribution of the surface -OH groups on the  $\text{WO}_3$ -(2) surface caused by the prolonged degassing period. Of course, the long degassing period may also alter the surface morphology to accommodate the present observation on the  $\text{WO}_3$ -(2) surface.

The spectrum (c) in Figure 6.5 showed a very poor S/N ratio, probably caused by personal error in measuring the desired amount of adsorbate, or a leak developed after the sample tube was sealed.

In general, the  $\text{WO}_3$  turned to a greenish color (from the original yellow color) upon the introduction of methanol,

but returned to the original yellow color when the samples were shaken. An attempt has been made to investigate if this is a photo effect, by storing the samples in complete darkness and under ordinary fluorescent light. The static  $^{13}\text{C}$  CP spectra in both cases were excellent reproductions of the original spectra after a storage period of 6 months. The photochromism of oxides like  $\text{WO}_3$  and  $\text{MoO}_3$  has been extensively studied (142). It was concluded that the tungsten was reduced from W(VI) to W(V) under ultraviolet irradiation. This reduction can also be caused by adsorption of  $\text{H}_2$ , alcohols, Pd or Pt metals (142). However, this change in the oxidation state in tungsten apparently does not change the observed  $^{13}\text{C}$  CP spectra of methanol on  $\text{WO}_3$ .

It is possible that the methanol- $\text{WO}_3$  systems did undergo reduction to some extent, to give rise to the green color. However, the conversion product(s) (from methanol) and the mechanism involved could not be elucidated by the present  $^{13}\text{C}$  results.

#### 6.A.IV. $^{13}\text{C}$ Static CP Spectra of Methanol- $\text{WO}_3$ at Elevated Temperatures

The representative  $^{13}\text{C}$  CP static spectra of the methanol- $\text{WO}_3$  systems at room temperature and after heating (170, 300°C) are shown in Figures 6.6 and 6.7 for  $\text{WO}_3$ -(1) and  $\text{WO}_3$ -(2) respectively. Both figures show essentially the same changes as the samples were heated to higher temperatures.

Figure 6.6

$^{13}\text{C}$  CP spectra of  $6.41 \mu\text{mole/m}^2$  of methanol (14%  $^{13}\text{C}$ -enriched) on  $\text{WO}_3$ -(1) treated at different temperatures. R.F. field = 40 kHz except (a) which is 70 kHz, contact period = 2 msec, except (a) which is 1 msec.

- (a) Room temp., rep rate =  $2 \text{ sec}^{-1}$ , 16,384 contacts
- (b)  $170^\circ\text{C}$  (3 hrs), rep rate =  $5 \text{ sec}^{-1}$ , 9,201 contacts
- (c)  $300^\circ\text{C}$  (3 hrs), rep rate =  $1 \text{ sec}^{-1}$ , 27,439 contacts

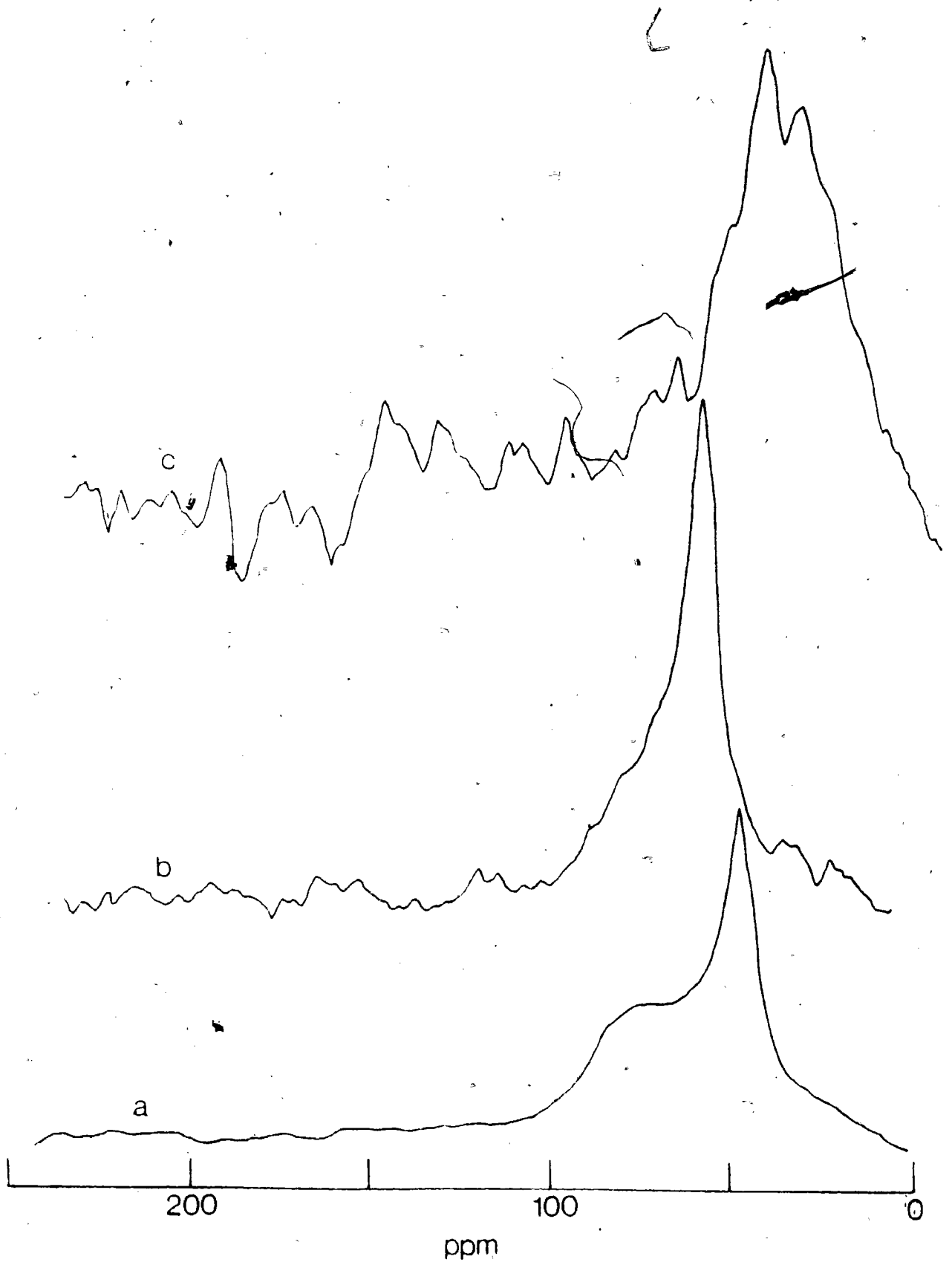


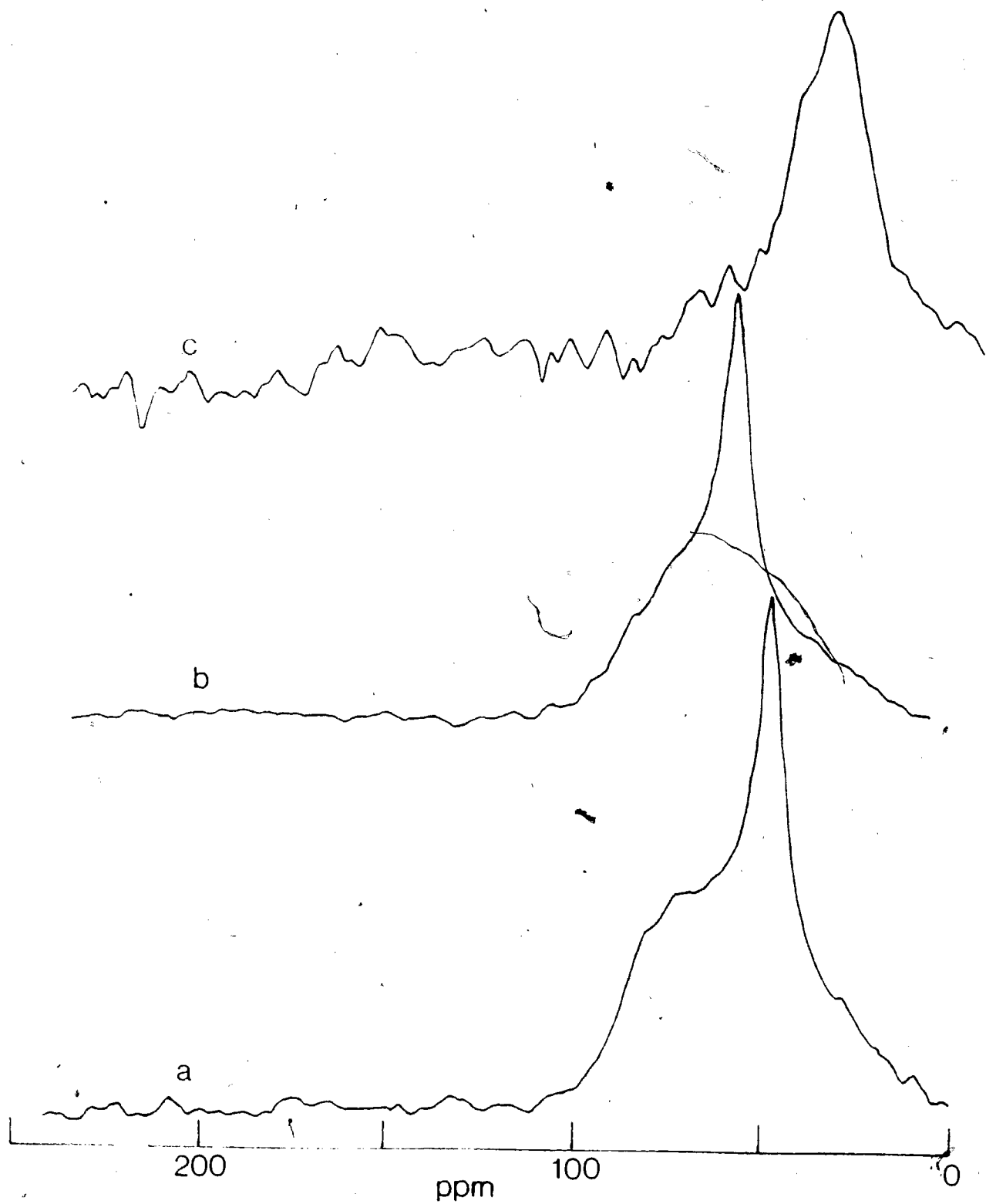
Figure 6.7

$^{13}\text{C}$  CP spectra of  $5.73 \mu\text{mole}/\text{m}^2$  of methanol on  $\text{WO}_3$ -(2) treated at different temperatures. R.F. field = 40 kHz except (a) which is 70 kHz. Contact period = 2 msec.

(a) Room temp., rep rate =  $3.03 \text{ sec}^{-1}$ , 29,522 contacts

(b)  $170^\circ\text{C}$  (3 hrs), rep rate =  $3.03 \text{ sec}^{-1}$ , 21,404 contacts

(c)  $300^\circ\text{C}$  (3 hrs), rep rate =  $2 \text{ sec}^{-1}$ , 126,200 contacts





Treated at 170°C, both spectra show a composite of two powder patterns: an isotropic peak at 61 ppm downfield from TMS superimposed on the original methoxide powder pattern. The liquid-like methanol resonance observed at room temperature was not present. It was suspected that some of the methanol may have undergone dehydration to a dimethyl ether species via:



This would involve surface protons, which should be abundant on the  $\text{WO}_3$  surface, since  $\text{WO}_3$  is an acidic catalyst. It could be further speculated that this dehydration involves an immobile methanol species (surface methoxide) and a mobile methanol (liquid-like methanol on the surface), and that the ether formation depends on the availability of the mobile methanol species. This hypothesis is certainly true if the active sites reside on W on the surface, and that the immobile methoxide species chemisorbed on these W atoms. This will make the chemisorbed methoxide species quite far apart, and any reaction taking place would involve the mobility of the physisorbed methanol species. Of course, this reaction could also be induced by the chemisorbed methoxide species, which start to "hop" to other sites (i.e. more mobile) at this treatment temperature.

Upon heating at 300°C for 3 hours, the methanol- $\text{WO}_3$  systems turned a bluish color, which indicates a significant

reduction of the  $WO_3$  from the original W(VI) to W(V) and W(IV) oxidation states. The  $^{13}C$  CP static spectra show a broad resonance at below 50 ppm downfield from TMS, with two peaks at 46 and 33 ppm respectively. Due to the poor S/N, the existence of other peaks could not be ascertained. From the positions of these resonances, it is apparent that they are alkanes and alkane derivatives, which have a low range of motional frequencies. However, the exact identity of these compound(s) is unknown.

When the samples were heated to  $500^\circ C$  for 3 hours, the color turned to a very intense blue. It was impossible to obtain any  $^{13}C$  CP static spectra for these samples.

One suspects that this is due either to paramagnetic interaction which broadens the  $^{13}C$  CP spectra, or most of the surface species have been distilled off the surface. Although it is not known exactly the oxidation state(s) of tungsten in the tungsten oxide at this experimental condition, one would expect that the oxidation state will vary from W(VI) to W(IV) (65, 142-146) indicating oxides of tungsten in the form of  $WO_{3-x}$  (where x varies from 0 to 1).  $WO_3$  (W in oxidation state VI) is not paramagnetic, but any lower oxidation states of tungsten will be paramagnetic as shown by ESR study (143). These paramagnets will certainly broaden the  $^{13}C$  CP spectra.

Single-pulse  $^{13}\text{C}$  NMR spectrum (performed on a Varian XL-100) on these samples treated at  $500^\circ\text{C}$  revealed resonances at 84, 125 and 157 ppm respectively. The resonances at 125 and 157 ppm probably correspond to ethylene and alkyl carbonate (146) respectively. However, the combination of the resonances at 84 and 157 ppm could be speculated to be a vinyl ether type species, and the resonance at 125 ppm probably indicates ethene. One is not sure about the origin of this vinyl ether, but it is possible that it arises from the dehydrogenation of a polymer-type species formed by the dimethyl ether.

#### 6.A.V. $^{13}\text{C}$ CP/MAS of Adsorbed Methanol on $\text{WO}_3$

To complete this preliminary study of adsorbed methanol on  $\text{WO}_3$ , two samples were prepared for  $^{13}\text{C}$  CP/MAS measurements. Two samples (from  $\text{WO}_3$ -(1) and -(2)) each of about one gram were loaded with about  $1.0 \mu\text{mole}/\text{m}^2$  of 90%  $^{13}\text{C}$ -enriched methanol in 5 mm o.d. NMR tubes. Sample preparations were the same as those for static samples. Their respective  $^{13}\text{C}$  CP/MAS spectra are shown in Figures 6.8 and 6.9.

At room temperature, the  $^{13}\text{C}$  CP/MAS spectra show a slight variation from the  $^{13}\text{C}$  CP static shown earlier. The striking feature is the appearance of a smaller peak at 68 ppm apart from the major resonance (of the methoxide resonances) at 53 ppm downfield from TMS.

Figure 6.8

$^{13}\text{C}$  CP/MAS spectra of  $0.96 \mu\text{mole/m}^2$  of 90%  $^{13}\text{C}$ -enriched methanol on  $\text{WO}_3$ (1), when treated at elevated temperatures. Field strength = 50 kHz. Contact period = 2 msec. Repetition rate =  $2 \text{ sec}^{-1}$ . Spinning speed = 1.8 kHz. All spectra are not normalized for the different number of contacts.

- (a) Room temp., 2,000 contacts
- (b)  $200^\circ\text{C}$  (3 hrs), 23,420 contacts
- (c)  $250^\circ\text{C}$  (3 hrs), 14,000 contacts
- (d)  $300^\circ\text{C}$  (3 hrs), 53,238 contacts

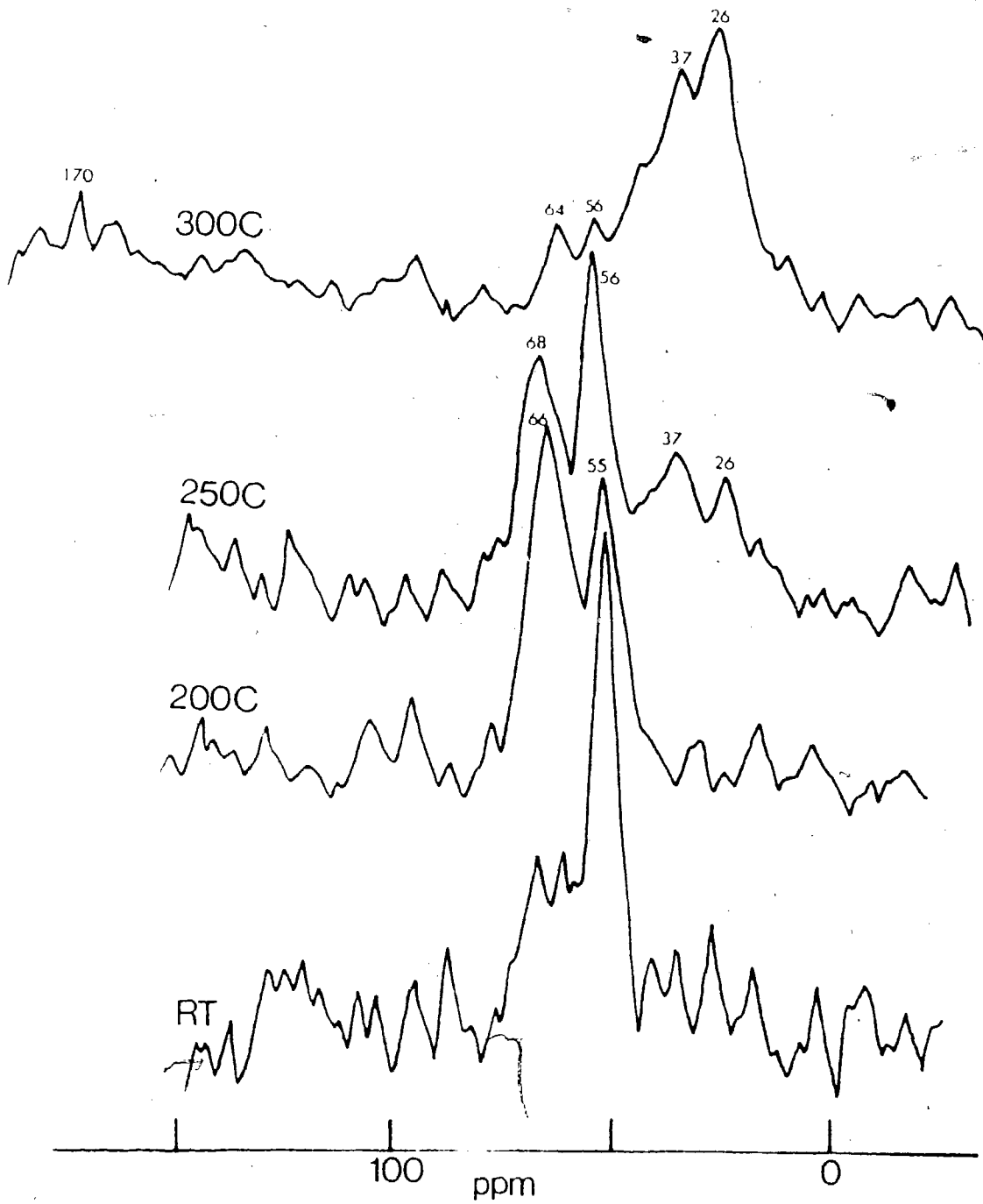


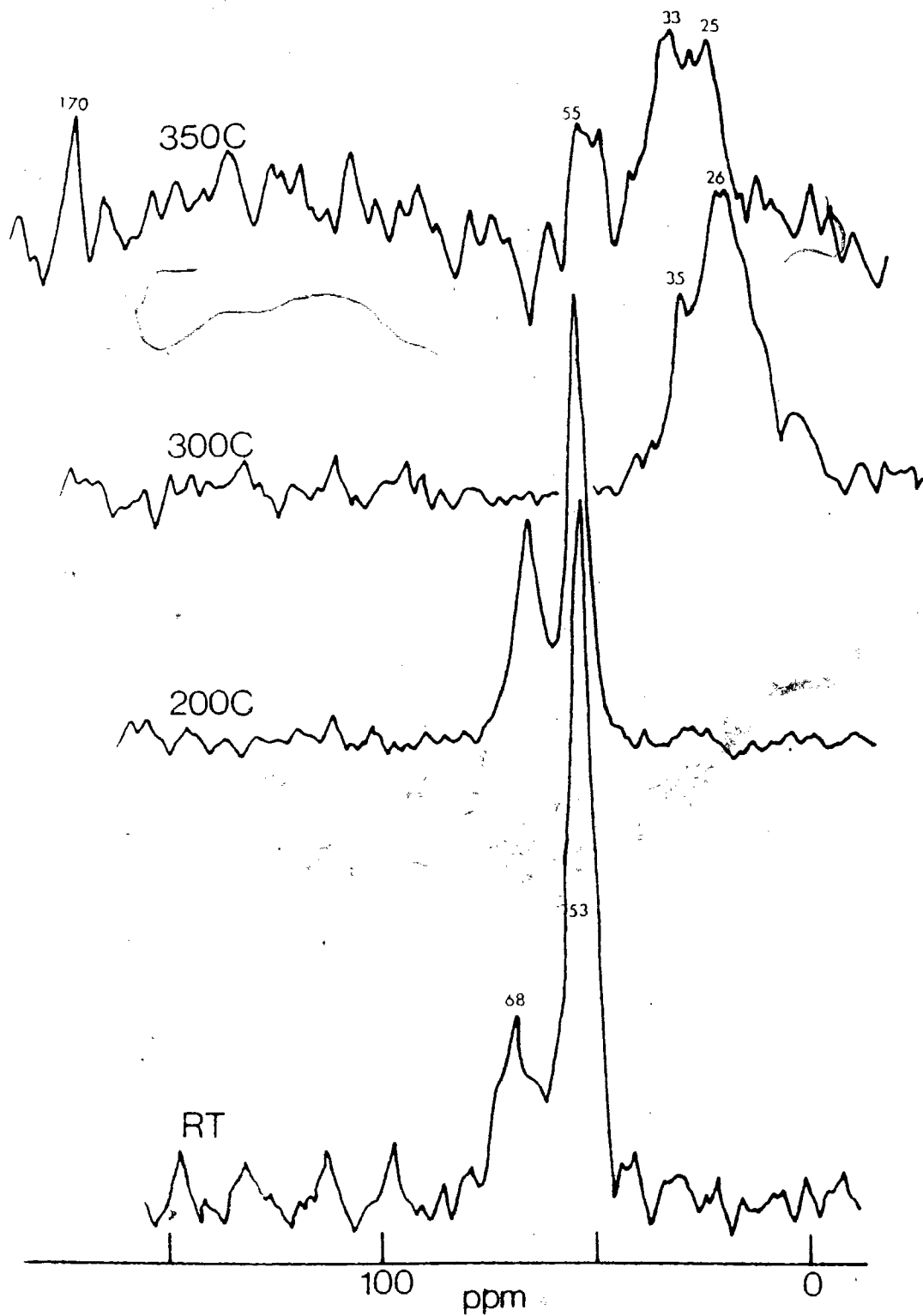
Figure 6.9

$^{13}\text{C}$  CP/MAS spectra of  $0.99 \mu\text{mole/m}^2$  of 90%  $^{13}\text{C}$ -enriched methanol on  $\text{WO}_3$ -(2) when treated at elevated temperatures. Field strength = 60 kHz. Contact period = 2 msec.

Repetition rate =  $2 \text{ sec}^{-1}$ . Spinning speed = 1.8 kHz.

All spectra are not normalized for the different number of contacts.

- (a) Room temp., 2,000 contacts
- (b)  $200^\circ\text{C}$  (3 hrs), 8,106 contacts
- (c)  $300^\circ\text{C}$  (3 hrs), 118,307 contacts
- (d)  $350^\circ\text{C}$  (3 hrs), 100,450 contacts



The downfield shift of about 4 ppm for the methoxide resonance (from the usual 49 ppm, e.g.  $Mg(OCH_3)_2$ ) is surprising. This may indicate that the surface tungsten atom exerts a rather strong interaction with the adsorbed methanol, by withdrawing electrons from the oxygen atom (in the methoxide species) so that the net effect is a deshielding effect on the methyl resonance.

However, it is well-known that tungsten exerts peculiar effects in the  $^{13}C$  chemical shifts of the organotungsten compounds (154). For example, the methyl resonance in  $W(CH_3)_6$  is at 84 ppm downfield from TMS, but at 35 ppm upfield from TMS for  $W(CH_3)(Cyclopentadienyl)(CO)_3$  (154). It is apparent then, that the electronic inductive effect from the tungsten atom is minimal. Recent  $^{13}C$  NMR studies on tungsten alkoxide complexes,  $W(O-t-Bu)_3(NO)(C_6H_5N)$  (155) and  $W_2(o-i-Pr)_6(C_6H_5N)$  (156), show that there exists a trend of downfield shifts of ca. 12 ppm for the  $\alpha$ -carbon on the alkoxide groups bonded to the tungsten atom, relative to the  $\alpha$ -carbon on the parent alcohols, i.e. tert-butanol and isopropanol. It is uncertain what causes this effect.

Returning to the spectra (a) in both Figures 6.8 and 6.9, it could be argued that the resonances at 53 and 68 ppm correspond to different kinds of surface methoxide species, e.g. unidentate methoxide species and multiple methoxide species all



bonded to the same tungsten atom. However, it is well-known that  $\text{WO}_3$  is strongly acidic (32), so it is not surprising that some methanol molecules are dehydrated as they adsorb on the  $\text{WO}_3$  surface. One could then identify the smaller resonance at 68 ppm as a dimethylether species. Both arguments seem to be possible due to the lack of  $^{13}\text{C}$  NMR data. In view of the complex nature of the  $^{13}\text{C}$  CP/MAS spectra of the samples of methanol- $\text{WO}_3$ , when they were treated to successively higher temperatures, one inclines to identify the smaller resonance at 68 ppm as a dimethether species.

There are no observable changes in the spectra until  $200^\circ\text{C}$  when the samples were treated to succesively higher temperatures at  $50^\circ\text{C}$  increments each. At  $200^\circ\text{C}$ , the resonance corresponding to the postulated dimethylether species grows much higher in intensity, and in Figure 6.8, it has higher intensity than the methoxide species. Since the acidity of the surface arises from the protons on the surface -OH groups, and following from the previous argument, if there are more surface -OH groups on the  $\text{WO}_3$ -(1) surface, more methanol molecules would be converted to the ether species.

When the samples were treated to  $250^\circ\text{C}$  (only one representative spectrum shown in Figure 6.8), the original resonances in the high-field region become very broad, with two sharp peaks at 26 and 37 ppm respectively.

It is suspected that these resonances represent either, the decomposition products of the chemisorbed methanol or the dimethylether species, or the cross-reaction products of methanol and the dimethylether species. The latter possibility seems more reasonable, since decomposition of methanol or dimethyl ether would only lead to small molecular weight alkanes which should appear more upfield in the spectrum.

It is almost impossible to speculate what are the cross-reaction products from methanol and dimethylether. However, a conjecture would be that the reaction path takes the form of propagation and elongation of the carbon chain, probably with the formation of polymers, and the resonances at 26 and 37 ppm would then correspond to the  $-CH_2$  carbons in the polymeric species.

$^{13}C$  NMR/MAS spectra were measured for these two samples after treatment at 250°C. Only one resonance at 125 ppm is observed. This resonance could be interpreted as an highly-mobile ethene species on the surface which could not be observed on the  $^{13}C$  CP/MAS spectra. The mechanism of its formation is not understood. The other identification for this resonance at 125 ppm is a physisorbed  $CO_2$  molecule, with no neighbouring surface -OH groups. Its formation probably arises from some decomposition of the surface methoxide or ether species.

When the samples were treated at 300°C, there is a complete disappearance of the resonances at 56 ppm (methoxide) and 68 ppm (dimethylether) in the spectrum in Figure 6.9 for methanol-WO<sub>3</sub>-(2). Only the broad resonances centered at 35 and 26 ppm remain. This indicates that the polymers previously postulated consist mainly of carbon and hydrogen only (no oxygen). The two resonances (for methanol and dimethylether) still persist on the spectrum in Figure 6.8 for the methanol-WO<sub>3</sub>-(1) sample. This probably indicates an incomplete conversion. An extra resonance at 170 ppm appears in the spectrum in Figure 6.8 (not observed for methanol-WO<sub>3</sub>-(2) in Figure 6.9), probably indicating the formation of a bicarbonate species. This resonance at 170 ppm eventually appears in Figure 6.9, after the sample was treated at 350°C. This further indicates that there is a slight difference between the two WO<sub>3</sub> sample due to different degassing procedures.

<sup>13</sup>C NMR/MAS shows the same resonance at 126 ppm downfield from TMS.

When treated at 350°C, both samples show the same spectrum (only one representative one shown in Figure 6.9). This spectrum is almost similar to the previous one treated at 300°C.

Beyond 350°C, it was impossible to obtain any <sup>13</sup>C CP/MAS spectrum, probably due to paramagnetic broadening as was

mentioned earlier, or changes on the surface of  $WO_3$ .

Paramagnetic species cause problems in the study of surface species by NMR in two ways (ignoring relaxation): first, line-broadening and, second, change in the positions of the chemical shifts of the observed nuclei (151). The latter has been observed in the  $^1H$  study of adsorbed benzene on  $CO^{2+}$ - $SiO_2$  (152) and  $^{13}C$  study of adsorbed CO on zeolites exchanged with transition metals (153). These changes in the chemical shifts are usually accompanied by broadened resonance lines. As the concentration of paramagnetic species increases, no  $^{13}C$  signals are observed because of the extremely broadened resonance line produced by the strong electron-nucleus interaction.

One could suggest that this is what happened on the  $WO_3$  oxide when treated at above  $400^\circ C$ .

#### 6.A.VI. Summary

It has been shown that  $WO_3$  samples degassed differently behaved similarly in their methanol adsorption/desorption isotherms. Apparently, degassing at  $300^\circ C$  for 2 hours essentially removed all the surface water, and a further degassing of 17 hours did not increase the adsorption of methanol in  $WO_3$ -(1). (It would seem that a longer period of degassing period would remove more surface -OH groups, thus producing more "vacant" sites for the adsorption of methanol.)

The proton spin-lattice relaxation times for both kinds of  $WO_3$  showed the same characteristics. A dipole-dipole interaction figures to be the major contribution towards relaxation.

The  $^{13}C$  CP spectra of adsorbed methanol on both types of  $WO_3$  resembled those measured for the methanol-MgO systems. However, the isotropic peak (corresponding to physisorbed methanol species) appeared at very low coverage. It is suspected that these physisorbed molecules adsorbed on sites of low activation energies, thus become easily desorbed, as shown in the desorption isotherms.

The  $^{13}C$  CP spectra of the methanol- $WO_3$  systems treated at higher temperatures are not very informative. The  $^{13}C$  CP/MAS spectra reveal a dimethylether species at room temperature. It is speculated that the surface of  $WO_3$  is sufficiently acidic to cause a dehydration of two adsorbed methanol molecules yielding an ether species. Also noticing that the methoxide is ca. 55 ppm downfield from TMS, it probably indicates that there is a strong interaction between the surface methoxide species and the surface.

At higher temperatures (ca.  $250^\circ$ ), a very broad resonance on the high field side of the methoxide resonance was observed. Since it was not accompanied with any resonance at

ca. 60-70 ppm (indicating alcohols or ethers) or the  $sp^2$ -carbon region, it is suggested that it is a mixture of branched-chain alkanes. At higher temperatures, a low field resonance at 170 ppm was observed, which probably indicates a carbonate species.

## CHAPTER 7

Conclusions and Future Outlook

In this dissertation, a model has been proposed for the adsorption of alcohols on the MgO surface. The magnesium ions on the surface act as active sites for the adsorption of alcohols. The first monolayer of these adsorbed alcohols exists as chemisorbed species, in the form of magnesium alkoxides.

There also exist some physisorbed alcohol molecules on the MgO surface. It is conjectured that these physisorbed methanol molecules adsorb on the less active sites (sites with lower energy of adsorption), rather than hydrogen-bond to other alcohol molecules or surface -OH groups. Observation of these species by the  $^{13}\text{C}$  CP technique precludes the possibility that they may be liquid-like alcohol molecules.

It is also shown that the two -OH groups on the alkanediols cannot adsorb onto the same  $\text{Mg}^{2+}$  ion on the surface, even if the -OH groups are four C-C bond distances apart (as in the case of 1,4-butanediol). Therefore, it is established that the adsorption mode of alcohols on MgO is a 1:1 ratio, i.e. no more than one alcohol molecule per active site ( $\text{Mg}^{2+}$ ) on the surface.

The methanol and  $\text{CO}_2$  adsorption isotherms measured at room temperature show slight variations among the four preparations of MgO. This may suggest different surface morphologies on the

MgO surface due to different methods of preparation. A variation in the concentration of surface -OH groups may also contribute to the difference in the measured adsorption isotherms. The  $^{13}\text{C}$  CP spectra of the adsorbed methanol on all four preparations of MgO fail to yield any information on how different these MgO are.

Employing the  $^{13}\text{C}$  CP/MAS technique, and  $^{13}\text{C}$  enriched alcohols, decomposition products were identified when the alcohol-MgO systems were treated at successively higher temperatures. It has been established that MgO is more than a dehydrogenation catalyst. It is shown that MgO can catalyze the formation of higher molecular weight alcohols from ethanol, which eventually decompose into hydrocarbons. The observations in this work differ from previous studies (by IR, TPD etc.) as detailed in Chapter 2. This substantiates that "MgO prepared differently has different catalytic activities" (24-28).

The application of the  $^{13}\text{C}$  CP and  $^{13}\text{C}$  CP/MAS techniques to other catalytic systems is fraught with some difficulties. The  $^{13}\text{C}$  spectra of the methanol- $\text{WO}_3$  system show slight variations with respect to the alcohol-MgO systems. An ether species and a methoxide species have been observed when methanol adsorbs on the  $\text{WO}_3$  surface. This dehydration of the methoxide to a dimethyl ether species is believed to be catalyzed by the acidic protons on the  $\text{WO}_3$  surface. However, surface paramagnets cause broadening of the  $^{13}\text{C}$  CP/MAS spectra as the methanol- $\text{WO}_3$  samples were treated to higher temperatures.



It has been demonstrated in this dissertation that the  $^{13}\text{C}$  cross-polarization and strong decoupling technique, when coupled with the magic-angle spinning technique provide a wealth of information in the study of surfaces and catalytic reactions. Many chemisorbed species on the MgO surface which were never identified before (such as by infrared spectroscopy), were found by this combined technique. Thus, a reaction mechanism could be proposed to give an overall picture of what happened on the surface at that particular experimental stage, and hopefully a general understanding of the catalytic property of the surface.

Despite its apparent success, there are still a few experimental difficulties and limitations with this technique:

(i) Sample Size: The adsorbents under investigation are packed into the 5 mm o.d. NMR tubings to a height of about 2-2.5 cm in height. Unless the adsorbent has a high density or is very tightly packed, the loading level of adsorbates per  $\text{cm}^3$  of sample would be very low. This raises the problem of sensitivity. Experiments which require long spectrometer time are forbidding if there is more than one user. A new magic-angle stator which holds 8 mm o.d. tubes and spinner has recently been developed in this laboratory. This would increase the sample size, and thus the loading level of the adsorbates. However, the spinning speed (3-4 kHz) normally obtained for the 5 mm spinner cannot be attained by this 8 mm spinner.

Another way to increase sample size is to press the adsorbent into pellets, and in the process increase its density, thus the amount of adsorbates introduced into the sample could be increased. However, one has to assume that there is no serious structural change on the adsorbent surface.

It is also possible to use  $^{13}\text{C}$ -enriched adsorbates which would improve the S/N ratio. However,  $^{13}\text{C}$ -enriched adsorbates are difficult to prepare, and quite expensive.

(ii) Spectrometer: Since the time this project was initiated, and by the time it was ready to write up, there have been a lot of improvements done on this "home-built" spectrometer. A new single-sideband filter has been installed to improve the sensitivity (although the theoretical  $\sqrt{2}$  enhancement was never attained). A broad-band amplifier has been built to investigate the feasibility of studying nuclei other than  $^{13}\text{C}$  on this spectrometer. Other improvements include the replacement of the magnet power supply by solid-state electronics, stabilization of the lock circuit, building a programmable pulse generator (for generation of every pulse sequence imaginable), and of course the magic-angle spinner, and its probe.

In spite of these improvements on the spectrometer, it is still desirable to use a high field NMR spectrometer, for example, an 150 MHz spectrometer with a superconducting magnet.

This will increase the sensitivity about four times. On top of this, a better resolution in the  $^{13}\text{C}$  CP/MAS spectra could also be obtained.

(iii) References: Both  $\text{MgO}$  and  $\text{WO}_3$  are not novel catalysts, most of the present results on these two catalysts could be inferred from other spectroscopic evidence, or results from other techniques. However, the hitch is that when the NMR results deviate from the other spectroscopic observations, one has to rely on other resources (e.g. intuition, experience with NMR data etc.). This can be illustrated in the following example. Alkanes do not adsorb on the  $\text{MgO}$  surface in any appreciable amount, and one does not expect to observe an adsorbed methane on  $\text{MgO}$  by the  $^{13}\text{C}$  CP/MAS technique. However, if there exists a resonance at ca. 10 ppm upfield from TMS on the  $^{13}\text{C}$  CP/MAS spectrum, one tends to identify it as a slowly-rotating methane on the surface. One way to make a positive identification is to prepare a reference sample, i.e. by introducing methane into a sample tube containing  $\text{MgO}$ , seal the tube, and heat the sample to  $500^\circ\text{C}$ , (in an attempt to duplicate some of the experimental conditions in this project) and then measure the  $^{13}\text{C}$  CP/MAS spectrum of this sample. Hopefully this may yield a spectrum of adsorbed methane on  $\text{MgO}$ . There are only two faults in this, first, the condition for the adsorption of methane may require the presence of other chemisorbed species, and, second, one may not be able to obtain any signal at all (if the sample tube hasn't exploded yet).

Another difficulty may arise from the interactions among chemisorbed species (like or unlike), which may cause changes in the chemical shifts, thus making a positive identification impossible, e.g. the 5 ppm downfield shift of the  $\alpha$ -carbon of 1,4-butanediol. It is also possible that two chemisorbed species could have similar chemical shifts, identifying one may miss the other species completely.

This problem could be "solved" by studying some well-characterized catalysts with standardized infrared or other spectroscopic data. By duplicating the experimental procedures, one would be able to obtain sets of  $^{13}\text{C}$  CP/MAS spectra of chemisorbed species which could be identified by inferring from previous spectroscopic data. Thus a set of reference chemical shift data could be obtained for future identifications.

(iv) Systems of Interest: This dissertation did not really demonstrate the full potential of the  $^{13}\text{C}$  CP/MAS technique in the study of surfaces. Surface methoxide species have an anisotropy of about 1 kHz, which is easily narrowed to ca. 80 Hz by the CP/MAS technique. Other alkoxide species have smaller anisotropies. Only in the case when fragmented and/or polymerized carbon species are suspected to be present on the surface (e.g. ethanol-MgO-(3) treated at 300°C and higher temperatures) is resolution in the spectrum is poor. One wonders how useful is this technique when extended to other catalytic systems.

Preliminary results from the study of adsorbed methanol on  $WO_3$  indicated that in the presence of paramagnetic ions; the  $^{13}C$  CP/MAS technique breaks down, and no  $^{13}C$  spectra could be obtained.

The  $^{13}C$  CP/MAS technique has been applied to other catalytic systems in this laboratory. Carbon monoxide and acetylene were shown to chemisorb on a high surface area Ru-SiO<sub>2</sub> catalyst (18). A ruthenium carbonyl species (ca. 250 Hz wide) is observed at 194 ppm downfield from TMS from the adsorption of CO on Ru-SiO<sub>2</sub>.

However, a more complicated spectrum resulted for the chemisorption of acetylene on the same catalyst. Apparently, a reaction has taken place at room temperature, yielding benzene (from cyclotrimerization) or a surface vinylidene species (18). The reaction is still under investigation in this laboratory.

It seems that a thorough understanding of any catalytic processes requires a complete characterization of the catalytic surface, on which the reactions takes place. Recent works by Fyfe et al. (152, 153) on zeolites utilizing  $^{27}Al$  and  $^{29}Si$  MAS/NMR and CP/MAS techniques have detailed the bulk structures of a variety of zeolites, mordenite and offretite with different ratios of Si/Al. This study could be extended to the investigation of interactions between the adsorbates and the

adsorbents by observing the change in the  $^{27}\text{Al}$  and/or  $^{29}\text{Si}$  chemical shifts upon the addition of the adsorbates on the zeolite catalysts.

## REFERENCES

- 1) J. Frailssard, R. Caillat, J. Elston and B. Imelik, J. Chem. Phys. 60, 1017 (1963).
- 2) D. Geschke, Z. Physik. Chem. (Leipzig) 249, 125, (1972); D. Michel, *ibid.* 252, 263 (1973); D. Michel, Surf. Sci. 42, 453 (1974).
- 3) I.D. Gay and S. Liang, J. Catal. 44, 306 (1976); I.D. Gay, *ibid.*, 48, 430 (1977); S.H.C. Liang and I.D. Gay, *ibid.* 66, 294 (1980).
- 4) T. Bernstein, L. Kitaev, D. Michel and H. Pfeifer, J. Chem. Soc. Farad. Trans. I 78, 761 (1982).
- 5) J.F. Kriz and I.D. Gay, J. Phys. Chem. 80, 2951 (1976); I.T. Ali and I.D. Gay, J. Catal. 62, 341 (1980).
- 6) A. Pines, M.G. Gibby and J.S. Waugh, J. Chem. Phys. 59, 569 (1973).
- 7) S.R. Hartmann and E.L. Hahn, Phys. Rev. 128, 2042 (1962).
- 8) F.M. Lurie and C.P. Slichter, Phys. Rev. A 33, 1108 (1964).
- 9) S. Kaplan, H.A. Resing and J.S. Waugh, J. Chem. Phys. 59, 5681 (1973).
- 10) J.J. Chang, A. Pines, J.J. Fripiat and H.A. Resing, Surf. Sci. 47, 661 (1975).
- 11) (a) E.O. Stejskal, J. Schaefer, J.M.S. Henis and M.K. Tripodi, J. Chem. Phys. 61, 2351 (1974); (b) M.D. Sefcik, J. Schaefer and E.O. Stejskal, A.C.S. Symp. Ser. 34, 109 (1976); (c) M.D. Sefcik, J. Am. Chem. Soc. 101, 2164 (1979).

- 12) T.M. Duncan, J.T. Yates Jr. and R.W. Vaughan, J. Chem. Phys. 71, 3129 (1979).
- 13) (a) W.H. Dawson, S.W. Kaiser, P.D. Ellis and R.R. Inners, J. Am. Chem. Soc. 103, 6780 (1981); (b) idem., J. Phys. Chem. 86, 867 (1982).
- 14) D.W. Sindorf and G.E. Marciel, J. Am. Chem. Soc. 105, 1848 (1983).
- 15) J.A. Ripmeester, J. Am. Chem. Soc. 105, 2925 (1983).
- 16) R.E. Taylor, L.M. Ryan, P. Tindall and B.C. Gerstein, J. Phys. Chem. 73, 5500 (1980).
- 17) D. Freude, M. Hunger and H. Pfeifer, Chem. Phys. Lett. 91, 307 (1982).
- 18) I.D. Gay, J. Mag. Res. 58, 413 (1984).
- 19) S.L. Meisel, J.P. McCullough, C.H. Lechthaler and P.B. Weisz, Chemtech. 6, 86 (1976).
- 20) C.D. Chang and A.J. Silvestri, J. Catal. 47, 249 (1977).
- 21) C.D. Chang, Catal. Rev. 25, 1 (1983).
- 22) See, for example: (a) J. Morikawa, T. Goto, Y. Moro-Oka and T. Ikawa, Chem. Lett. 1667 (1982); (b) R.M. Dessau and R.B. Lapierre, J. Catal. 78, 136 (1982); (c) T. Inue, N. Morinaga, T. Ishihara, T. Kanie and Y. Takegami, J. Catal. 79, 176 (1983); (d) J.H.C. van Hooff, C.D. Chang, C.T.W. Chu and G.W. Skeels, *ibid.* 79, 242 (1983).
- 23) I.D. Gay, J. Phys. Chem. 84, 3230 (1980).
- 24) D.C. Foyt and J.M. White, J. Catal. 47, 260 (1977).
- 25) T. Iizuka, M. Saito and K. Tanabe, J. Res. Inst. Catalysis, Hokkaido Univ. 28, 189 (1980).



- 26) T. Matsuda, J. Tanabe, N. Hayashi, Y. Sasaki, H. Miura and K. Sugiyama, Bull. Chem. Soc. Japan 55, 990 (1982).
- 27) K. Miyahara, Y. Murata, I. Toyoshima, Y. Tanaka and T. Yokoyama, J. Catal. 68, 186 (1981).
- 28) S. Coluccia, A.J. Tench and R.L. Segall, J. Chem. Soc. Farad. Trans. I 75, 1769 (1979).
- 29) P.J. Anderson and P.L. Morgan, Trans. Farad. Soc. 60, 930 (1964).
- 30) R.I. Razouk, R. Sh. Mikhail and J. Ragai, J. Appl. Chem. Biotechnol. 23, 51 (1973).
- 31) B.H. Davis, J. Chem. Soc. Farad. Trans. I 76, 92 (1980).
- 32) (a) K. Tanabe, in "Solid Acids and Bases" p. 50-58, Acad. Press (1970); (b) idem, "Catalysis: Science and Technology" (J.R. Anderson and M. Boudart ed.), vol. 2 p. 231-273, Springer-Verlag (1981).
- 33) H. Hattori, N. Yoshii, K. Tanabe, Proc. 5th Internat. Congr. Catalysis 10, 223 (1973).
- 34) K. Tanabe, Y. Fukuda, React. Kinet. Catal. Lett. 1, 21 (1974).
- 35) K. Tanabe, K. Saito, J. Catal. 35, 247 (1974).
- 36) P.O. Scokart and R.E. Rouxhet, J. Coll. Interface Sci. 86, 96 (1982).
- 37) St. Mallinowski, S. Szczepanska, A. Bielanski and J. Slocznski, J. Catal. 4, 324 (1965).
- 38) O.V. Krylov, Z.A. Markova, I.I. Tretiakov and E.A. Fokina, Kinetics and Catalysis, 6, 107 (1965).

- 39) See, for example: (a) H. Zeitlin, R. Frei and M. McCarter, *J. Catal.* 4, 77 (1965); (b) H.E. Zaugg and A.D. Schaffer, *J. Am. Chem. Soc.* 87, 1857 (1965); (c) R.L. Nelson, A.J. Tench and B.J. Harmsworth, *Trans. Farad. Soc.* 63, 1427 (1967); (d) A.J. Tench and R.L. Nelson, *ibid.* 63, 2254 (1967).
- 40) Y. Inoue and I. Yasumori, *Bull. Chem. Soc. Japan* 54, 1505 (1981).
- 41) M. Iwamoto and J.H. Lunsford, *J. Phys. Chem.* 84, 3079 (1980).
- 42) R.B. Akhverdiev, A.P. Mamedov, F.V. Aliev, G.N. Asmolov and O.V. Krylov, *Kinetics and Catalysis*, 21, 999 (1980).
- 43) J.A. Lercher, H. Noller and G. Ritter, *J. Chem. Soc. Farad. Trans. I* 77, 621 (1981).
- 44) F. Koubowetz, J. Latzel and H. Noller, *J. Coll. Interface Sci.* 74, 322 (1980).
- 45) T. Ushikubo, H. Hattori and K. Tanabe, *Chem. Lett.* 649 (1984).
- 46) R.O. Kagel and R.G. Greenler, *J. Chem. Phys.* 49, 1638 (1968).
- 47) A.J. Tench, D. Giles and J.F.J. Kibblewhite, *Trans. Farad. Soc.* 67, 854 (1971).
- 48) H. Hattori, K. Shimazu, N. Yoshi and K. Tanabe, *Bull. Chem. Soc. Japan* 49, 969 (1976).
- 49) D.C. Foyt and J.M. White, *J. Catal.* 47, 260 (1977).
- 50) S.L. Parrott, J.W. Rogers and J.M. White, *Appl. Surf. Sci.* 1, 443 (1976).

- 51) N. Takezawa, C. Hanamaki and H. Kobayashi, J. Res. Inst. Catalysis, Hokkaido Univ. 28, 347 (1980).
- 52) N. Takezawa and H. Kobayashi, J. Catal. 73, 120 (1982).
- 53) N. Takezawa, C. Hanamaki and H. Kobayashi, J. Catal. 38, 101 (1975).
- 54) H. Noller and G. Ritter, J. Chem. Soc. Farad. Trans. I 80, 275 (1984).
- 55) O.V. Krylov and E.A. Fokiva, Kinet. i Katal. 1, 421 (1961).
- 56) M.E. Winfield, in "Catalysis" (P.H. Emmett, ed.) 2, 93, Reinhold Publ. Co., New York (1960).
- 57) See, for example: (a) B.A. Morrow, L.W. Thomson and R.W. Wetmore, J. Catal. 28, 332 (1973); (b) N. Takezawa and H. Kobayashi, J. Catal. 28, 335 (1973).
- 58) O.V. Krylov in "Catalysis by Nonmetals" p. 113-134, Acad. Press (1970).
- 59) See, for example: (a) T. Yamaguchi, Y. Tanaka and K. Tanabe, J. Catal. 65, 442 (1980); (b) A.J. van Roosmalen, D. Koster and J.C. Mol, J. Phys. Chem. 84, 3075 (1980); (c) A. Andreini and J.C. Mol, J. Coll. Interface Sci. 84, 57 (1981); (d) F. Penella, J. Catal. 69, 206 (1981); (e) A.J. van Roosmalen and J.C. Mol, J. Catal. 78, 17 (1982); (f) L.L. Murrell, D.C. Grenoble, R.T.K. Baker, E.B. Prestridge, S.C. Fung, R.R. Chianelli and S.P. Cramer, J. Catal. 79, 203 (1983).
- 60) R. Thomas, J.A. Moulijn, J. Medema and V.H.J. de Beer, J. Mol. Catal. 8, 161 (1980).

- 61) R.I. Alekseyeva, T.G. Alkazov, P.M. Bidzinova and M.S. Belenky, Azerb. Khim. Zh. 6, 45 (1965); Chem. Abstr. 71, 64601v (1969).
- 62) Y. Kamiya and E. Ogata, Proc. 5th Intern. Congr. Catalysis, II 93-1291, North-Holland Publishing Co. (1973).
- 63) H. Hattori, N. Asada and K. Tanabe, Bull. Chem. Soc. Japan 51, 1704 (1978).
- 64) M. Schiavello, F. Pepe, M. Cannizzaro, S. de Rossi and R.J.D. Tilley, Z. Physik. Chem. Neue Folge 106, 45 (1977), and references therein.
- 65) B.H. Davis, J. Catal. 55, 158 (1978).
- 66) H.A. Resing, Adv. Molecular Relaxation Processes 1, 109 (1967); and references therein.
- 67) See, for example: (a) W.F. Wurzbach and S. Gade, Phys. Rev. B6, 1724 (1972); (b) E.T. Cheng and J.D. Memory, Phys. Rev. B6, 1714 (1972); (c) D.K. Hutchins and S.M. Day, Phys. Rev. 180, 432 (1969).
- 68) See, for example: (a) I.J. Lowe and S. Gade, Phys. Rev. 156, 817 (1967); (b) G.W. Leppelmeier and J. Jeener, Phys. Rev. 175, 498 (1968); (c) D. Tse and S.R. Hartmann, Phys. Rev. Lett. 21, 511 (1968).
- 69) (a) J. Jeener, Adv. Mag. Reson. 3, 206 (1968); (b) A.G. Redfield, Science 164, 1015 (1969); (c) M. Goldman, in "Spin Temperature and Nuclear Magnetic Resonance in Solids" Oxford Univ. Press, London (1970).

- 70) (a) A. Abragam, in "The Principles of Nuclear Magnetism" Chapters 4 and 7, Oxford Univ. Press, London (1961);  
(b) G.E. Pake, J. Chem. Phys. 18, 317 (1948); (c) R. Bersohn and H.S. Gutowsky, J. Chem. Phys. 22, 651 (1954).
- 71) See, for example: (a) D.C. Look and I.J. Lowe, J. Chem. Phys. 44, 2995 (1966); (b) T.B. Cobb and C.S. Johnson Jr., J. Chem. Phys. 52, 6224 (1970); D.W. McCall, Acct. Chem. Res. 33, 223 (1971).
- 72) J.H. Van Vleck, Phys. Rev. 74, 1168 (1948).
- 73) (a) E.R. Andrew, A. Bradbury and R.G. Eades, Arch. Sci. 11, 223 (1958); (b) E.R. Andrew and V.T. Wynn, Proc. Royal Soc. A 291, 257 (1967).
- 74) H. Kessemeier and R.E. Norberg, Phys. Rev. 155, 321 (1967).
- 75) E.R. Andrew, in "Progress in NMR Spectroscopy" (J.W. Emsley, J. Feeney and L.H. Sutcliffe eds.) vol. 8, p. 1 Pergamon Press, New York (1971).
- 76) M. Maricq and J.S. Waugh, J. Chem. Phys. 70, 3300 (1979).
- 77) J.S. Waugh, C.H. Wang, L.M. Huber and R.L. Vold, J. Chem. Phys. 48, 662 (1968).
- 78) J.S. Waugh, L.M. Huber and U. Haeberlen, Phys. Rev. Lett. 20, 180 (1968).
- 79) U. Haeberlen and J.S. Waugh, Phys. Rev. 175, 453 (1968);  
ibid. 185, 420 (1969).
- 80) P. Mansfield, in "Progress in NMR Spectroscopy" (J.W. Emsley, J. Feeney and L.H. Sutcliffe eds.) vol. 8, p. 41, Pergamon Press, New York (1971).

- 81) (a) L.R. Sarles and R.M. Cotts, Phys. Rev. 111, 853 (1958);  
(b) M. Mehring, A. Pines, W.K. Rhim and J.S. Waugh,  
J. Chem. Phys. 54, 3239 (1971).
- 82) M. Mehring, in "NMR: Basic Principles and Progress"  
(P. Diehl, E. Fluck and R. Kosfeld eds.) vol. 11,  
Springer-Verlag, New York (1976).
- 83) A. Abragam and W.G. Procter, Phys. Rev. 109, 1441 (1958).
- 84) A.G. Redfield, Phys. Rev. 98, 1787 (1955).
- 85) E.P. Jones and S.R. Hartmann, Phys. Rev. 36, 757 (1972).
- 86) C.P. Slichter and W.C. Holton, Phys. Rev. 122, 1701 (1961).
- 87) (a) A. Pines, M.G. Gibby and J.S. Waugh, J. Chem. Phys. 56,  
1776 (1972); (b) idem., Chem. Phys. Lett. 15, 373 (1972).
- 88) I. Solomon, Compt. Rend. 248, 92 (1950).
- 89) A.G. Anderson and S.R. Hartmann, Phys. Rev. 128, 2023  
(1960).
- 90) (a) J. Jeener and P. Broekaert, Phys. Rev. 157, 232 (1967);  
(b) J. Jeener, R. Du Bois and P. Broekaert, Phys. Rev. 139  
A, 1959 (1965).
- 91) D.A. McArthur, E.L. Hahn and R.E. Walstedt, Phys. Rev. 188,  
609 (1969).
- 92) D. Demco, J. Tegenfeldt and J.S. Waugh, Phys. Rev. B11,  
4133 (1975).
- 93) (a) P.K. Grannell, P.K. Mansfield and M.A. Whittaker, Phys.  
Rev. B8, 4149 (1973); (b) H. Ernst, Wiss. Z. Karl-Marx  
University, Leipzig, Math. Naturev. 23, 449 (1974);

- (c) O. Kanert and M. Mehring, in "NMR: Basic Principles and Progress" vol. 3, Springer (1971); (d) D. Schmid, "Springer Tracts in Modern Physics" Springer (1973).
- 94) M.J. Sullivan and G.E. Marciel, *Anal. Chem.* 54, 1615 (1982).
- 95) H.E. Bleich and A.G. Redfield, *J. Chem. Phys.* 55, 5405 (1971).
- 96) A. Pines and T.W. Shattuck, *J. Chem. Phys.* 61, 1255 (1974).
- 97) M. Mehring, H. Raber and G. Sinning, 18th Congress Ampere, p.35, Nottingham, England (1974).
- 98) E.R. Andrew, *Arch. Sci. (Geneva)* 12, 103 (1959).
- 99) I.J. Lowe, *Phys. Rev. Lett.* 2, 285 (1959).
- 100) E.R. Andrew, A. Bradbury and R.G. Eades, *Nature* 183, 1802 (1959).
- 101) E.R. Andrew and R.G. Eades, *J. Chem. Soc. Farad. Soc. Disc.* 34, 38 (1962).
- 102) E.R. Andrew and R.A. Newing, *Proc. Phys. Soc.* 72, 959 (1958).
- 103) J. Dreitlin and H. Kessemeier, *Phys. Rev.* 123, 835 (1961).
- 104) E.R. Andrew and G.T. Genks, *Proc. Phys. Soc.* 80, 663 (1962).
- 105) S. Clough and K.W. Gray, *Proc. Phys. Soc.* 79, 457 (1962); *ibid.* 80, 1382 (1962).
- 106) S. Clough and I.R. McDonald, *Proc. Phys. Soc.* 86, 833 (1965).
- 107) W.A.B. Evans and J.G. Powles, *Proc. Phys. Soc.* 92, 1046 (1967).

- 108) (a) J. Schaefer and E.O. Stejskal, J. Am. Chem. Soc. Soc. 98, 1031 (1976); (b) J. Schaefer, E.O. Stejskal and R. Buchdahl, Macromolecules 10, 384 (1977).
- 109) E.O. Stejskal, J. Schaefer and J.S. Waugh, J. Mag. Res. 28, 105 (1977).
- 110) E.O. Stejskal and J. Schaefer, J. Mag. Res. 18, 560 (1975).
- 111) A.L. Brooke, I.D. Gay, P.K. Morris and T.R. Openshaw, unpublished results.
- 112) J.R. Zimmerman and W.E. Brittin, J. Phys. Chem. 61, 1328 (1957).
- 113) J.K. Thompson, J.J. Krebs and H.A. Resing, J. Chem. Phys. 4, 3853 (1965).
- 114) A.G. Whitney, Ph.D. Thesis, Simon Fraser University (1975).
- 115) M.E. Stoll, A.J. Vega and P.W. Vaughan, Rev. Sci. Instr. 48, 800 (1977).
- 116) V.R. Cross, R.K. Hester and J.S. Waugh, Rev. sci. Instr. 47, 1486 (1976).
- 117) Andrew Corp., type LDF4-50.
- 118) American Technical Ceramics, types 100E, 100B.
- 119) Polyflon Corp., type VC.
- 120) A.L. Brooke, unpublished.
- 121) Mini-Circuits Laboratories, type MCL-SRA-3.
- 122) B. Gerand, G. Nowogrocki, J. Guenot and M. Figlaiz, J. Solid State Chem. 29, 429 (1979).
- 123) W.F.N.M. de Vleesschauwer, in "Physical and Chemical Aspects of Adsorbents and Catalysts" (B.G. Linsen, ed.) p. 284, Acad. Press, London (1970).



- 124) A. Murray III and R.L. Williams, in "Organic Synthesis with Isotopes" Part 1, p. 905, Wiley Interscience Publ. Co. (1958).
- 125) P.J. Anderson, R.F. Horlock and J.F. Oliver, Trans. Farad. Soc. 61, 2754 (1965); P.J. Anderson, in "Structure of Metallic Catalysts" p. 63, Acad. Press (1975).
- 126) H. Pfeifer, in "NMR: Principles and Progress" vol. 7, Springer-Verlag (1972).
- 127) L. Muller, A. Kumar, T. Baumann and R. Ernst, Phys. Rev. Lett. 32, 1402 (1974).
- 128) R.K. Hester, V.R. Cross, J.L. Ackerman and J.S. Waugh, J. Chem. Phys. 63, 3606 (1975).
- 129) S.J. Opella and M.H. Frey, J. Am. Chem. Soc. 101, 5854 (1979).
- 130) L.B. Alemany, D.M. Grant, T.D. Alger and R.J. Pugmire, J. Am. Chem. Soc. 105, 6697 (1983).
- 131) N. Takezawa and H. Kobayashi, J. Catal. 25, 179 (1972).
- 132) M.E. Winfield, Catalysis (P.H. Emmett, ed.) vol. 7, 93 (1960).
- 133) We have measured the  $^{13}\text{C}$  chemical shifts of 58.8 and 22.5 ppm downfield from TMS by  $^{13}\text{C}$  CP/MAS for the magnesium ethoxide polymer.
- 134) J.B. Stothers, in "Carbon-13 NMR Spectroscopy", Acad. Press, New York (1970).
- 135) S. Ganapathy, V.P. Chacko and R.G. Byrant, J. Mag. Res. 52, 239 (1984).
- 136) A. Ejchart, Org. Mag. Res. 2, 351 (1977).

- 137) J.D. Roberts, F.J. Wright, J.I. Kroschwitz and H.J. Reich, J. Am. Chem. Soc. 92, 1338 (1970).
- 138) L.P. Lindeman and J.Q. Adams, Anal. Chem. 43, 1245 (1971).
- 139) R.M. Silverstein, G.C. Bassler and T.C. Morrill, in "Spectrometric Identification of Organic Compounds", 4th ed. John Wiley and Sons, New York (1981).
- 140) We have measured the shielding component of the methine carbon in diammonium tartronate as 59.8, 83.1 and 90.9 ppm downfield from TMS.
- 141) These  $^{13}\text{C}$  chemical shift data for 1,3-butanediol was measured neat on our Bruker WM-400 NMR spectrometer.
- 142) T.H. Fleisch and G.J. Mains, J. Chem. Phys. 76, 780 (1982); and references therein.
- 143) A.M. Alquie and C. Lamy, Comptes Rendu 175, 1207 (1972).
- 144) R.A. Aronovitch, I.G. Fal'kov, A.I. Yablonskaya, L.S. Tuktarova, V.F. Grigor'ev, D.A. Bol'shakov and O.P. Yablonskii, Kinet. i. Katal. 23, 1489 (1982).
- 145) J. Haber, J. Janas, M. Schiavello and R.J.D. Tilley, J. Catal. 82, 395 (1983).
- 146) N. Tsuda, T. Mori, N. Kosaka and Y. Sakai, J. Mol. Catal. 28, 183 (1985).
- 147) M.J. Sullivan and G.E. Marciel, Anal. Chem. 54, 1606 (1982).
- 148) W.T. Dixon, J. Schaefer, M.D. Sefcik, E.O. Stejskal and R.A. McKay, J. Mag. Res. 45, 173 (1981).
- 149) T. Yoshida, Y. Maekawa and T. Fujito, Anal. Chem. 55, 390 (1983).

- 150) C.A. Wilkie, T.C. Ehlert and D.T. Haworth, *J. Inorg. Nucl. Chem.* 40, 1983 (1978).
- 151) H. Pfeifer, W. Meiler and D. Deininger, in "Annual Reports on NMR Spectroscopy" (G.A. Webb ed.) vol. 15, p. 321, Acad. Press (1983).
- 152) V. Ju. Borovkov and V.B. Kazansky, *Kinet. i. Katal.* 13, 1356 (1972).
- 153) Y. Ben Taarit, *Chem. Phys. Lett.* 62, 211 (1979).
- 154) B.E. Mann and B.F. Taylor, in "<sup>13</sup>C NMR Data for Organometallic Compounds" (P.M. Maitlis, F.G.A. Stone, and R. West eds.) Acad. Press (1981).
- 155) M.H. Chisholm, F.A. Cotton, M.W. Extine and R.L. Kelly, *Inorg. Chem.* 18, 116 (1979).
- 156) M. Akiyama, M.H. Chisholm, F.A. Cotton, M.W. Extine, D.A. Haitko, D. Little and P.E. Fanwick, *Inorg. Chem.* 18, 2266 (1979).